Report No. 952

PHYSICS OF FLAMES (U)

Final Report

by

Irvin Glassman, William A. Sirignano and Martin Summerfield

Guggenheim Laboratories
Department of Aerospace and Mechanical Sciences
Princeton University
Princeton N. J.

Prepared For

U. S. Army
Ballistic Research Laboratories
Aberdeen Proving Grounds, Md.

September 1970

2.50

AD

Final Report Under Contract No. DAA05-68-C-0450

for

U. S. Army
Ballistic Research Laboratories
Aberdeen Proving Ground, Md.

PHYSICS OF FLAMES

by

Irvin Glassman, William A. Sirignano and Martin Summerfield

Guggenheim Laboratories
Department of Aerospace and Mechanical Sciences
Princeton University
Princeton, N. J.

September 1970

Summary

The long range objectives of the research were to discover and describe in general theoretical form the fundamental factors that govern ignitability, rate of flame spreading, and rate of burning of fully developed flames in sprays, vapors and/or pools of liquid hydrocarbon fuels under various conditions of exposure. Because of early termination of the program, only ignitability and flame spreading characteristics across pools have been considered and are reported upon here.

Early in the work it was discovered that, for fuels below their flashpoint, hydrodynamic currents in the liquid fuel itself play perhaps the dominant role in flame spreading. These currents are induced by either surface tension or buoyancy forces. Since it was concluded then that the physical characteristics of the fuel are important in flame spreading, extensive experiments were performed in which the flame spreading rate across normal decane was measured as a function of fuel temperature, viscosity, depth, pan size, etc. It is these results which must be compared to the comprehensive theory sought.

The problem of a two-dimensional flame spreading across a horizontal fuel surface has been analyzed when the liquid fuel temperature is below its flash point. It has been demonstrated that the liquid phase convective heat transfer in the direction of the flame propagation occurs when surface tension variation is taken into account. The flow field has been completely analyzed for shallow pools. In the case of deep pools, the boundary layer approximation is valid and it has been shown that the buoyancy terms are of higher order and hence negligible compared to surface tension terms. Some velocity profiles in the liquid phase are presented.

The program on ignition characteristics of pools was divided into two parts; one considered ignition of a pool of fuel above its flash temperature, and the other dealt with ignition of the pool below its flash temperature. In the first case, the ignition zone could be predicted from a given geometry of pool and air flow above the fuel surface. The theoretical model considered the fuel surface to be rigid and hence used the known boundary layer solutions over a flat plate to calculate the profiles of the fuel vapor concentration and the air velocity in the boundary layer. The knowledge of the lean and rich limit concentrations for ignition of the vapor/air mixture and the burning velocity of the fuel as a function of vapor/air mixture then determines the ignition zone above the fuel surface. In fact, the experimental ignition data obtained in the air flow system were in good agreement with the theory. Both theory and experiment indicated that the ignitable mixture in the air flow can be produced only if the liquid pool is at or above its flash temperature.

In the case of the pool at subflash temperatures, the ignitable mixtures can be achieved if local heating of the fuel by the proximity of the igniter can sufficiently increase the fuel vaporization rate. The local heating of the fuel entails a subsurface fuel circulation which complicates the phenomena involved in producing the ignitable mixture above the pool. At present, no proven model has been suggested for this type of ignition. The observations can be summed up in the following statements:

1. Ignition of a liquid at subflash temperature can be effected by a hot igniter if it is placed very close to the surface, much closer in general than in the case of a liquid fuel at a temperature above the flash temperature. It is evident that heat transfer by radiation and by conduction to the surface of the adjacent liquid is an essential part of the process; this is not essential in the case of a liquid above the flash temperature.

2. Under such conditions of ignition, the presence of a wind does not affect noticeably the required igniter height or the ignition delay; this is contrary to the case of a fuel at above-flash temperature, where the wind is definitely a strong factor.

3. The presence of the hot igniter near the liquid surface causes two observable fluid dynamic phenomena. One is a sustained vortex, with the streamlines running away from the igniter along the surface, and returning to the igniter upward from below the surface. The higher the igniter temperature, the faster the liquid circulates in the vortex. The second phenomena is a definite depression of the surface below the igniter, in some cases as much as a millimeter, which becomes more pronounced as the igniter temperature is raised or as it is brought closer to the surface.

4. Unless the induced circulation in the body of the fuel near the hot igniter is restricted by some artificial means, such as a mechanical barrier or a thickening additive, the induction interval before ignition may be very long, from a few seconds to a hundred seconds or more, depending on the temperature of the igniter, its closeness to the surface, and other conditions.

5. Although a liquid pool at subflash temperature may have been brough successfully to ignition, the flame may die out soon after the igniter is withdrawn. However, it was observed that if the burning area exceeds some minimum size, the flame will continue to propagate over the surface of the subflash liquid fuel. The preignition motion of the fuel, induced by the heat flux from the hot igniter at the upper surface, was studied to determine the driving mechanisms of the motion. It was found that buoyancy and surface tension forces were combining to cause the complex motion. A numerical scheme was formulated to obtain more details of the fluid motion.

In conclusion, this research has shown that the ignition data for the boundary layer above the pool at superflash temperature is in satisfactory agreement with the theoretical model. On the other hand ignition above the pool at subflash temperature depends strongly on subsurface motion of the fuel.

The problem of ignition of a combustible mixture by a hot projectile also has been analyzed by considering independently three flow regimes, the leading stagnation point, the lateral surface, and the wake. The dependence of the projectile velocity on its temperature and/or its length is determined numerically for different values of quantities relating to the properties of propane-air mixture. An empirical correlation of the numerical results is also given.

A simplified model has been proposed for the ignition of unmixed reactants by a hot inert gas, and the numerical results are, at present, being obtained.

Foreward

The Princeton program on "The Physics of Flames" began on July 1, 1968 under the sponsorship of the U. S. Army Ballistics Research Laboratory (Contract No. DAAD05-68-C-0450). The program was terminated on July 31, 1970 and this document is the final report of the progress made.

The principal investigators directing this effort were Professors Irvin Glassman, William A. Sirignano and Martin Summerfield. The overall program was divided into three major parts: flame spreading across liquid pools, ignition of pools, and a theoretical effort on flame spreading and projectile ignition. As a matter of administrative convenience to the sponsoring agency, a small study on ignition of solid propellants directed by Professor Summerfield was added to the program under the same contract.

Considering the scope of the effort, it was deemed most logical to write this report in four separate parts which would include each of the major aspects of the flame study and the solid propellant study. Each part is written as if it were a separate document and includes its own table of contents, text, references and figures. Co-authors who have contributed to the program are listed at the beginning of each part.

Table of Contents

Part I

Table of Contents

Part I: Flame Spreading Over Liquid Fuel Surfaces in Quiescent Atmospheres

List of Tables

List of Figures

Part I. Flame Spreading Over Liquid Fuel Surfaces in Quiescent Atmospheres (R. MacKinven and I. Glassman)

Of the four stages (ignition, flame spreading, steady burning and extinguishment) involved in the burning of large pools of flammable liquids, flame spreading has received the least attention in the literature. Only two contributions, which are specific to the better understanding of flame spreading over liquid fuels, could be found. One is by Tarifa and Torralbo[1] in 1967 and the other is a doctoral thesis by Roberts[2] which is referenced in a comment by Roberts on the above paper*. Partly because of this dearth of information on flame spreading over liquid fuels, a co-ordinated program of fundamental tests and experiments was planned. During the course of the contract (24 months) many of these plans were implemented. Due to the number and diversity of the experiments which were performed and the multiplicity of conclusions that were drawn, the research is best described under six main sub-headings:

A. Preliminary Concepts, Models and Experiments.
B. Experimental Procedures for Flame Spreading Measurements.
C. Investigation of the Influence of Laboratory Parameters on the Rate of Flame Spread.
D. Investigation of the Influence of Changes in the Physical Properties of the Fuel on the Rate of Flame Spread.
E. Investigation of the Convective Flow Patterns in the Liquid Which Accompany Flame Spreading.
F. Measurement of the Physical Properties of the Fuels.

A. Preliminary Concepts, Models and Experiments

Since ignition, flame spreading. "steady" burning, and extinction are intimately interrelated, one process cannot adequately be studied without a knowledge of the other three processes. Consequently, the initial task in the program was a review of the field of Pool Burning[6]. This review formulated some basic concepts which have been the keystones to the research effort. Firstly, the flash temperature and the fire temperature were given

---

*It was only after the present research effort began that a copy of this copyrighted thesis could be obtained from the Imperial College Library, London. The date of the thesis is 1959 although it is erroneously reported as 1966 in Roberts' comments to Tarifa and Torralbo's paper[1] in the 11th Combustion Symposium. This work has since been published in the Proceedings of the Royal Society under the co-authorship of Burgoyne and Roberts with Quinton (see References 3-5).

a basic definition in terms of fundamental combustion theory. The flash point is that temperature at which the liquid fuel ignites (i.e., flashes) in air when a pilot flame is passed at a specified, constant, distance above the fuel surface. It therefore specifies the temperature at which the liquid exerts a sufficient vapor pressure such that the mixture of fuel vapor and air is just within the flammability limit of the fuel. (Obviously the flash point varies somewhat with the height of the ignition source, but for a fixed height, the flash point is a fixed property of the fuel).

The fire point is the temperature at which the liquid not only ignites, but also burns in a self-sustaining manner. Fundamentally, it is the temperature which creates a mixture ratio near the surface such that the transfer number is large enough so that the energy release at the fuel surface (due to combustion) maintains a sufficient evaporation rate to sustain a flammable mixture ratio.

These definitions led to the concept that there are two distinct mechanisms of flame spread, one controlling above the flash point and the other below the flash point. When a fuel which is above it flash/fire point is ignited the flame can spread through the vapor-air mixture without requiring further vaporization from the liquid. In such cases, gas phase phenomena are postulated to control the rate of flame spread and the order of magnitude of the spread rate should be the laminar flame speed.

Liquid fuels below their flash point are known to sustain a spreading flame and eventually burn in a 'steady' manner. The most logical process of sustaining the spreading flame is to have the liquid ahead of the flame front heated to its flash point. There are three distinct ways in which the fuel ahead of the flame may be heated, namely:

(i) RADIATION from the flame to the non-ignited fuel surface. [See Figure 1, heat transfer mode 6].

(ii) CONDUCTION through the gas ahead of the flame to the fuel surface [See Figure 1, heat transfer mode 5].

(iii) Heating (CONDUCTIVE, CONVECTIVE AND RADIATIVE) of the fuel beneath the established flame and then transfer of heat forward through the liquid fuel. [See Figure 1, heat transfer modes 3, 4 and 11].

For small flames, radiative heating is negligible, leaving only the slower conductive and convective mechanisms, (ii) and (iii) above. It was postulated, therefore, that flame spreading rates would be much slower in fuels below the flash point than in fuels above the flash point. This conception is shown schematically in Figure 2 as a plot of flame spreading rate as a function of fuel temperature. It was found later that Roberts[2] had previously postulated such curves and made the experimental measurements to support them.

Armed with these considerations, certain key preliminary experiments[7] were performed in which close visual observation was made of flame spreading over kerosene* below its flash point. These experiments showed, as Roberts'[2] experiments apparently had, that the liquid fuel ahead of the flame moves in the same direction as the flame. This observation was verified by noting the movement of styrofoam particles which were floated on the fuel surface during the flame propagation experiments. It was speculated that convection currents in the liquid fuel were a most important factor in the flame propagation process. This conclusion was supported by two other series of experiments. In one, the fuel was absorbed in sintered metal and refractory wicks, with the reasoning that the metal wick had a higher thermal conductivity and thus the flame should propagate more rapidly if heat conduction through the liquid is important. The flame spread very slowly across the metal wick (the flame propagation rate was trivial compared to the rates in free liquid fuels) while with the refractory wick the flame was essentially stationary and the fuel was transferred to the stationary flame by capillary action. The solid wicks therefore stopped the initiation of convective flows and flame spreading was much slower.

In the second series of experiments a group of barriers were placed in the experimental tray such that the top of the barriers almost penetrated the fuel-air interface, i.e., the fuel just wetted the tops of the barriers. Barriers made of cardboard (thermal conductivity equal to that of the fuel), steel and glass (thermal conductivity greater than that of the fuel) had the same effect in that flame propagation was halted at the first barrier. (If allowed to burn for a few minutes, the fuel on the other side of the barriers would eventually heat up, ignite and flame propagation would begin again). If the barriers were lowered a little (a few mm) below the fuel surface the flame propagated normally over the barriers. It was concluded that liquid phase convection was the major driving force for flame spread across liquids.

In a final series of preliminary experiments the viscosity of the kerosene fuel was increased by adding a polyisobutylene of molecular weight $\approx$ 200,000, Vistanex MM L-140, in small percentages to the fuel. Such thickening agents were not expected to alter the vapor pressure of the kerosene (this was later verified experimentally, see Section F.2). As was anticipated if convection currents were important, when the viscosity of the fuel increased the flame spreading rate decreased. These data are shown in Figures 3 and 4. The decrease in flame spreading is of significant proportions.

Following the accepted practice for research, the feed-back of information from the experiments to the model showed that there were

---

*A 3.6 mm thick layer of kerosene was floated on a 15.3 mm layer of water in an aluminum tray, 48 inches long, 6 inches wide and 1 inch deep.

two logical ways in which convection currents (cells) could be established by surface tension induced flows* (Marangoni effect) or buoyancy induced flows (gravity effect).

The conclusions of this preliminary study can be summarized as:-

(i) Flash and fire points were given much greater significance.

(ii) There are two regimes of flame spread.

(iii) Above the flash point, gas phase phenomena control the flame spreading rate.

(iv) Below the flash point, liquid phase phenomena control the flame spreading rate.

(v) Below the flash point convection currents play an important role in flame spreading mechanisms.

(vi) Flame spreading over solids and liquids may differ considerably and great care must be taken in applying theories for solids to liquids.

B. Experimental Procedures for Flame Spreading Measurements

At the start of this program many decisions had to be made as to the experimental techniques to be used for measuring flame spreading rates. The two previous studies used widely different techniques. Burgoyne and co-workers[3-5] used a wick as an ignitor, narrow channels (0.9" to 2.5", but usually 1.3" wide) as fuel containers and a circulating water bath to maintain the temperature of the containers. Tarifa and Torralbo used a large tray (20 inches wide by 16 feet long), gasoline as an ignitor fluid and a moving screen which extinguished the flames about one foot behind the flame front. It was considered essential that all the procedural details of the flame spreading experiments should be investigated critically so as to give results which were independent of the procedures. To this end, various fuels, modes of ignition and methods for measuring the flame spreading rate were investigated. This section describes the procedures and the next section describes the investigation of the influence of the laboratory parameters on the rate of flame spread.

1. Fuels

Two types of fuels were recognized as being important, (1)

---

*The concept of surface tension induced flows first arose in discussions with Professor S. H. Lam.

mixed fuels, like kerosene, which are in commercial use, and (2) pure fuels which are constituents of the mixed fuels, e.g., nonane, decane, undecane, dodecane, tetradecane, hexadecane, cymene and dipentene. The fuels which have been used, their purity and their source are shown in Table 1. Initially kerosene was used as the test fluid, but its wide variation in composition caused scatter in the results and dipentene then was substituted. Eventually the more expensive n-decane was used for the majority of the tests because it burned much more cleanly and with less carbon formation than dipentene.

A distillation apparatus was constructed to repurify the unburned n-decane remaining after each test. The fraction distilling in the range 173-174°C was collected and used in subsequent tests.

2. Procedures

Early in the experimental program, it became obvious that great care must be taken in controlling the initial conditions in order to obtain reproducible flame spreading data. In particular, external air currents and variations in the temperature of the fuel cause discrepancies and must be eliminated. Accordingly, all experiments were performed in a test cell (25 feet long by 9 feet wide by 10 feet high) which was virtually free of drafts so that flame spreading phenomena were studied under conditions free of forced convection. Furthermore, the temperature of the cell was controlled to $\pm$ 1°C using heaters and air conditioners. The fuel was equilibrated to the required temperature ($\pm$ 0.1°C) in a temperature controlled water-bath.

In most experiments (except those with water-soluble fuels and some experiments with decane and kerosene) the fuel was floated on water in order to give a well defined depth of fuel and to conserve fuel supplies. (The effect of the presence of this water layer has been investigated, see Sections D.1 and 4).

In a typical run, it was decided what fuel, depth of fuel, initial temperature, and tray size to use. A wide variety of tray sizes were available. Most trays were made of 1.6 mm (1/16 inch) thick aluminum, but two were constructed of 6.3 mm (¼ inch) thick plates of Pyrex (which were cemented together with epoxy) to allow visual observation of the liquid phase phenomena and to change the thermal properties of the tray walls. Change of the thermal properties of the tray walls also was achieved by lining the inside of the aluminum trays with plate glass. (Table 2 gives the dimensions of the trays). The method of measuring the progress of the spreading flame was also chosen (see next section). The fuel (and water if required) was added to the tray and time was allowed for currents in the air and liquid to subside before igniting the fuel. After the flame had spread the required distance and the necessary measurements had been taken, the flame was extinguished by covering

Table 1

Source and urity of the Liquid Fuels

Fuel	Grade (mole per cent)	Source
n-Nonane	Technical (95%)	Phillips 66
n-Decane	Practical (95%)	Humphrey Chemical Co.
n-Decane	Technical (95%)	Phillips 66
n-Decane	Pure (97%)	Phillips 66
n-Decane	97%	Humphrey Chemical Co.
n-Decane	99%	Humphrey Chemical Co.
n-Decane	Research (99.5%)	Phillips 66
n-Undecane	Technical (95%)	Phillips 66
n-Dodecane	Technical (95%)	Phillips 66
n-Dodecane	Practical (90% + Isomers)	Humphrey Chemical Co.
n-Tetradecane	Practical (91% + Isomers)	Humphrey Chemical Co.
n-Hexadecane	Practical (91% + Isomers)	Humphrey Chemical Co.
Dipentene	Technical	Eastman Organic Co.
Dipentene	Reagent	J. T. Baker Co.
p-Mentha-1,8 diene (Dipentene)	Technical	Matheson, Coleman & Bell
Cymene	Technical	Fisher Scientific Co.
Mesitylene	Technical	Fisher Scientific Co.
n-Butanol	Reagent	Matheson, Coleman & Bell
n-Butanol	Technical	Fisher Scientific Co.

Table 2

Size and Material of the Trays

Material	Dimensions, cm (inches		
	Length	Width	Depth
Aluminum	120(48)	2.9(1.13)	2.5 (1)
Aluminum	120(48)	5.6(2.25)	2.5 (1)
Aluminum	120(48)	7.8(3.13)	2.5 (1)
Aluminum	120(48)	10.6(4.25)	2.5 (1)
Aluminum	120(48)	15 (6)	1.9 (0.75)
Aluminum	120(48)	15 (6)	2.5 (1)
Pyrex	120(48)	15 (6)	2.5 (1)
Aluminum	120(48)	15 (6)	3.2 (1.25)
Aluminum	120(48)	17.5(7)	2.5 (1)
Aluminum	120(48)	22.5(9)	2.5 (1)
Aluminum	120(48)	60 (24)	2.5 (1)
Aluminum	120(48)	75 (30)	2.5 (1)
Aluminum	180(72)	19.7(7.9)	1.0 (0.4)
Aluminum	180(72)	19.7(7.9)	2.5 (1)
Aluminum	180(72)	19.7(7.9)	5.0 (2)
Aluminum	180(72)	45 (18)	2.5 (1)
Aluminum	240(96)	30 (12)	2.5 (1)
Aluminum	300(120)	19.7(7.9)	2.5 (1)
Aluminum	300(120)	75 (30)	2.5 (1)

with a smother board. Reproducibility was much improved by adopting this standard procedure, and by repeating each determination four or five times the scatter of results was reduced to about ± 3%.

Three different ignition methods* were investigated. The first used an aluminum barrier to segment a small (approx. 5-8 cm wide) section of the fuel at the end of the tray which was ignited with a Bernz-O-Matic propane torch. When the flame was fully established in this section, the barrier was removed and the flame allowed to spread.

In the second mode of ignition, a small volume (approx. 1cc) of a volatile fuel, usually hexane, was poured onto the fuel at one end of the tray and spark ignited.

In the third method, an asbestos or ceramic wick was placed near the end of the tray and the fuel vapor above the wick was ignited with a flame.

The barrier/torch mode of ignition was used in the majority of tests, but the hexane/spark ignition was used periodically throughout the tests in order to test the reproducibility of the flame spreading data with a different mode of ignition. The wick ignition method was used only occasionally in specialized tests. (The advantages and disadvantages of these procedures are discussed in more detail later; see Section C.4).

3. Techniques used for measuring flame spreading rates

There are numerous methods available for measuring the rate of progress of the flame across the surface of fuels (V_F). Some methods give mean velocities between two fixed positions while others give values of the instantaneous spreading velocity at a specific position. Many methods were tried in order to arrive at the 'best' possible method. By 'best', it was obviously considered that the method should be accurate (and preferably give some idea of the accuracy), but also it should be easy to use and set up and give results quickly because of the large number of experiments which were anticipated. The method should also minimize the amount of subjectivity in deciding the position of the flame front.

The main methods used to measure flame spreading rates are described below.

---

*Unconfined fuels below their flash points cannot be ignited by simply applying a source of energy such as a propane torch.

(a) Method 1 - Stopwatch timing between two fixed points.

This was the first method used and had the advanatage that it was very simple in that it entailed marking positions on the tray and timing the progress of the flame with a stopwatch. This method has the disadvantage that it only gave mean velocities and it was subjective. (It depended on the experimentalists eyesight in determining the position of the leading edge of the flame).

(b) Method 2 - Cinematography of flame position and time.

A Bolex 16 mm movie camera was used to record simultaneously the time and the position of the flame in a graduated tray. This method had the advantage that it gave plots of flame position against time and, therefore, gave instantaneous velocities. It had a marked disadvantage due to the delays in processing and tedious analysis of the film.

(c) Method 3 - Photo-transistor detection with electronic counter display

Photo-transistors were arranged at known positions along the tray in specially designed housings such that the view-angle was very small and in a direction perpendicular to the direction of flame spread. The output from these photo-transistors was fed into Schmidt triggers so that when the output reached a certain value a Berkeley counter was initiated. One photo-transistor started the counter when the flame passed and another stopped the counter. the counter was calibrated in seconds. This method had the advantage that it was very rapid to use, but had the disadvantages that it only gave mean spreading rates and that it gave no idea of the magnitude of the errors involved in each measurement.

(d) Method 4 - Photo-transistor detection with Visicorder display

This method used the identical photo-transistor detectors to the previous method but the output from the transistors was displayed directly on a Visicorder. Although this method was slightly more time consuming and still only gave mean velocities, it did give an idea of the errors involved in each measurement since it supplied a continuous record.

In many runs, combinations of the above methods were used. For example, the photo-transistor/counter method was backed-up by stopwatch measurement or the photo-transistor/visicorder method was backed up with cinematography.

4. Automated system for measuring flame spreading rates in the standard tray

While the investigation of the effect of the experimental parameters was in progress, it was not possible to automate the system. [No system could be devised which would allow a 30 fold variation in the tray width, a 3 fold variation in the tray length and a 5 fold variation in the tray depth]. It is advantageous to have an automated system, however, not only for the aesthetic reason that it is much more pleasant for the operator to perform the tests away from the fumes and smoke of the experiment (although with particular fuels which emit toxic fumes this is a necessity) but also the technical reason that if the test room is isolated without any personnel the flame spreading results are less variable. This is because the operator causes drafts and forced convection currents with the movements of his body that are necessary to perform the experiment.

When experiments indicated a standard tray size, the system was automated so as to be operated from outside the test cell. Figure 5 shows an overall view of the apparatus. Ignition was achieved by pouring 1 cc of hexane from a container by actuating a solenoid valve. The measurements were performed as described previously using the Visicorder and the photodetectors. Extinguishment was achieved by smothering the flames by actuating a motorized box which moved to cover the burning fuel while at the same nitrogen jets purged the oxygen from the enclosed area hence "starving" the flames. The operator viewed the experiment through a window. After each run the noxious fumes were evacuated from the test cell by a remotely operated extractor fan. When the room air was freshened using air conditioners, the operator entered the test area to prepare for the next run.

C. Investigation of the Influence of Laboratory Parameters on the Rate of Flame Spread Across Liquid Fuels[8]

The prime reason for this work was to investigate the effects of laboratory parameters (such as tray width, tray length and tray depth) with the view to obtaining flame spreading data which were independent of the apparatus.

1. Qualitative observations and a physical description of the spreading flame

A great deal of insight was gained from close observation of the spreading flame.

With all fuels, the main flame was preceded by a blue flame very close to the surface of the fuel. It is considered that this precursor flame is a premixed fuel and air flame. With most fuels this precursor flame oscillated back and forward in front of the well-developed flame.

This observation is in agreement with the concept that the flash point of the fuel is important in controlling the mechanism of flame spread. Initially the temperature of the fuel is lower than its flash point, and there is insufficient fuel vapor to form a flammable mixture above the liquid surface. As the flame approaches, heat is transferred ahead of the flame front until the liquid temperature attains the flash point. At this temperature there is sufficient fuel vapor to form the lean flammable mixture and a pre-mixed flame flashes through this mixture, at a speed of the order of the laminar flame velocity, consuming the flammable mixture. At the flash temperature, the rate of vaporization is not high enough to sustain the flame and thus the premixed flame is extinguished (i.e., appears to flash back). This sequence of events is repeated, with the premixed flame flashing backward and forward, until the requisite amount of heat is transferred forward of the flame to raise the fuel temperature to the fire point. The flame is now developed at this point and the flame progresses further along the fuel surface.

When n-butanol is used as the fuel, the observations are slightly different in that the precursor flame progresses steadily over the fuel surface rather than oscillate back and forward. This observation is again in agreement with the above description since experimental measurement of the flash and fire points of n-butanol (see Section F.1) shows the two to be very close together (both 29°C, Tag Open Cup Method, A.S.T.M., 1968). There is approximately 6°C difference between the flash and fire points of the other fuels studied.

Behind the blue pre-mixed flame was a short transition region in which the flame builds up to its fully developed height. The full-developed flame itself was composed of semi-discrete flamelets which pulsate causing the flame height to fluctuate.

It is obvious from this description of the flame spreading phenomenon that it is not a completely steady process, and any method which utilizes the flame phenomenon to measure spreading rates will be susceptible to some error.

It is useful, at this point, to attempt a description of the physical processes which accompany the flame spreading phenomenon. The spread of flame across a liquid fuel surface below its flash point presents a complex problem of coupled interactions which include heat transfer processes (conductive, convective and radiative), mass transfer processes (in-draft of air, up-draft of hot combustion products) and hydro-dynamic processes (convective motion of the non-uniformly heated liquid fuel). Further, there are processes associated with the presence of the tray. The purpose of the experiments described in this section were to identify the important processes and to separate the processes involved with the tray and not intrinsically accompanying the flame spreading.

Figure 1 schematically illustrates the physical processes which can be postulated as occurring. These can be summarized as follows:

(a) Heat transfer from the flame and the pre-cursor flame to the atmosphere [(1) and (2) on Figure 1].

(b) Heat transfer from the flame to the fuel surface below the flame [(3) and (4)].

(c) Heat transfer from the flame to the fuel surface ahead of the flame [(5) and (6)].

(d) Heat transfer from the precursor to the fuel surface below the pre-cursor (7).

(e) Heat transfer from the flame to the tray edges [(8) and (9)].

(f) Heat transfer from the surface of the fuel to the bulk of the fuel (10).

(g) Heat transfer from fuel under flame to the fuel ahead of the flame [convective (11)].

(h) Heat transfer from fuel layer to the water layer and then to the tray (12).

(i) Heat transfer from fuel layer to the tray walls (13).

(j) Heat transfer from the tray rim to the bulk of the tray and then to the table top [(14) and (15)].

(k) Heat transfer from the tray to fuel layer (16).

(l) Evaporative mass transfer of fuel from the surface.

(m) Mass transfer upwards of the hot combustion products.

(n) Mass transfer of air into the flame both ahead of the spreading flame and over the tray edges.

Some of these processes are heat losses and slow down propagation; it remains to identify the important processes by means of experimentation.

2. <u>The effect of the environmental parameters (atmospheric pressure, relative humidity and air temperature) on the flame spreading velocity</u>.

Although it was difficult to test the effects of changes in atmospheric pressure and relative humidity directly, experiments

were repeated on different days and the environmental parameters were noted. Analysis of a large number of experiments from many different days showed that the atmospheric pressure and the relative humidity had no discernible effect on the flame spreading data. Furthermore, slight variations in the air temperature ($\pm$ 5°C), had negligible effect on the flame spreading velocity.

3. The constancy of the flame spreading rate along the tray length.

One of the necessary first steps in the experimental program was to determine that the flame spreading rate (V_F) was indeed constant along the length of the tray. Movie films were taken of the flame spreading along the entire length of three different trays, and plots were made of the position of the leading edge of the flame against time. (See Figure 5). In all these plots, the flame spreading rate reached a constant value after a short acceleratory period (approx. 25 cm from the ignition end).

It can be seen from Figure 6 that individual points showed a relatively large deviation from the mean line. In fact, a line joining all the points in a run with n-decane was sinusoidal in character. This gave substance to the argument that the flame spreading was not steady in nature but rather an unsteady oscillation super-imposed on an average velocity. It was felt, however, that these tests adequately justified the use of mean velocity measurements, provided, of course, the measurement region was sufficiently downstream from the ignition end not to be in the acceleratory region and also that the detection points were sufficiently far apart to minimize the errors of the oscillatory motion.

It was estimated that results with accuracy of $\pm$ 3% reflect the unsteadiness of the flame propagation.

4. The effect of different modes of ignition.

A series of experiments were performed in which the mode of ignition was varied in order to assess the effect of the ignition method on the flame spreading velocity.

In one set of runs with 4 mm depth of n-decane floated on 14.8 mm of water in a 120 x 15 x 2.5 cm aluminum tray at an initial temperature of 23°C, the width of the ignition zone and the time of ignition with the propane torch were varied in the barrier/torch ignition method (see Section B.2). Three ignition widths (2.5, 5 and 7.5 cm) and three ignition times (10,20,30 seconds) were investigated. The measured rates of flame spread agreed, within experimental limits, in all nine tests showing that the results were not sensitive by slight changes in the mode of ignition.

Comparative tests on the three different modes of ignition were run with n-decane in the 120 x 15 x 2.5 cm tray. The barrier/torch method and the hexane/spark method gave results that agreed very closely, whereas the wick ignition gave completely different data. In the wick ignition the flame did not spread immediately, but rather remained on the wick for a long period of time (about 5-10 minutes) before spreading over the liquid fuel surface at a much faster rate than given by either of the other two ignition methods.

The induction period and the faster rate of flame spread are considered to be direct consequences of the convective flows which are generated by the flame on the wick. These currents efficiently remove heat from the fuel in the vicinity of the wick. It is not until all of the fuel in the tray is heated sufficiently to permit the fuel adjacent to the wick to attain the flash temperature that flame spreading begins. Flame spreading is more rapid because of the increase in the bulk fuel temperature caused by the convection currents. Because of the variability of the initial fuel temperature, the wick ignition method was not used to obtain flame spreading data.

As was stated before (page), Burgoyne and Roberts [3-5] used wick ignition. Our work, however, casts doubt on the validity of their use of an "initial" fuel temperature.

5. The effect of fuel purity on the rate of flame spread.

The initial studies of flame spreading were conducted with kerosene in order to compare the results with Tarifa and Torralbo[1] but it was recognized that such mixed fuels come in different compositions depending on the batch and that the flame spreading data may be susceptible to scatter. Accordingly, it was decided that a mono-fuel which is a constituent of these "mixed" fuels was more amenable to accurate study. Normal decane was chosen as a suitable fuel for the majority of tests, but since this also comes in various grades it was essential to test if the flame spreading rate varied with the source or the purity of n-decane. (The high cost of ultra-pure n-decane, $160/gallon, prohibited its use in large number of runs. Also, the moderately expensive 95 mole percent n-decane, $30/gallon, necessitated the recovery, by distillation of the unconsumed fuel). Thus, the flame spreading velocities of four grades of fuel, nominally 95, 97, 99, 99.5 mole percent, and the redistilled n-decane have been measured. There was no difference in the flame spreading velocity (within experimental scatter) with any of the grades of n-decane; thus, the Humphrey 97 mole percent (the least expensive) and the redistilled n-decane were used for all tests. This result was to be expected since the main impurities of n-decane are isomers of decane with similar flammability characteristics.

Other fuels (see Table 2) were used less frequently.

6. The effect of variations in fuel temperature on the flame spreading velocity.

The main purpose of this study was to determine the accuracy with which the fuel temperature should be controlled in order to minimize the errors in the flame spreading data. The spreading velocity was investigated using a 4 mm depth of n-decane floated on 14.8 mm depth of water in the 120 x 15 x 2.5 cm aluminum tray over a temperature range of 13-30°C. As can be seen from Figure 7, the flame spreading velocity increased from 1.9 cm/sec at 13°C to 2.7 cm/sec at 30°C. The rate of increase was much less in the low temperature region than in the high temperature region. These findings indicated that a variation of ± 0.2°C at a temperature of 23°C caused a change of ± 0.7% in the flame spreading velocity and indicated that a temperature control to ± 0.1°C was adequate to minimize the errors.

7. The effects of variation of the tray dimensions on the flame spreading velocity.

The study of liquid phase flame spreading phenomena differs from similar studies of solid materials in that the fuel is fluid and thus necessitates the use of a tray to contain the fuel. The dimensions and materials of this tray may have a tremendous influence on the validity of the flame spreading results, and it is imperative that the phenomena caused by the tray and thos intrinsically connected with the physics of the process be separated.

Accordingly, from the outset a program of experiments was drawn up in which the effects of (a) the height of the tray wall and the related parameter, the height of the tray rim above the fuel surface, (b) the tray width, and (c) the tray length, on the flame spreading velocity were studied systematically. All runs were conducted at a constant liquid temperature (23.0 ± 0.1°C) and with a constant depth of fuel (4 mm) floated on a constant depth of water (14.8 mm). In most cases, the runs were duplicated both in aluminum trays and aluminum trays lined with 3 mm thick plate glass in order to change the physical properties (in particular, the thermal conductivity and the thermal diffusivity) of the wall.

(a) The height of the tray wall and its effect on the flame spreading velocity.

Three aluminum trays, all 120 cm long by 15 cm wide, but 18.8, 25.4 and 31.7 mm deep respectively, were used for this study. The fuel was dipentene.

Since the length/width ratio of the trays was comparatively large (8:1) and the flame effectively propagated through a narrow channel, it was expected that the long walls of the tray, rather than the end walls, would have the most perturbing effect on the flame spreading velocity. The experiments were conducted in different sets in order to separate the various effects of the walls and the bottom of the tray. The experiments can be divided into five groups. (Figure 8 illustrates diagrammatically the various wall configurations).

(i) The regular unlined aluminum trays (see (A), (B), (C) in Figure 8).

(ii) The aluminum trays lined along its entire long sides with 18.8 mm wide and 2.5 mm thick plate glass (see (D), (E) and (F) of Figure 8). In addition, some runs were performed with glass liners along the end walls.

(iii) The aluminum trays with 6.3 mm thick plate glass lining the bottom, both with and without glass liners along the long sides. (See (G) and (H) of Figure 8).

(iv) The 31.7 mm high aluminum tray lined along its entire long sides with 12.7 mm wide and 2.5 mm thick plate glass such that the glass obscured only the aluminum wall above the fuel surface. (See (I) of Figure 8).

(v) The 6.3 mm thick Pyrex tray. (See (J) of Figure 8).

In addition, some runs were performed similar to group (ii) above, except that the glass insulators were used only in the central 45 cm of the tray.

The results of these studies are summarized in Figure 9 as a plot of the flame spreading velocity as a function of the height of the tray rim above the fuel surface.

The flame spreading velocity in the aluminum trays fell from 4.08 cm/sec in the 13.8 mm tray to 3.4 cm/sec in the 25.4 mm and 31.7 mm trays. A similar pattern was observed in the aluminum trays lined with glass inside the long walls [4.47 cm/sec at zero pan rim height (18.8 mm tray) but 4.03 cm/sec at 5.6 and 12.9 mm pan rim height (25.4 and 31.7 mm height tray)] except that the flame spreading rate was in all cases faster in the glass lined trays than in the equivalent unlined aluminum tray.

The fall in flame spreading velocity as the free board height was increased from zero (i.e., fuel level flush with the top of the pan) to 5.6 mm and 12.9 mm was probably due to the aerodynamic consequences of the tray rim which inhibits the flow of oxygen to the fuel surface.

The overall increase in V_F, regardless of the free board height, when glass liners were inserted in the trays was undoubtedly due to the reduction in the thermal conductivity (and thermal diffusivity) of the tray wall material which reduced the heat losses from the fuel layer to the tray wall (i.e., heat transfer mode No. 13 in Figure 1 was reduced).

When the 6.3 mm thick glass bottom was used (which effectively reduces the height of the tray rim above the fuel surface by 6.3 mm and also changes the heat transfer characteristics of the tray bottom)there was no change in the spreading rate in the 31.7 mm deep tray (i.e., now equivalent to 25.4 mm deep tray). This showed that a negligible amount of heat was lost through the bottom of the tray. In the 25.4 mm deep tray the spreading rate increased from 3.4 cm/sec to 4.07 cm/sec when the glass bottom is inserted. This was equivalent to changing the free board height from 5.6 mm to zero, and again demonstrated that heat losses through the bottom of the pan were negligible.

The use of glass liners inside the end walls did not change the flame spreading velocity indicating that heat losses through the end walls were not important.

The 25.4 mm deep Pyrex tray gave very similar results to those obtained in the 25.4 mm and 31.7 mm deep aluminum trays lined with glass along their long edge. This result was to be expected and demonstrated that a glass lined aluminum tray was equivalent to an all-glass tray.

When glass was used to insulate only the central 45 cm of the tray (i.e., the distance over which V_F was measured) the flame spreading rate was 3.80 cm/sec in the 25.4 mm deep tray and 3.75 cm/sec in the 31.7 mm deep tray. These values are intermediate between those obtained with glass liners along the entire length of the tray and those without glass liners. This indicated that processes behind the leading edge of the flame were also important in determining the rate of flame propagation.

When the 12.7 mm wide glass liners were inserted along the long side of the 31.7 mm tray such that the glass obscures only the aluminum wall above the surface of the fuel (see Figure 8-I) the flame spreading velocity was reduced to 3.04 cm/sec (as opposed to 3.4 cm/sec in the 31.7 mm aluminum tray without glass liners).

This interesting experime gave a great deal of insight into the important heat transfer processes which occurred at the tray wall. The heat loss from the fuel layer to the tray wall has already been identified as an important process. The flame, however, can heat up the tray rim and this heat is dissipated throughout the pan. In the absence of glass liners, the flame heats the aluminum wall appreciably and the hot aluminum wall acts as a source of heat feed-back into the fuel layer (i.e., tends to diminish the heat loss shown as (13) in Figure 1). When glass obscures the aluminum free board, the wall is heated by the flame to a much lesser extent and the heat feed-back from the wall to the fuel is markedly diminished. This has the effect of increasing the heat loss from the fuel layer and thus diminishing the spreading velocity.

(b) The effect of tray width.

The flame spreading velocity over n-decane was measured in twelve different width aluminum trays, both with and without glass liners attached to the inside of the long wall. The results are shown in Figure 10. In all cases the tray length was constant at 120 cm and the tray height was 2.5 cm.

There are several interesting points to be made from these data. Again the flame spreading velocity was faster in aluminum trays lined with glass than it was in unlined aluminum trays. This difference persisted until the tray width reached 60 cm at which width the results with and without glass insulators were indistinguishable. These results confirmed that heat losses from the liquid fuel to the tray wall become less important as the tray width was increased, and in the limit, at 60 cm width, the heat losses can be neglected.

As can be seen from Figure 10, there was a significant change in the slope of V_F against tray width, both with and without glass liners, in the 2.5, 5, 7.5 and 10 cm wide trays. This more rapid diminution of the flame spreading velocity as the tray width was decreased below 15 cm was attributed to the viscous effects at the tray wall, which of course, gave rise to a non-uniform velocity across the fuel channel. Thus, the heat convection in the direction of propagation is altered. The appearance of the flame plume is also noticeably changed in these narrow trays from a large coherent flame in the wide trays to a series of small flamelets, which are basically independent of one another, in the 2.5 cm wide tray.

These results again cast doubt on the <u>absolute</u> validity of the work of Burgoyne and Roberts[3-5]. These pioneer workers used channels which were only 2.3, 3.3 and 6.2 cm wide. It would appear that in such narrow channels wall effects must be very important.

In the wider trays, 30 to 75 cm wide, the flame height increased markedly from approximately 60 cm in the 30 cm wide tray

to approximately 180 cm in the 60 and 75 cm tray. This increase in flame height was accompanied by an increase in radiant energy output from the flame. This radiant increase was thought to account for the more gradual increase in V_F in this width regime.

The flame spreading velocity at tray widths between 15 and 22.5 cm was of great interest. Without glass liners, the flame spreading velocity increased from 2.40 cm/sec to 2.75 cm/sec when the tray width was increased from 15 to 22.5 cm. With glass liners, however, the flame spreading velocity was constant at 2.97 $\pm$ 0.08 cm/sec in this same width regime. This 'plateau' value, which was thoroughly checked by repeated tests, was thought to correspond to a region in which V_F was not only unaffected by the viscous drag at the tray walls and the heat losses from the fuel layer to the tray walls, but also was unperturbed by radiative heat transfer from the flame. This hypothesis was to some extent corroborated by a series of experiments in which manually operated boards were used; (a) to shield the surface of the unlit fuel from the flame radiation, or (b) to extinguish the flame 5 or 25 cm and, thus, reduce the flame height and the radiative heat transfer). Although these devices did produce marked decreases in the flame spreading velocities in the wider trays (see Figure 10), a considerable number of tests showed that the techniques were difficult to use with precision. The qualitative results were, however, interesting. For example, when the 'radiation-excluding boards' were used in the 15 cm wide tray there was no change in the spreading velocity. When, however, the boards were used in the 45 cm wide tray V_F fell from 3.45 cm/sec without the 'radiation excluder' to 3.04 cm/sec with the 'radiation excluder' (i.e., the 'plateau' value which was obtained in the 15 to 22.5 cm wide trays). In the 75 cm wide tray, (which was the widest tray in which it is feasible to study the flame spreading phenomenon, because of spatial limitations of the test cell and the increased hazards of burning large areas of fuel) the flame spreading velocity was the same, within experimental error, as was measured in the 60 cm wide tray. It appears, therefore, that a second 'plateau' had been reached beyond which no further increases in the flame spreading rate were possible. The flame plume increases in height as the tray width was increased (in the 75 cm wide tray the flame plume was approximately 150-180 cm high). It was likely that when the flame reaches these heights there is no significant increase in the 'view factor' of the liquid fuel adjacent to the flame (i.e., the flame plume is effectively infinite) and thus there is little or no increase in the radiative heat transfer to the fuel. Similar results were reported by Anderson [9] for flame spread through solid fuel beds. In order to substantiate that this plateau was indeed a real phenomenon associated with flame spreading (i.e., the experiments were scaled properly) and not a consequence of the size of the test cell (the ceiling of the cell is only 180 cm (6 feet) above the fuel and may perturb the flame plume) or the

non-homologous nature of the trays (the length/width ratio of the 75 cm wide tray is only 1.625), several tests were performed in a much larger test room with a ceiling height of 900 cm (30 feet).

Tests were performed both in the 120 x 75 x 2.5 cm tray (to repeat the earlier determinations) and in a much longer tray, 300 x 75 x 2.5 cm. In the 120 x 75 x 2.5 cm tray, lined with glass, the spreading velocity was very similar in the large test facility as had been measured in the smaller test cell (3.55 cm/sec and 3.67 cm/sec respectively). The flame spreading rate was constant along the length of the tray and the flame height was similar to before at 150-240 cm (5-8 feet). In the 300 x 75 x 2.5 cm tray, however, the flame spreading rate was accelerating along the length of the tray and was faster than in the shorter tray (V_F was 4.47 cm/sec in the upstream region and rose to 6.10 cm/sec in the downstream region). Furthermore, the flame height was greater (pulsating to over 300 cm). It would appear that the second plateau in the curve of V_F against tray width (Figure 10) was a consequence of the shortness (120 cm) of the trays used and not a real phenomenon associated with flame spreading. These experiments show that V_F was sensitive to flame height and the radiative output of the flame. Unfortunately, these experiments did not indicate an upper bound to the flame spreading velocity in large pans, because of the increasing intensity of the flame radiation.

(c) The effects of variations in tray length.

The effects of variations in tray length on V_F were studied in trays 2.5 cm deep and 20 cm wide (i.e., in the width range in which the flame spreading is controlled by convective effects). Six tray lengths, 300, 240, 180, 150, 120 and 90 cm were studied. The results are shown in Figure 11 as a plot of V_F against tray length. The fuel was n-decane, the initial temperature was 23°C, and as before the trays were lined with 19 mm wide plate glass.

As can be seen from the figure, the flame spreading velocity was insensitive to further increases in tray length above 180 cm*. Below 180 cm length, the flame spreading velocity fell below the maximum value of 3.04 cm/sec to a minimum of 2.8 cm/sec in a 90 cm long tray.

These results were as expected since the length of the tray does not alter the heat loss characteristics to the walls, and the only probable effect of length is that the short trays perturb the flow characteristics of the convective motion.

---

*No effort was made to determine whether the length to width ratio was applicable to other tray widths, since it was decided to standardize on a width of 20 cm.

8. Conclusions

(a) These experiments define a tray of dimension 180 x 20 x 2.5 cm, lined inside its long wall with glass, in which flame spreading data is uneffected by the presence of the tray.

(b) Convection in the liquid phase is again identified as an important mode of heat transfer.

(c) Radiative heat transfer only begins to be important in trays which are wider than 22.5 cm.

(d) Because of the importance of convective heat transfer in the liquid phase, care must be taken in the use of wicks to ignite the sub-flash temperature fuel, because of the difficulty in assigning an initial temperature to the fuel.

(e) Care must be taken in assigning theories of flame spreading to liquid fuels below their flash point. Radiation is undoubtedly a major mode of heat trans- in the large scale problem, but convective heat transfer is the major mode of heat transfer both in smaller scale fire spreading and in the transitional period of the large scale fires. Many of the theories of flame spreading are assigned to both solid and liquid fuel, whereas it is the opinion of the authors that the relative contributions of conduction, convection and radiation vary markedly both in liquids and in solids and in 'small' and 'large' fires.

D. Investigation of the Influence of Changes in the Physical Properties of the Fuel on the Rate of Flame Spread

There are three physical properties of the fuels which were initially recognized as being of importance; the viscosity, the surface tension (and the gradient of surface tension with respect to temperature) and the flash/fire points. The depth of the fuel layer, although not strictly a physical property of the fuel, was also investigated and it is included in this section since it directly influences the form of the convection currents generated by flame spread.

Changes in other properties of the liquid fuel (density, heat capacity, thermal conductivity, coefficient of bulk expansion) have not been investigated systematically in this work.

All experiments were conducted in the standard tray (see Section B; 72" long, 8" wide and 1" deep) and using the automatic system unless otherwise noted.

1. The effect of changes in the viscosity of the fuel.

As was described in Section A, the viscosity of kerosene was altered by additions of small amounts ($\sim$ 2%) of a polyisobutylene called Vistanex MM L-140 (Enjay Chemical Co.). Although these tests were highly instructive, they were, by necessity, of a preliminary nature. (The tray was smaller than the standard size and without glass liners to insulate the walls so the results may have been perturbed by edge effects, and more importantly, the viscosity measurements were made by the less reliable falling-ball method, see Section F.2). It was considered important to check the effect of increasing viscosity with a more rigorously controlled series of tests.

Two sets of tests were performed. In the first, a 4mm deep layer of n-decane was floated on a 14.8 mm deep layer of water, and in the second, a 4mm deep layer of n-decane was used without a water layer. In both sets of runs the free board height was held constant at 6.3 mm (¼ inch) since a 1" deep tray was used with the water layer and a 0.4" deep tray was used in the series with n-decane alone. The two sets of tests were aimed at investigating the effect of a change in the lower boundary condition of the fuel from water (thermal diffusivity, 14.3×10^{-4} cm^2/sec) to aluminum (thermal diffusivity, 0.92 cm^2/sec) while keeping all other parameters constant.

The results are shown in Figures 12 and 13 as plots of flame spreading velocity (V_F) as a function of reciprocal viscosity ($1/\mu$). In both cases V_F varies between 2.90 cm/sec for pure n-decane (μ = 0.88 centipoise at 23°C) to 1.3 cm/sec for n-decane thickened to a viscosity of 20 centipoise. The results with and without a water layer show good correspondence indicating that the presence of the water substrate does not alter the flame spreading rate. Since the water and aluminum differ in thermal diffusivity by a factor in excess of 600, the logical conclusion is that heat losses through the fuel perpendicular to the surface are unimportant in a 4mm deep n-decane layer. This conclusion confirms and extends the results of a previous study in which no change in V_F was measured when a ¼ inch thick glass bottom was inserted into the tray. (See Section C.7.a.). The water layer was used initially as a way of ensuring a uniform fuel layer and also as a fuel conservation device. This series of tests has demonstrated that in n-decane layers, which are over 4mm thick, the results are independent of the lower boundary condition. This result greatly increased the applicability of these results and justified the continued use of a water substratum.

The shape of the V_F vs. $1/\mu$ curve is difficult to analyze quantitatively. (It appears to follow a V_F $(1/\mu)^{\frac{1}{4}}$ dependence over the viscosity range 1.6 centipoise to 6 centipoise). Qualitatively, however, the shape of the curves in good agreement with our preliminary studies with kerosene (see Figures 3 and 4). The curves are also in qualitative agreement with a liquid phase convection controlling mechanism of flame spread.

2. The effect of changes in the surface tension of the fuel.

The earliest and most completely formulated model [10] of flame spreading over liquid fuels was based on convective flows generated by surface tension gradients. Because of this, one of the principal objectives of the experimental program was to directly test this model by changing the surface tension (σ) and the gradient of surface tension with respect to temperature ($\partial\sigma/\partial T$) of the fuel, n-decane. After a painstaking search, a surfactant designated FC-176 by the 3M Co. was found to alter both σ and $\partial\sigma/\partial T$ of n-decane (see Section F.3 and Figure 25).

Six different experiments were performed with n-decane plus 1.5% FC-176 by volume in three fuel depth (2, 4 and 16.8 mm), both with and without a water sub-layer. In no case was the measured flame spreading velocity significantly changed by the addition of the surfactant. In two further tests, the proportion of FC-176 was increased to 5%, but again there was no measurable alteration in the flame spreading velocity.

At first sight, this seems to be contrary to the predictions of the Glassman-Sirignano surface tension induced flow model of flame spreading. However, two points remain to be investigated. Firstly, the exact nature of the effect of FC-176 on the surface tension of n-decane should be evaluated. Secondly, the smallest depth of fuel with which it is feasible to make tests is 2 mm, (below 1.5 mm depth of n-decane at 23°C, the flame will not spread), and it is considered that the consequences of surface tension gradients may be important in thinner fuel layers (< 1 mm). Time did not permit the investigation of these two effects before the expiration of the contract.

3. The influence of changes in the depth of the fuel layer.

The dependence of the flame spreading velocity on the depth of fuel is important from both a theoretical and a practical viewpoint. Experiments were conducted with n-decane at 23°C in the standard tray and a water layer was used as was necessary to maintain the free board height at 6.3 mm. Some of the tests were completed using the automatic system while others used the manual system. The results with the two methods were in excellent agreement. Figure 14 shows the results as a plot of V_F as a function of the depth of the n-decane layer. The results fall into two regimes; those below 2 mm depth where the flame did not spread and those above 2 mm depth.

(a) Experiments with fuel layers less than 2mm deep.

One and 1.5 mm depths of n-decane did not support a propagating flame although ignition of a portion of the surface could be easily achieved either by the barrier ignition method or the hexane ignition method.

Close visual observation and movie photography of the processes occurring in thin films of n-decane indicated that the absence of flame spreading was due to a break up of the film which isolated the burning portion from the main body of the fuel. This break up was observed to occur when the decane was floated on water or was in contact with the aluminum tray. The fact that the ignited section burned almost to completion (only a few cc of fuel remained) indicated that heat loss to the water sub-layer was not an important mechanism for inhibiting the flame propagation. (This was also to be expected from consideration of the thermal diffusivities of n-decane and water; 3.27×10^{-3} cm^2/sec and 1.43×10^{-3} cm/sec at $23^{\circ}C$ respectively). Furthermore, experiments showed that propagation did occur in a one mm layer of n-decane which had been thickened by additions of small percentages of Vistanex MM 4-140. This is in accord with the postulate that break-up of the fuel layer is important in stopping flame spreading since increases in viscosity of the fuel would inhibit the break up of the fuel film.

Time did not permit an exhaustive investigation of the cause of the break up of the fuel layer. There are two mechanisms which can be envisaged as causing this effect. The first, and more unlikely, is that the oscillation of the precursor flame causes flows in the fuel which break up the film. In order to test this hypothesis, flame spreading experiments were conducted over very thin films of n-butanol. It should be remembered that the combustion of n-butanol is not accompanied by an oscillatory precursor flame (see Section C.1.). Butanol sustained a propagating flame down to 0.5 mm thick layer. (This was the thinnest butanol layer that could be investigated since this is the order of magnitude of the imperfections in the trays). This is not considered definite proof that oscillation of the precursor causes the film break-up since the alcohol, butanol, differs significantly in its physical properties from the hydrocarbon, decane.

The second, and more likely, cause of the break up of the film is surface tension forces. In an analogous experiment in which a heated piece of metal was brought in close proximity to the surface of a thin film of n-decane, the film spontaneously parted beneath the heated metal. Again, no conclusive evidence has been gathered to support the hypothesis of surface tension induced film break up, but the experiment does show that the fuel layer will spontaneously break up without the oscillating forces of the precursor flame.

(b) Experiments with fuel layers greater than 2mm deep.

A 2mm depth of n-decane at 23°C does support a propagating flame, the flame spreading rate being 2.12 ± 0.1 cm/sec. As the depth of n-decane is increased the spreading rate rises steadily and tends to a maximum value of 6.5 ± 0.2 cm/sec in decane depths greater than 25mm.

In the preliminary conceptual thinking [6] the propagation velocity was related to the velocity of the fuel surface, the motion of which was induced either by surface tension of buoyancy forces. It is shown elsewhere in this report (see Section II C) that for thin films corresponding to low Reynold's number in the flowing liquid that in the case of surface tension induced flow, the surface velocity is proportional to the ratio $\sigma_x L/\mu$ where σ_x is the surface tension gradient, L is a critical dimension (in this case, the fuel thickness) and μ the viscosity of the liquid.

For large fuel depths (large Reynold's number), it would be expected that the flow becomes boundary layer in character. This boundary layer flow was indeed observed in experiments in which the 120 x 15 x 2.5 cm pyrex tray was filled with n-decane to a depth of 18.8 mm and backlighted. After the fuel was ignited and steady flame spreading had begun, surface flows were observed to extend approximately 8 cm ahead of the precursor flame.

The first point of movement (a stagnation point) appears as a leading edge for the growth of a boundary-layer type structure within the fuel (see Figure 15). For about 5cm the layer grew in what appeared to be a laminar fashion, but just beneath the leading edge of the precursor flame a circulating zone about 1cm in size developed. This "eddy" decays in depth until below the fully developed flame there was a stratified flow 0.5 cm in depth.

The surface tension induced boundary layer flow problem is more difficult to treat analytically. One can estimate, however, the trend of the surface velocity with increasing fuel depth by assuming that the critical dimension in the induced velocity expression given above can be replaced with the Blasius expression for the laminar boundary layer. This estimate indicates that the surface velocity should be independent of fuel depth for a fully developed boundary layer. A thin film calculation gives the surface velocity as a function of the fuel thickness to the first power and the data in Figure 14 show such a trend. Above 15mm deep layer the flame spreading velocity tends to an asymptote and indicates that a boundary layer flow has developed.

Other experiments, using the Hydrogen Bubble technique have been developed to investigate the flows in a quantitative manner. (See Section E).

4. Flash/Fire Point Changes - Flame spreading velocity as a function of temperature for different fuels

The majority of the tests so far described were with the hydrocarbon fuel, n-decane (kerosene, dipentene and n-butanol were used to a lesser extent), and have attempted the independent variation of one parameter at a time. Of great practical importance, however, is how the flame spreading characteristics change from one fuel to another. In the last few weeks of the contract period it was decided to measure the flame spreading velocity of a range of fuels as a function of the bulk temperature. Because of the multiplicity of changes in the physical properties in going from fuel to fuel it was considered that only the most simplistic correlations of V_F could be made in the time available. [This type of study was felt to be more fruitful than the originally projected tests of adding various percentages of a fuel with different flammability characteristics to the original fuel, n-decane].

Four hydrocarbon fuels were chosen, n-decane, $C_{10}H_{22}$; n-dodecane, $C_{12}H_{26}$; n-tetradecane, $C_{14}H_{30}$ and n-hexadecane, $C_{16}H_{34}$. These fuels were chosen partly for economic reasons (the odd number hydrocarbons $C_{11}H_{24}$, $C_{13}H_{28}$, $C_{15}H_{32}$ cost twenty times those chosen) but more importantly because they give a wide range of flash points (56°C to 146°C) and the physical properties of all fuels are very similar at their flash point (see Section F.1). To this list was added dipentene and p-cymene which differ significantly in their physical properties from the straight chain hydrocarbons.

All runs were conducted in the standard tray using 4 mm depth of fuel floated on a 14.8 mm deep water layer. The results are shown in Figure 16 as a plot of V_F versus the bulk temperature of the fuel, T_L.

The most simple minded approach of all is to assume that the physical properties of all the fuels are equal and to equate the flame spreading velocity to the amount of heat required to raise the temperature of the fuel from the initial bulk temperature to the flash point. Figure 17 illustrates a plot of V_F as a function of $(T_{FL} - T_L)$. The straight chain hydrocarbon fuels all lie on one curve within the experimental error. The results for dipentene however are significantly faster than the hydrocarbon values. This discrepancy was postulated to be due to the lower heat capacity of dipentene liquid; however, no literature value for this property could be found. The available heat capacity data for liquid fuels were surveyed and p-cymene was chosen as a suitable fuel with a relatively low heat capacity (C_p for p-cymene is approximately 0.45 cal/g deg C over the temperature range of interest, in contrast to the typical value of 0.55 cal/g deg C for straight chain hydrocarbons). The value of the flash and fire points for p-cymene were measured as 56 and 62 °C respectively (identical to the values for pure n-decane). As was

predicted, the flame spreading velocity of p-cymene (3.97 cm/sec) was significantly higher than for n-decane (2.97 cm/sec), and lay well above the correlation curve of V_F against T (see Figure 17). Qualitatively, the importance of the heat capacity of the liquid fuel was therefore demonstrated. Unfortunately, time did not permit quantitative correlations to be made, but these tests did indicate the important possibility of predicting flame spreading velocities from the physical properties of the fuel (flash point, heat capacity and density).

E. Direct Quantitative Investigation of the Flow Patterns in the Liquid Fuel During Flame Spreading

1. Preliminary Studies

There are many methods available for measuring velocities in fluids. One of the simplest methods is to disperse neutral density particles in the fluid and photographically observe the particle tracks. To use neutral density particles, however, it is necessary to intersperse the particles in the fuel by agitating the liquid. Herein lies the problem in using this method to study the flow patterns in liquid fuels during flame spreading. The density of most liquid fuels is low (0.7 to 0.8 g/cc) and the lower the density of the fluid then the more difficult it becomes to obtain particles which have a truly neutral density. The settling velocity of most particles is therefore high and it becomes necessary to agitate the fluid to suspend the particles just prior to flame spreading. This was found to be totally unsuitable since to get an accurate picture of the flow patterns due to flame spreading, the fuel must be completely quiescent.

The second method investigated was that of dye injection, where the movement of a dye stream, which is injected into the fluid, is recorded photographically. This method runs into much the same difficulty as the first method. Since the flows due to flame spreading are relatively slow it is difficult to inject the dye with a slow enough imposed velocity that it does not significantly perturb the velocities that are of interest. Dyes also diffuse very rapidly making accurate measurements at various depths in the fuel almost impossible.

Optical methods (shadowgraph, Schlieren or interferometry) were originally thought to be the most probable method of obtaining an accurate quantitative measure of the velocity (and simultaneously temperature) profiles in the liquid fuel during flame spreading. The shadowgraph method was tried first since it is the least sensitive of the three and it is the easiest to set up. It was found, however, that the width of the tray (15 cm) necessary to perform flame spreading experiments and the integrated path effect which is inherent with any optical method were incompatible and produced obliterated images. Thus, although the gross flow characteristics could be observed (these were described briefly in Section D.3, see Figure 15), it was impossible to discern the fine structure of the convective motions or to make quantitative measurements.

At this point in the preliminary studies, all the classical methods of measuring velocities in liquids had been investigated and all had been found inappropriate to even semi-quantitative studies of flame induced convection currents. Our attention was then drawn* to another method, the hydrogen-bubble technique, which had been used with some success in water tunnel flow studies. Preliminary experimentation demonstrated that this method, although only previously used for flows as slow as 16 cm/sec, held promise of being adaptable to the purpose of studying flame spreading (velocities of the order of 1 cm/sec).

2. The hydrogen-bubble technique

The principle of this method is to apply an electrical potential across an electrolytic liquid such that the liquid is electrolyzed and gas bubbles are generated at the electrodes. If one of the electrodes takes the shape of a very fine wire which extends vertically from the bottom of the liquid to the top, the bubbles which are generated are very small and they follow the flow lines in the fluid. Moreover, if the electrical potential is pulsed, the bubbles form discrete rows and velocities can easily be obtained from the spacing of the rows.

This method has previously been used with water as the electrolytic fluid and thus hydrogen bubbles are generated at the cathode and oxygen bubbles at the anode. Since two hydrogen are produced for every one oxygen, the cathode is always used as the test electrode and, hence, the name, "Hydrogen-Bubble Technique".

As was mentioned earlier, this method had previously been used to study flow patterns over airfoils in the velocity regime about 60 cm/sec (2 ft/sec). The technique had also been extended to higher velocities (700 cm/sec) and lower velocities (16 cm/sec). This application required the method to work in the 0-2 cm/sec velocity range. There were two questions to be answered to prove the usefulness of the method.

(i) Does the hydrogen-bubble technique work in the 0-2 cm/sec velocity range?

(ii) Can a liquid be found which will propagate a flame (i.e., a fuel below its flash point) and also electrolyse?

The first question was answered by a series of experiments in water. The mechanism of flame spreading has been related to surface tension gradients in the liquid fuel.[10] It has long been known, however, that when a drop of detergent is added to water the surface tension is altered locally and flows are induced. (These induced flows can easily be demonstrated by adding talcum powder to the water surface). Thus, assuming the surface tension induced flow model of

---

*We thank D. R. Hardesty for this suggestion and Professor G. E. Mattingly for many discussions which were helpful in setting up the experimental arrangement.

flame spreading to be correct, the effect of the flame may be "simulated" by addition of a drop of detergent to water.

The water was contained in a Pyrex tray (120 cm long by 15 cm wide by 2.5 cm deep). A 0.0004" diameter platinum - 13% rhodium wire was supported vertically in the water with a bracket, and served as the cathode. A copper plate was used for the anode and these were connected by a pulse-generator. (A schematic of the apparatus is given in Figure 18, and a photograph of a general view of the equipment is shown in Figure 19). When a drop of detergent was added to the water at one end of the Pyrex tray, flow patterns were established and these set up bubble patterns which could be photographed. Figure 20 shows a representative experiment, in which the drop of detergent was added to the water at the left hand side. Notice the left to right flow near the water surface and the return flow deeper in the liquid.

Many experiments of this type showed the applicability of the hydrogen bubble technique to flame spreading studies. Further preliminary studies were carried out using an infrared lamp as a source of heat to simulate the flame and similar flow patterns were obtained.

Although quantitative analysis of these preliminary runs was not made, qualitatively the velocity profiles are in good agreement with the Glassman-Sirignano surface tension induced flow model (see Section II C, Figure 1).

The research for an electrolytic fuel was more involved. The most likely fuels to electrolyse were the alcohols and the carboxylic acids. Butanol and butyric acid were tried, but neither would electrolyse at the potentials available. After considerable testing a solution of dilute hydrochloric acid in butanol was found to both burn and electrolyse. The combustion characteristics of this mixed fuel were similar to pure butanol. Preliminary flame spreading experiments with hydrochloric acid/butanol mixture indicated it was feasible to study the sub-surface flow patterns in the presence of a spreading flame.

The hydrogen-bubble technique has the advantage over other methods in that specific locations in the fuel can be studied because the flow of bubbles is essentially confined to one plane parallel to the side of the fuel container. Thus, there is no integrated path effect which is inherent in optical methods.

The feasibility of the method having been proved, it remained to develop and refine method to obtain quantitative results. The technique has been dogged with problems, but all have been of a technologic nature and have been overcome. For example, in order to have hydrogen bubbles with a low rising velocity, the bubbles must be very small necessitating the use of very thin cathode wires (ca 0.0004" diameter). This cathode wire is very fragile and prone to breaking. However, after modifying the cathode bracket holder

three times this problem was eliminated. After three months of trouble-shooting the technique was refined to such an extent where quantitative measurements were available via movie photography. The first results were obtained almost at the end of the contract period and at the time of writing quantitative results were not available. However, a movie film analyser has been borrowed which permits a frame-by-frame analysis to be punched out on I.B.M. cards and a computer program has been written and the data should be forthcoming in the near future. Figure 21 shows a representative bubble profile frame from the movie film.

F. Measurement of the Physical Properties of the Fuels

Although the physical properties of straight chain hydrocarbon fuels are well documented[11] [12], it was considered highly desirable to have the capability of measuring the physical properties for two reasons; firstly, some of the fuels which have been investigated, e.g., dipentene, are more exotic and the documentation of their properties is far from complete. Secondly, and more importantly, it was intended to add thickening agents and surface tension agents to the fuels and it was important to measure the properties of these fuels with additives.

The vast majority of the flame spreading tests were with n-decane hence the physical property measurements have centered on those of n-decane and n-decane with additives. The properties of other fuels were measured in a non-systematic manner.

1. Flash and Fire Points

There are two different procedures for measuring flash points; the closed cup method in which the liquid fuel is totally enclosed with a known amount of air and the open-cup flash point in which there is a free surface of fuel in contact with the atmosphere. The open cup flash point which is higher than the closed cup flash point by about 10°C, was chosen as more applicable to the flame spreading experiments.

Two flash testers have been used, the first, the TAG Open Flash Point Tester (Fisher Scientific Co.) which is designated for use with fuels whose flash point is below 79°C and, the second, the CLEVELAND open cup, ("Precision", Scientific Glass Apparatus Co.) which is designated for use with fuels whose flash point is above 79°C. Both of these instruments have A.S.T.M. designations[13] [14]. The fire point can also be measured using these instruments, but it is less well defined and is more difficult to reproduce from laboratory to laboratory.

The procedures for measuring flash and fire points followed the appropriate A.S.T.M. designation exactly, a preliminary run being used to determine the correct flash tester. The tag tester was calibrated using p-xylene and found to have a correction factor of + 1°C.

The flash point of n-decane was measured to be 56°C with a reproducibility of less than 1°C (well within the A.S.T.M. designation). No literature value of the open cup flash point for n-decane could be found in the literature although the closed cup flash point was listed as 115°F or 46°C[15]. The fire point of pure n-decane was measured as 62°C.

Decane thickened with Vistanex MM L-140 to a viscosity of 60 centipoise (approx. 2% addition of thickener) had identical flash and fire points to pure decane with a reproducibility again of less than 1°C.

Addition of 1.5% of the surfactant FC-176 did not alter the flash or fire points, but the reproducibility was somewhat worse at 3°C.

The values of the flash and fire points of the other fuels are given in Table 3.

2. Viscosity Measurements

There are a number of different methods available for measuring the absolute viscosity (μ) and the dynamic viscosity (η). The measurement of viscosity is governed by an A.S.T.M. designation (Number D445).

In the preliminary experiments (see Section A) a Falling Ball Viscosimeter was used. This instrument was found not to have the required degree of accuracy (readings are high in the low viscosity region and low in the high viscosity region) and the use of this instrument was discontinued.

Accurate viscosity measurements were made with A.S.T.M. approved and calibrated UBBELOHDE VISCOSIMETER TUBES (Scientific Glass Apparatus Co., Catalog Number V-7050). This method was chosen because of the ease of operation in a constant-temperature water bath thus permitting the measurement of viscosity over a range of temperature.

The viscosity data for pure n-decane (research grade) and for thickened n-decane (2% Vistanex MM L-140 added) are shown in Figure 22. The results for pure n-decane are in good agreement with the literature values.

The addition of the surface tension agent FC-176 in 1.5% proportions did not alter the viscosity of n-decane.

3. Surface Tension Measurements

Surface tension measurements were made using a CAPILLARY RISE INSTRUMENT (Fisher Scientific Co.; Catalog Number 14-817). All capillaries were rigorously cleaned in chromic acid and were calibrated using liquids of known surface tension (acetone, hexane, methanol and carbon tetrachloride).

Table 3

Measured Values of the Open Cup Flash and Fire Points of Selected Fuels

Fuel	Flash Point* (°C)	Fire Point (°C)
n-Nonane	44	44
n-Decane	56	62
n-Dodecane	86-88**	95
n-Tetradecane	116	124
n-Hexadecane	146**	152
Dipentene	56	62
p-Cymene	56	62
Butanol	29	29

* All values are the mean of at least three determinations.

** The values of the flash point of these fuels was somewhat variable and in some cases the flash point co-incided with the quoted value of the fire point.

The surface tension of pure n-decane (viscosity 0.92 centipoise at 20°C) and thickened n-decane (2% addition of Vistanex MM L-140, viscosity 64.8 centipose at 20°C) were measured at 20, 30, 40 and 50°C. The data (each point represents the mean of at least three trials) are shown in Figure 23. These results confirm that additions of Vistanex does not alter either the absolute value of the surface tension or the gradient of surface tension with respect to temperature.

One of the most important aspects of the surface tension measurements was the search for a compound which alters the surface tension (σ) and hopefully the gradient $d\sigma/dT$ of the fuels and in particular n-decane. This is a difficult proposition since the surface tension of pure hydrocarbons is already low and it is difficult to find a surface agent which will reduce σ further. Twelve chemicals (AROMOX C/12-50%, AROMOX DMC-40%, AROMOX DMHT-40%, AROMOX 18/12-50%, ETHOMEEN C/12, ETHOMEEN T/12, ETHOMEEN 18/12, ARQUAD ZC-75, ARQUAD ZHT-75, ARQUAD ZS-75, KESSCO ISOPROPYLMYRISTRATE & KESSCO ISOPROPYLPALMITATE) were supplied by the Armour Industrial Chemical Co. for preliminary trials. Addition of these compounds in 1% proportions had no measurable influence on the surface tension of n-decane.

In the continuing search the FLUORAD brand of compounds (manufactured by the 3M Company) was brought to our attention. These are fluorochemical surfactants and the specification made them appear to be ideally suited to our purpose. The compound designated FC-176 was chosen because of its stated solubility in the hydrocarbon, heptane.

Addition of about 1.3% of FC-176 reduced the surface tension of n-decane from 24 dynes/cm to 19 dynes/cm at a temperature of 20°C. Moreover, FC-176 altered the $d\sigma/dT$ of n-decane from 0.09 dynes/cm °C to approximately 0 dynes/cm°C. These results are shown in Figure 24.

FC-176 did not alter the viscosity of n-decane.

The exact nature of the effect of FC-176 on the surface tension is not clear at the moment and more work is necessary. Two experimental points were disturbing. Firstly, it was very difficult to obtain reproducible surface tension data with a solution of FC-176 in decane. (This difficulty is reflected in the experimental error bars in Figure 24). Secondly, after the capillaries had been in contact with solutions of FC-176 it was not possible to reproduce the value of 24 dynes/cm for pure n-decane even after the most rigorous cleaning procedure (hot potassium hydroxide solution followed by chromic acid). It appeared that F-176 left a film inside the capillary which was impossible to remove. This raises the interesting question - does FC-176 dissolve in n-decane, or does it form a microscopic surface layer? This question, as yet unresolved, has important consequences in the flame spreading experiments with decane and FC-176.

4. Vapor Pressure Measurements

The static isoteniscope method of the Smith and Menzies type[16] was selected to measure the vapor pressure of the fuels, in particular the pure n-decane and the thickened n-decane.

The data for n-decane and n-decane with various amounts of added Vistanex MM L-140 are shown in Figure 25. The data scatter amounts to about ± 10% which is much larger than desirable. Part of this may be due to the difficulty in removing dissolved air from the decane sample especially when it is thickened with Vistanex. However, this data indicates that the vapor pressure of thickened decane does not differ from that of pure n-decane in a consistent manner. This is in agreement with the flash point measurements, since if there were any significant change in the vapor pressure on adding Vistanex this would manifest itself in a change in the flash point.

5. Density Measurements

For completeness the densities of pure n-decane and thickened n-decane were measured using pyknometers (Scientific Glass Apparatus Co.; Catalog Number JB-2530/10). The density of n-decane was measured as 0.7278 g/cc at 25°C (in good agreement with the literature value of 0.7300 at 20°C) whereas the density of n-decane thickened with 2% addition of Vistanex was measured at 0.7699 g/cc at 25°C (i.e., a 0.4% increase).

References

1. Tarifa, C. S. and Torralbo. A. M., "Flame Propagation Along the Interface Betwe n a Gas and a Reacting Medium", Eleventh Symposium (International) on Combustion, Combustion Institute, 533 (1967).

2. Roberts, A. F., Spread of Flame on a Liquid Surface", Ph.D. Thesis, Imperial College, London, 1959.

3. Burgoyne, J. H., Roberts, A. F. and Quinton, P. G., "The Spread of Flame Across a Liquid Surface I. The Induction Period", Proc. Roy. Soc. A308, 39 (1968).

4. Burgoyne, J. H. and Roberts, A. F., "The Spread of Flame Across a Liquid Surface II. Steady-State Conditions", Proc. Roy. Soc. A308, 55 (1968).

5. Burgoyne, J. H. and Roberts, A. F., "The Spread of Flame Across a Liquid Surface III. A Theoretical Model", Proc. Roy. Soc. A308, 69 (1968).

6. Glassman, I. and Hansel, J. G., "Some Thoughts and Experiments on Liquid Fuel Fire Spreading, Steady Burning and Ignitability in Quiescent Atmospheres", Fire Research Abstracts and Reviews, 10, 217 (1968).

7. Glassman, I., Hansel, J. G., and Eklund, T., "Hydrodynamic Effects in the Flame Spreading, Ignitability and Steady Burning of Liquid Fuels", Combustion and Flame, 13, 99 (1969).

8. MacKinven, R., Glassman, I. and Hansel, J. G., "Influence of Laboratory Parameters on Flame Spread Across Liquid Fuels", Combustion Science and Technology, 1, 293 (1970).

9. Anderson, H. E., "Fire Spread and Flame Shape", Fire Technology 4, 51 (1966).

10. Sirignano, W. A. and Glassman, I., "Flame Spreading Above Liquid Fuels: Surface-Tension-Driven Flows", Combustion Science and Technology 1, 307 (1970).

11. National Bureau of Standards Circular C461, "Selected Values of Properties of Hydrocarbons", U.S. Department of Commerce, Washington, D. C. (1947).

12. American Petroleum Institute, "Technical Data Book - Petroleum Refining", New York, New York (1966).

13. A.S.T.M. Standards, Designation D1310-67, "Standard Method of Test for Flash Point of Volatile Flammable Materials by Tag Open-Cup Apparatus", American Society for Testing and Materials, Philadelphia, Pa., 17, 484 (1968).

14. A.S.T.M. Standards, Designation D92-66, "Standard Method of Test for Flash and Fire Points by Cleveland Open Cup", American Society for Testing and Materials, Philadelphia, Pa., 17, 31 (1968).

15. "Handbook of Laboratory Safety", Ed. N. V. Steere, Chemical Rubber Co., Cleveland, Ohio (1967).

16. Glasstone, S., "Textbook of Physical Chemistry, van Nostrand Co., New York, N. Y. (1946).

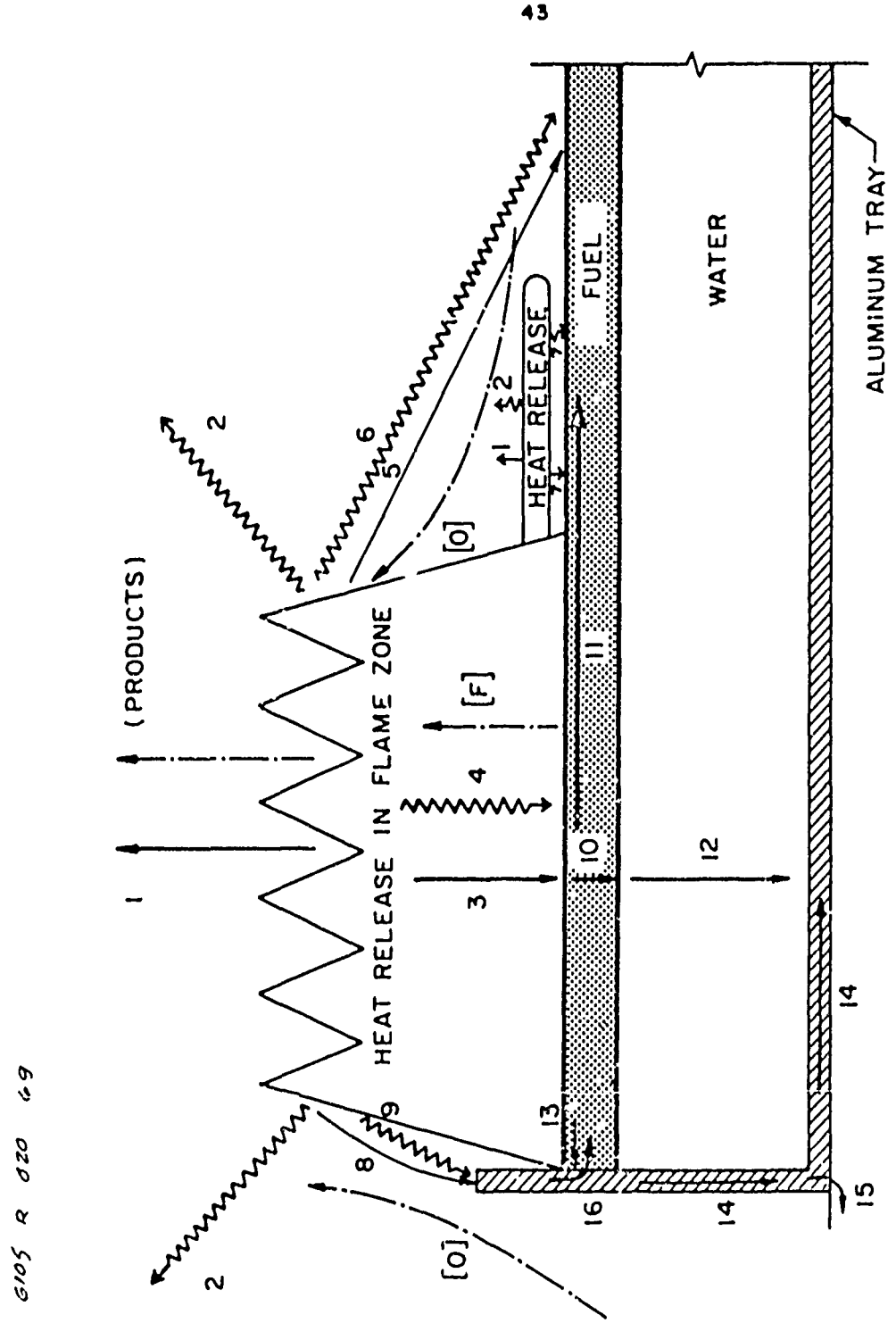

SCHEMATIC REPRESENTATION OF THE PHYSICAL PROCESSES ACCOMPANYING THE FLAME SPREADING PHENOMENON

FIGURE 1

6105 R 020 69

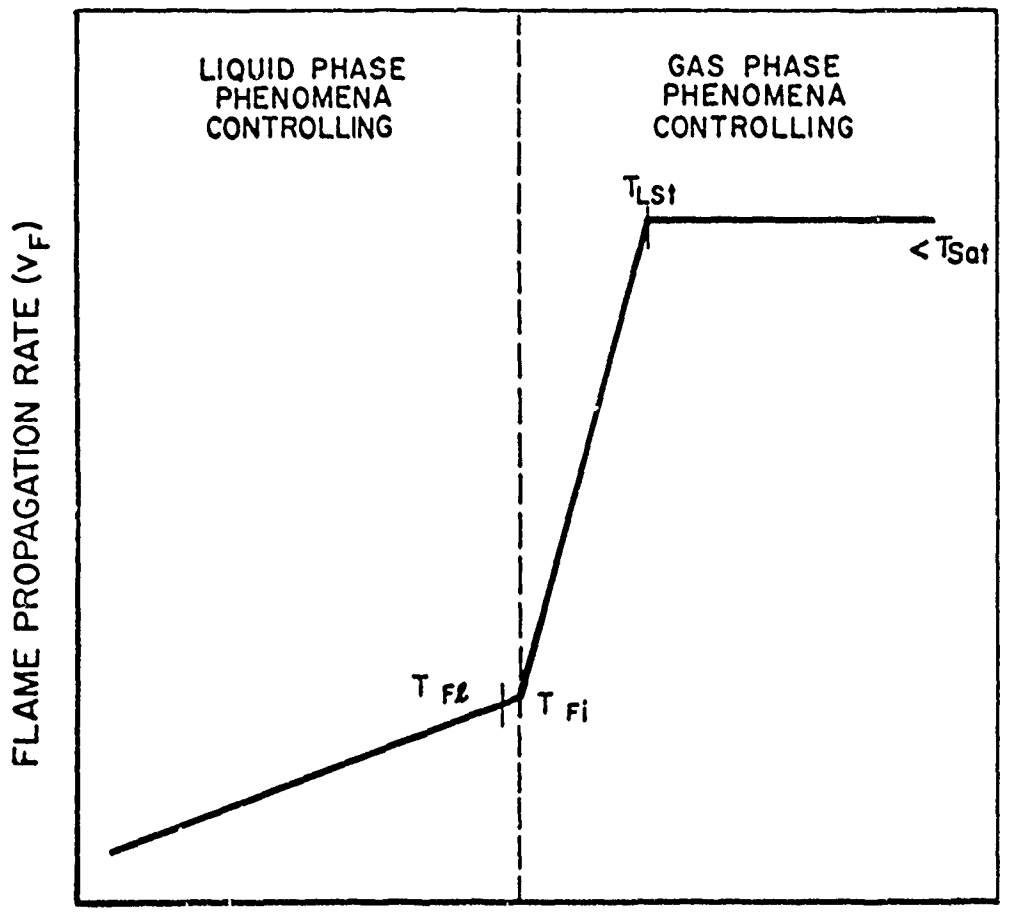

6105 R 001-68

SCHEMATIC OF THE FLAME SPREADING RATE AS A FUNCTION OF THE BULK TEMPERATURE OF THE FUEL

(T_{Fl} is the flash point, T_{Fi} is the fire point, T_{LSt} is the temperature of the fuel which creates a stoichiometric mixture somewhere above the surface).

FIGURE 2

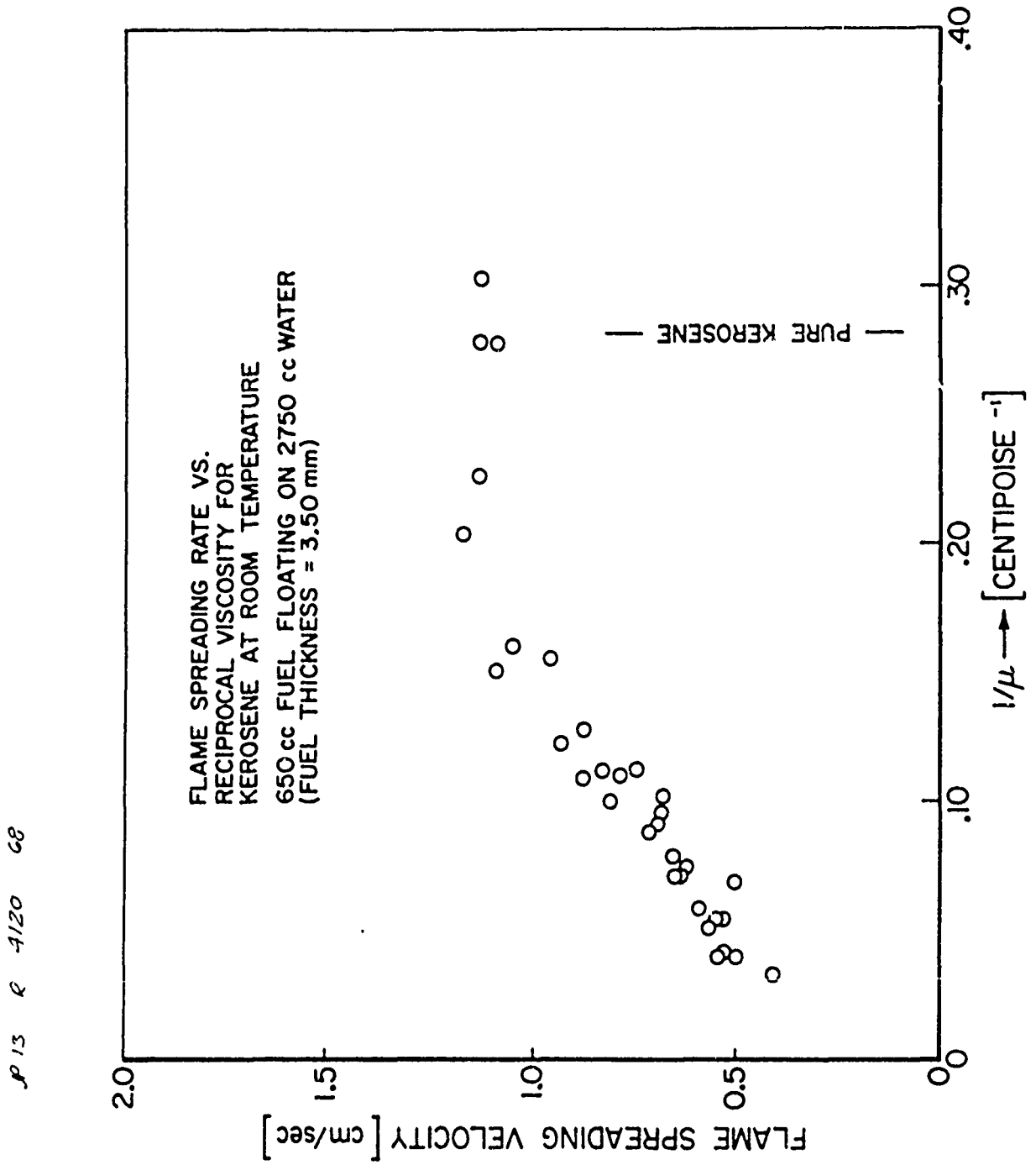
FLAME SPREADING RATE VS.
RECIPROCAL VISCOSITY FOR
KEROSENE AT ROOM TEMPERATURE
650 cc FUEL FLOATING ON 2750 cc WATER
(FUEL THICKNESS = 3.50 mm)
PURE KEROSENE
FLAME SPREADING VELOCITY [cm/sec]
2.0
1.5
1.0
0.5
0.0
.10
.20
.30
.40
1/μ → [CENTIPOISE -1]

FIGURE 3

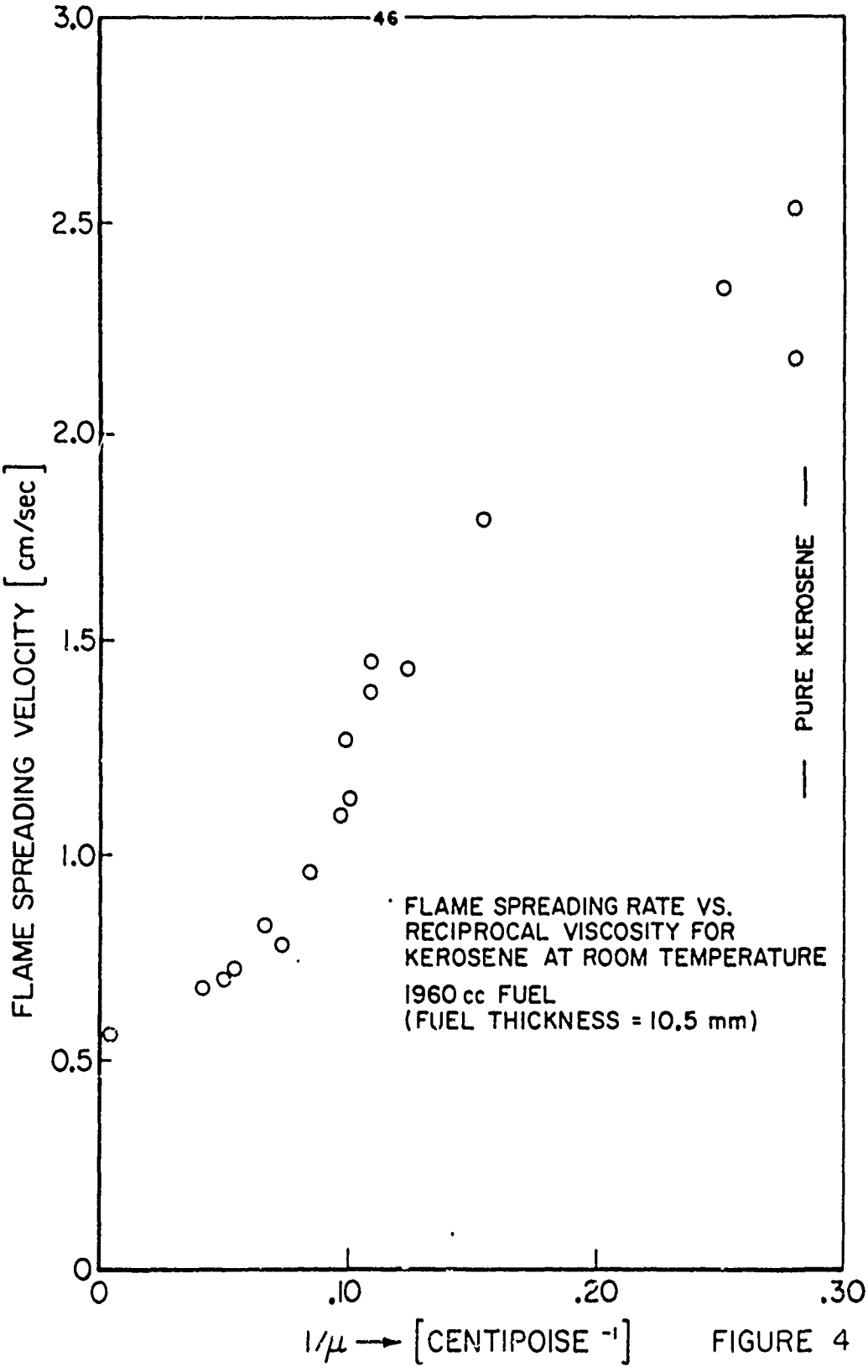
3.0
2.5
2.0
1.5
1.0
0.5
0
0
.10
.20
.30
FLAME SPREADING VELOCITY [cm/sec]
1/μ → [CENTIPOISE⁻¹]
— PURE KEROSENE —
FLAME SPREADING RATE VS.
RECIPROCAL VISCOSITY FOR
KEROSENE AT ROOM TEMPERATURE
1960 cc FUEL
(FUEL THICKNESS = 10.5 mm)

FIGURE 4

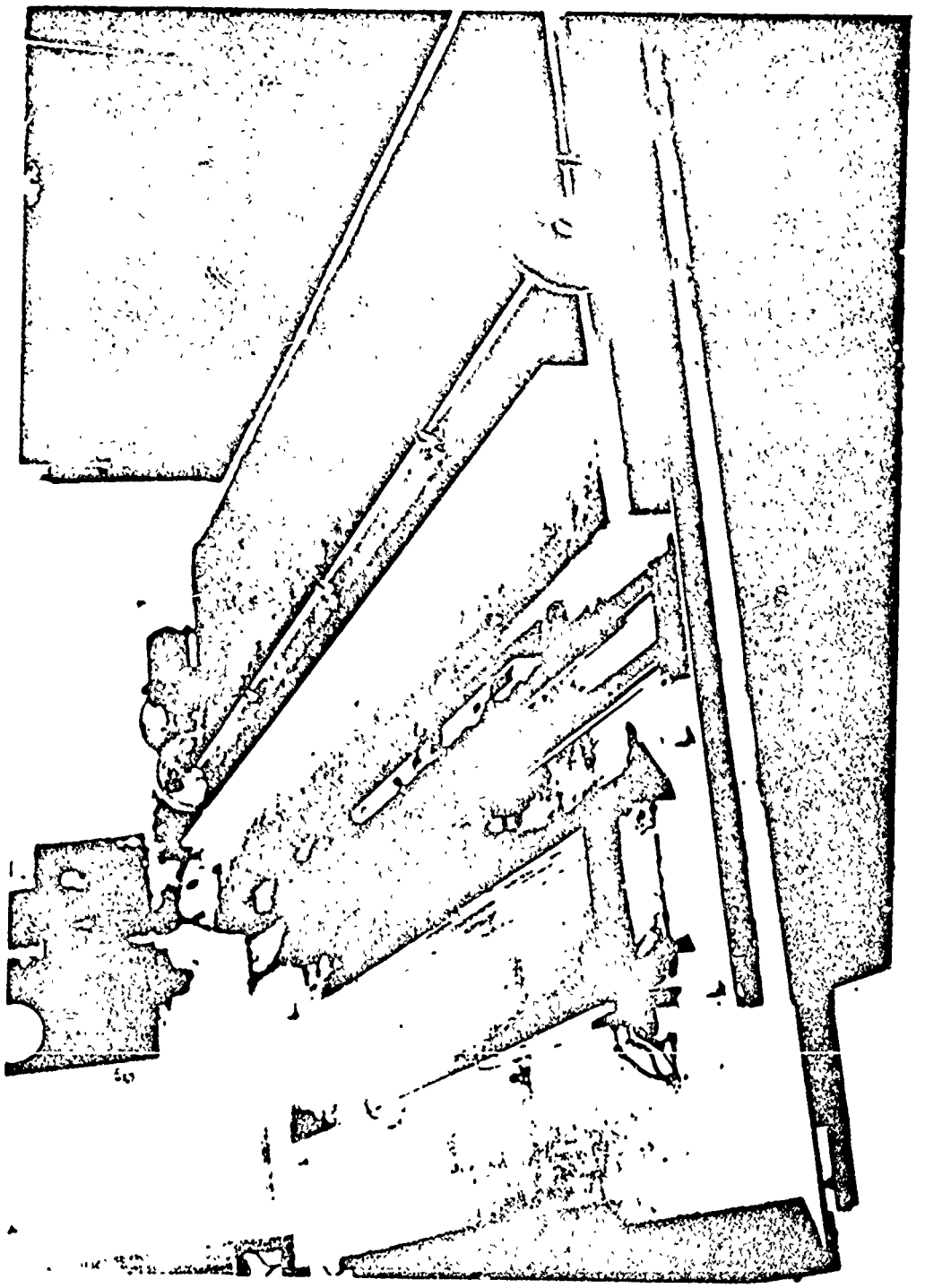

FLAME SPREADING APPARATUS

FIGURE 5

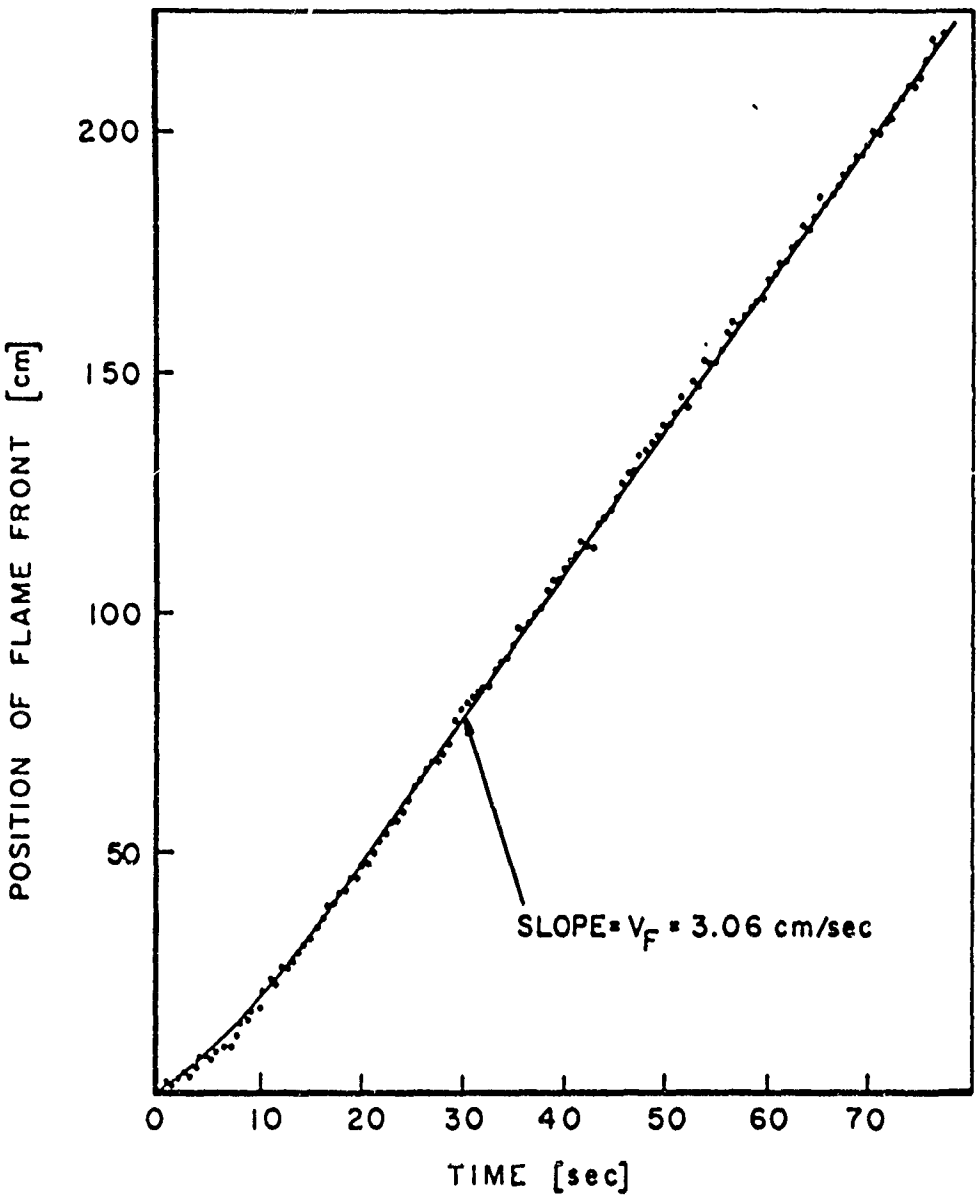

THE POSITION OF THE LEADING EDGE OF THE FLAME AS A FUNCTION OF TIME.

(Conditions: 4 mm depth of n-decane floated on 14.8 mm of water in the 240 x 19.5 x 2.5 cm tray lined with glass inside the long walls; initial temperature of fuel = 23.0 ± 0.1°C).

FIGURE 6

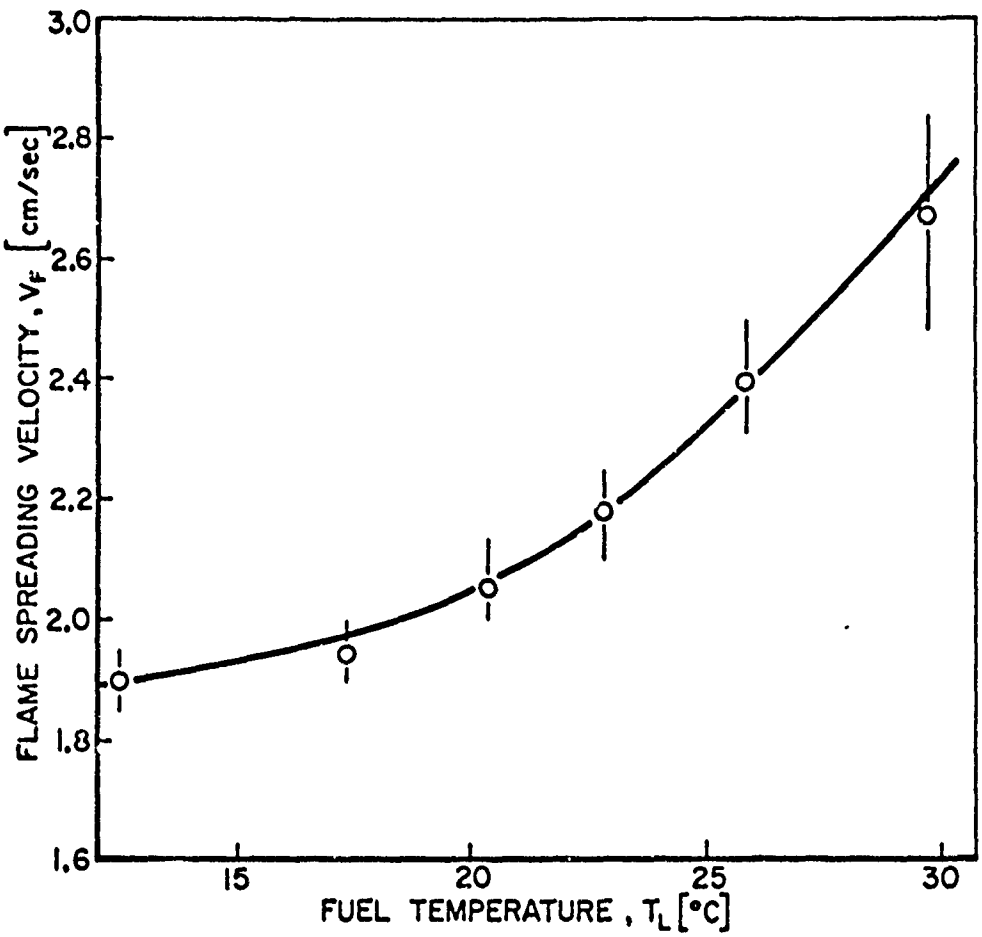

FLAME SPREADING VELOCITY OF n-DECANE AS A FUNCTION OF THE FUEL TEMPERATURE

(Conditions: 4 mm depth of n-decane floated on 14.8 mm depth of water in the 120 x 15 x 2.5 cm aluminum tray).

6105 K 023 69

FIGURE 7

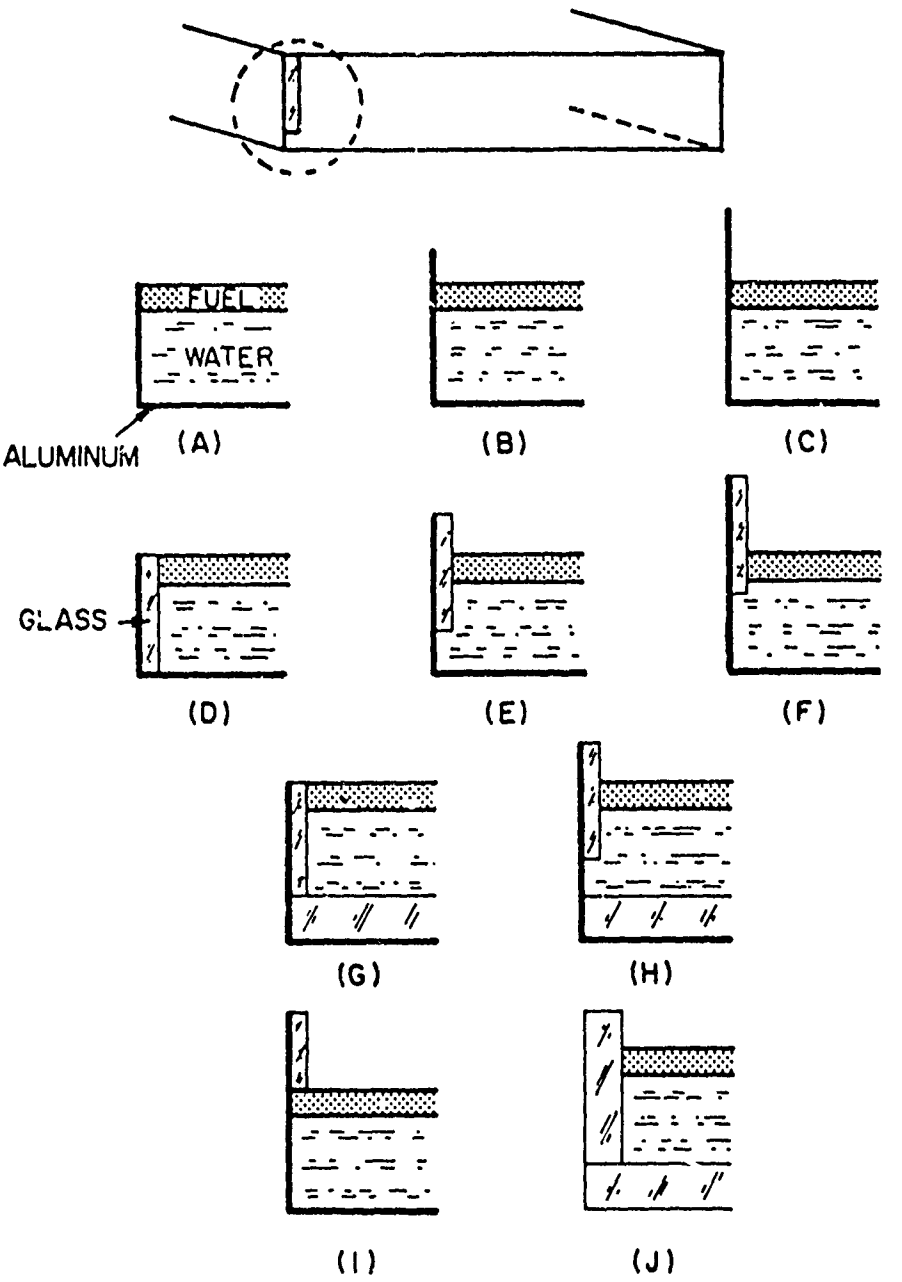

ILLUSTRATION OF THE POSITIONING OF THE GLASS INSULATORS USED TO LINE THE SIDES AND THE BOTTOM OF THE ALUMINUM TRAYS

FIGURE 8

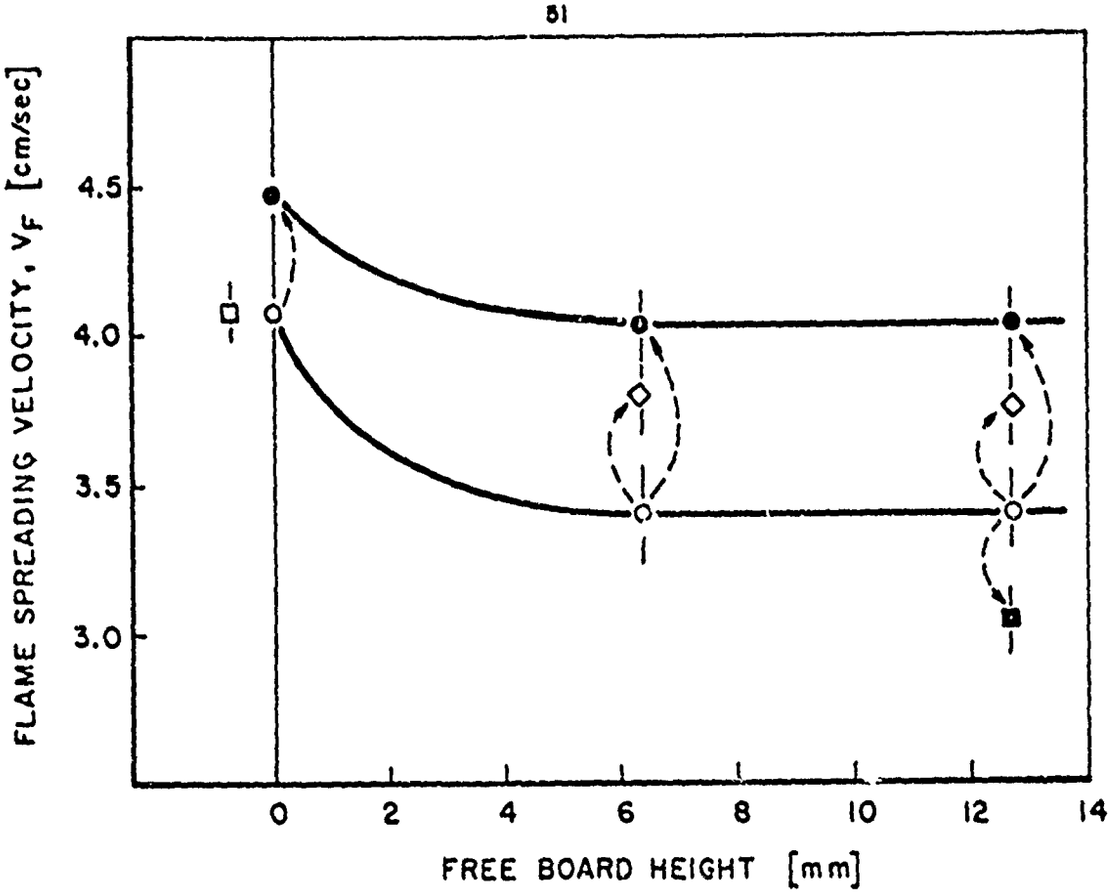

FLAME SPREADING VELOCITY OF DIPENTENE AS A FUNCTION OF THE HEIGHT OF THE TRAY RIM ABOVE THE LIQUID LEVEL (THE FREE BOARD HEIGHT).

[Conditions: 4 mm depth of dipentene floated on 14.8mm of water in trays 120 cm long by 15 cm wide; ○ aluminum tray, ● aluminum tray lined with 19 mm wide plate-glass inside the entire long wall, ◇ aluminum tray lined with 19 mm wide plate-glass inside the central 45 cm of the length, ◧ aluminum tray lined with 13 mm wide plate-glass inside the entire length such that the glass obscures the aluminum only, □ pyrex tray with 6.3 mm free board height].

6105 2 025 69

FIGURE 9

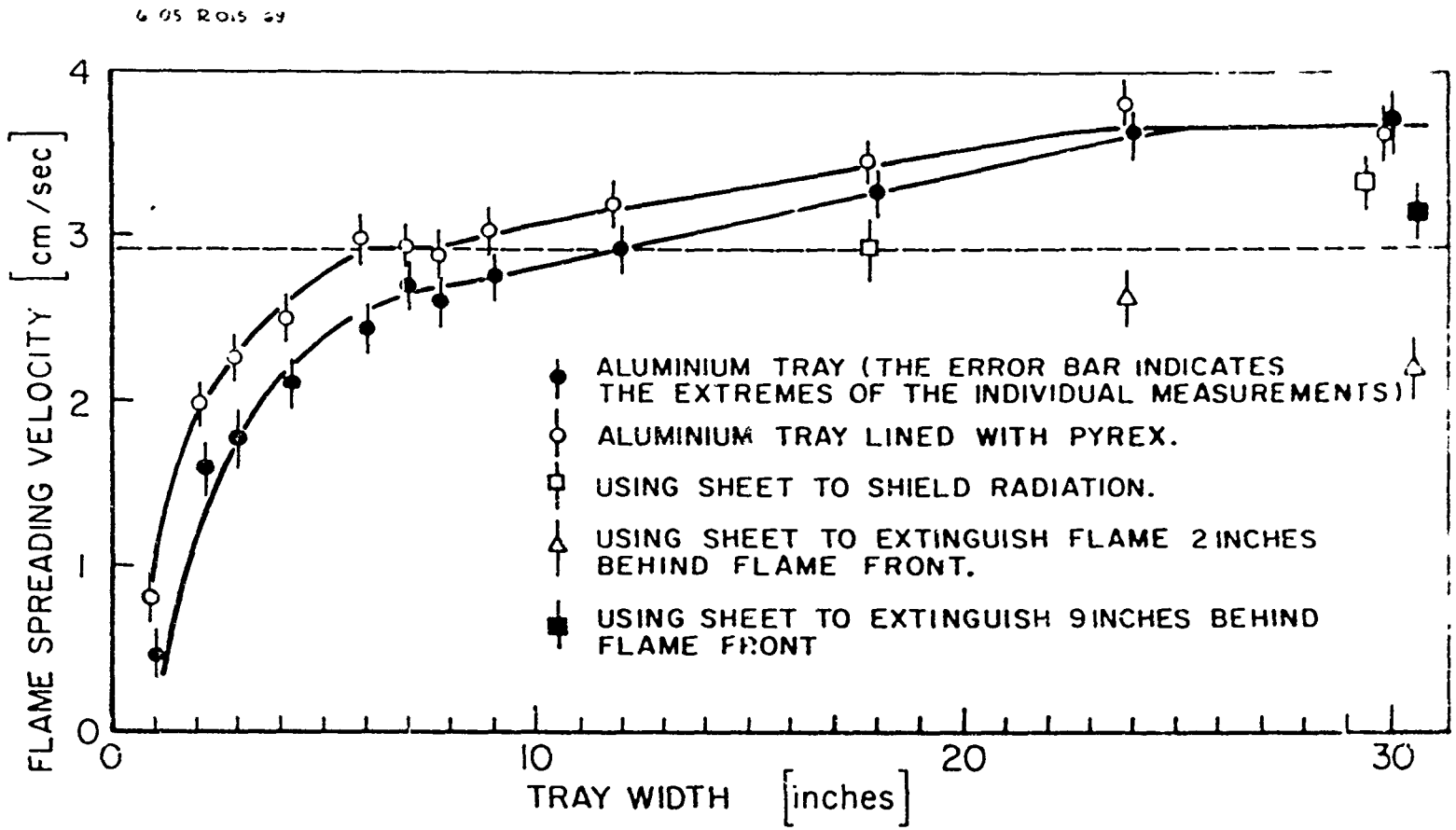

FIGURE 10

FLAME SPREADING VELOCITY OF n-DECANE AS A FUNCTION OF TRAY WIDTH. (FUEL DEPTH 4mm; WATER DEPTH 14.8mm; LIQUID TEMPERATURE 23.0 ± 0.2° C).

6105 R 027 69

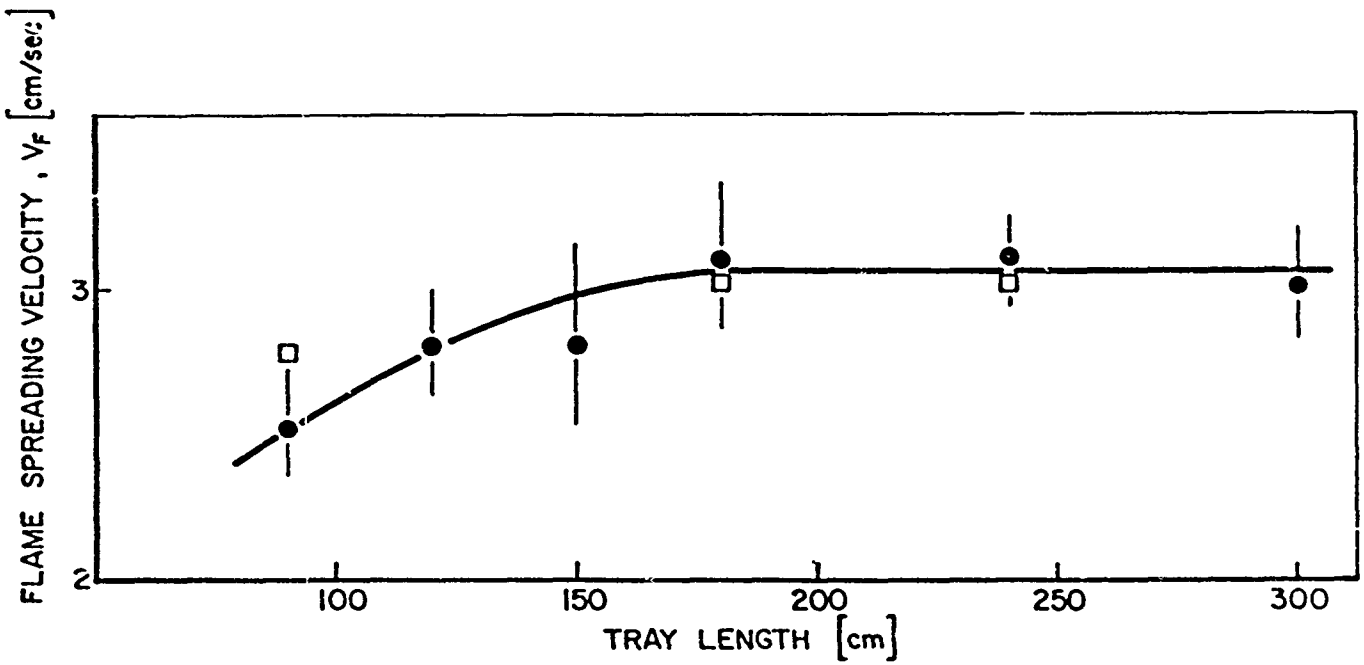

FLAME SPREADING VELOCITY OF n-DECANE AS A FUNCTION OF TRAY LENGTH

(Conditions: 4 mm depth of n-decane floated on 14.8 mm depth of water in trays 19.5 cm wide by 2.5 cm deep lined with glass inside the long wall; initial temperature of fuel = 23.0 ± 0.1°C. □ indicates cinematographic runs).

FIGURE 11

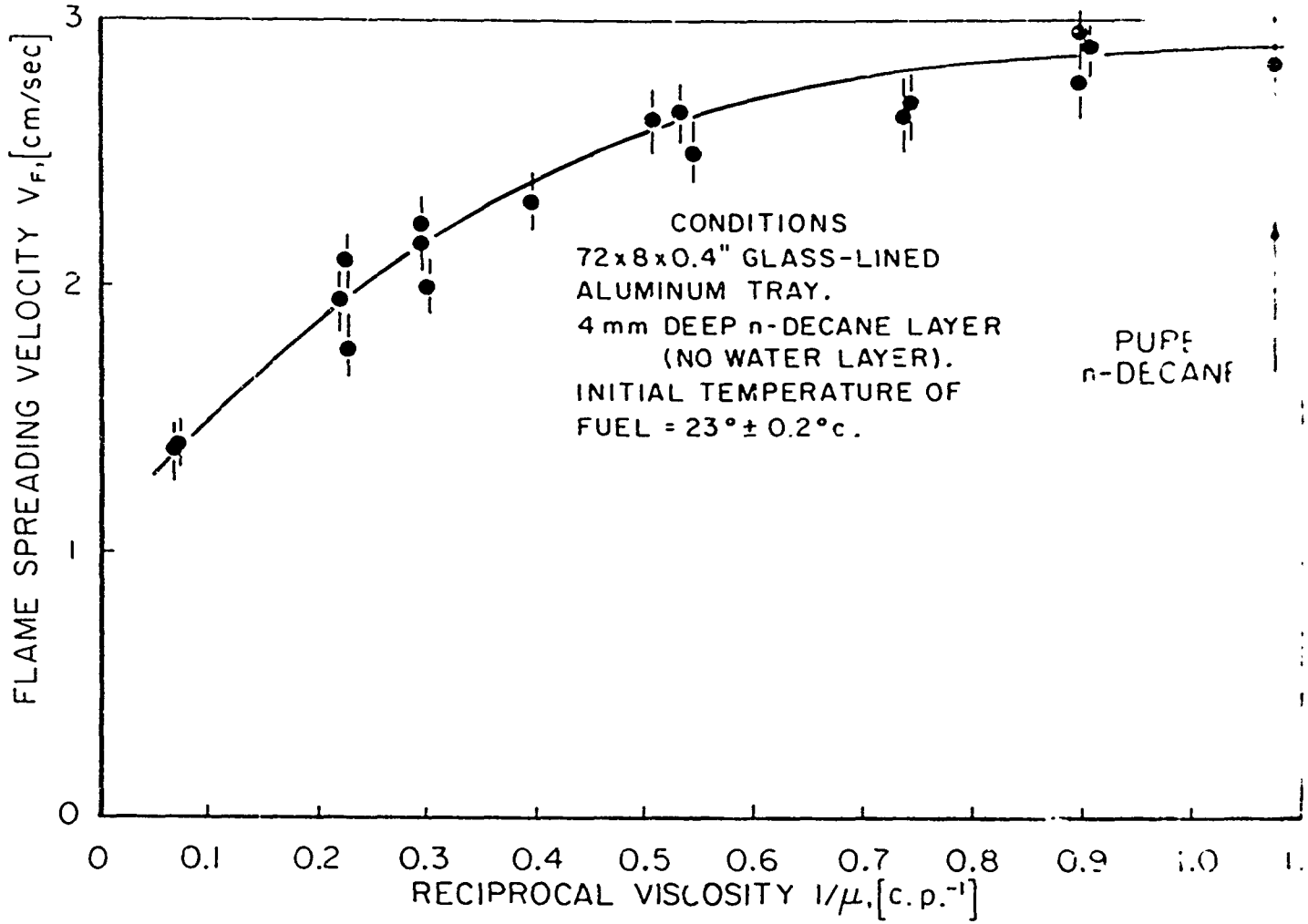

FIGURE 12

FLAME SPREADING VELOCITY OF n-DECANE AS A FUNCTION OF THE RECIPROCAL VISCOSITY

G105 R 037 70

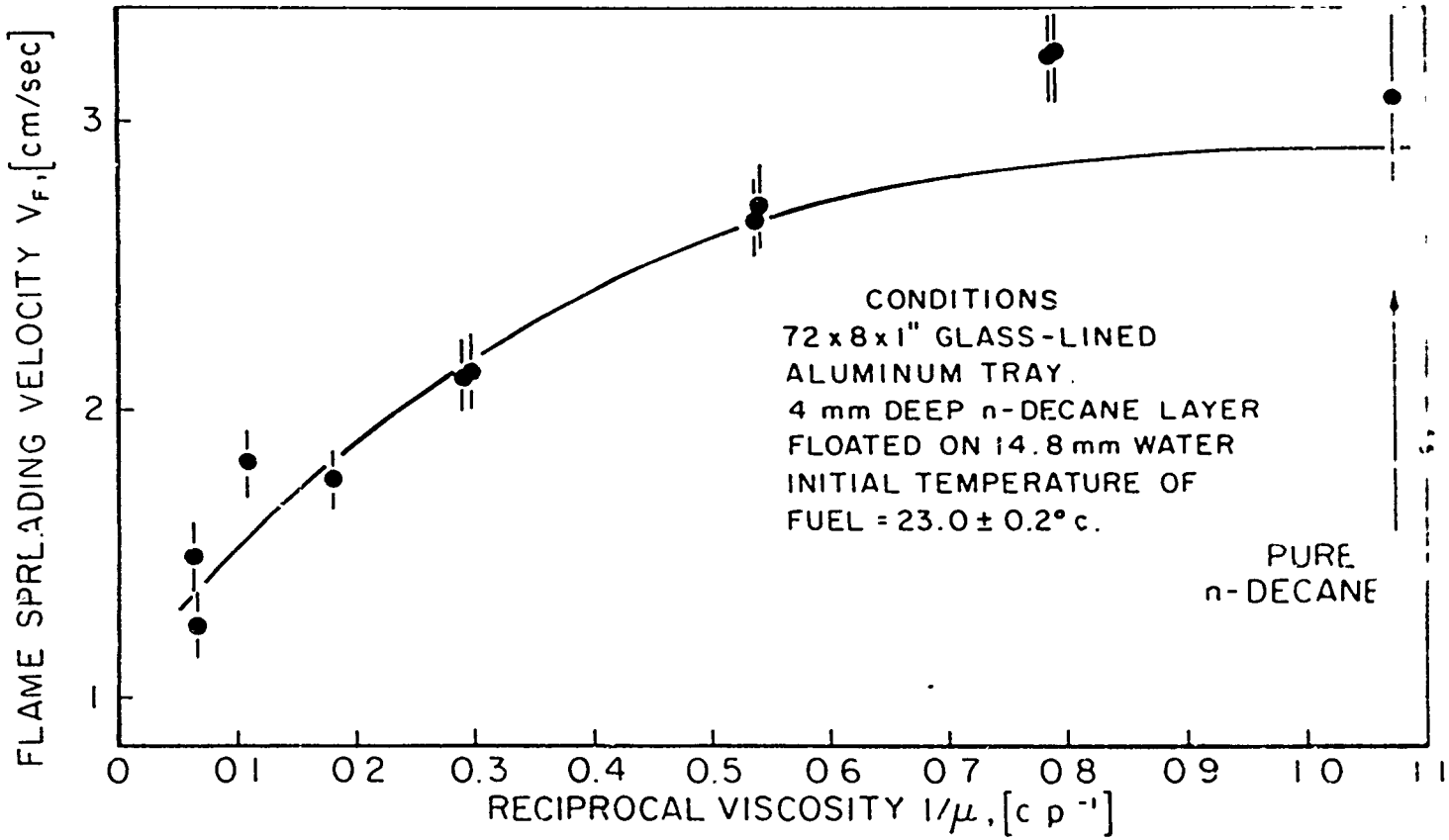

FIGURE 13

FLAME SPREADING VELOCITY OF n-DECANE
AS A FUNCTION OF THE RECIPROCAL VISCOSITY

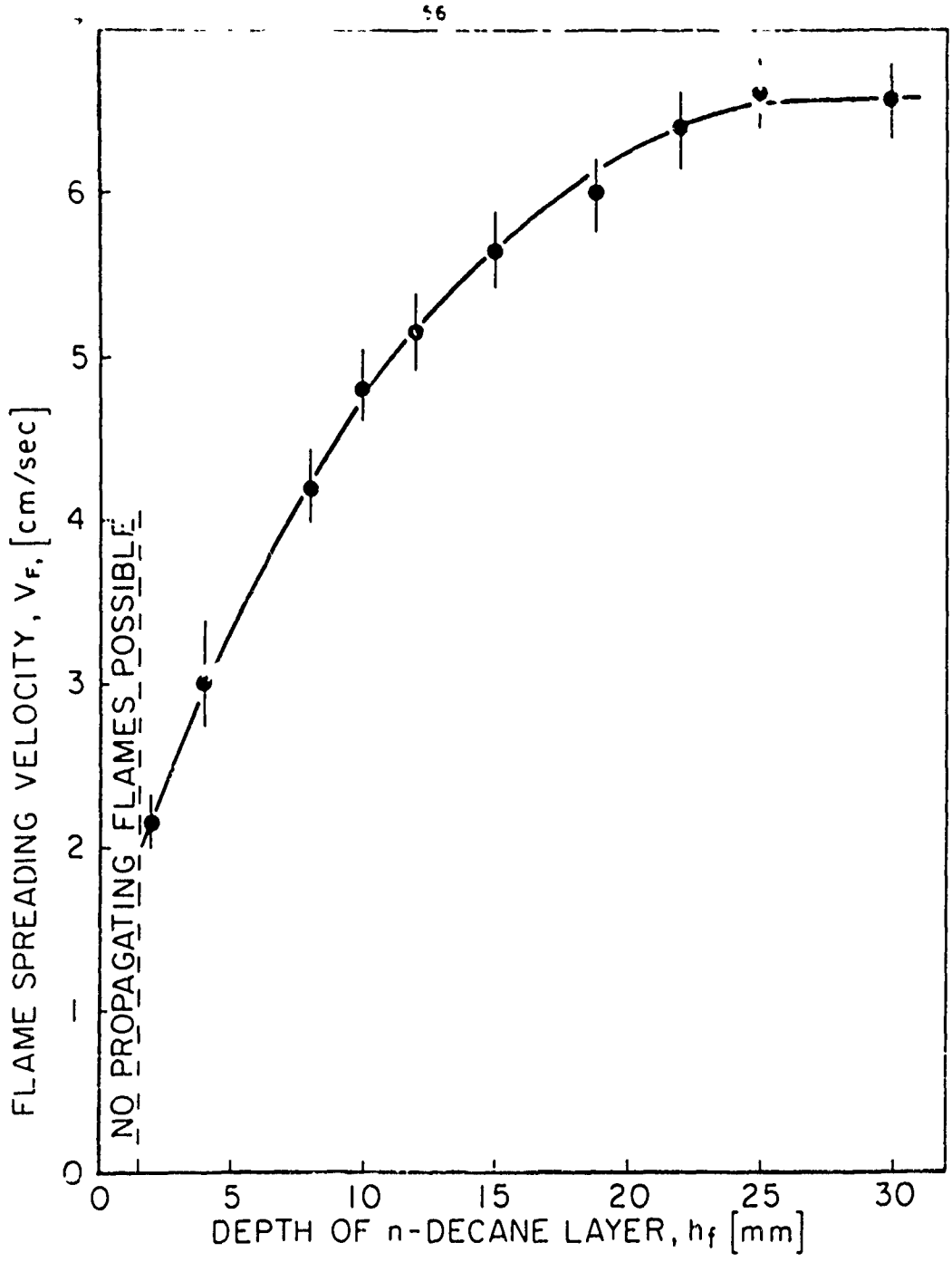

FLAME SPREADING VELOCITY OF n-DECANE
AS A FUNCTION OF THE DEPTH OF THE FUEL LAYER

FIGURE 14

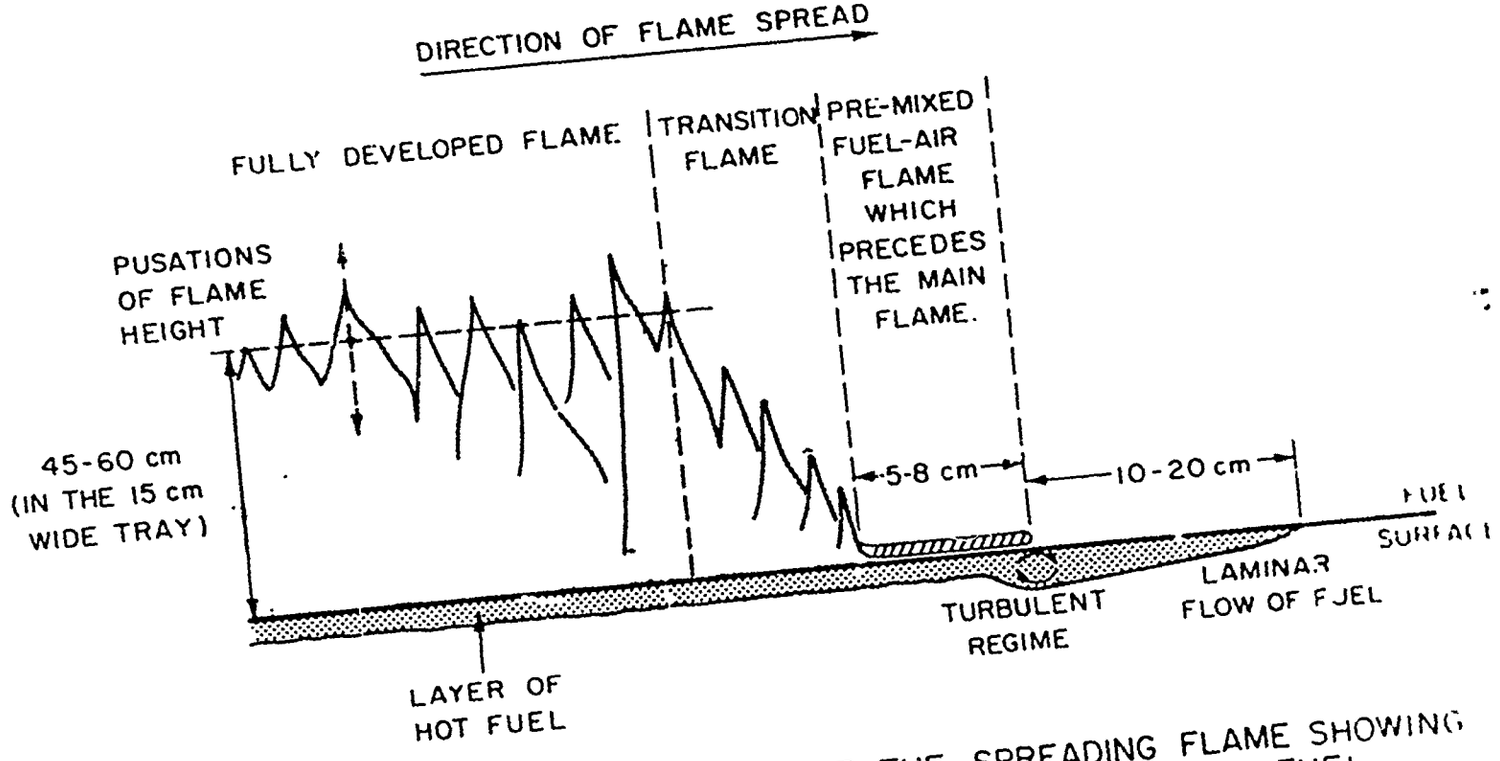

FIGURE 15

SCHEMATIC REPRESENTATION OF THE SPREADING FLAME SHOWING THE "BOUNDARY LAYER" TYPE FLOW IN THE LIQUID FUEL

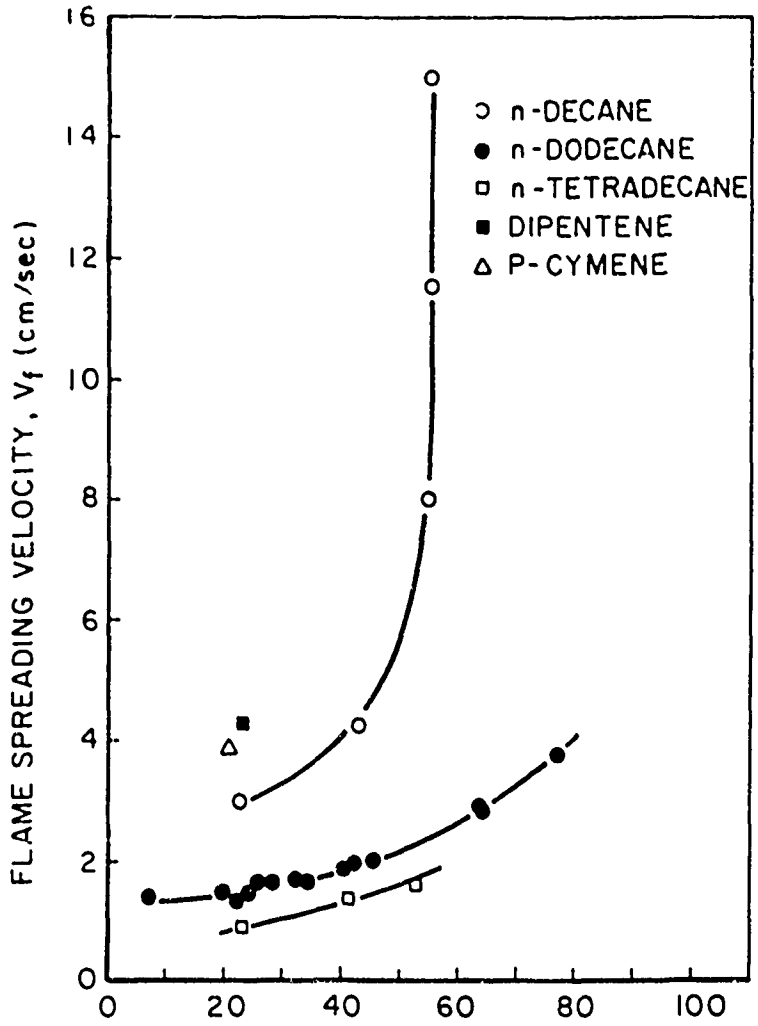

FLAME SPREADING VELOCITY AS A FUNCTION OF BULK FUEL TEMPERATURE FOR FIVE FUELS: "STANDARD" CONDITIONS

G105 R 047 TO

FIGURE 16

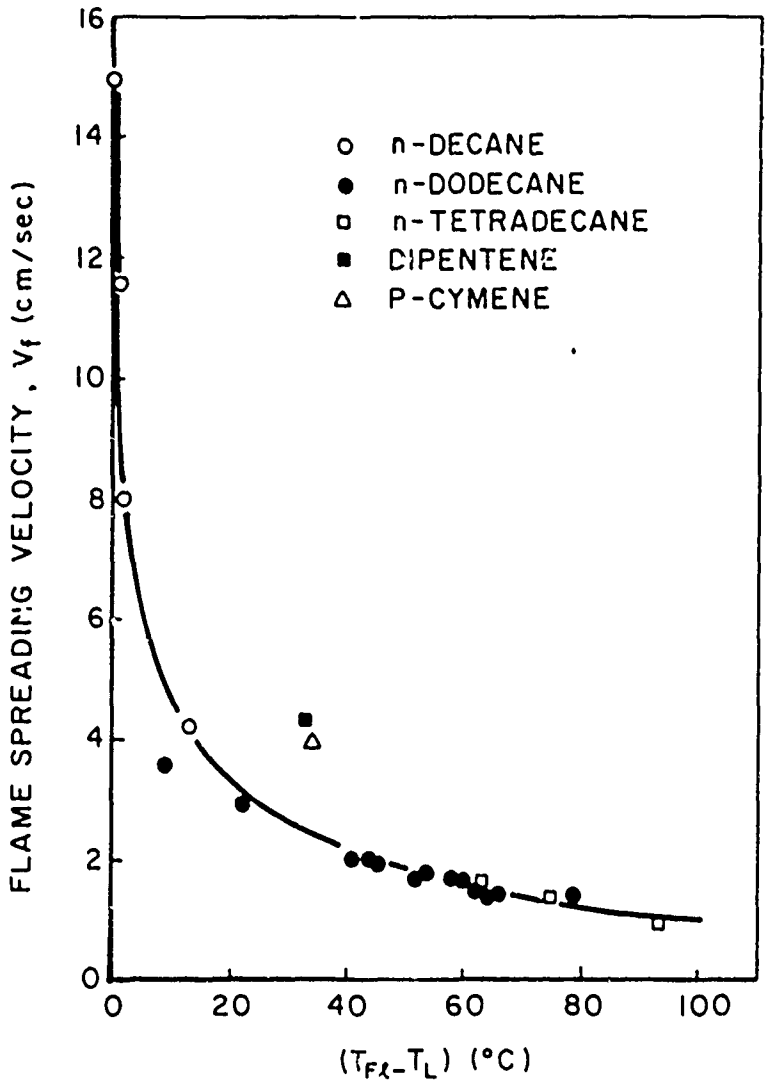

6105 R 048 70

FLAME SPREADING VELOCITY AS A FUNCTION OF $(T_{Fl}-T_L)$ FOR FIVE FUELS: "STANDARD" CONDITIONS

FIGURE 17

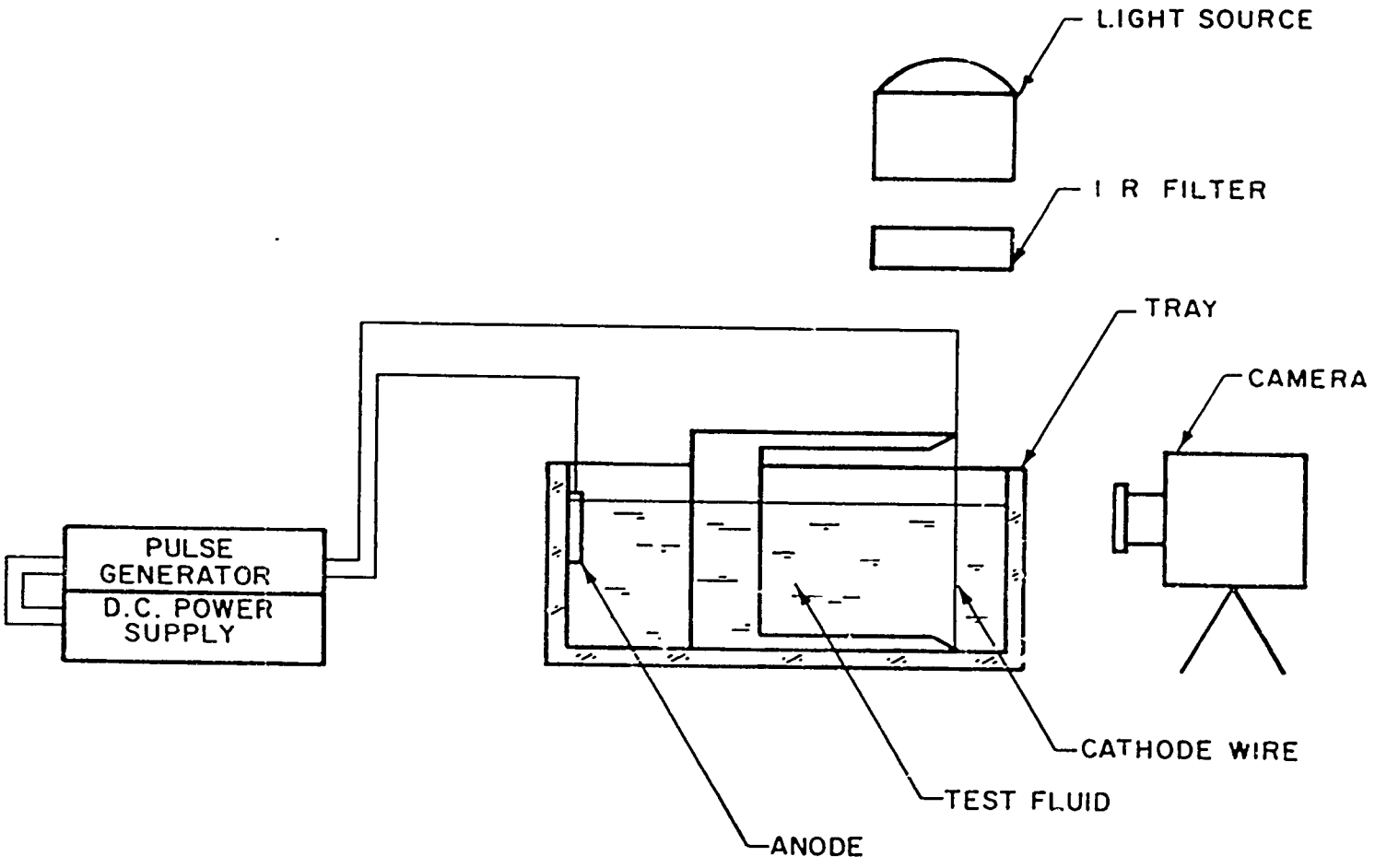

FIGURE 18

SCHEMATIC OF EQUIPMENT USED IN THE HYDROGEN BUBBLE TECHNIQUE

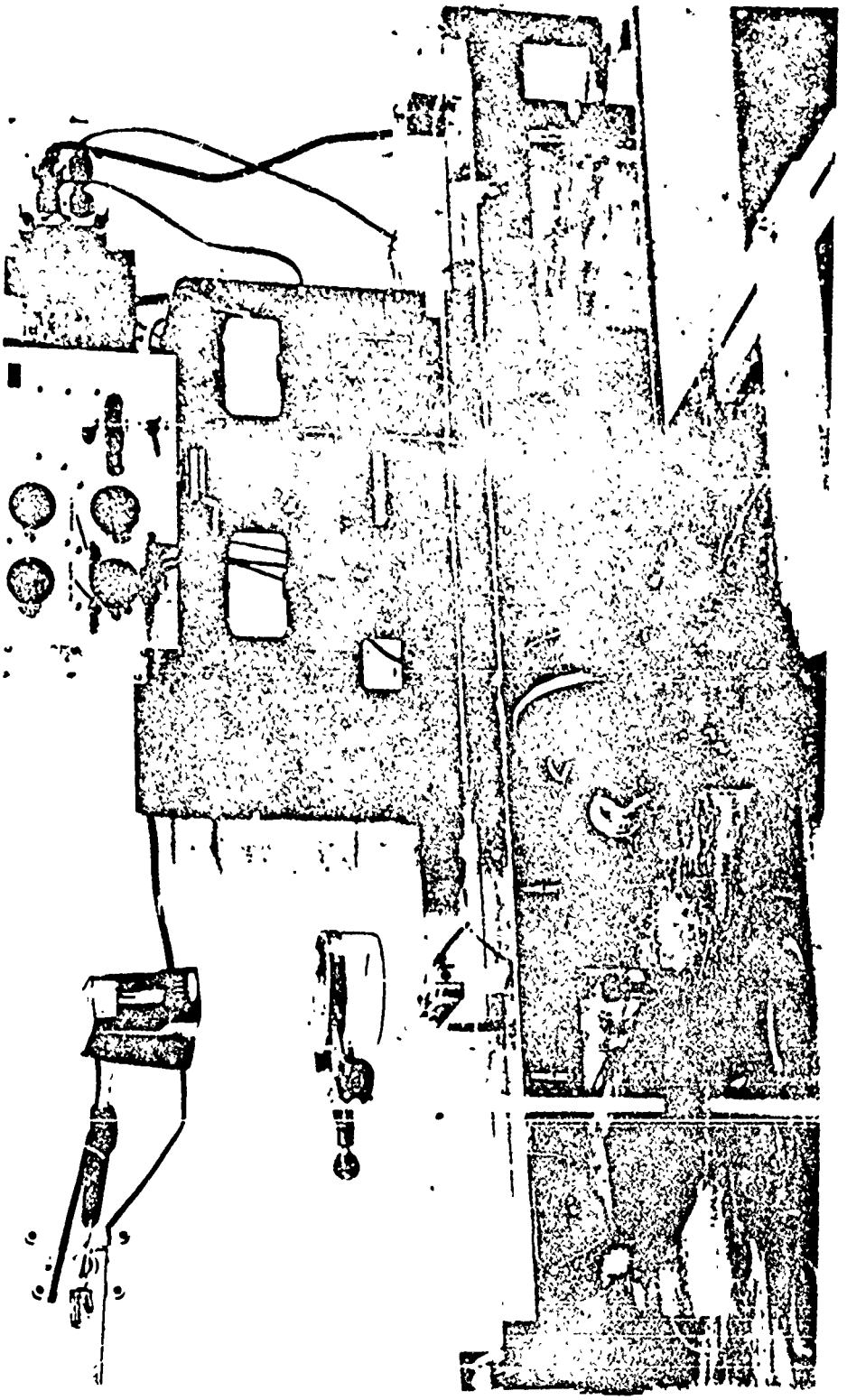

HYDROGEN BUBBLE APPARATUS

FIGURE 19

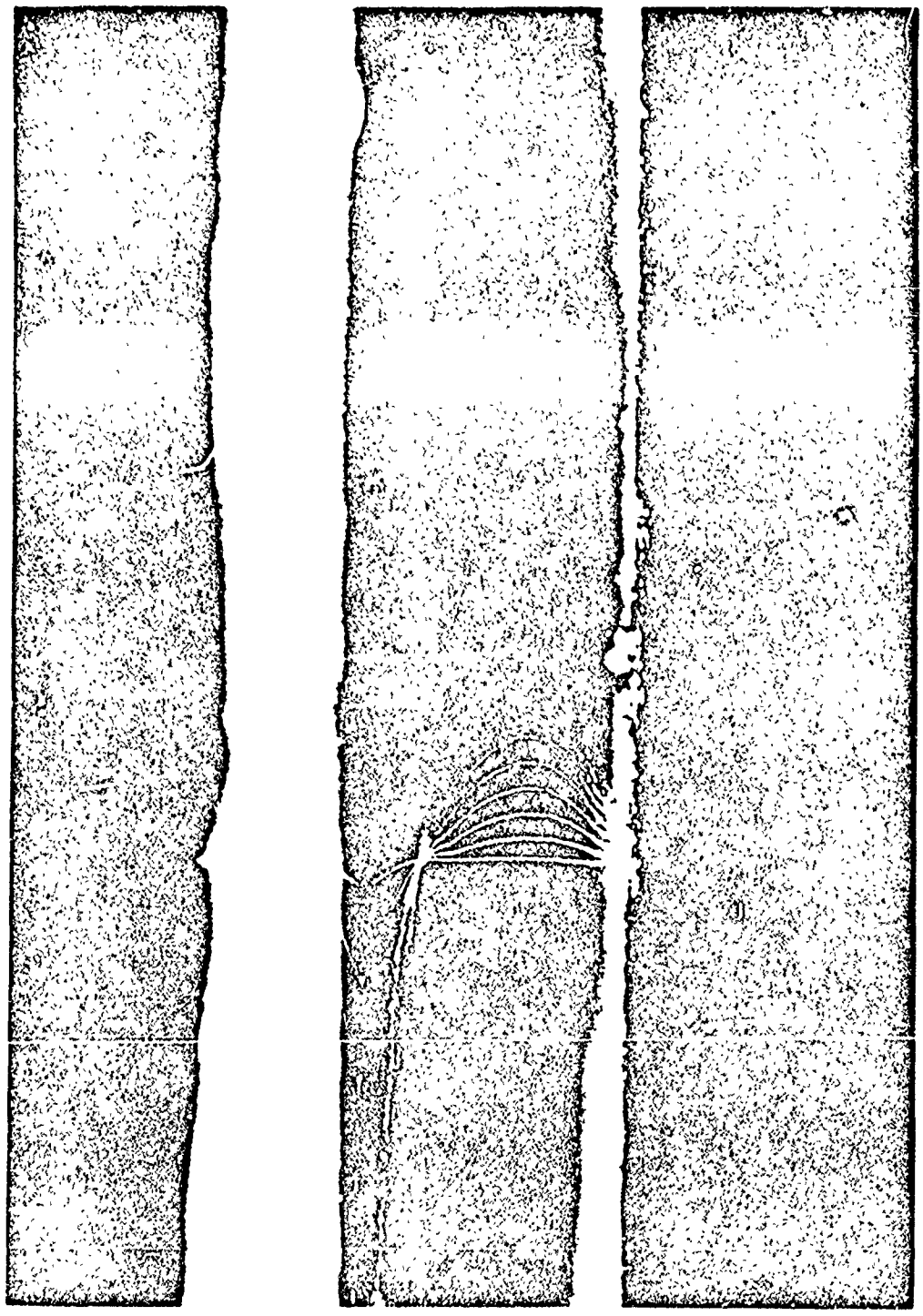

FLOW PATTERN IN SURFACE TENSION INDUCED FLOW IN WATER

FIGURE 20

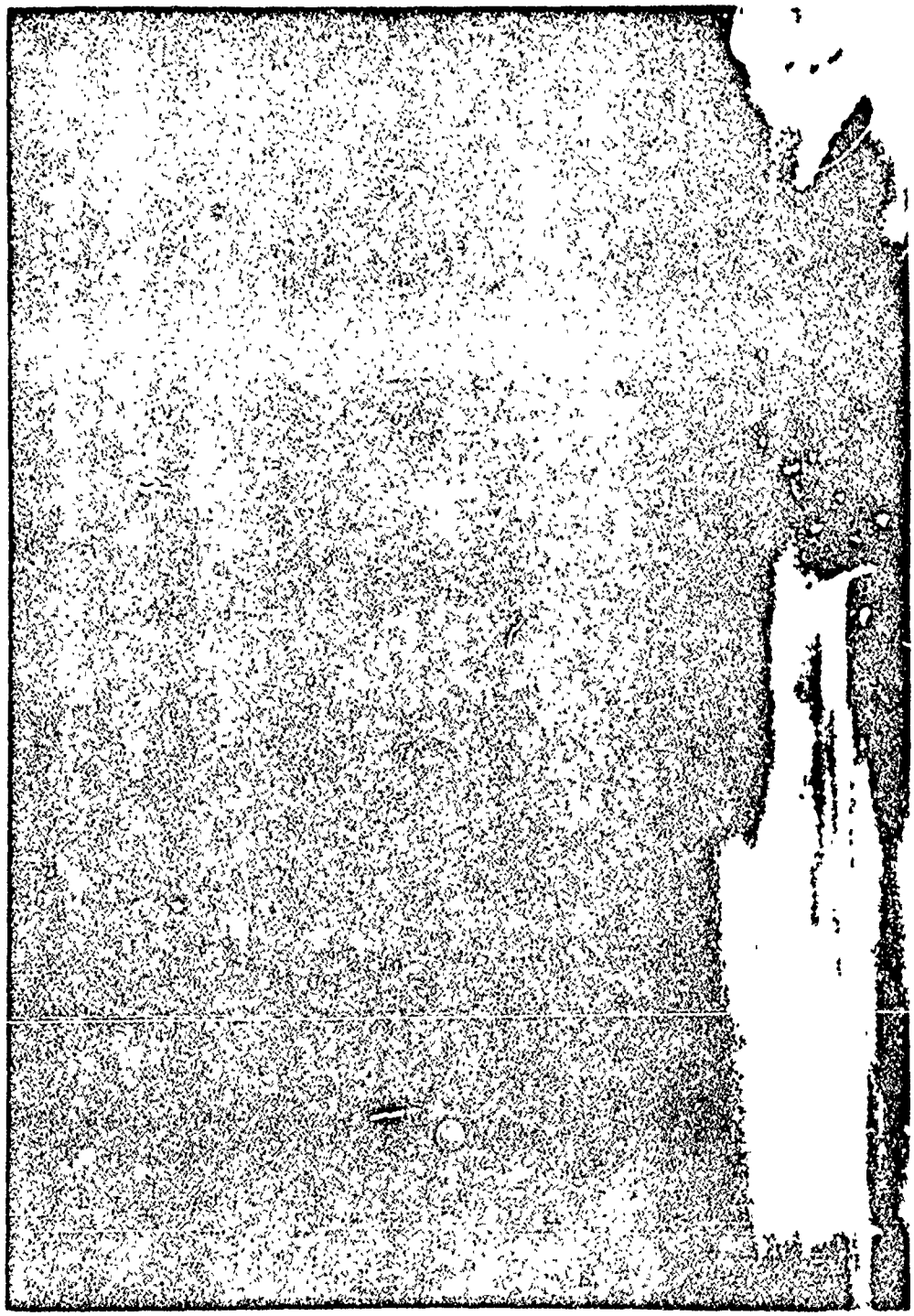

FLOW PATTERN IN NORMAL BUTANOL AS INDUCED BY PROPAGATING FLAME

FIGURE 21

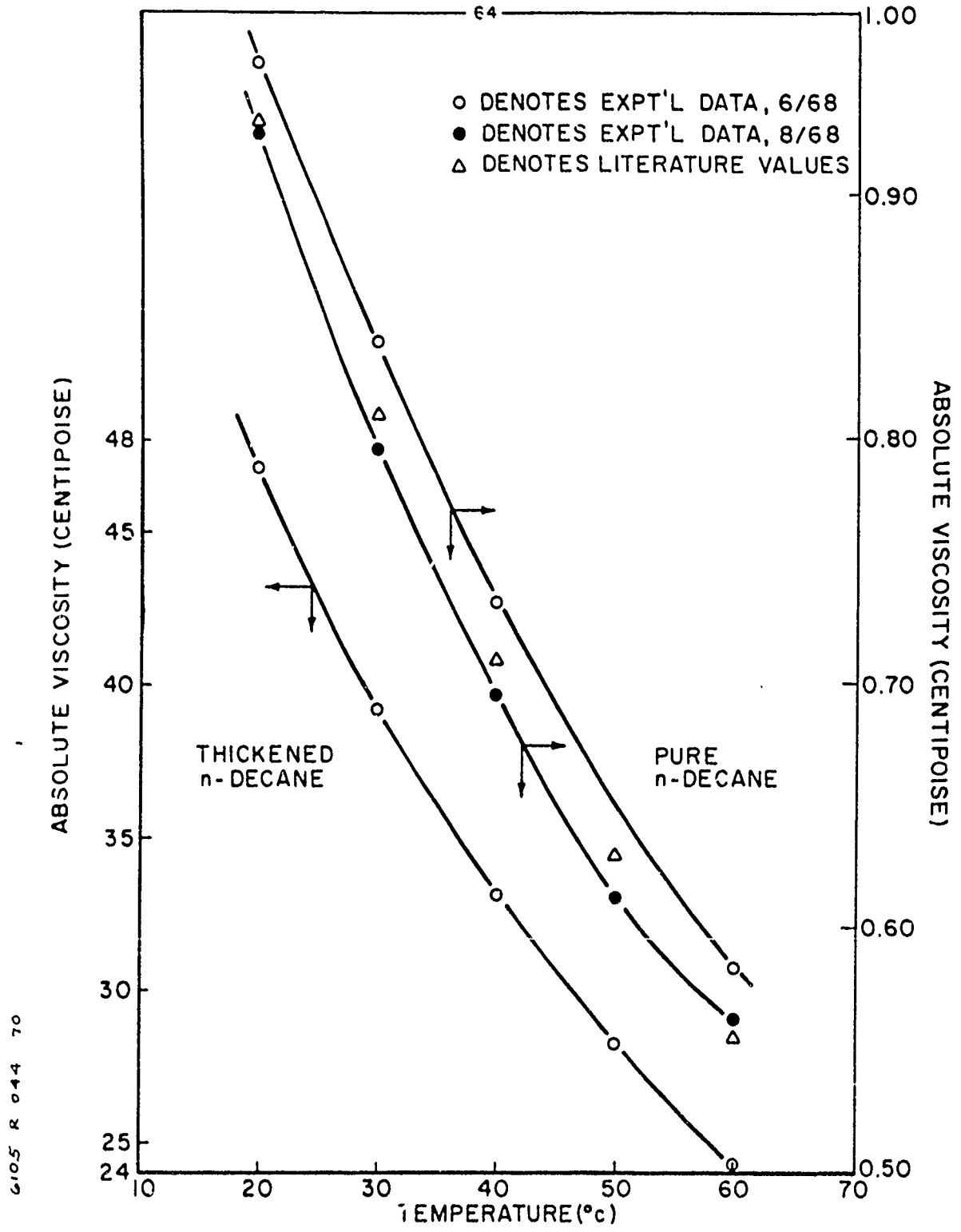

6105 R 044 70

ABSOLUTE VISCOSITY OF PURE AND THICKENED n-DECANE AS A FUNCTION OF TEMPERATURE FIGURE 22

6105 R 046 70

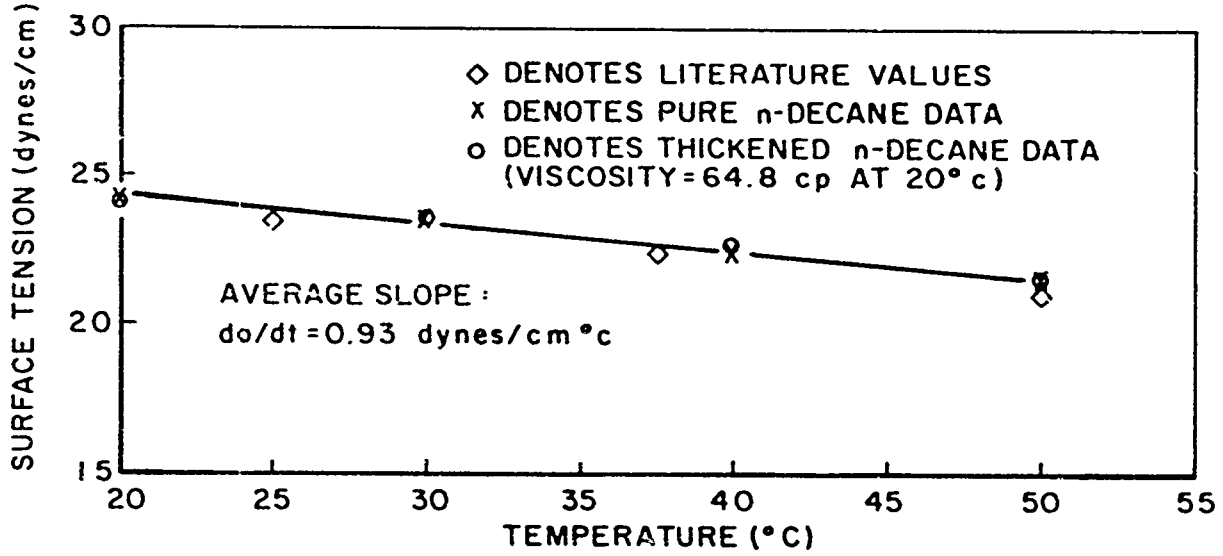

SURFACE TENSION OF n-DECANE AND THICKENED n-DECANE AS A FUNCTION OF TEMPERATURE

FIGURE 23

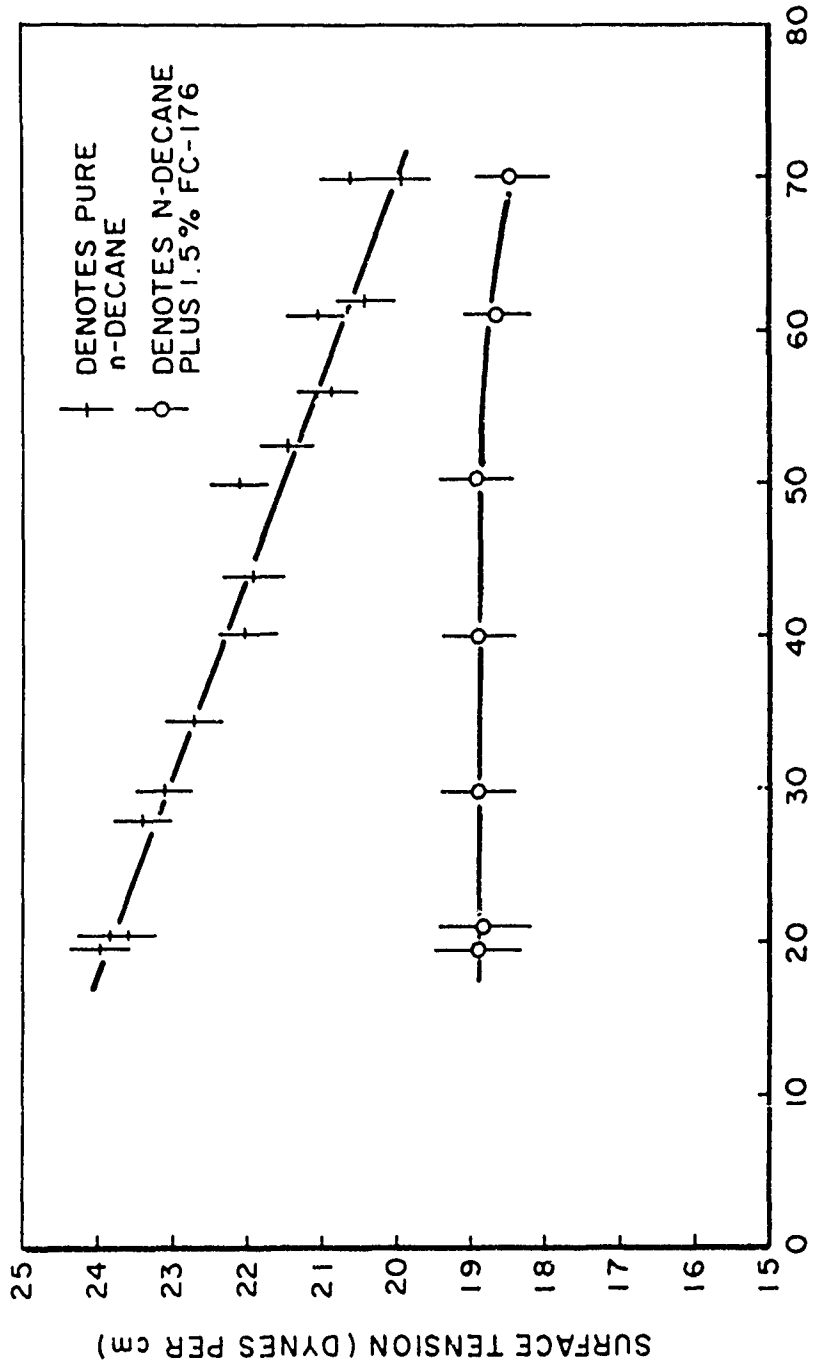

SURFACE TENSION OF PURE n-DECANE PLUS 1.5% FC-176 AS A FUNCTION OF TEMPERATURE

FIGURE 24

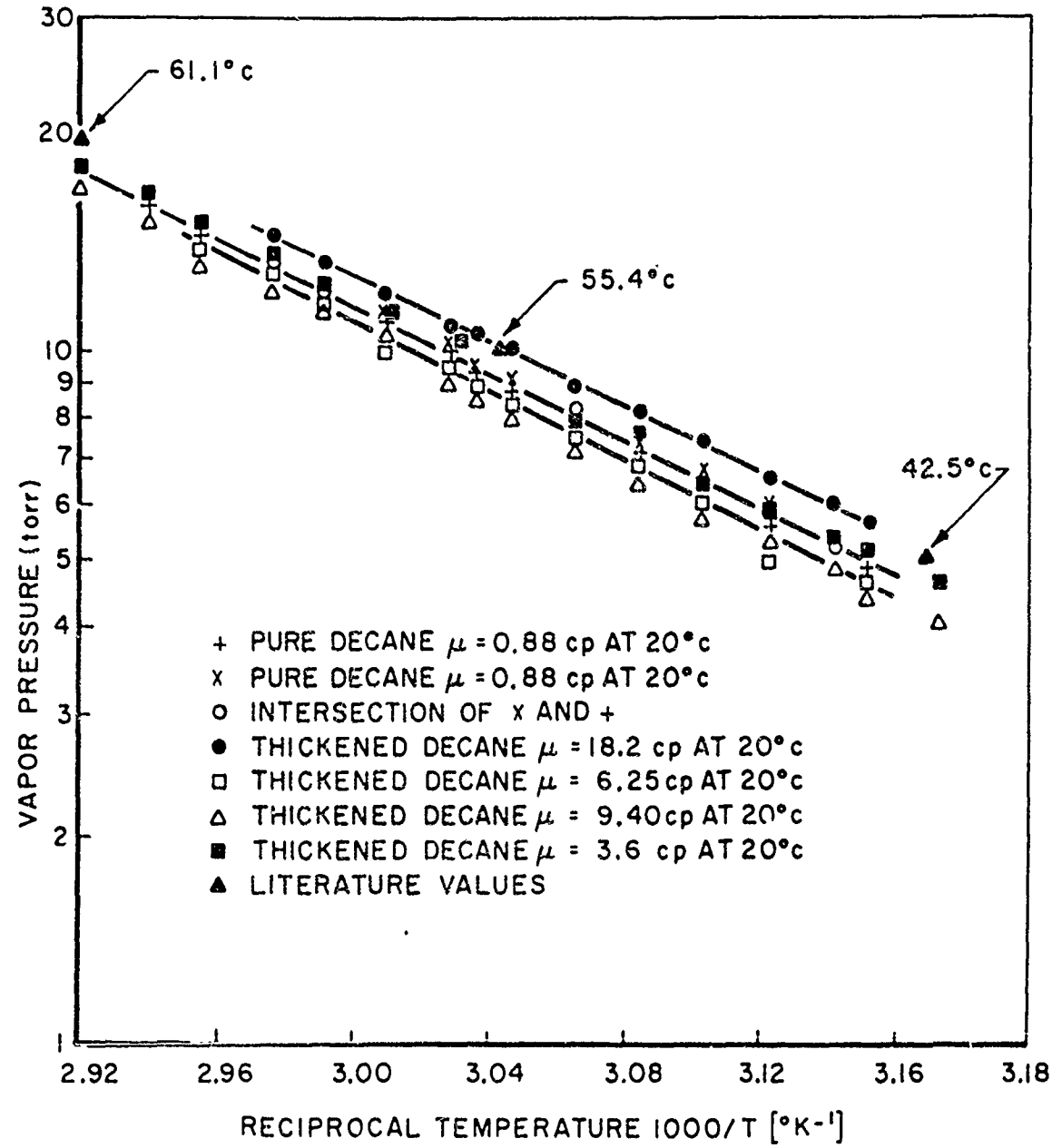

6105 R 049 70

VAPOR PRESSURE OF PURE n-DECANE AND THICKENED n-DECANE AS A FUNCTION OF RECIPROCAL TEMPERATURE

FIGURE 25

Part II

Table of Contents

Part II: Theoretical Studies: Ignition by a Hot Projectile and Flame Spreading Over Liquid Fuel Surfaces

List of Figures (Part A)

List of Figures (Part C)

Part II. Theoretical Studies: Ignition by a Hot Projectile and Flame Spreading Over Liquid Fuel Surfaces (O. P. Sharma and W. A. Sirignano)

This work is described under the following three main headings:

A. Ignition by a Hot Projectile.
B. Ignition of Unmixed Fuel and Oxidizer by a Hot Inert Gas.
C. Flame Spreading Over Liquid Fuel Surfaces.

Each section consists of its own sequence of numbers for the equations, the figures and the references. Section A is further divided into four sub-sections; namely, A-I. Stagnation Point Flow, A-II. Flow on the Cylindrical Surface, A-III. The Wake Flow, and A-IV. General Discussion and Empirical Correlations. Section C consists of two parts; C-I, deals with shallow pools while C-II. is concerned with the analysis of deep pools of liquid fuel.

A. Ignition By a Hot Projectile.

The physical mechanism of ignition of a combustible air-fuel mixture by a hot projectile of moderate speeds is relatively simple and may be described as follows. The temperature of the fluid elements which come in contact with the hot surface of the projectile rises due to conduction and convection of heat. The chemical reaction is, therefore, accelerated, and more heat is released in the gaseous phase which further raises its temperature. When the amount of heat evolved is sufficient to sustain the chemical reaction without relying upon heat from the projectile, it will be said that ignition has occurred. In other words, the zero heat transfer condition at the (non-catalytic) surface of the projectile was used as the ignition criterion.

The heat exchange as well as the chemical reaction take place within the boundary layer surrounding the projectile. In order to circumvent the numerical complexities associated with the solution of unsteady boundary layer flows, the velocity and the temperature of the projectile were assumed to remain steady. We obtained some interesting parameters of the problem (like the temperature or the length of the projectile) by solving steady boundary layer equations when the chemical time was shorter than the characteristic flow time. The projectile was assumed to be a blunt-nosed body with a cylindrical aft-body (see Fig. 1). The problem was analyzed by considering independently three flow regimes, the leading stagnation point region[1], the flow on the cylindrical surface[2], and the wake.[2] The details of the analyses in each flow regime are described below under separate headings.

There is an extensive literature concerning the ignition of explosive gases by heated surfaces in which the systems considered are static or in a low velocity regime associated with natural convection. The ignition of inflammable gases by hot moving particles[3] as well as the ignition of high velocity streams of combustible gases by heated cylindrical rods[4] has also been studied

experimentally. There are also some attempts to correlate the experimental data in terms of the influence of rod diameter, rod temperature, free flow velocity, etc.[5] We have not come across any experimental investigation of the ignition problems restricted to the stagnation region of a hot body. Moreover, some attempts at correlating other experimental data to the present analysis were not successful either due to the lack of kinetics data or due to the absence of some other parameters like the mass fraction of the combustible component of the mixture at ignition point.

A-I. Stagnation Point Flow

In this regime, the problem is to determine the critical surface temperature at which zero heat transfer occurs. We are dealing here with four time scales: namely, the characteristic flow time, the chemical reaction time, the diffusion time, and the heat conduction time. This led us to three non-dimensional quantities described by Pr, Sc, and D_n (see Section A-I-1). We performed calculations for different values of Pr, Sc, and D_n.

Chambré[6] studied analytically the ignition of a planar stagnation flow. This analysis is restricted to cases for which the Lewis number (Le=Sc/Pr) is unity, a first order Arrhenius rate law is valid, and the quantity $(E_a/RT_w) >> 1$, where E_a represents the activation energy for the reaction, T_w is the (unknown) surface temperature, and R is the universal gas constant. The last assumption is required in order to make the reaction zone very thin and close to the surface so that an estimate of the temperature gradient needed in his calculations can be made from the results of earlier non-reacting boundary layer flow calculations.

In the present study, numerical solutions have been obtained for a mixture of propane and air by assuming a more realistic second-order Arrhenius rate law and a constant value of Lewis number. It is possible, in principle, to include more realistic transport properties of the mixture in the present calculations. In Section A-I-1, the differential equations describing the flow are discussed and some simplifying assumptions are given. In Section A-I-2, we give the essential steps of the numerical scheme employed for the solution of differential equations. Finally, the various results are discussed in Section A-I-3.

A-I-1. Governing equations.

The steady state two-dimensional and axisymmetric laminar boundary layer flow for a chemically reacting mixture is described by the following set of equations[7].

Mass

$$\frac{\partial(\rho u R')}{\partial x} + \frac{\partial(\rho v R')}{\partial y} = 0 \qquad (1)$$

Momentum

$$\rho\left(u\frac{\partial u}{\partial x} + v\frac{\partial u}{\partial y}\right) = -\frac{dp}{dx} + \frac{\partial}{\partial y}\left(\mu\frac{\partial u}{\partial y}\right) \qquad (2)$$

Energy

$$\rho\left(\sum_i h_i Y_i\right)\left(u\frac{\partial T}{\partial x}+v\frac{\partial T}{\partial y}\right)-u\left(\frac{\partial p}{\partial x}\right)$$
$$=-\left(\frac{\partial q}{\partial y}\right)-\sum_i h_i\left[-\frac{\partial}{\partial y}(\rho Y_i V_i)+\dot{\omega}_i\right]+\mu\left(\frac{\partial u}{\partial y}\right)^2 \qquad (3)$$

Species

$$\rho\left(u\frac{\partial Y_i}{\partial x}+v\frac{\partial Y_i}{\partial y}\right)=-\frac{\partial}{\partial y}(\rho Y_i V_i)+\dot{\omega}_i \qquad (4)$$

Ideal gas equation of state

$$p=\left(\sum_i Y_i/W_i\right)\rho R T \qquad (5)$$

The distance coordinates (x, y) and the velocity components (u, v) are shown in Figures 2a and 2b. $R^j(x)$ describes the curvature of the surface of the body such that j=0 for two-dimensional flow and j=1 for axisymmetric flow (see Fig. 2b). Here

$$h_i=\int_{T^\circ}^{T} c_{p,i}\,dT+h_i^\circ$$

and denotes the static specific enthalpy of species i. ρ, T, p, and μ are the density, temperature, pressure, and viscosity coefficient of the reacting gas mixture, respectively. W_i, Y_i, $c_{p,i}$, V_i and h_i^0 denote the molecular weight, mass fraction, constant pressure specific heat, y-component of diffusion velocity, and the heat of formation at the temperature T_o of the ith species, respectively. The symbol $\dot{q}$ stands for an expression of the heat flux in the y-direction, and $\dot{w}_i$ represents the mass rate of formation of the species i per unit volume.

We make a simplifying assumption that the mixture under consideration consists of only three components, namely; the reactants (e.g. propane + oxygen), reaction products (e.g. water vapor + carbon dioxide), and an inert gas (e.g. nitrogen). For a mixture having the reactants and the reaction products of nearly the same molecular weights and also, having an inert gas as a major component, it is reasonable to neglect the dependence on the chemical composition in equation (5) and, instead, use a value of the molecular weight corresponding to the free stream composition ($\hat{W}$). It is further assumed that the specific heats (at constant pressure) of different components of the mixture are the same and are constant with temperature changes.

Neglecting thermal diffusion, and assuming that the diffusion of reactants can be described by Fick's law, we get

$$Y_c V_c=-D(\partial Y_c/\partial y) \qquad (6)$$

where D denotes the coefficient of diffusion of the reactive component in the mixture. In view of our assumptions regarding c_p, the rate of heat energy transported across the streamlines is expressed as

$$\dot{q} = -\lambda \left(\frac{\partial T}{\partial y}\right) + \sum_i \rho Y_i V_i h_i^c \qquad (7)$$

where λ denotes the coefficient of thermal conductivity of the mixture. Using Bernoulli's law for the pressure distribution in the boundary layer,

$$-\left(\frac{dp}{dx}\right) = \rho_e u_e \left(\frac{du_e}{dx}\right) \qquad (8)$$

The subscript e refers to the variables in the free stream.

Making use of the equations (6) and (8) and other simplifications mentioned earlier, equations (2) to (5) can be rewritten as

$$\rho\left(u\frac{\partial u}{\partial x} + v\frac{\partial u}{\partial y}\right) = \rho_e u_e\left(\frac{du_e}{dx}\right) + \frac{\partial}{\partial y}\left(\mu\frac{\partial u}{\partial y}\right) \qquad (9)$$

$$\rho c_p\left(u\frac{\partial T}{\partial x} + v\frac{\partial T}{\partial y}\right) = \frac{\partial}{\partial y}\left(\lambda\frac{\partial T}{\partial y}\right) - q\dot{\omega}_c - u\rho_e u_e\left(\frac{du_e}{dx}\right) + \mu\left(\frac{\partial u}{\partial y}\right)^2 \qquad (10)$$

$$\rho\left(u\frac{\partial Y_c}{\partial x} + v\frac{\partial Y_c}{\partial y}\right) = \frac{\partial}{\partial y}\left(\rho D\frac{\partial Y_c}{\partial y}\right) + \dot{\omega}_c \qquad (11)$$

$$p = \rho RT / \bar{w} \qquad (12)$$

Here q denotes the heat released due to the chemical reaction per unit mass of the reactant.

The boundary conditions for the velocity, temperature, and reactant mass fraction are the following. At the surface, both velocity components vanish while far away from the surface, the velocity is given by the potential flow. Thus,

$$u(x,0) = v(x,0) = 0, \quad u(x,\infty) = u_e \qquad (13)$$

The free stream temperature has a prescribed constant value (T_e), and a constant surface temperature (T_w) is obtained for the ignition criterion of no heat transfer, that is,

$$(\partial T/\partial y)_{y=0} = 0 \quad , \quad T(x,\infty) = T_e \tag{14}$$

Note that T_w becomes an eigenvalue of the problem at the ignition point. The species mass fraction has a known constant value in the external flow and, since there is no diffusion of the reactants into the surface, we get

$$[\partial Y_c(x,0)/\partial y] = 0 \quad , \quad Y_c(x,\infty) = Y_{c,e} \tag{15}$$

Following Howarth and Dorodnitsyn, we introduce the new variables as defined below[7]

$$s = \int_0^x \rho_e(x')\,\mu_e(x')\,u_e(x')\,R^{2j}(x')\,dx' \tag{16}$$

$$\eta = \left(\frac{u_e R^j}{\sqrt{2s}}\right) \int_0^y \rho(x,y')\,dy' \tag{17}$$

and

$$f(s,\eta) = \psi(x,y)/\sqrt{2s} \tag{18}$$

The stream function ψ satisfies the following equations

$$\rho u R^j = (\partial\psi/\partial y) \quad , \quad \rho v R^j = -(\partial\psi/\partial x) \tag{19}$$

such that the continuity equation (1) is now automatically satisfied. The velocity components in terms of the new variables are given by the following expressions

$$\left(\frac{u}{u_e}\right) = \left(\frac{\partial f}{\partial \eta}\right) \tag{20}$$

and

$$\rho v = -\left(\frac{\rho_e \mu_e u_e R^j}{\sqrt{2s}}\right)\left[f + 2s\left(\frac{\partial f}{\partial s}\right) + \frac{2s}{\rho_e \mu_e u_e R^{2j}}\left(\frac{\partial \eta}{\partial x}\right)\left(\frac{\partial f}{\partial \eta}\right)\right] \tag{21}$$

Now, the boundary layer equations (9) to (11) assume the following forms:

$$\frac{\partial}{\partial\eta}\left(C\frac{\partial^2 f}{\partial\eta^2}\right) + f\left(\frac{\partial^2 f}{\partial\eta^2}\right) + \beta\left[\frac{\rho_e}{\rho} - \left(\frac{\partial f}{\partial\eta}\right)^2\right] = 2s\left[\left(\frac{\partial^2 f}{\partial s\,\partial\eta}\right)\left(\frac{\partial f}{\partial\eta}\right) - \left(\frac{\partial f}{\partial s}\right)\left(\frac{\partial^2 f}{\partial\eta^2}\right)\right] \tag{22}$$

$$\frac{\partial}{\partial\eta}\left(\frac{C}{Pr}\frac{\partial\theta}{\partial\eta}\right) + f\left(\frac{\partial\theta}{\partial\eta}\right) = 2s\left[\left(\frac{\partial f}{\partial\eta}\right)\left(\frac{\partial\theta}{\partial s}\right) - \left(\frac{\partial f}{\partial s}\right)\left(\frac{\partial\theta}{\partial\eta}\right)\right] + \alpha\left(\frac{\rho}{c_p T_e}\right)\dot{\omega}_c + \beta\left(\frac{\rho_e}{\rho}\right)\left(\frac{u_e^2}{c_p T_e}\right)\left(\frac{\partial f}{\partial\eta}\right) - C\left(\frac{u_e^2}{c_p T_e}\right)\left(\frac{\partial^2 f}{\partial\eta^2}\right)^2 \tag{23}$$

$$\frac{\partial}{\partial\eta}\left(\frac{C}{Sc}\frac{\partial Y_c}{\partial\eta}\right) + f\left(\frac{\partial Y_c}{\partial\eta}\right) = 2s\left[\left(\frac{\partial f}{\partial\eta}\right)\left(\frac{\partial Y_c}{\partial s}\right) - \left(\frac{\partial f}{\partial s}\right)\left(\frac{\partial Y_c}{\partial\eta}\right)\right] - \alpha\,\dot{\omega}_c \tag{24}$$

Here $C \equiv (\rho\mu/\rho_e\mu_e)$; Prandtl number, $Pr = (\mu c_p/\lambda)$; Schmidt number, $Sc = (\nu/D)$; $\theta \equiv (T/T_e)$, $\beta \equiv (2s/u_e)(du_e/ds)$ and $\alpha \equiv (2s/\rho_e\mu_e u_e^2 R^2)$. The magnitude of the quantities α and β depend on the external flow. It can be easily shown that, for plane stagnation flow, $\beta = 1$ and $\alpha = (1/2a\rho)$; while, for axisymmetric stagnation flow, $\beta = \frac{1}{2}$ and $\alpha = (1/2a\rho)$, where a is defined by the equation, $u_e = ax$, describing the external flow in each case. Note that η now becomes proportional to $\int_0^y \rho\,dy$ and is in a direction normal to the surface. Assuming that the coefficient of viscosity varies directly as the temperature, we set $C = 1$. It is further assumed that the Prandtl and Schmidt numbers remain constant. We can replace (ρ_e/ρ) in Eq. (22) by θ with the help of Eq. (12). The rate of consumption of the combustible component of the mixture will be described by an overall single step second order Arrhenius rate law, that is,

$$\dot{\omega}_c = -A\,\rho^2\,Y_c^2\exp\left(-E_a/RT_e\theta\right) \tag{25}$$

where A is assumed to be a known constant and E_a denotes the activation energy for the combustion process. For $u_e \sim 10^3$ cm/sec and $T \sim 3 \times 10^2$ °K, $(u_e^2/c_p T_e) \ll 1$ so that the last two terms in equation (23) may be neglected. Restricting the present analysis

in the neighborhood of a stagnation point, and after some rearrangements, equation (22) to (24) become

$$f''' + f f'' + \beta [\theta - (f')^2] = 0 \tag{26}$$

$$\theta'' + Pr\, f\, \theta' = -Pr\, Q_n D_n (Y_c^2 | \theta) \exp[-E_a | R T_e \theta] \tag{27}$$

$$Y_c'' + Sc\, f\, Y_c' = +Sc\, D_n (Y_c^2 | \theta) \exp[-E_a | R T_e \theta] \tag{28}$$

The prime here denotes differentiation with respect to η . Y_c has been normalized by its value in the external flow ($Y_{c,e}$). The symbol Q_n stands for ($q Y_{c,e} / c_p T_e$), and D_n represents ($A \rho_e Y_{c,e} / a$) for plane stagnation flow or ($A \rho_e^2 Y_{c,e} / 2a$) for axisymmetric stagnation flow. The boundary conditions (13), (14), and (15) become

$$f(0) = f'(0) = 0 \quad , \qquad f'(\infty) = 1 \tag{29}$$

$$\theta'(0) = 0 \quad , \qquad \theta(\infty) = 1 \tag{30}$$

$$Y_c'(0) = 0 \quad , \qquad Y_c(\infty) = 1 \tag{31}$$

At the ignition point, we find that, for Lewis number (Le) equal to unity, equation (27) and (28) can be suitably combined, and then integrated by making use of the equation (30) and (31), such that

$$Y_c = 1 - (\theta - 1) / Q_n \tag{32}$$

In this case, the problem reduces to the solution of only one of the equations (27) and (28), which is obtained by eliminating Y_c between equations (27) and (32), that is,

$$\theta'' + Pr\, f\, \theta' = -Pr\, Q_n D_n \{ [1 - (\theta - 1)/Q_n]^2 / \theta \} \times \exp[-E_a | R T_e \theta] \tag{33}$$

For plane stagnation flow ($\beta = 1$), we extended Chambré's analysis to second order reaction by considering equations (26) and (33) subject to the boundary conditions (29) and (30). Following Chambré, we multiply Eq. (33) by θ' and

integrate over the complete η range and obtain

$$\int_c^{\infty} f(\theta')^2 d\eta = Q_n D_n \int_1^{\theta_w} d\theta \left[\left(\frac{1}{\theta}\right)\left(1 - \frac{\theta-1}{Q_n}\right)^2 \exp\left(-E_a/RT_e\theta\right)\right] \tag{34}$$

Here we have made use of the fact that θ' vanishes at the surface ($\eta = 0$) as well as at the outer edge of the boundary layer ($\eta = \infty$). Under suitable assumptions, Chambré has made an estimate of the integral on the left hand side of equation (34), which then becomes

$$Q_n D_n \int_1^{\theta_w} d\theta \left[\left(\frac{1}{\theta}\right)\left(1 - \frac{\theta-1}{Q_n}\right)^2 \exp\left(-E_a/RT_e\theta\right)\right] = 0.18 \tag{34'}$$

By solving the integral in equation (34'), we then obtain the following expressions in the limit $(E_a/RT_e\theta_w) \gg 1$,

$$\left(\frac{D_n}{Q_n}\right)\left(\frac{RT_e\theta_w}{E_a}\right)\left[Q_n - (\theta_w - 1)\right]^2 \exp\left(-E_a/RT_e\theta_w\right) = 0.18 \tag{35}$$

up to first order in $(RT_e\theta_w/E_a)$ in the pre-exponential factor

and

$$\left(\frac{D_n}{Q_n}\right)\left(\frac{RT_e\theta_w}{E_a}\right)\left\{ \left[Q_n - (\theta_w - 1)\right]^2 - \left[(Q_n+1)^2 - 4\theta_w(Q_n+1) + 3\theta_w^2 \right]\left(\frac{RT_e\theta_w}{E_a}\right)\right\} \exp\left(-E_a/RT_e\theta_w\right) = 0.18 \tag{35'}$$

up to second order in $(RT_e\theta_w/E_a)$ in the pre-exponential factor

A-I-2. Method of Solution.

Numerical integration of equations (26) to (31) has been performed by following a method due to Fay and Kaye[8]. For the sake of completeness, it is summarized in the following four steps:

(i) Linearization. The boundary layer equations (26) to (28) are first linearized about an initial trial solution (or previous iteration). The method of linearization (or quasi-linearization) essentially involves the approximation of the non-

linear terms by a first order Taylor series expansion about the 'previous' solution[9,10]. The equations (26) to (31) are now uncoupled except through the initial guess or the results of the earlier iteration.

(ii) Finite Difference Equations. The differential equations are cast into an implicit finite difference form by replacing the derivatives by central difference formulas (without any correction terms). Equation (26), is reduced to a second order form in terms of ϕ by defining $\phi = f'$. Furthermore, in the process of linearizing the source terms in equations (27) and (28), we include the Taylor expansion with respect to θ alone on the right hand side of equation (27), while with respect to Y_c alone in equation (28). Thus, equations (26) to (28) become

$$-\left[1-\tfrac{1}{2}h f_{(i-1)}^{(k)}\right]\phi_{(i-1)}^{(k+1)} + 2\left[1+\beta h \phi_{(i)}^{(k)}\right]\phi_{(i)}^{(k+1)} - \left[1+\tfrac{1}{2}h f_{(i)}^{(k)}\right]\phi_{(i+1)}^{(k+1)} = \beta\left\{\theta_{(i)}^{(k)} + \left[\phi_{(i)}^{(k)}\right]^2\right\} \qquad i = 2,3,\cdots,N$$

$$-\left[1-\tfrac{1}{2}h\,Pr\, f_{(i)}^{(k+1)}\right]\theta_{(i-1)}^{(k+1)} + \left\{2 + h^2 Pr\, Q_n D_n \left(Y_{c(i)}^{(k)}\right)^2 \times \left(1 - Ea/RT_e\theta_{(i)}^{(k)}\right) \exp\left[-Ea/RT_e\theta_{(i)}^{(k)}\right]/\left[\theta_{(i)}^{(k)}\right]^2\right\}\theta_{(i)}^{(k+1)} - \left[1+\tfrac{1}{2}h\,Pr\, f_{(i)}^{(k+1)}\right]\theta_{(i+1)}^{(k+1)} = h^2 Pr\, Q_n D_n \left(Y_{c(i)}^{(k)}\right)^2 \left(2 - Ea/RT_e\theta_{(i)}^{(k)}\right)\exp\left[-Ea/RT_e\theta_{(i)}^{(k)}\right]/\theta_{(i)}^{(k)} \qquad i = 2,3,\cdots,N \qquad (36)$$

$$-\left[1-\tfrac{1}{2}h\,Sc\, f_{(i)}^{(k+1)}\right]Y_{c(i-1)}^{(k+1)} + 2\left\{1 + h^2\, Sc\, D_n \left(Y_{c(i)}^{(k)}\right)^2 \times \exp\left[-Ea/RT_e\,\theta_{(i)}^{(k+1)}\right]/\theta_{(i)}^{(k+1)}\right\}Y_{c(i)}^{(k+1)} - \left[1+\tfrac{1}{2}h\,Sc\, f_{(i)}^{(k+1)}\right]Y_{c(i+1)}^{(k+1)} = h^2\, Sc\, D_n \left(Y_{c(i)}^{(k)}\right)^2 \exp\left[-Ea/RT_e\,\theta_{(i)}^{(k+1)}\right]/\theta_{(i)}^{(k+1)} \qquad i = 2,3,\cdots,N \qquad (37)$$

$$(38)$$

Here h denotes the interval length. The subscripts refer to the mesh points while the superscripts represent the numbers of the steps in the interative process.

(iii) Solution of the Difference Equations. Each of the equations (36) to (38) form a tridiagonal matrix which can be easily inverted by using a procedure called 'line-inversion'[11]. The boundary conditions at the wall, i = 1, were incorporated by using a three point formula for the derivatives, that is,

$$\theta_1^{(k+1)} = \left[4\,\theta_2^{(k+1)} - \theta_3^{(k+1)}\right]/3 \qquad (39)$$

$$Y_{c,1}^{(k+1)} = \left[4\,Y_{c,2}^{(k+1)} - Y_{c,3}^{(k+1)}\right]/3 \qquad (40)$$

Equation (39) is used only at the ignition point. The boundary conditions at the end point i = N + 1 are added into the terms on the right hand side of equations (36), (37), and (38). In order to obtain various temperature profiles before ignition, we assume different values of the surface temperature (θ_w) lower than the ignition temperature at which equation (39) is satisfied.

(iv) Iteration. Assuming some initial profiles for f, p, θ, and Y_c, we first solve equation (36) by the 'line-inversion' procedure, and obtain a new profile for p in order to get a profile for f. Then, the new profile of f is utilized in the solution of equation (37). Finally, equation (38) is solved by making use of the newly calculated profiles of both f and θ. Having obtained the values of f, p, θ, and Y_c once, the procedure is repeated till a prescribed convergence, $^{c}1$ in 10^4, is achieved for certain values of successive iterations. The procedure is quite fast except when (39) becomes the boundary condition, in which case the convergence between the results of the successive iterations becomes slow and, therefore, a convergence test of 1 in 10^3 was employed at this stage.

A-I-3. Results

Besides the mathemat. l operations associated with the solution of the boundary layer equations (26) to (28), there is an additional task of specifying reasonably the physical quantities Pr, Sc, Q_n, and D_n for the reacting mixture before any numerical computation is attempted. We performed the numerical calculations for a combustible mixture (at the edge of the boundary layer) of propane and air in stoichiometric proportions, at a temperature of 300°K, and 1 atmosphere pressure. From the data for propane and air[12,13], we calculated c_p ($= \Sigma_i c_{p_i} Y_i$); and μ, D, and λ for the external stream by combining the individual values according to the appropriate rules for a binary mixture[14]. We thus obtained Pr=0.75 and Sc=1.32, and used them in the calculations. These numbers were later varied arbitrarily to find their effect on the ignition temperature. Taking into account the standard heats of formation of the products CO_2 and H_2O[15], the heat released due to the chemical reaction per unit mass of the reactant was found to be 2.39 kcal/gm. Myers and Bartle[16] obtained an expression for the reaction time from empirical correlations of their experimental data on the oxidation of propane in a shock tube. Based on their results, we made estimates of the quantities A and E_a [see equation (25)] which were used in the entire calculations. Since the empirical correlations had shown two distinct temperature regimes, we had two sets of values, namely, $A \simeq 10^{10}$ (cm^3/gm-sec), E_a = 17.01 kcal/mole, for 1000°K < T < 1250°K, and $A \simeq 3 \times 10^{13}$ (cm^3/gm-sec), E_a = 31.29 kcal/mole, for 1600°K > T > 1250°K. We made use of only the first set of values.

The results of the detailed calculations when Q_n = 8.84 and $D_n = 10^4$ are shown in Figures 3a, b, c and 4a, b, c. The general qualitative features of the corresponding profiles when Le = 1 and 1.76 are the same. Due to the release of chemical heat, there occurs an overshoot of the velocity profiles within the boundary layer (see Figures 3c and 4c). As the temperature of the surface increases, this overshoot becomes more pronounced and moves closer to the surface. In Figure 3a or 4a, the various temperature profiles are not similar because of the fact that different boundary conditions have been used at the surface. As mentioned earlier, we specify the surface temperature before the ignition point while we make use of equation (39) as the appropriate surface boundary condition in order to determine the ignition temperature (θ_w) as an eigenvalue. A plot of θ_w vs θ'_w is also given in Figure 5 to indicate heat transfer variation near the ignition point. The effect of the external stream on the ignition temperature can be studied by varying D_n. This is shown in Figure 6 (solid curve). As D_n is increased by decreasing a (or u_e), the ignition temperature also decreases due to an increase in the characteristic flow time. Also, at low temperatures less of the combustible gas ($Y_{c,w}$) is consumed which is indicated by the dotted curve in Figure 6.

Some additional calculations were done to determine quantitatively the effect on the ignition temperature due to different values of the transport parameters Pr and Sc. For Q_n = 8.84 and $D_n = 10^4$, these results are summarized in Table I. For Le = 1, ($Y_{c,w}/Y_{c,e}$) is calculated with the help of equation (32). It should be noted that the variations in the values of the ignition temperatures or ($Y_{c,w}/Y_{c,e}$) are relatively minor due to those of Pr or Sc. Of course, the overall trend of the variations is as expected. For the same Sc, the increase in Pr lowers the ignition temperature while for same Pr, the increase in Sc decreases ($Y_{c,w}/Y_{c,e}$).

Table I

	Pr	Sc	Le	θ_w	($Y_{c,w}/Y_{c,e}$)
1	0.75	0.75	1	3.75	0.689
½	0.75	0.75	1	3.62	0.704
½	0.75	1.32	1.76	3.82	0.576
½	0.75	1.00	1.33	3.70	0.646
½	0.75	0.70	0.93	3.60	0.716
½	1.00	1.32	1.32	3.64	0.655

Using equations (35) and (35'), we calculated the ignition temperatures according to Chambre's analysis for plane stagnation flow and Le = 1, and the results are, respectively,

$$(\theta_w)_{\text{Chambre'}} = 2.76 \text{ and } 2.82$$

Thus, we find that Chambre's value is about 25% lower than the present one.

A-II. Flow on the Cylinderical Surface

For sufficiently high Reynolds number and Prandtl number about unity, the boundary layer is thin compared to the radius of the cylinder, and, therefore, a 'flat plate' approximation has been employed for the second region [see Fig. 7(a)]. Now the characteristic parameter of the problem is the distance from the leading edge at which ignition occurs, and is identified by the presence of a temperature maximum. Dooley[17] as well as Toong[18] have independently studied the problem of ignition in the laminar boundary layer of a heated plate. Dooley[17] developed an iterative procedure for the solution of energy equation and obtained detailed results for the thermal decomposition of azomethane. This analysis is restricted to the special case of unitary Lewis number, and in addition, to an arbitrary specification of chemical composition at the wall. Toong[18] employed a series expansion to a set of ordinary differential equations, and solved the latter on a computer for specific values of the various dimensionless parameters. He obtained convergence by including only five terms of the series, and also found that it became poor near the ignition point. In the present study, we directly integrated the non-similar boundary layer equations by using a numerical scheme described in Section A-II-2. Besides, the effect of different values of Prandtl and Schmidt numbers as well as that of the speed and the dimensions of the projectile was calculated.

A-II-1. Governing equations.

Making all the simplifying assumptions described in Section A-I-2, and noting that the pressure remains constant on a flat plate, equations (1) and (9) to (12), describing the steady state two dimensional boundary layer flow, can be rewritten as

$$\frac{\partial(\rho u)}{\partial x} + \frac{\partial(\rho v)}{\partial y} = 0 \tag{41}$$

$$\rho\left(u\frac{\partial u}{\partial x} + v\frac{\partial u}{\partial y}\right) = \frac{\partial}{\partial y}\left(\mu\cdot\frac{\partial u}{\partial y}\right) \tag{42}$$

$$\rho c_p\left(u\frac{\partial T}{\partial x} + v\frac{\partial T}{\partial y}\right) = \frac{\partial}{\partial y}\left(\lambda\frac{\partial T}{\partial y}\right) + \mu\left(\frac{\partial u}{\partial y}\right)^2 - q\dot{\omega}_c \tag{43}$$

$$\rho\left(u\frac{\partial Y_c}{\partial x}+v\frac{\partial Y_c}{\partial y}\right)=\frac{\partial}{\partial y}\left(\rho D\frac{\partial Y_c}{\partial y}\right)+\dot{\omega}_c \tag{44}$$

$$p=\rho RT/\bar{W} \tag{45}$$

Here q denotes the heat released due to the chemical reaction when a unit mass of the reactant is consumed.

The boundary conditions for the velocity, temperature, and reactant mass fraction are summarized next. At the surface both velocity components vanish while far away from the surface, the velocity is given by the potential flow. Thus

$$u(x,0)=v(x,0)=0\quad,\quad \lim_{y\to\infty}u(x,y)=u_e \tag{46}$$

Both the free stream temperature and the surface temperature have prescribed constant values

$$T(x,0)=T_w\quad,\quad \lim_{y\to\infty}T(x,y)=T_e \tag{47}$$

The problem can also be solved by the same procedure even when the surface temperature is a prescribed function of x. The species mass fraction has a known constant value in the external flow, and since there is no diffusion of the reactants into the surface, we get

$$\left[\partial Y_c/\partial y\right]_{y=0}=0\quad,\quad \lim_{y\to\infty}Y_c(x,y)=Y_{c,e} \tag{48}$$

The proper initial conditions for equations (41) to (44) are the specifications of u, v, T, and Y_c at some initial station, x_i. We note that the boundary layer approximation breaks down near the leading edge of the flat plate ($x = 0$). Furthermore, we are dealing here with a non-similar flow because of the chemical reaction which accelerates as the mixture moves away from the leading edge. In view of these observations, we will proceed with an integration at a small distance away from the leading edge and utilize the results of a similar solution for non-reacting flow as our initial conditions.

Next we introduce the new variables as defined below [7]

$$s=(x/L) \tag{49}$$

$$\eta=\left[u_e/2sL\rho_e\mu_e\right]^{1/2}\int_0^y\rho(x,y')\,dy' \tag{50}$$

and

$$f(s,\eta)=\left[\psi(x,y)/(2sL\rho_e\mu_e u_e)^{1/2}\right] \tag{51}$$

The stream function ψ satisfies the following equations

$$\rho u = (\partial\psi/\partial y) \quad , \quad \rho v = -(\partial\psi/\partial x) \tag{52}$$

such that the continuity equation (1) is now automatically satisfied. The velocity components in terms of the new variables are given by the following expressions

$$\left(\frac{u}{u_e}\right) = \left(\frac{\partial f}{\partial \eta}\right) \tag{53}$$

and

$$\rho v = -\left(\frac{\rho_e \mu_e u_e}{2\xi}\right)^{1/2}\left[f + 2\xi\left(\frac{\partial f}{\partial \xi}\right) + 2\xi L\left(\frac{\partial \eta}{\partial x}\right)\left(\frac{\partial f}{\partial \eta}\right)\right] \tag{54}$$

Now the boundary layer equations (42) to (44) assume the following forms:

$$\frac{\partial}{\partial \eta}\left(C\frac{\partial^2 f}{\partial \eta^2}\right) + f\left(\frac{\partial^2 f}{\partial \eta^2}\right) = 2\xi\left[\left(\frac{\partial f}{\partial \eta}\right)\left(\frac{\partial^2 f}{\partial \xi \partial \eta}\right) - \left(\frac{\partial f}{\partial \xi}\right)\left(\frac{\partial^2 f}{\partial \eta^2}\right)\right] \tag{55}$$

$$\frac{\partial}{\partial \eta}\left(\frac{C}{P_r}\cdot\frac{\partial \theta}{\partial \eta}\right) + f\left(\frac{\partial \theta}{\partial \eta}\right) = 2\xi\left[\left(\frac{\partial f}{\partial \eta}\right)\left(\frac{\partial \theta}{\partial \xi}\right) - \left(\frac{\partial f}{\partial \xi}\right)\left(\frac{\partial \theta}{\partial \eta}\right)\right] - C\left(\frac{u_e^2}{c_p T_e}\right)\left(\frac{\partial^2 f}{\partial \eta^2}\right)^2 + \alpha\left(\frac{q}{c_p T_e}\right)\dot{\omega}_c \tag{56}$$

$$\frac{\partial}{\partial \eta}\left(\frac{C}{S_c}\frac{\partial \gamma_c}{\partial \eta}\right) + f\left(\frac{\partial \gamma_c}{\partial \eta}\right) = 2\xi\left[\left(\frac{\partial f}{\partial \eta}\right)\left(\frac{\partial \gamma_c}{\partial \xi}\right) - \left(\frac{\partial f}{\partial \xi}\right)\left(\frac{\partial \gamma_c}{\partial \eta}\right)\right] - \alpha\dot{\omega}_c \tag{57}$$

Here $G \equiv (T/T_e)$, $C \equiv (\rho\mu/\rho_e\mu_e)$; Prandtl number, $Pr = (\mu c_p/\lambda)$; Schmidt number, $Sc = (\mu/\rho D)$; and $\alpha \equiv (2\xi L/\rho u_e)$. The rate of consumption of the combustible component of the mixture will be described by an over-all single step, second order Arrhenius rate law; that is,

$$\dot{\omega}_c = -A\rho^2\gamma_c^2 \exp(-E_a/RT_e\theta) \tag{58}$$

where A is assumed to be a known (positive) constant and E_a denotes the activation energy for the combustion process under consideration.

The problem can be greatly simplified by neglecting the dependences of μ, λ, and D on the various components of the mixture and the temperature. We will perform numerical computations for constant values of C, Pr, and Sc. The momentum conservation equation (55) is now no longer coupled to energy equation (56) or the species equation (57). Furthermore, if we use similar profiles as our initial conditions, it is then evident that equation (55) reduces to the Blasius case which has been already computed [see, for example, Reference (19)]. Hence, the boundary layer equations finally reduce to the following forms:

$$\left(\frac{d^3f}{d\eta^3}\right) + f\left(\frac{d^2f}{d\eta^2}\right) = 0 \tag{59}$$

$$\left(\frac{\partial^2\theta}{\partial\eta^2}\right) + Pr\, f\left(\frac{\partial\theta}{\partial\eta}\right) = -Pr\left(\frac{u_e^2}{c_p T_e}\right)\left(\frac{d^2f}{d\eta^2}\right)^2 + 2s\, Pr\left(\frac{df}{d\eta}\right)\left(\frac{\partial\theta}{\partial s}\right) - 2s\, Pr\, Q_n D_n (Y_c^2/\theta)\exp(-E_n/RT_e\theta) \tag{60}$$

$$\left(\frac{\partial^2 Y_c}{\partial\eta^2}\right) + Sc\, f\left(\frac{\partial Y_c}{\partial\eta}\right) = 2s\, Sc\left(\frac{df}{d\eta}\right)\left(\frac{\partial Y_c}{\partial s}\right) + 2s\, Sc\, D_n (Y_c^2/\theta)\exp(-E_n/RT_e\theta) \tag{61}$$

Here Y_c has been normalized by its value in the external flow $(Y_c)_e$. The symbol Q_n stands for $(qY_{c,e}/c_pT_e)$, and D_n represents $(AL\,\xi_e Y_{c,e}/u_e)$. The boundary conditions (46) to (48) become

$$f(0) = \frac{df(0)}{d\eta} = 0 \quad , \quad \lim_{\eta\to\infty}\left(\frac{df}{d\eta}\right) = 1 \tag{62}$$

$$\theta(s\,0) = \theta_w \quad , \quad \lim_{\eta\to\infty}\theta(s,\eta) = 1 \tag{63}$$

$$\left[\partial Y_c/\partial y\right]_{y=0} = 0 \quad , \quad \lim_{\eta\to\infty} Y_c(s,\eta) = 1 \tag{64}$$

The initial profiles, as discussed earlier, will be taken as the solution of the following equations

$$\left(\frac{d^2\theta}{d\eta^2}\right) + Pr\, f\left(\frac{d\theta}{d\eta}\right) = -Pr\left(\frac{u_e^2}{c_p T_e}\right)\left(\frac{d^2f}{d\eta^2}\right)^2 \tag{65}$$

$$\left(\frac{d^2 Y_c}{d\eta^2}\right) + Sc\, f\left(\frac{dY_c}{d\eta}\right) = 0 \tag{66}$$

subject to the boundary conditions stated in equations (63) and (64). These profiles can be easily shown to be

$$\theta = \theta_w + (d\theta/d\eta)_w \int_0^{\eta} d\eta' \exp\left(-Pr \int_0^{\eta'} f(\eta'')\, d\eta''\right) - Pr\,(u_e^2/c_p T_e) \int_0^{\eta} d\eta' \left[\exp\left(-Pr \int_0^{\eta'} f(\eta'')\, d\eta''\right) \times \int_0^{\eta'} d\eta'' \,(\partial^2 f/\partial\eta^2)^2 \exp\left(Pr \int_0^{\eta''} f(\eta''')\, d\eta'''\right)\right] \tag{67}$$

with

$$(d\theta/d\eta)_w = \left\{-\theta_w + 1 + Pr\,(u_e^2/c_p T_e) \times \int_0^{\infty} d\eta \left[\exp\left(-Pr \int_0^{\eta} f(\eta')\, d\eta'\right) \int_0^{\eta} d\eta' \,(\partial^2 f/\partial\eta^2)^2 \times \exp\left(Pr \int_0^{\eta'} f(\eta'')\, d\eta''\right)\right]\right\} \Big/ \left[\int_0^{\infty} d\eta \exp\left(-Pr \times \int_0^{\eta} f(\eta')\, d\eta'\right)\right]$$

and

$$Y_c = 1 \tag{68}$$

A numerical procedure is discussed in Section A-II-2 for solving equations (60) and (61) with initial conditions given in equations (67) and (68) and subject to the boundary conditions of equations (63) and (64).

A-II-2. Method of Solution.

Numerical integration of equation (60) and (61) subject to the initial profiles given in equations (67) and (68) and the boundary conditions stated in equations (63) and (64) was done by using a slight modification of the scheme described in Section A-I-2.

The partial differential equations (60) and (61) are first put individually into a form of difference-differential or an ordinary differential equation in η by substituting a three point formula for the first derivatives with respect to s. For example, we write

$$\left(\frac{\partial\theta}{\partial s}\right)_{i,j} = \left(\frac{1}{2h_i}\right)\left[\theta_{i-2,j} - 4\,\theta_{i-1,j} + 3\,\theta_{i,j}\right] \tag{69}$$

Here h_1 stands for the step size in the s-direction, and the subscripts i, j represent the mesh points in the s- and η-directions respectively. From equation (69), it is evident that we need to know the solution at two s-stations before proceeding to the next one. To start step by step integration in the s-direction, we will, therefore, initially use a two point formula with half of the regular step size ($h_1' = h_1/2$). Thus, we have

$$\left(\frac{\partial\theta}{\partial s}\right)_{i,j} = \left(\frac{1}{h_1'}\right)\left(\theta_{i,j} - \theta_{i-1,j}\right) \qquad (70)$$

After having obtained a solution at an s-station next to the initial one, we go back to equation (69) for further calculations. The difference-differential equations in η are then solved at each s-station by using the procedure described in Section A-I-2. Equations (60) and (61), after transformation into ordinary differential equations with respect to η, also linearization of the non-linear terms, and replacement of the η derivatives by central difference formulae, become

$$\begin{aligned}
&-\left(1-\tfrac{1}{2}h_2\,Sc\,f_{(i,j)}\right)Y_{c(i,j-1)}^{(k+1)} + \left\{2 + 3(i-1)h_2^2\,Sc\,(df/d\eta)_{(i,j)}\right.\\
&+ 4(i-1)h_1h_2^2\,Sc\,D_n\left[Y_{c(i,j)}^{(k)}/\theta_{(i,j)}^{(k)}\right]\exp\left[-E_a/RT_e\,\theta_{(i,j)}^{(k)}\right]\Big\}Y_{c(i,j)}^{(k+1)}\\
&-\left(1+\tfrac{1}{2}h_2\,Sc\,f_{(i,j)}\right)Y_{c(i,j+1)}^{(k+1)}\\
&= (i-1)h_2^2\,Sc\,(df/d\eta)_{(i,j)}\left[4\,Y_{c(i-1,j)} - Y_{c(i-2,j)}\right]\\
&\quad + 2(i-1)\,h_1h_2^2\,Sc\,D_n\left[\left(Y_{c(i,j)}^{(k)}\right)^2/\theta_{(i,j)}^{(k)}\right]\\
&\quad\times\exp\left(-E_a/RT_e\,\theta_{(i,j)}^{(k)}\right) \qquad (71)
\end{aligned}$$

and

$$\begin{aligned}
&-\left(1-\tfrac{1}{2}h_2\,Pr\,f_{(i,j)}\right)\theta_{(i,j-1)}^{(k+1)} + \left\{2 + 3(i-1)h_2^2\,Pr\,(df/d\eta)_{(i,j)}\right.\\
&- 2(i-1)h_1h_2^2\,Pr\,Q_n\,D_n\left[Y_{c(i,j)}^{(k+1)}/\theta_{(i,j)}^{(k)}\right]^2\left[1+E_a/RT_e\,\theta_{(i,j)}^{(k)}\right]\\
&\left.\times\exp\left[-E_a/RT_e\,\theta_{(i,j)}^{(k)}\right]\right\}\theta_{(i,j)}^{(k+1)} - \left(1+\tfrac{1}{2}h_2\,Pr\,f_{(i,j)}\right)\theta_{(i,j+1)}^{(k+1)}\\
&= h_2^2\,Pr\,(u_e^2/c_pT_e)\left[(d^2f/d\eta^2)_{(i,j)}\right]^2\\
&\quad + (i-1)h_2^2\,Pr\,(df/d\eta)_{(i,j)}\left[4\,\theta_{(i-1,j)} - \theta_{(i-2,j)}\right]\\
&\quad - 2(i-1)h_1h_2^2\,Pr\,Q_n\,D_n\left[\left(Y_{c(i,j)}^{(k+1)}\right)^2/\theta_{(i,j)}^{(k)}\right]\\
&\quad\times\left[-2+E_a/RT_e\,\theta_{(i,j)}^{(k)}\right]\exp\left[-E_a/RT_e\,\theta_{(i,j)}^{(k)}\right] \qquad (72)
\end{aligned}$$

Here the superscript k refers to the number of iterations, and δ_2 denotes the step size in the η-direction. Note that in making use of equation (69), we include the iterative index k only as $\theta^{(k+1)}_{(i,j)}$ because all the other quantities have presumably been determined by the previous calculations.

The initial profiles given in equations (67) and (68) for θ and Y_C were determined by using extended Simpson's rule for the integrations. A choice of an initial value of $s, s_i = 0.02$ was arbitrarily made. We first solved equation (71) by the use of 'line-inversion' procedure to obtain a profile for Y_C at the next s-station. This new profile of Y_C was then utilized in the solution of equation (72). These values of Y_C and θ were used in the next step of the iteration to determine new values at this same s-station. This procedure was repeated until a prescribed convergence, 1 in 10^4, was achieved for certain values of successive iterations. This gave us the final profiles at the station next to s_i. By making use of these results, we can then proceed another step in the s-direction, and perform the same iteration at that position. Eventually all stations of interest are covered. The step-size in the η-direction was kept fixed at 0.10, while that in s-direction varied from 0.1 to 0.01. Near the ignition point, the smaller step-size in the s-direction was needed for better convergence especially for the case of the laminar mixing problem.

A-II-3. Results and Discussion

The calculations were done for a mixture of propane and air at 1 atmosphere pressure. Earlier estimates for Pr, Sc and Q_n were used (see Section A-I-3). Later, some arbitrary variations of these numbers were also considered in order to find their effect on the location of the ignition point. Since Myers and Bartle's[16] correlations of their experimental data on the oxidation of propane indicate different behavior above and below $T = 1250^{\circ}K$ we have, unlike the stagnation point flow case, added the two second order Arrhenius rate terms obtained from these correlations in order to get a continuous chemical source term. Thus, in equations (60) and (61), we replace $D_n \exp(-E_a/RT_e\theta)$ by $[D_{n,1}\exp(-E_{a,1}/RT_e\theta) + D_{n,2}\exp(-E_{a,2}/RT_e\theta)]$ where $E_{a,1} = 17.01$ kcal/mole, $E_{a,2} = 31.29$ kcal/mole, $D_{n,1} = (A_1 L \rho_e Y_{c,e}/\mu_e)$, with $A_1 \simeq 10^{10}$ cm^3/gm-sec, and $D_{n,2} = (A_2 L \rho_e Y_{c,e}/\mu_e)$, with $A_2 \simeq 3^1 \times 10^{13}$ cm^3/gm sec. The above combined expression possesses correct asymptotic behavior, and excepting for the neighborhood of the transition temperature, it gives values in each region which are in close agreement with the ones obtainable from the relevant individual term. Note that this manipulation is necessary even when the temperature of the flat plate is less than $1250^{\circ}K$ because when we go beyond the ignition point, the temperature of the gas begins to be higher than that of the flat plate.

The detailed results of a solution of equations (60), (61), (63), (64), (67), and (68), describing the temperature and the reactant mass fraction profiles over a flat plate, are shown in Figures 8a and 8b when $\theta_w = 3.50$. The specific values for the dimensionless quantities Pr, Sc, Q_n, $D_{n,1}$, $D_{n,2}$ and $(u_e^2/c_p T_e)$, used in the above calculations are respectively 0.75, 1.32, 8.84, 3×10^3, 9×10^6, and 0.025 (or, see line 8 of Table II). It is to be noted that as the value of s increases, the temperature profile is modified due to chemical reaction such that the temperature gradient at the wall increases from a negative value to a positive one. In order to make a more accurate determination of the ignition point, that is, the location of zero heat transfer condition we have also shown the variation of θ_w with s in Figure 9. For the above mentioned data, we find that ignition occurs at $s_{ig} = 0.373$ when $\theta_w = 3.50$. For $s > s_{ig}$, note that the heat is transferred from the reacting mixture to the body, and that the temperature maximum moves in the direction toward the free stream. Furthermore, as the numerical solution is continued beyond the ignition point, the temperature gradient in the s-direction starts increasing. For example, it was found that when $\theta_w = 3.50$, the second derivative of temperature in s-direction became larger than that in η-direction (both evaluated at $s = 0.66$ and $\eta = 0.1$) by a factor of three. The boundary layer equations are then clearly invalid. The numerical procedure also breaks down because of a lack of convergence between different iterates.

The effect on the location of the ignition point due to different values of Sc, L, u_e, and θ_w has also been determined, and some of the results are summarized in Table II. The numbers in the last column refer to an approximate analysis which is discussed at the end of this section. The temperature as well as the reactant mass fraction profiles for different values of θ_w are similar to those shown in Figures 8a and 8b where $\theta_w = 3.50$ except that the corresponding similar features of these profiles are now observed at lower or higher values of s depending on whether the value of θ_w is respectively greater or smaller than 3.50. Since $(u_e^2/c_p T_e)$ is very small compared to unity especially for lower velocities, it is evident from equations (60) and (61) that as long as the ratio (u_e/L) is kept constant, the ignition point (s_{ig}) for the same value of θ_w also remains unaltered, and furthermore, if we increase the velocity of the external stream (u_e) by a certain factor, the ignition distance (s_{ig}) also gets increased by almost the same factor. These facts are supported by the numerical results of Table II. Note that a minor change in temperature (θ_w) leads to a much bigger change in the ignition distance (s_{ig}) and that the variations in the value of Sc do not alter the ignition distance substantially. Finally, it is expected that, for a fixed value of T_w and u_e, the distance of the ignition point from the leading edge (x_{ig}) should remain independent of the length L as long as $x_{ig} < L$. The slight discrepancy between the numerical results given in Table II is due to the fact that s_{ig} [or, $(Y_{c,w}/Y_{c,e})_{s=s_{ig}}$] has been determined, as stated earlier, from a graphical plot of the type given in Figure 9.

Table II

θ_w	L (cm)	u_e (cm/sec)	(Sc/Pr)	$(Y_{c,w}/Y_{c,e})_{s=s_{ig}}$	s_{ig}	$(s_{ig})_{appr.}$
2.00	10	10^2	1.76	0.912	0.94	1 (=1.28)
3.00	5	10^3	1.76	0.818	0.322	0.333
	10	10^3	1.76	0.828	0.158	0.166
	10	2×10^3	1.76	0.818	0.322	0.333
	10	2×10^3	1.00	0.872	0.294	
	10	2×10^3	0.88	0.882	0.288	
	10	6×10^3	1.76	0.818	0.966	0.998
3.50	8	8.84×10^3	1.76	0.771	0.373	0.332
	8	8.84×10^3	1.00	0.838	0.327	
	8	1.768×10^4	1.76	0.772	0.727	0.663
	10	2×10^4	1.76	0.774	0.65	0.601
	10	2×10^4	1.00	0.842	0.575	
	10	2×10^4	0.88	0.853	0.563	
	10	3×10^4	1.76	0.78	0.925	0.901
4.00	10	3×10^4	1.76	0.727	0.255	0.204

A-III. The Wake Flow.

If ignition does not occur at the stagnation point or on the lateral surfaces of the projectile, there is a possibility of it occurring in the wake on account of a larger residence time for the same fluid elements due to recirculation. These elements may undergo almost complete combustion. Furthermore, the flow in this region is usually turbulent. However, due to lack of information about the transport properties of a turbulent mixture as well as the complexities involved in the description of a bluff-body wake flow pattern, we employ a simplified flow model of the Marble and Adamson[20] type to describe the ignition of the incoming cold combustible mixture by the hot products of combustion which are considered to have accumulated in the base region as the first event in the ignition process. This analysis will determine whether an ignition process that may have started in the base region of a projectile results in the flame spreading to the surrounding combustible mixture. Marble and Adamson[20] assumed uniform initial velocities and initial temperatures for the two streams, the cold combustible mixture and the already-burned hot gas, which were considered to flow adjacent and parallel to each other after the point of contact. Using boundary layer approximation, they did an extensive study of the problem by using a regular perturbation method. Later, Cheng and Kovitz[21], and Cheng and Chiu[22] considered the effect of non-uniform velocity and temperature profiles by developing suitable series expansions. These solutions are good in the neighborhood of the point of contact and the numerical results were given for a first order Arrhenius rate law. As in the case of the flat plate approximation, we will obtain numerical solutions of the steady non-similar boundary layer equations describing the mixing for various values of the external uniform conditions. However, the initial profiles for the two streams at the point of contact need not be uniform.

A-III-1. Governing equations.

Under the simplifying assumptions described in Section A-I-2, the flow in the mixing zone [see Figure 7(b)] is again described by equations (41) to (45) but with modified boundary conditions. Let U_u and U_r, respectively, denote the uniform velocities of the unreacted and the reacted streams outside the mixing zone. Then the boundary conditions on the x-component of velocity are

$$\lim_{y\to-\infty} u(x,y) = U_r \quad , \quad \lim_{y\to+\infty} u(x,y) = U_u \qquad (73)$$

Unlike the flat plate case (Sec. A-II-2), the y-component of velocity is not known a priori anywhere in the flow field. An additional physical condition which determines uniquely the orientation of the wake was first suggested by von Kármán. It states

that there must not be any resultant force on a 'free' wake in the direction normal to the main flow. Thus, according to von Kármán, we have [33]

$$(\rho_u U_u) \lim_{y \to +\infty} v(x,y) = -(\rho_r U_r) \lim_{y \to -\infty} v(x,y) \qquad (74)$$

where ρ_u and ρ_r, respectively, denote the uniform densities of the unreacted mixture and the hot combustion products outside the mixing zone. The boundary conditions for the temperature field and the reactant mass fraction are easily specified in terms of the values outside the wake, that is, the uniform temperature of the hot combustion products (T_r), the uniform temperature (T_u), and the reactant mass fraction ($Y_{c,e}^r$) of the unreacted mixture. Thus

$$\lim_{y \to -\infty} T(x,y) = T_r \quad , \quad \lim_{y \to +\infty} T(x,y) = T_u \qquad (75)$$

$$\lim_{y \to -\infty} Y_c(x,y) = 0 \quad , \quad \lim_{y \to +\infty} Y_c(x,y) = Y_{c,e} \qquad (76)$$

Besides, we must specify suitable initial prodiles for u, T, and Y_c. Here again, we will follow the prescription discussed previously for the case of a flat plate (Section A-II-2). In other words, we begin integration at a station which is slightly away from the point of contact and up to which no significant chemical reaction has occurred. Thus, we use non-reacting similar profiles as our initial conditions, and, consequently, our solution is not necessarily restricted to the case of uniform conditions of the two streams at the point of contact.

Before proceeding any further with the solution of these equations, it should be noted that the third boundary condition for the momentum equation, that is, equation (74), is rather cumbersome to use. However, it has been shown that this boundary condition is unessential and can be accounted for by making use of the transposition theorem of Prandtl [19,23]. Thus, if we introduce the following new independent variables

$$\bar{x} = x \quad , \quad \bar{y} = y + g(x) \qquad (77)$$

and the dependent quantities

$$\left.\begin{aligned}
&\bar{\rho}(\bar{x},\bar{y}) = \rho(x,y)\ ,\quad \bar{u}(\bar{x},\bar{y}) = u(x,y)\\
&\bar{v}(\bar{x},\bar{y}) = v(x,y) + (dg/dx)\,\bar{u}(\bar{x},\bar{y})\\
&\qquad\qquad = v(x,y) + (dg/dx)\,u(x,y)\\
&\bar{T}(\bar{x},\bar{y}) = T(x,y)\\
&\bar{Y}_c(\bar{x},\bar{y}) = Y_c(x,y)
\end{aligned}\right\} \qquad (78)$$

we find that equations (41) to (45) remain invariant. Note that amongst the dependent quantities, it is only the y-component of velocity which changes due to the transformation defined by equation (77). Regarding the boundary conditions, we find that equations (73), (75), and (76) remain unaltered while equation (74) becomes

$$\left(\frac{dg}{dx}\right) = \frac{\lim_{\bar{y}\to\infty} \bar{v}(\bar{x},\bar{y}) + (\rho_r U_r/\rho_u U_u) \lim_{\bar{y}\to-\infty} \bar{v}(\bar{x},\bar{y})}{U_u + (\rho_r U_r/\rho_u U_u)\, U_r} \qquad (79)$$

In order to keep the origin of coordinates fixed, we set $g(0) = 0$. Due to the above invariance of the boundary layer equations, we can now arbitrarily impose a convenient boundary condition on the y-component of velocity, say,

$$\bar{v}(\bar{x}, \bar{y}=0) = 0 \qquad (80)$$

The above choice implies that the streamline through origin coincides with $\bar{x}$-axis. After having obtained a solution using equation (80), we can, if necessary, go back to the physical variables y and v(x,y) by means of equation (79).

Since the governing equations for the mixing zone in $(\bar{x},\bar{y})$ plane are identical to those for the flat plate case in (x,y) plane, we can put them into the forms given in equations (59) to (61) by incorporating all the relevant simplifying assumptions, and by applying the transformations defined in equations (49) to (52) after having replaced (x,y) by $(\bar{x},\bar{y})$ as well as all the variables referring to the external stream by those corresponding to the unreacted mixture. In the present analysis, it is again reasonable to work with a similar solution of the momentum equation. The boundary conditions given in equations (73), (75), (76), and (80) become

$$\lim_{\bar{\eta}\to-\infty}\left(\frac{d\bar{f}}{d\bar{\eta}}\right) = \lambda\ ,\quad \bar{f}(0) = 0\ ,\quad \lim_{\bar{\eta}\to+\infty}\left(\frac{d\bar{f}}{d\bar{\eta}}\right) = 1 \qquad (81)$$

$$\lim_{\bar{\eta}\to-\infty} \bar{\theta}(s,\bar{\eta}) = \theta_r \quad , \quad \lim_{\bar{\eta}\to+\infty} \bar{\theta}(s,\bar{\eta}) = 1 \tag{82}$$

$$\lim_{\bar{\eta}\to-\infty} Y_c(s,\bar{\eta}) = 0 \quad , \quad \lim_{\bar{\eta}\to+\infty} Y_c(s,\bar{\eta}) = 1 \tag{83}$$

Here $\lambda \equiv (U_r/U_u)$, $\theta_r \equiv (T_r/T_u)$, and the reactant mass fraction has been normalized by its value $(Y_{c,e})$ as $\bar{\eta}\to+\infty$.

The initial profiles for $\bar{\theta}$ and $\bar{Y}_c$ given by the solutions of equations (65) and (66) subject to the boundary conditions, equations (82) and (83), respectively, are

$$\begin{aligned}
\bar{\theta}(\bar{\eta}) &= 1 + Pr\,(u_e^2/c_pT_e)\int_{\bar{\eta}}^{\infty} d\eta' \left\{ \exp\left(-Pr\int_0^{\eta'} \bar{f}(\eta'')d\eta''\right) \right. \\
&\quad \left. \times \left[\int_0^{\eta'} d\eta'' \left(d^2\bar{f}/d\eta''^2\right)^2 \exp\left(Pr\int_0^{\eta''} \bar{f}(\eta''')d\eta'''\right)\right]\right\} \\
&\quad - \left(d\bar{\theta}/d\bar{\eta}\right)_{\bar{\eta}=0} \int_{\bar{\eta}}^{\infty} d\eta' \exp\left(-Pr\int_0^{\eta'} \bar{f}(\eta')d\eta''\right) \\
&\qquad\qquad \text{for} \quad 0 < \bar{\eta} \le +\infty \\
&= \theta_r - Pr\,(u_e^2/c_pT_e)\int_{-\infty}^{\bar{\eta}} d\eta' \left\{ \exp\left(-Pr\int_0^{\eta'} \bar{f}(\eta'')d\eta''\right) \right. \\
&\quad \left. \times \left[\int_0^{\eta'} d\eta'' \left(d^2\bar{f}/d\eta''^2\right)^2 \exp\left(Pr\int_0^{\eta''} \bar{f}(\eta''')d\eta'''\right)\right]\right\} \\
&\quad + \left(d\bar{\theta}/d\bar{\eta}\right)_{\bar{\eta}=0} \int_{-\infty}^{\bar{\eta}} d\eta' \exp\left(-Pr\int_0^{\eta'} \bar{f}(\eta'')d\eta''\right) \\
&\qquad\qquad \text{for} \quad -\infty \le \bar{\eta} < 0
\end{aligned} \tag{84}$$

where

$$\begin{aligned}
\left(d\bar{\theta}/d\bar{\eta}\right)_{\bar{\eta}=0} &= \left\{ 1 - \theta_r + Pr\,(u_e^2/c_pT_e)\int_{-\infty}^{\infty} d\bar{\eta}\left[\exp\left(-Pr\right.\right.\right. \\
&\quad \left.\left.\left. \times \int_0^{\bar{\eta}} \bar{f}(\eta')d\eta'\right)\int_0^{\bar{\eta}} d\eta' \left(d^2\bar{f}/d\eta'^2\right)^2 \exp\left(Pr\right.\right.\right. \\
&\quad \left.\left.\left. \times \int_0^{\eta'} \bar{f}(\eta'')d\eta''\right)\right]\right\} \Big/ \left[\int_{-\infty}^{\infty} d\bar{\eta} \exp\left(-Pr\int_0^{\bar{\eta}} \bar{f}(\eta')d\eta'\right)\right]
\end{aligned}$$

And

$$\bar{Y}_c(\bar{\eta}) = 1 - (d\bar{Y}_c/d\bar{\eta})_{\bar{\eta}=0} \int_{\bar{\eta}}^{\infty} d\eta' \exp\left(-Sc \int_0^{\eta'} \bar{f}(\eta'')\, d\eta''\right) \qquad 0 < \bar{\eta} \leq \infty$$

$$= (d\bar{Y}_c/d\bar{\eta})_{\bar{\eta}=0} \int_{-\infty}^{\bar{\eta}} d\eta' \exp\left(-Sc \int_0^{\eta'} \bar{f}(\eta'')\, d\eta''\right) \qquad -\infty \leq \bar{\eta} < 0 \qquad (85)$$

where

$$(d\bar{Y}_c/d\bar{\eta})_{\bar{\eta}=0} = \left[\int_{-\infty}^{\infty} d\bar{\eta} \exp\left(-Sc \int_0^{\bar{\eta}} \bar{f}(\eta')\, d\eta'\right)\right]^{-1}$$

The critical distance (S_{cr}) for flame stabilization is now determined from a solution of equations (59) to (61) subjected to their respective boundary conditions given by equations (81) to (83) and the appropriate initial profiles of equations (84) and (85). The details of the numerical procedure employed are described in the following section.

A-III-2. Method of solution.

Note that, after appropriate changes of notation, equations (71) and (72) are equally valid for the laminar mixing problem, and it is also true of the numerical scheme described in Section A-II-2. Moreover, even though some numerical solutions of equation (59) when subjected to the boundary conditions given by equations (81) are available in the literature (see, for example, Reference 23) we obtained profiles of $\bar{f}$, $(d\bar{f}/d\bar{\eta})$, and $(d^2\bar{f}/d\bar{\eta}^2)$ by using the present scheme which, unlike the other calculations, allows easily to make use of any simple choice for a value of λ. Again, the initial profiles given in equations (84) and (85) for $\bar{\theta}$ and $\bar{Y}_c$ were determined by using extended Simpson's rule for the integrations.

A-III-3. Results.

The velocity profiles resulting from solutions of equations (59) and (81) are shown in Figure 10 when λ = 0.01, 0.25, and 0.50. Solutions to the equations (60), (61), and (82) to (85), which describe the planar laminar mixing of the combustible gas with the hot combustion products, were obtained for different values of Sc, L', λ and θ_r. The temperature and the reactant

mass fraction profiles for $\lambda = 0.25$ and $\theta_r = 5.0$ are shown in Figures 11a and 11b. Here we used the same values for the dimensionless constants as in the case of Figure 3a and 3b. The occurrence of ignition is identified with the first appearance of a local temperature maximum. Like the flat plate case, the profiles for the other input data are similar, and the dependence of the ignition distance on different external conditions is summarized in Table III. The ignition distance is, again, a sensitive function of the temperature ratio (θ_r) and has a weaker dependence on the changes in λ. Unlike the flat plate case, the ignition distance is changed considerably by the variations in the value of Sc. This is not surprising because in this case the rate of heat transfer to the ignitable mixture depends on the mixing rate for the reactants and the hot products. Due to the presence of an additional variable λ, the previous observations in connection with the dependence of s_{ig} on u_e and (u_e/L'), which were made for the flat plate case, are no longer valid.

Table III

θ_w	L' (cm)	U_r (cm/sec)	U_u (cm/sec)	(Sc/Pr)	s_{ig}	$(s_{ig})_{appr.}$
3.00	5	10	25	1.76	0.30	0.32
			50	1.76	0.52	0.55
				1.00	0.16	
				0.88	0.12	
			10^2	1.76	0.94	>1 (=1.01)
	10	10	50	1.76	0.25	0.275
			10^2		0.46	0.505
3.50	5	10	10^2	1.76	0.22	0.219
			2×10^2		0.40	0.417
			4×10^2		0.78	0.815
	10	10	2×10^2	1.76	0.20	0.209
4.00	5	2.5×10^2	5×10^2	1.76	0.43	0.404
				1.00	0.155	
				0.88	0.12	
			10^3	1.76	0.74	0.673
			1.25×10^3	1.76	0.86	0.808
5.00	8	2.21×10^3	8.84×10^3	1.76	0.58	0.573
		4.42×10^3			0.67	0.659
6.00	8	2.21×10^3	8.84×10^3	1.76	0.17	0.156

A-IV. General Discussion and Empirical Correlations.

In order to find the ignitability limit, we determined the maximum velocity at which ignition would occur when the projectile has a temperature T_w (or, T_r of the hot products in the case of the wake) and a length L (or L' of the eddy size in the case of the wake). The numerical procedure was, therefore, repeated thrice by varying u_e for fixed values of θ_w (or θ_r) and L (or L'). Then, from a graphical plot of u_e vs. s_{ij}, we found a value of $(u_e)_{max}$ corresponding to $s_{ij} = 1$ by extrapolation. Proceeding in the same manner for other values of θ_w and L, we obtained the curves shown in Figure 12. For the purpose of comparison, we replotted in Figure 12 some results for ignition at an axisymmetric stagnation point taken from Figure 6 by letting $a = (u_e/R)$, R being the radius of curvature of the front end of the projectile. For the case of the wake, we found that the thickness of the mixing layer starts increasing when λ gets smaller than 0.05. Therefore, to avoid using more computer time, the results for the case when $U_r = 10$ cm/sec and L' = 10 cms were not obtained.

The above calculations indicated, for example, that a projectile of length 5 cm and temperature 900°K would initiate ignition on its lateral surface only if its speed were less than or equal to 3.2×10^3 cm/sec. Also, for the same values of the characteristic length and temperature, the corresponding speeds for ignition at the stagnation point or in the wake are, respectively, 26 cm/sec and 1.05×10^2 cm/sec. In other words, for a projectile at a fixed temperature, a particular value of its speed imposes a condition on the relevant characteristic length in order to ignite the combustible mixture. Furthermore, it should be noted that $(u_e)_{max}$ for the lateral surface is two orders of magnitude bigger than that for the stagnation point. From our choice of L and R, we could have expected as much as one order of magnitude difference. The extra difference can be explained in terms of the heat transfer from the projectile to the gas. The boundary layer thickness near the stagnation point is constant and of the order of $R(Re)^{-\frac{1}{2}}$ where $Re = (\rho_e u_e R/\mu_e)$, while in the case of the flat plate, the boundary layer grows as $\sqrt{x}$. Since the heat transfer is more for a thin boundary layer, it decreases as we go away from the leading edge of the flat plate. Therefore, the total heat transfer over a flat plate of length R could be greater than the heat transfer at the stagnation point having a radius of the nose equal to R. Clearly, this argument holds good when the two flows are studied independently, which is the case in the present analysis. In case of the wake, we note that due to the presence of a finite relative speed and of mixing between the reactant and the hot inert streams, the ignition point lies somewhere in the mixing zone where the magnitudes of the velocity, reactant mass fraction, and temperature do not correspond so closely to the conditions at the hot edge of the layer as in the case of the flat plate where the ignition point lies close to the hot surface.

Neglecting transport effects, we attempt a rough estimate of the location of the ignition point by defining

$$x_{ig} = u' \tau \tag{86}$$

where u' is some characteristic flow velocity of the reacting mixture and τ denotes the chemical reaction time. In other words, the ignition distance is being approximated by the actual distance traversed by a certain fraction (α) of the initial amount of the reactive component in the mixture having a constant temperature (T^*) and a uniform speed (u') in a period of time equal to the ignition delay time evaluated at α and T^*. From equation (58), we may express the reaction time as

$$\begin{aligned} \tau &= (-\rho Y_c / \dot{\omega}_c) = \exp(E_a / R T_e \theta^*) / (\alpha A \rho Y_{c,e}) \\ &= \theta^* \exp(E_a / R T_e \theta^*) / (\alpha A \rho_e Y_{c,e}) \end{aligned} \tag{87}$$

where we have also made use of the ideal gas equation of state, equation (45). Since the ignition criterion is applied at the surface of the flat plate, it is reasonable to choose θ^* equal to θ_w. Therefore, combining equations (86) and (87) we obtain the following expression for the ignition distance on a flat surface,

$$x_{ig} = \beta \theta_w \exp(E_a / R T_e \theta_w) / (\alpha A \rho_e Y_{c,e} / u_e) \tag{88}$$

where β is a suitable fraction of the velocity of the external stream (u_e). Equation (88), when appropriately modified to account for the continuous source term at all temperatures, becomes

$$\begin{aligned} x_{ig} = \theta_w (\beta/\alpha) \Big[&(A_1 \rho_e Y_{c,e} / u_e) \exp(-E_{a,1} / R T_e \theta_w) \\ &+ (A_2 \rho_e Y_{c,e} / u_e) \exp(-E_{a,2} / R T_e \theta_w) \Big]^{-1} \end{aligned} \tag{89}$$

It is difficult to guess a priori any suitable values of α and β except for the fact that α lies closer to unity while β to zero. After making some trial calculations by using the data given in Table II, we found that there were large variations in the value of (β/α) with θ_w. Instead, if we arbitrarily set

$$(\beta/\alpha) = (\theta_w - 1)(\beta'/\alpha') \tag{90}$$

the values of (β'/α') remain nearly the same (within about 30%) for the data used in the earlier calculations. We chose an average value of 0.136 for (β'/α'). We may look upon this value of (β'/α')

as resulting from $\alpha' \simeq 0.74$ and $\beta \simeq 0.1$, which are reasonable numbers at the ignition point. Combining equations (89) and (90), we get

$$x_{ig} = 0.136\, L\, \theta_w (\theta_w - 1) \left[(A_1 L \rho_e Y_{c,e} / u_e) \exp(-E_{a,1}/RT_e\theta_w) + (A_2 L \rho_e Y_{c,e} / u_e) \exp(-E_{a,2}/RT_e\theta_w) \right]^{-1} \quad (91)$$

The results of the approximate calculations based on equation (91) for different cases are given in the last column of Table II. We can conclude that equation (91) describes fairly well the dependence of ignition distance (x_{ig}) on the surface temperature (θ_w) and the velocity of the external stream (u_e) provided, of course, (β/α) is known or guessed correctly. Note that equation (91) does not possess any explicit dependence on the Reynolds number. Except for an estimation of Prandtl number (Pr), we thus never made use of the value of coefficient of viscosity for propane-air mixture in the determination of the ignition distance.

In a similar fashion, we can obtain an expression for the ignition distance in the mixing layer, namely, (see, also Reference 24)

$$x_{ig} = 15.0\, L' \theta_r (\theta_r - 2) \left[(1+\lambda)/2 \right] \left[(A_1 L' \rho_u Y_{c,u} / v_u) \times \exp(-E_{a,1}/RT_v\theta_r) + (A_2 L' \rho_u Y_{c,u} / v_u) \times \exp(-E_{a,2}/RT_v\theta_r) \right]^{-1} \quad (92)$$

Here a suitable value for the constant (β'/α') turns out to be 15.0 which, when split up as $\alpha \simeq 0.05$ and $\beta \simeq 0.75$, corresponds to a reasonable number at the ignition point. The estimates for s_{ig} based on equation (92) are given in the last column of Table III, and the agreement with the numerical results is within about 10%.

References

1. Sharma, O. P. and Sirignano, W. A., 1969, Ignition of Stagnation Point Flow by a Hot Body, Combustion Science and Technology 1, 95-104.

2. Sharma, O. P. and Sirignano, W. A., 1970, "On the Ignition of a Premixed Fuel by a Hot Projectile", Combustion Science and Technology 1, 481-494.

3. Paterson, S., 1940, "The Ignition of Inflammable Gases by Hot Moving Particles, II", Phil. Mag. 30, 487.

4. Mullen, J. W., Fenn, J. B. and Irby, M. R., 1949,"Ignition of High Velocity Streams of Combustible Gases by Heated Cylindrical Rods." Third Symposium on Combustion, Flame, and Explosion Phenomena, 317-329, Williams and Wilkins Co., Baltimore.

5. Adomeit, G., 1965,"Ignition of Gases at Hot Surfaces under Non-steady State Conditions", Tenth Symposium (International) on Combustion, 237-243, The Combustion Institute.

6. Chambré, P. L., 1956,"On the Ignition of a Moving Combustible Gas Stream", J. Chem. Phys. 25, 417-421.

7. Chung, P. M., 1965,"Chemically Reacting Non-Equilibrium Boundary Layers", Advances in Heat Transfer, Academic Press, New York, N. Y., 2, 109.

8. Fay, J. A., and Kaye, H., 1967, "A Finite Difference Solution of Similar Non-Equilibrium Boundary Layers", AIAA Journal, 5, 1949-1954.

9. Radbill, J. R., 1964,"Application of Quasilinearization to Boundary Layer Equations", AIAA Journal, 2, 1860-1864.

10. Libby, P. A. and Chen, K. K., 1966,"Remarks on Quasilinearization Applied in Boundary Layer Calculations", AIAA Journal, 4, 937-939.

11. Wachspress, E. L., 1962,"The Numerical Solution of Boundary Value Problems", Mathematical Methods for Digital Computers, edited by A. Ralston and H. S. Wilf, Vol. I, 121-132, John Wiley and Sons, Inc.

12. Weast, R. C., 1967-68, Handbook of Chemistry and Physics, 48th Edition, The Chemical Rubber Co., Cleveland, Ohio.

13. API, 1966, Technical Data Book - Petroleum Refining, American Petroleum Institute, New York, New York.

14. Penner, S. S., 1957, Chemistry Problems in Jet Propulsion, The Macmillan Company, New York, N. Y.

15. NBS, 1965, 1966, National Bureau of Standards Technical Notes 270-1 and 270-2.

16. Myers, B. F. and Bartle, E. R., 1968,"Reaction Times of Hydrocarbon Oxidation Behind Incident Shock Waves in a Shock Tube, AFAPL-TR-67-152, pp. 1-68. Also, see AIAA Journal 7, 1862-1869 (1969).

17. Dooley, D. A., 1957,"Ignition in the Laminar Boundary Layer of a Heated Plate", Proceedings of the 1957 Heat Transfer and Fluid Mechanics Institute, Stanford University Press, Stanford, California, 321.

18. Toong, Tau-Yi, 1957,"Ignition and Combustion in a Laminar Boundary Layer over a Hot Surface", Sixth Symposium (International) on Combustion, Reinhold Publishing Corporation, New York, N. Y., 532.

19. Rosenhead, L., 1963, Laminar Boundary Layers , Oxford University Press, London, p. 211 and p. 224.

20. Marble, F. E. and Adamson, T. C., Jr., 1954, "Ignition and Combustion in a Laminar Mixing Zone", Jet Propulsion 24, 85.

21. Cheng, S. I. and Kovitz, A. A., 1957, "Ignition in the Laminar Wake of a Flat Plate", Sixth Symposium (International) on Combustion, Reinhold Publishing Corporation, New York, N. Y., 418.

22. Cheng, S. I. and Chiu, H. H., 1961,"Mixing and Chemical Reaction in an Initially Non-Uniform Temperature Field", Int. J. Heat Mass Transfer 1, 280.

23. Napolitano, L. G., 1957, "Critical Study of the Adequacy of Integral Methods in Plane Mixing Problems", AFOSR-TN-57-757, pp. 1-66.

24. Williams, F. A., 1965, Combustion Theory, Addison-Wesley Publishing Co., Inc., Palo Alto, California, 319.

JPR-3:2 R023 69
A

SCHEMATIC DIAGRAM OF THE DIFFERENT FLOW FIELDS AROUND A PROJECTILE

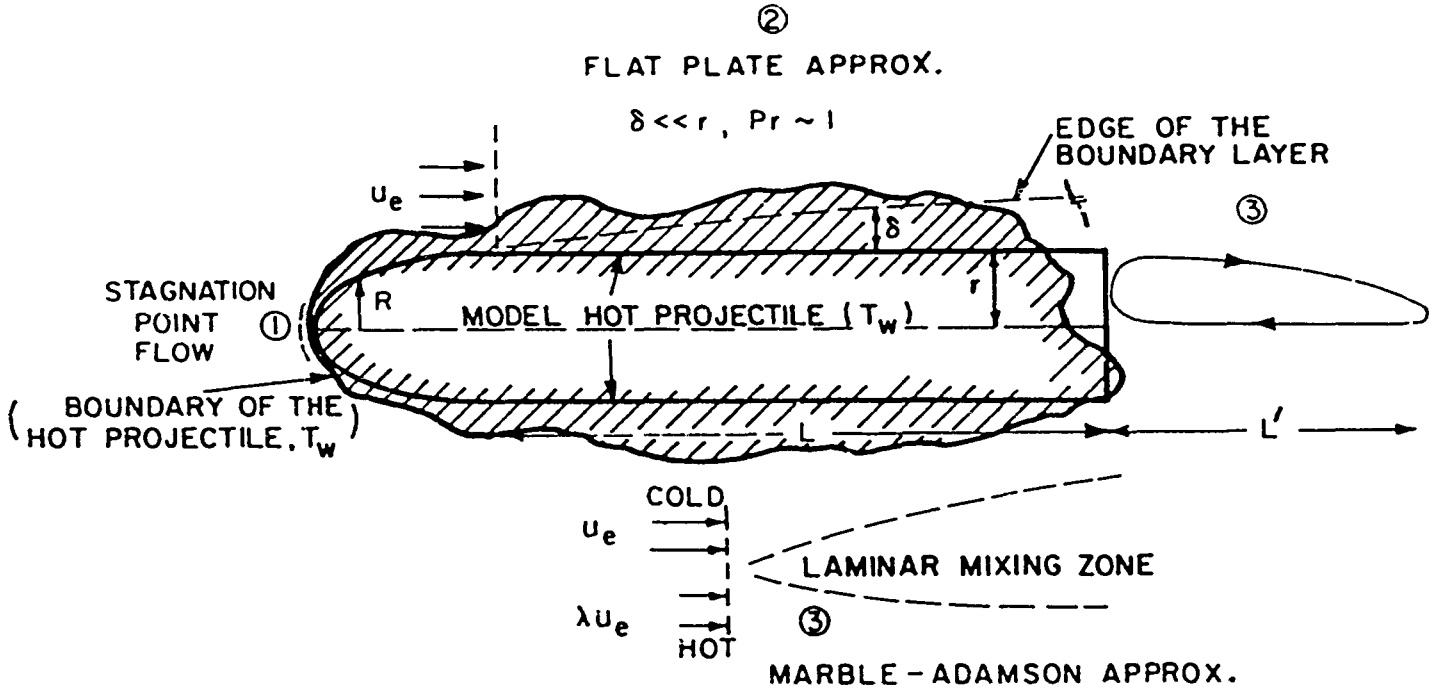

FIGURE 1

COORDINATE SYSTEM

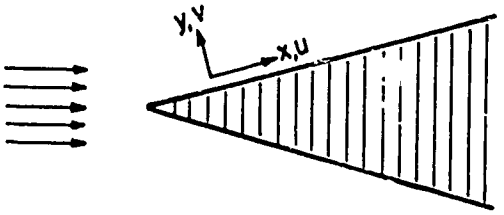

(a) TWO DIMENSIONAL FLOW

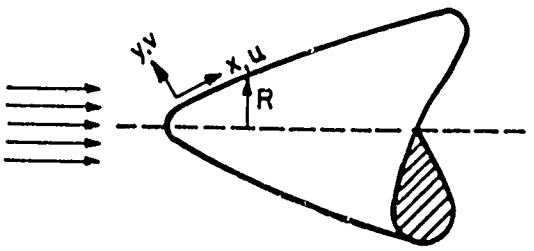

(b) AXISYMMETRIC FLOW

FIGURE 2

TEMPERATURE PROFILES FOR AXISYMMETRIC STAGNATION FLOW WHEN $L_e = 1$

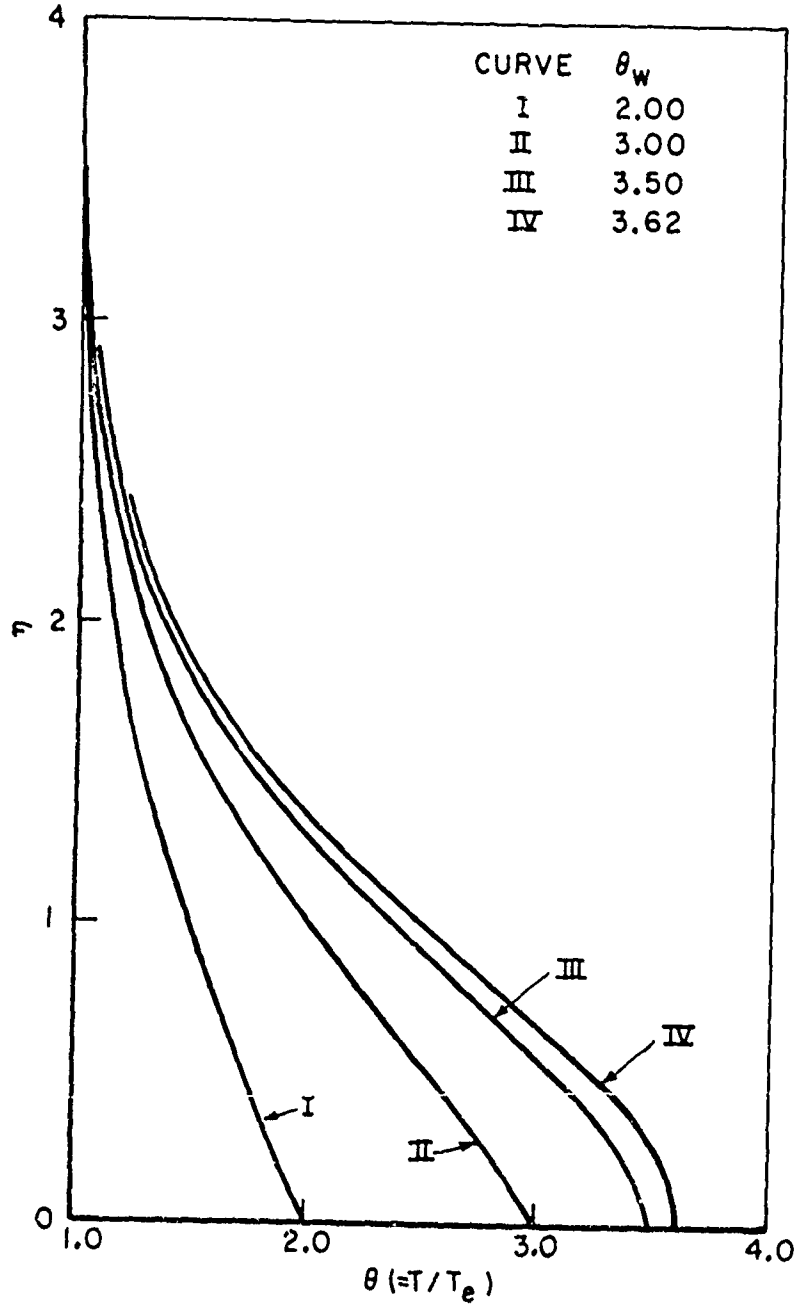

FIGURE 3c

REACTANT MASS FRACTION PROFILES FOR AXISYMMETRIC STAGNATION FLOW WHEN $L_e = 1$

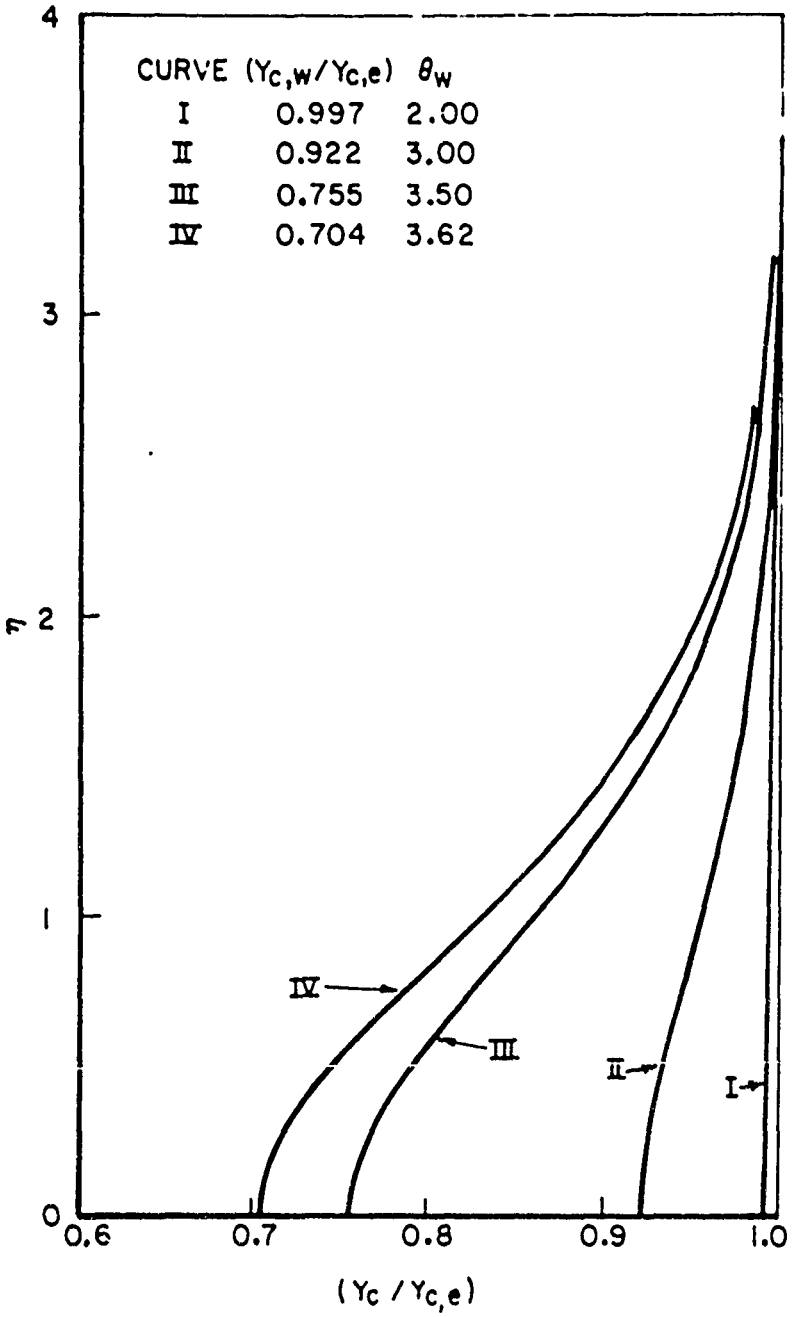

FIGURE 3b

VELOCITY PROFILES FOR AXISYMMETRIC STAGNATION FLOW WHEN $L_e = 1$

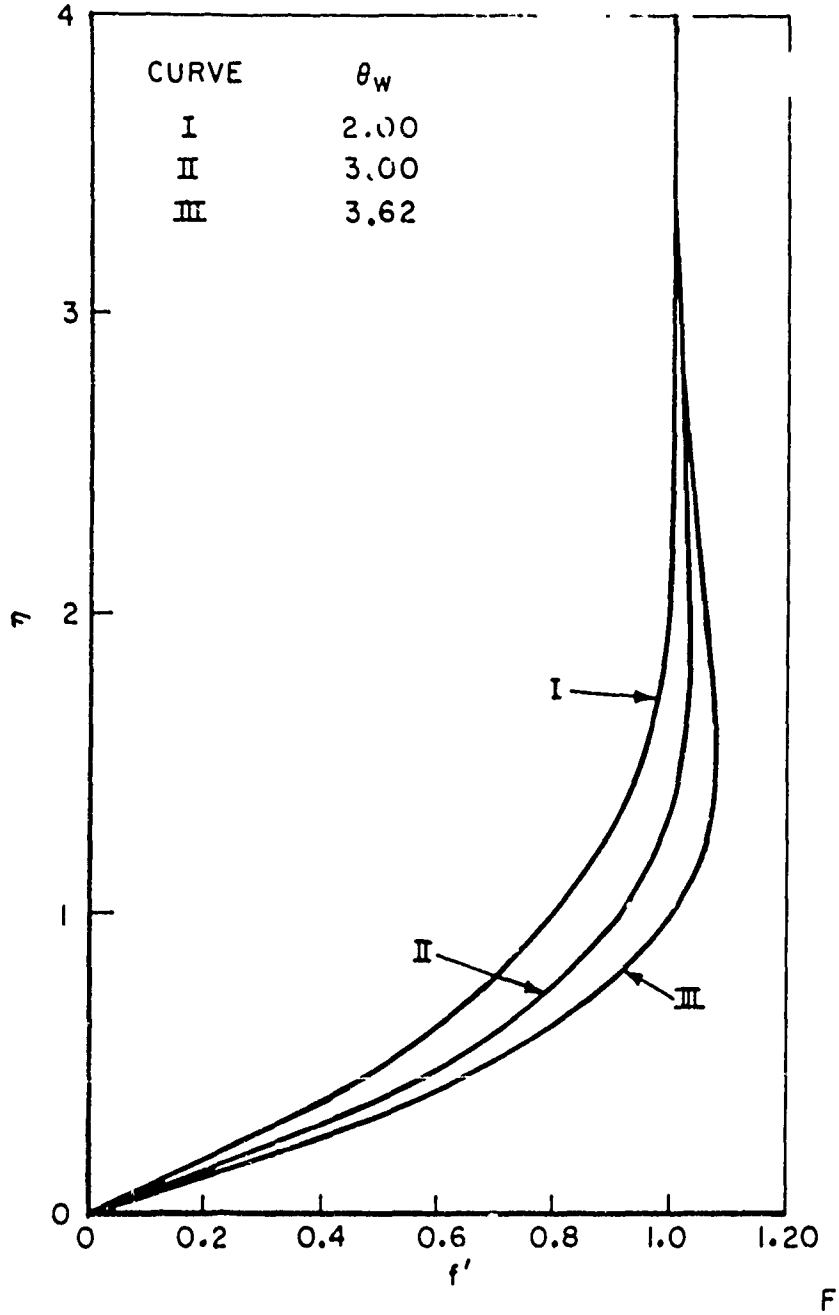

FIGURE 3c

TEMPERATURE PROFILES FOR AXISYMMETRIC STAGNATION FLOW WHEN $L_e = 1.76$

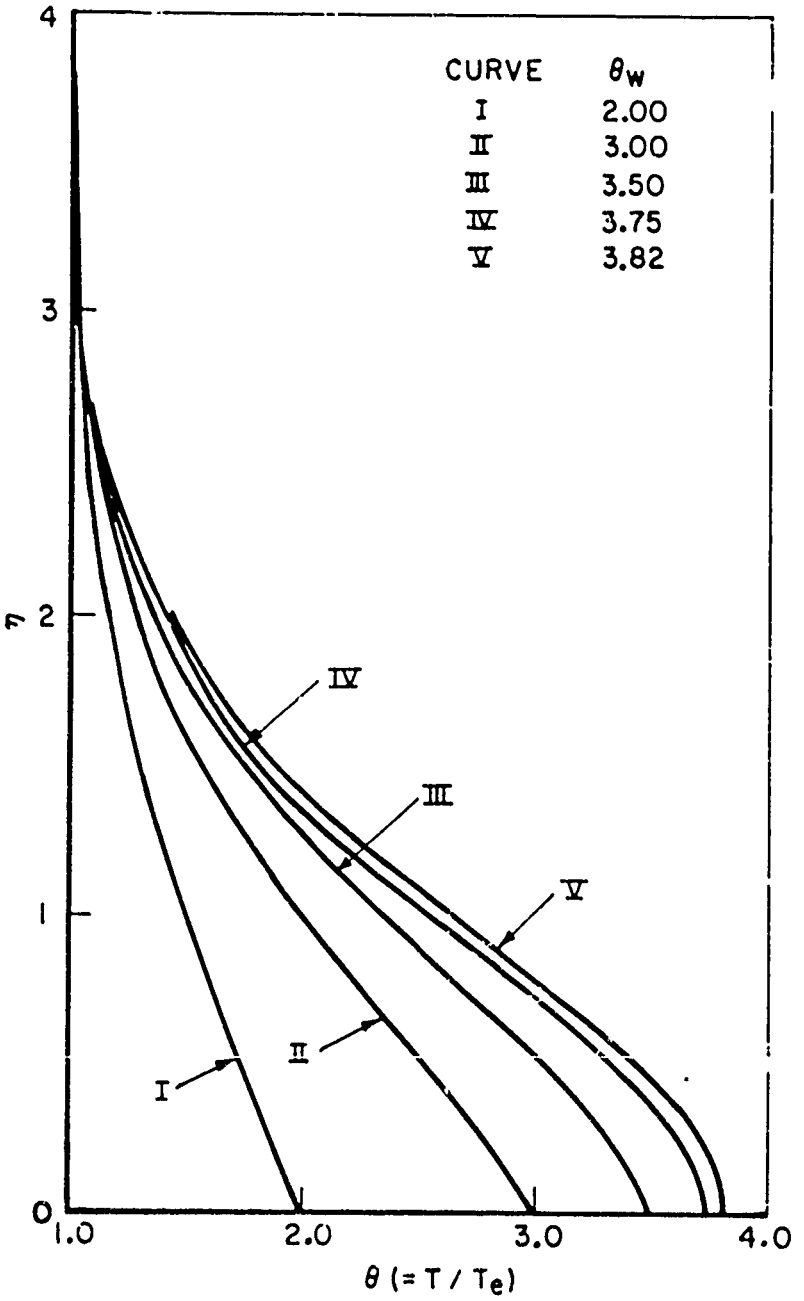

FIGURE 4a

REACTANT MASS FRACTION PROFILES FOR AXISYMMETRIC STAGNATION FLOW WHEN $L_e = 1.76$

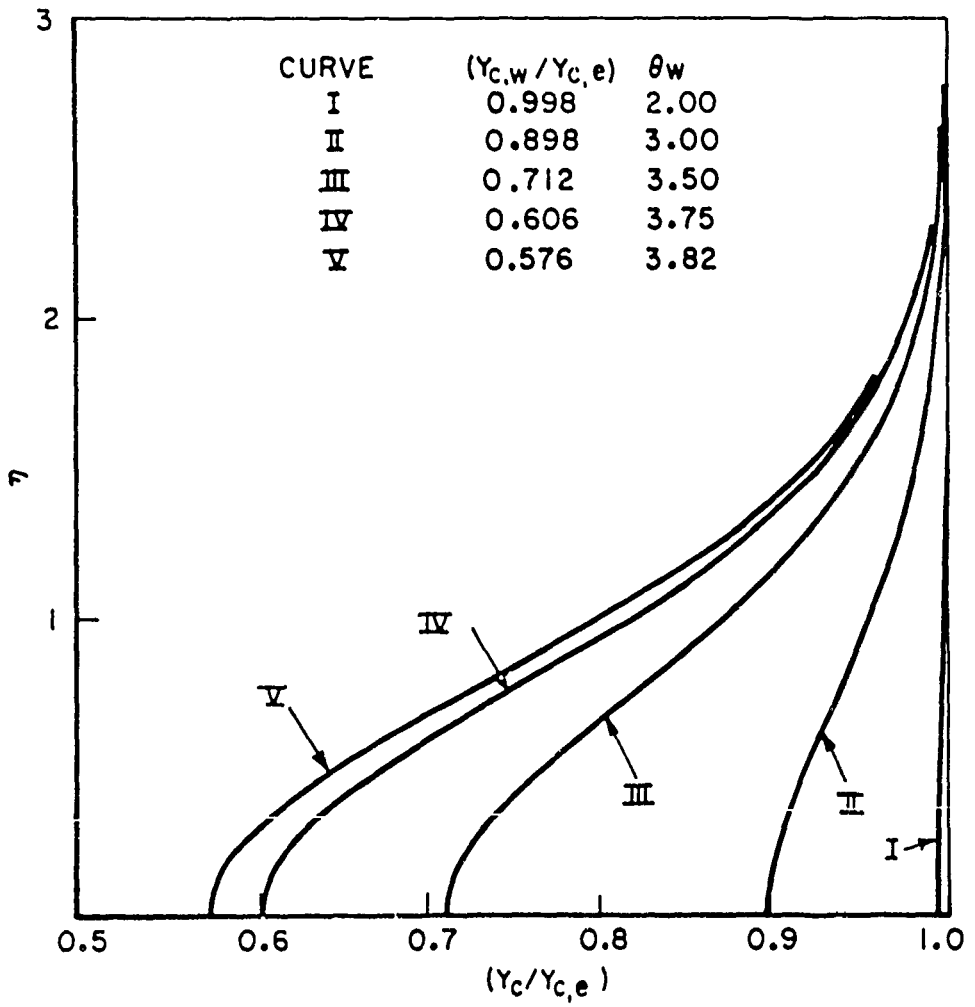

FIGURE 4b

VELOCITY PROFILES FOR AXISYMMETRIC STAGNATION FLOW WHEN $L_e = 1.76$

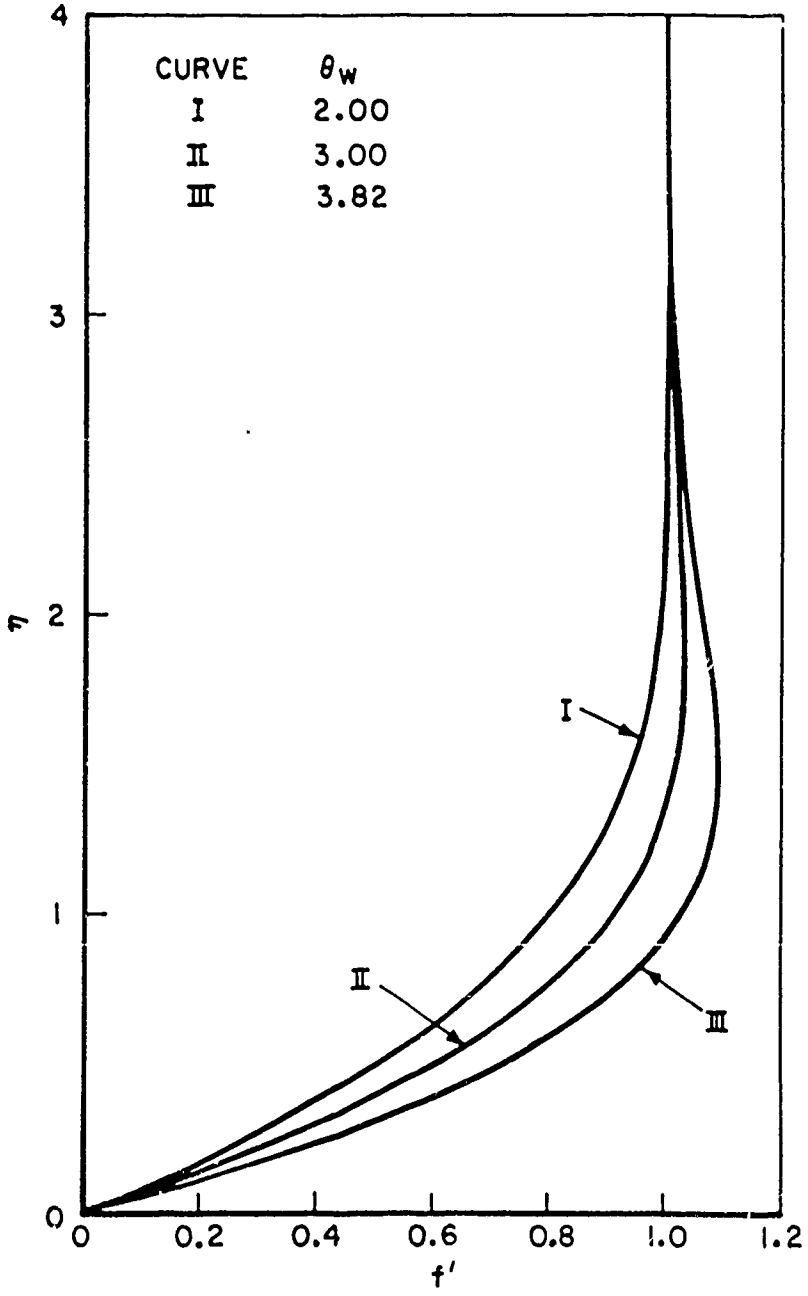

FIGURE 4 c

VARIATION OF TEMPERATURE GRADIENT WITH TEMPERATURE AT THE SURFACE FOR PLANE AND AXISYMMETRIC STAGNATION FLOW

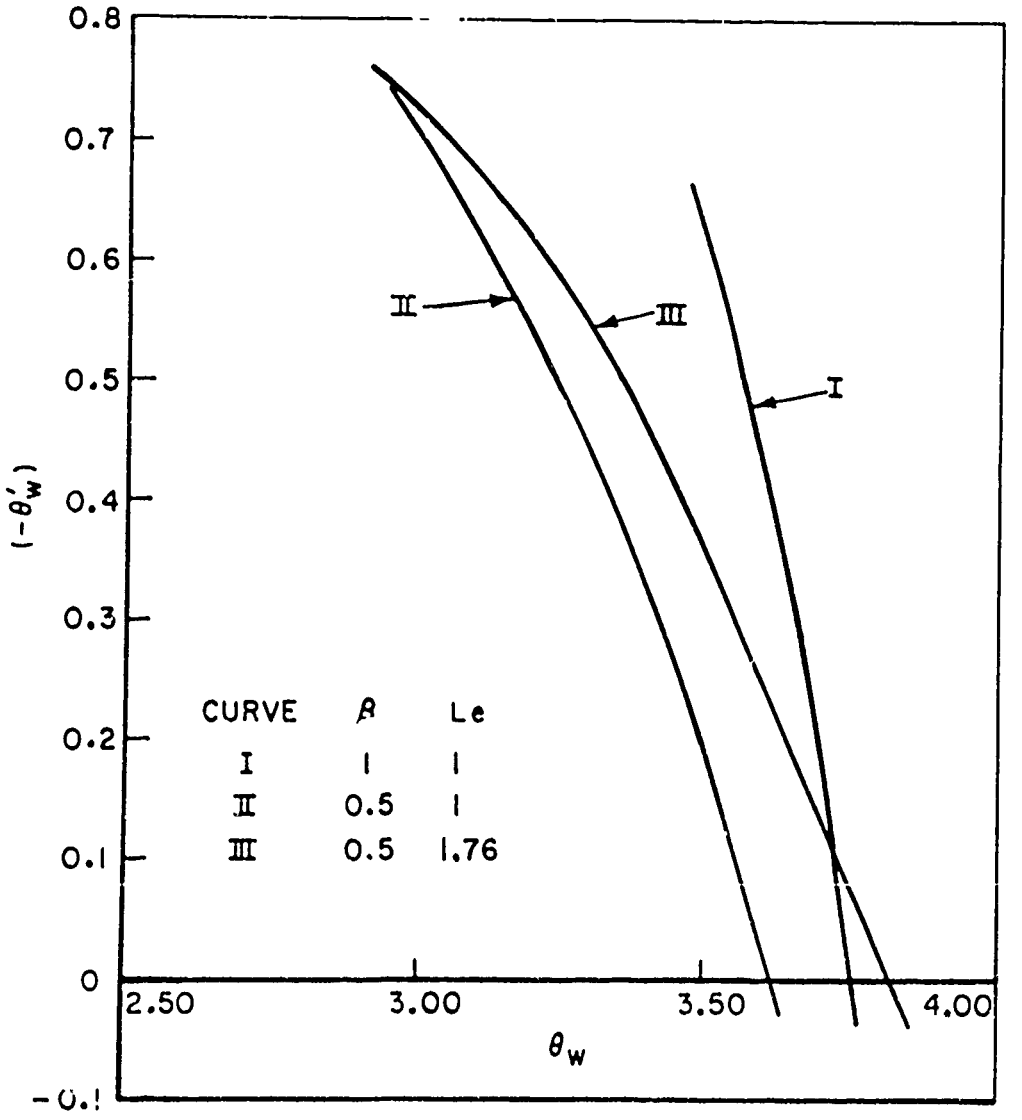

FIGURE 5

VARIATION OF THE WALL VALUE OF THE REACTANT MASS FRACTION AND THE IGNITION TEMPERATURE WITH THE PARAMETER D_n

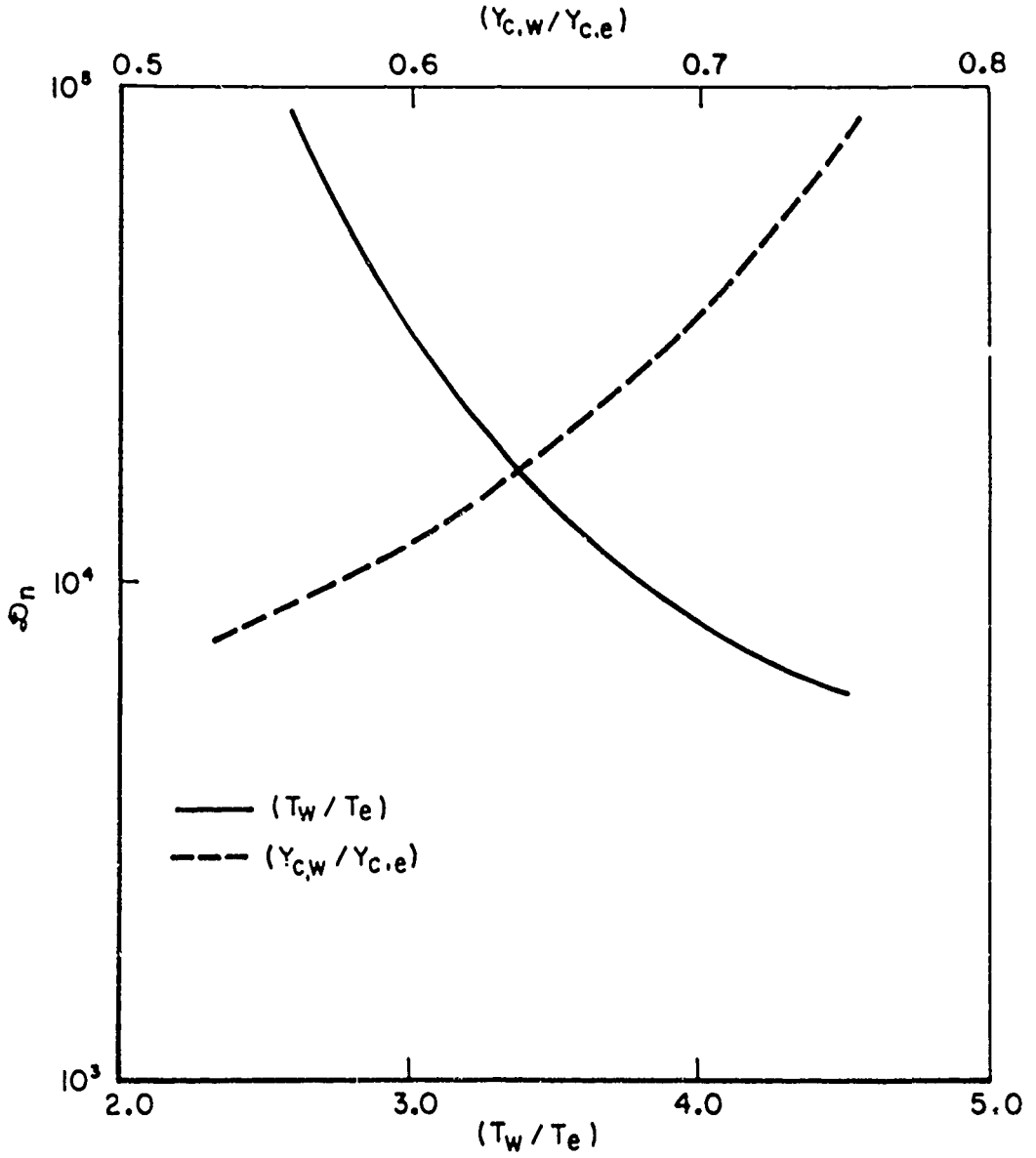

G106 R004, 69

FIGURE 6

COORDINATE SYSTEM

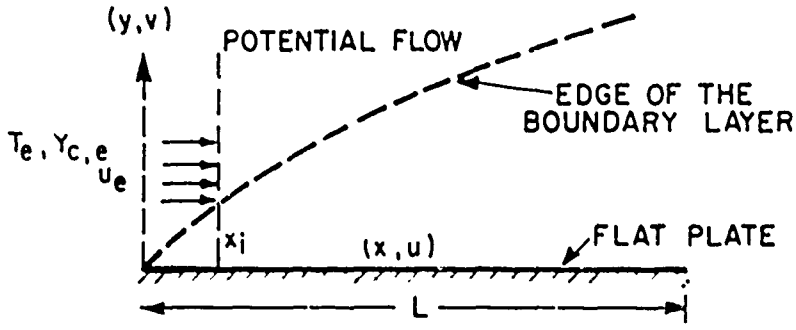

(a) FOR A FLAT PLATE

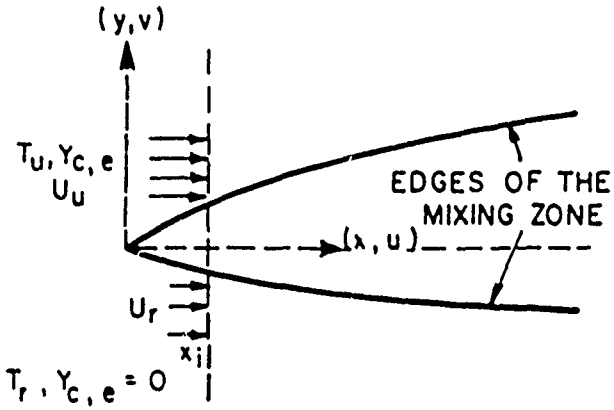

(b) FOR THE MIXING ZONE

FIGURE 7

TEMPERATURE PROFILES AT DIFFERENT POINTS ALONG THE FLAT SURFACE WHEN $\theta_w = 3.50$

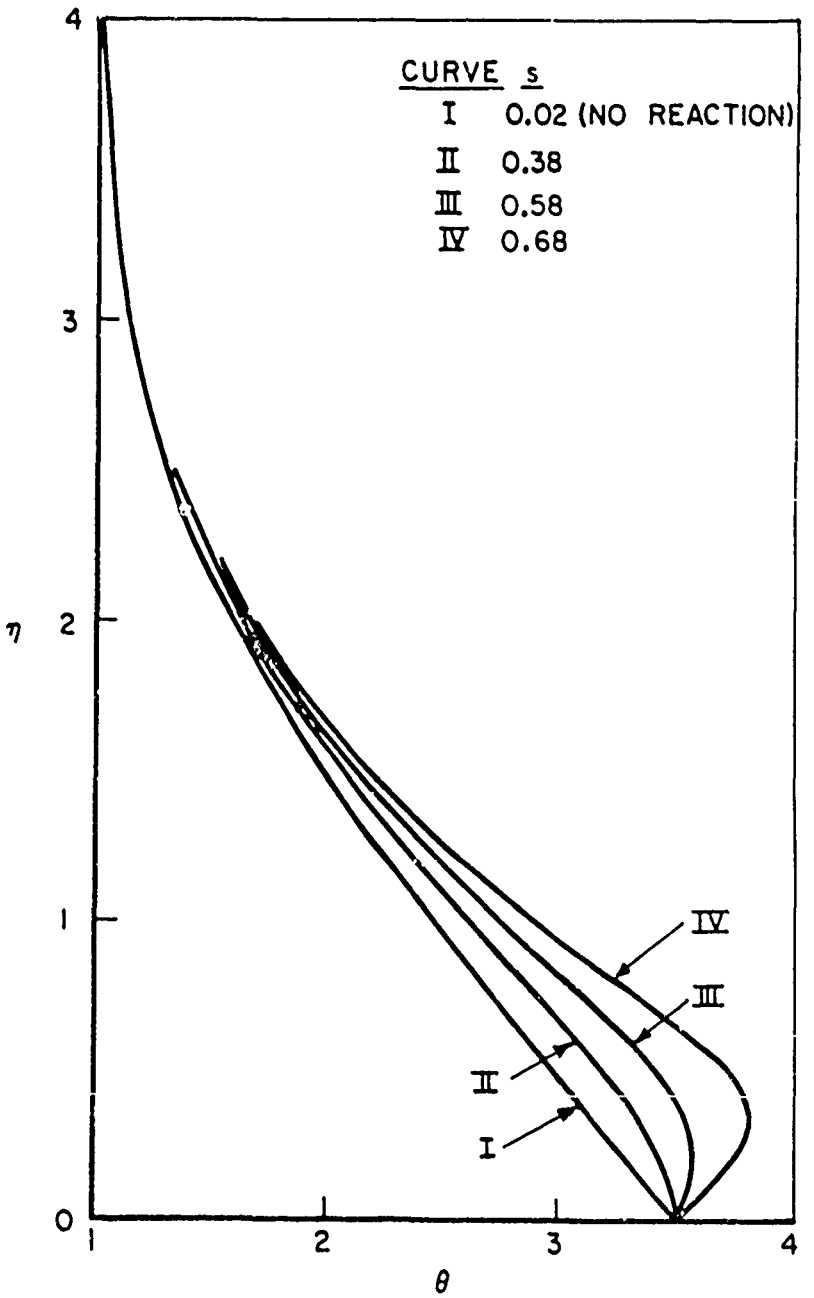

6106 R 013 69

FIGURE 8 a

REACTANT MASS FRACTION PROFILES AT DIFFERENT POINTS ALONG THE FLAT SURFACE WHEN θ_w=3.50

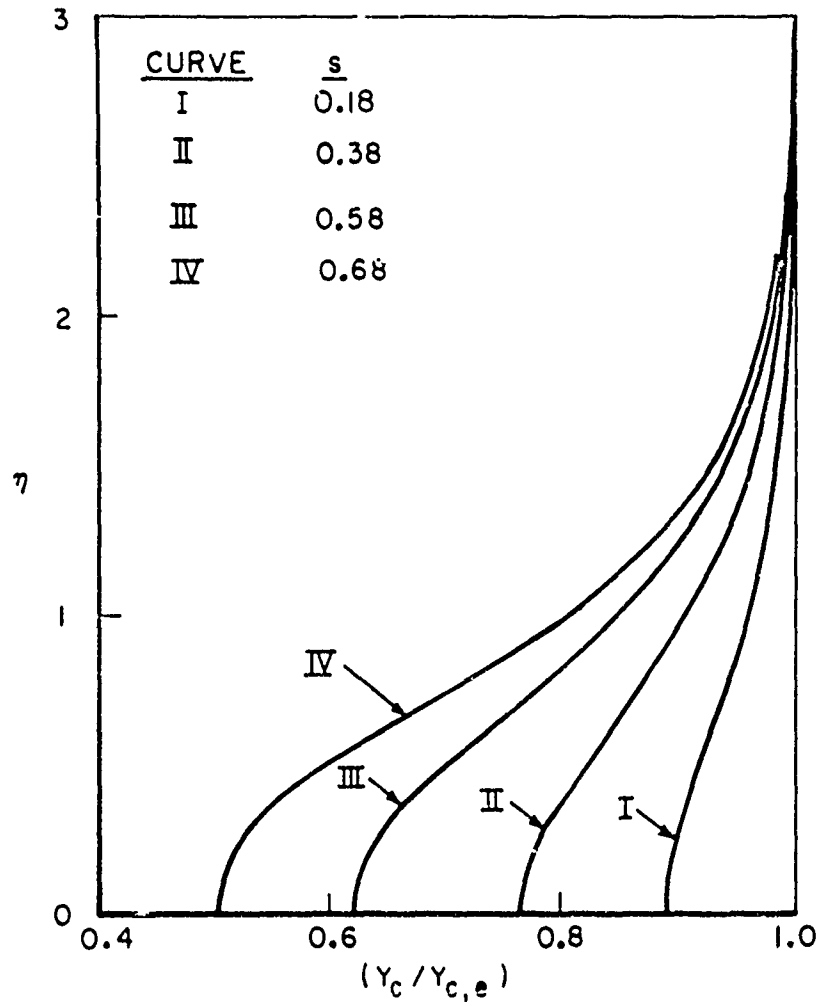

6106 R 014 GY

FIGURE 8b

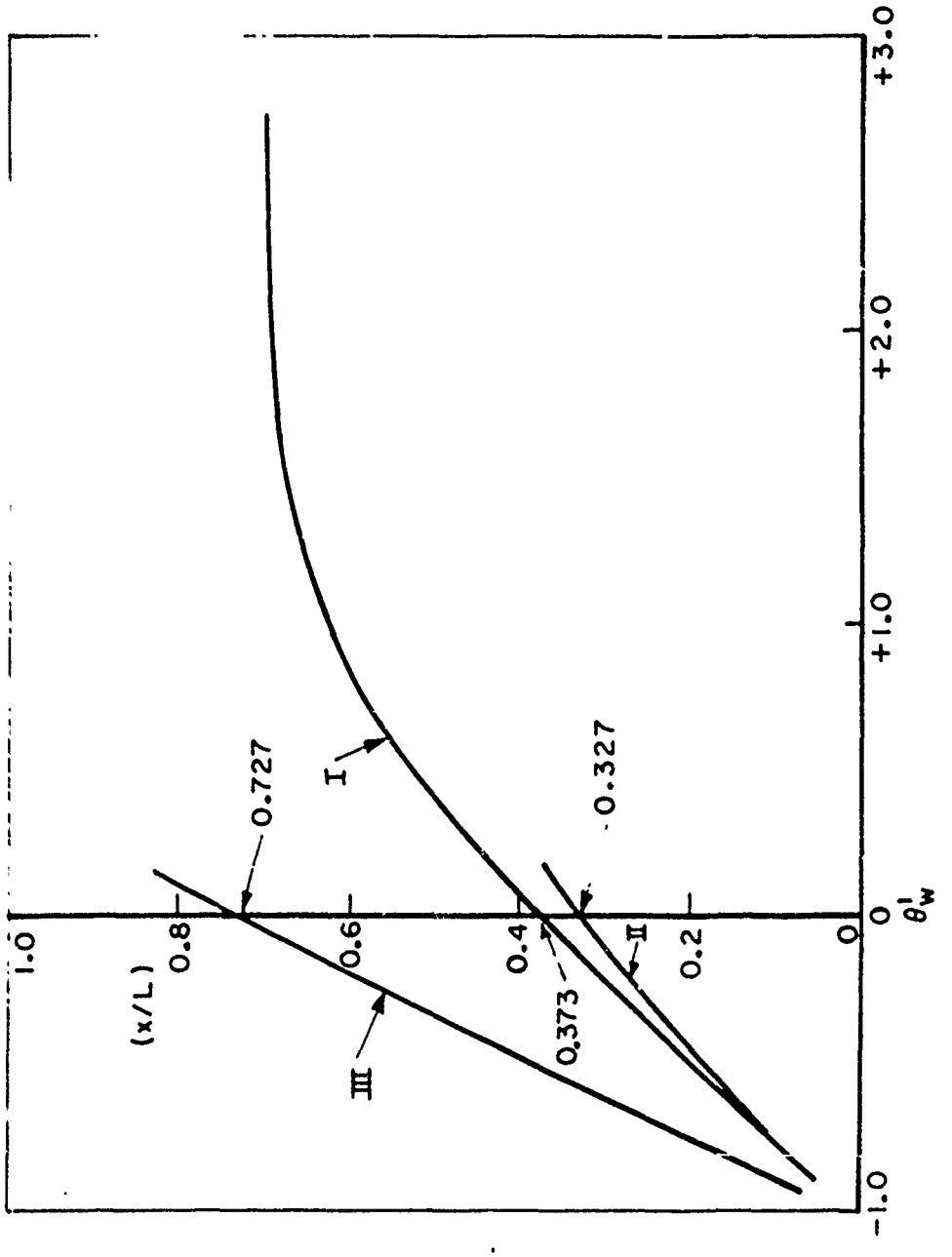

6106 R 015 69

FIGURE 9

VELOCITY PROFILES IN A PLANE LAMINAR MIXING PROBLEM FOR DIFFERENT VALUES OF λ

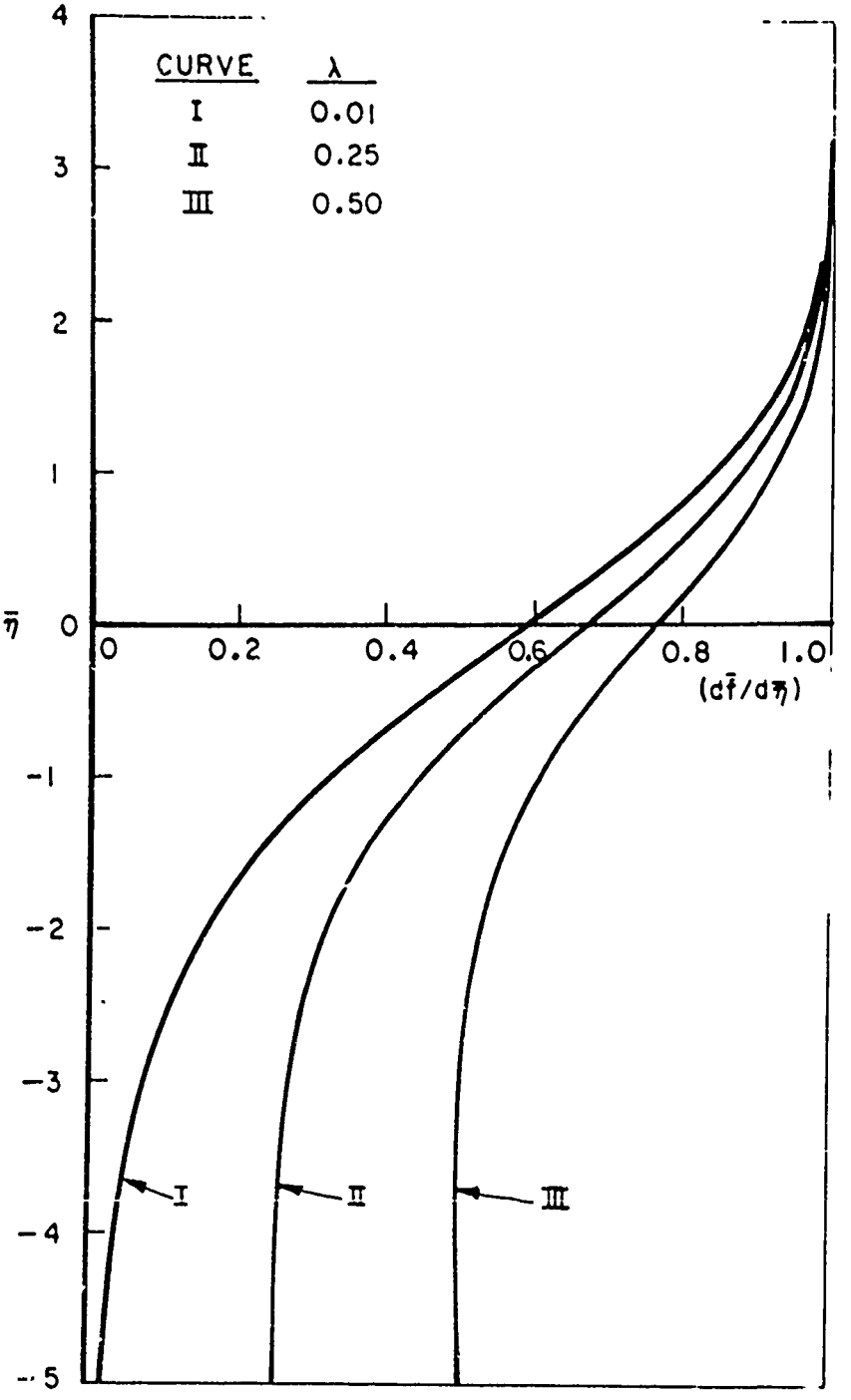

FIGURE 10

DETAILED DEVELOPMENT OF REACTANT MASS FRACTION PROFILES BEFORE FLAME STABILIZATION IN CASE OF A PLANE LAMINAR MIXING PROBLEM WHEN $\lambda=0.25$ AND $\theta_f=5.0$

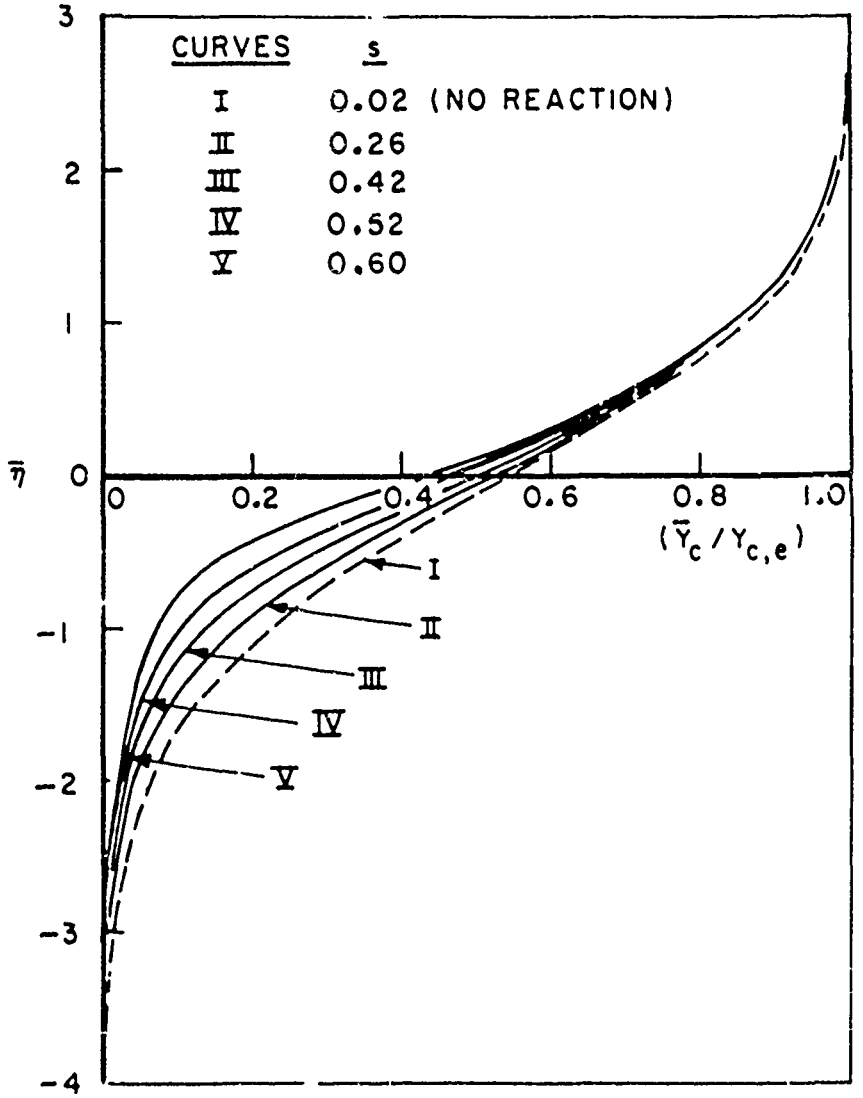

6106 R 017 69

FIGURE II a

DETAILED DEVELOPMENT OF TEMPERATURE PROFILES BEFORE FLAME STABILIZATION IN CASE OF A PLANE LAMINAR MIXING PROBLEM WHEN $\lambda = 0.25$ AND $\theta_r = 5.0$

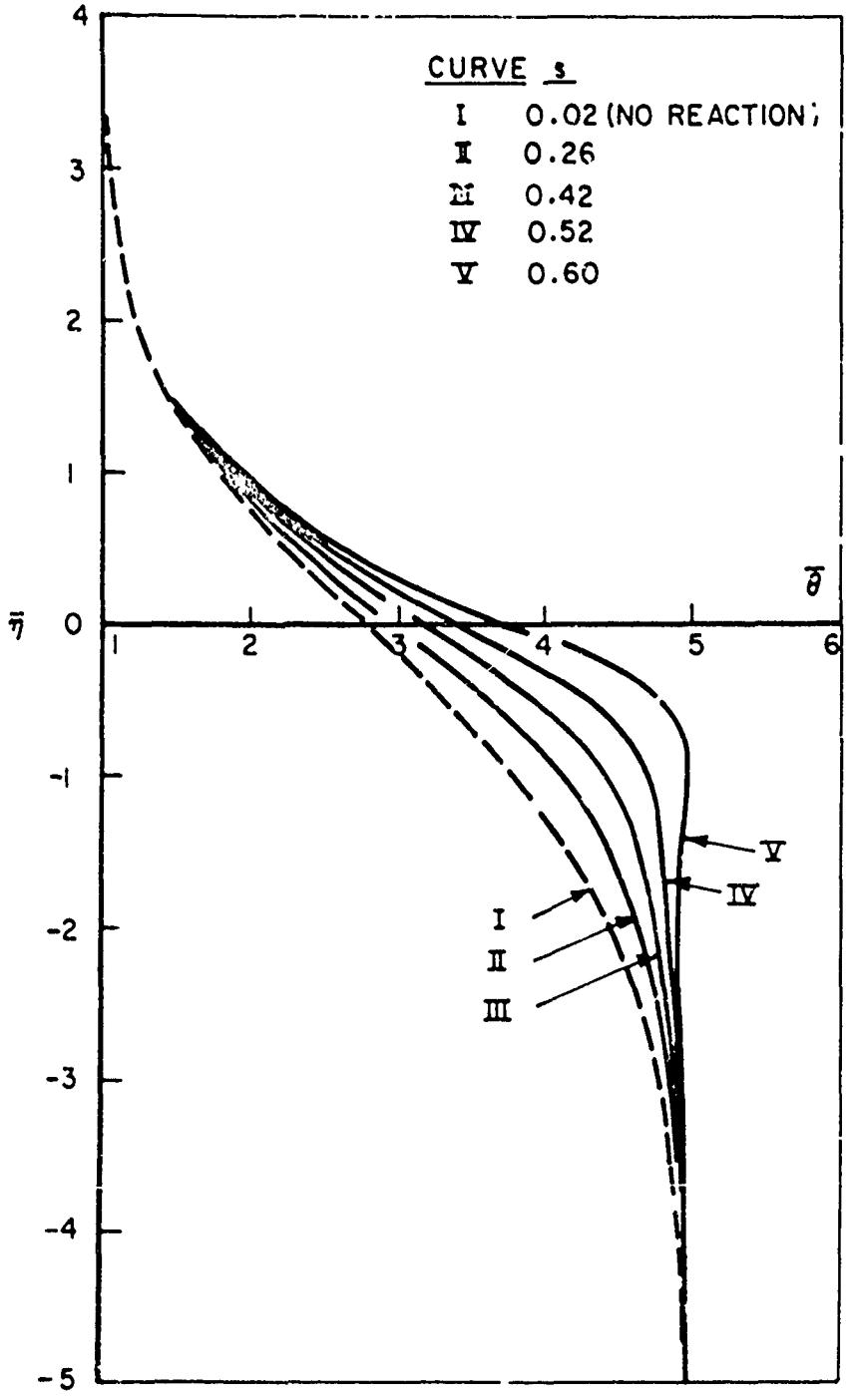

6106 R 018 69

FIGURE 11b

DEPENDENCE OF THE MAXIMUM SPEED OF A PROJECTILE ON ITS TEMPERATURE (T_w) AND ITS LENGTH (L) OR ITS RADIUS OF CURVATURE (R) OR THE CHARACTERISTIC LENGTH OF THE MIXING ZONE (L') WHEN IGNITION TAKES PLACE

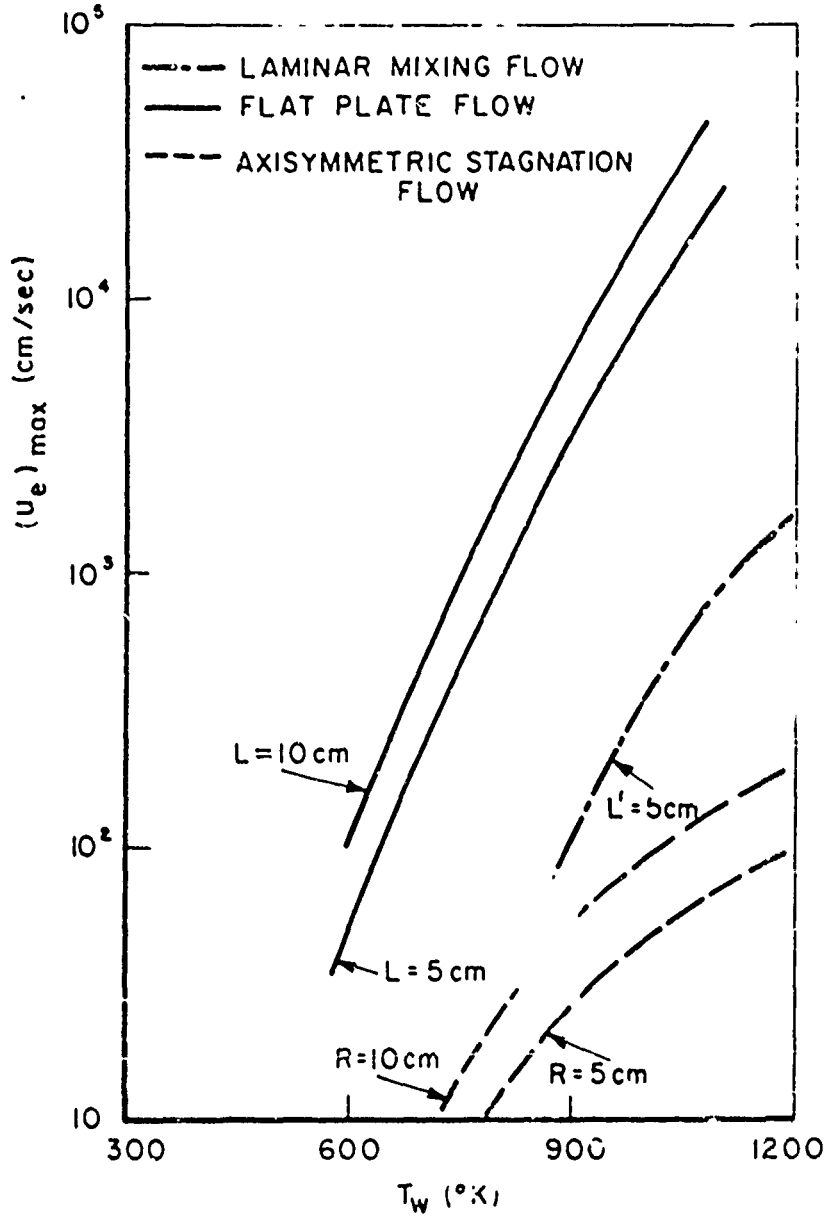

FIGURE 12

B. Ignition By a Hot Inert Gas

During the passage of a hot projectile through the premixed combustible mixture existing above a pool of liquid fuel, ignition occurs under certain circumstances, and, therefore, some hot products are left behind(1,2). The burning will, of course, stop as soon as the premixed mixture is exhausted. But, simultaneously more fuel is being vaporized from the liquid pool by the heat transfer from the hot products, and both oxidizer and fuel vapors diffuse towards each other while raising their temperatures at the same time. The question then arises that under what conditions ignition can take place so that the burning continues.

We have first considered a very simple model consisting of three parallel gaseous streams moving uniformly at the same speed such that the hot inert gas is sandwiched between the oxidizer and the fuel streams. Fixing ourselves on a coordinate system moving with the same velocity as that of the gaseous streams, we are then dealing with a non-convective situation. The diffusion of species and the heat transfer are, respectively, described by the simple Fick's law of diffusion and the Fourier's law of heat conduction (see, for example, reference 3). The ignition delay time will be computed as a function of the initial temperature as well as the width of the hot inert gas stream. Ignition will be said to have taken place when a local temperature maximum or a rapid change in the chemical reaction rate occurs. We will next describe the theoretical analysis of the problem.

We assume that the density (ρ), the specific heat (c_p), and the coefficient of thermal conductivity (k) remain independent of temperature and mixture composition. Let T_i (i = I, II, III) denote the temperature in the oxidizer stream (I), the hot inert region (II), and the fuel zone (III). The mass fraction of the oxidizer, the hot products, and the fuel vapors in regions I, II, and III will be represented by Y_{ij} (i = O, P, F and j = I, II, III) . Let L denote the width of the hot inert stream, and D be the coefficient of binary diffusion. The governing equations are now summarized below.

In region I, $L < x < \infty$,

$$\left.\begin{aligned}
&\left(\frac{\partial T_I}{\partial t}\right) = \kappa \left(\frac{\partial^2 T_I}{\partial x^2}\right) \quad , \quad t > 0 \\
&T_I(0,x) = T_\infty \\
&T_I(t,\infty) = T_\infty \\
&T_I(t,L) = T_{II}(t,L) \\
&\left(\frac{\partial T_I}{\partial x}\right)_{x=L} = \left(\frac{\partial T_{II}}{\partial x}\right)_{x=L}
\end{aligned}\right\} \quad (1)$$

$$\left(\frac{\partial Y_{O,I}}{\partial t}\right) = D\left(\frac{\partial^2 Y_{O,I}}{\partial x^2}\right) \quad , \quad t > 0$$

$$Y_{O,I}(0,x) = 1$$

$$Y_{O,I}(t,\infty) = 1$$

$$Y_{O,I}(t,L) = Y_{O,II}(t,L)$$

$$\left(\frac{\partial Y_{O,I}}{\partial x}\right)_{x=L} = \left(\frac{\partial Y_{O,II}}{\partial x}\right)_{x=L} \qquad (2)$$

In region II, $0 < x < L$,

$$\left(\frac{\partial T_{II}}{\partial t}\right) = \alpha\left(\frac{\partial^2 T_{II}}{\partial x^2}\right) - \left(\frac{1}{\rho C_p}\right)\sum_{i=1}^{3} h_i^c \omega_i \quad , \quad t > 0$$

$$T_{II}(0,x) = T_F$$

$$T_{II}(t,0) = T_{III}(t,0)$$

$$\left(\frac{\partial T_{II}}{\partial x}\right)_{x=0} = \left(\frac{\partial T_{III}}{\partial x}\right)_{x=0} \qquad (3)$$

$$\left(\frac{\partial Y_{O,II}}{\partial t}\right) = D\left(\frac{\partial^2 Y_{O,II}}{\partial x^2}\right) + \left(\frac{\omega_O}{\rho}\right) \quad , \quad t > 0$$

$$Y_{O,II}(0,x) = 0$$

$$Y_{O,II}(t,0) = 0 \qquad (4)$$

$$\left(\frac{\partial Y_{F,II}}{\partial t}\right) = D\left(\frac{\partial^2 Y_{F,II}}{\partial x^2}\right) + \left(\frac{\omega_F}{\rho}\right) \quad , \quad t > 0$$

$$Y_{F,II}(0,x) = 0$$

$$Y_{F,II}(t,L) = 0$$

$$Y_{F,II}(t,0) = Y_{F,III}(t,0)$$

$$\left(\frac{\partial Y_{F,II}}{\partial x}\right)_{x=0} = \left(\frac{\partial Y_{F,III}}{\partial x}\right)_{x=0} \qquad (5)$$

In region III, $-\infty < x < 0$,

$$\left(\frac{\partial T_{III}}{\partial t}\right) = \alpha\left(\frac{\partial^2 T_{III}}{\partial x^2}\right) \quad , \quad t > 0$$

$$T_{III}(0,x) = T_\infty$$

$$T_{III}(t,-\infty) = T_\infty \qquad (6)$$

$$\left(\frac{\partial Y_{F,III}}{\partial t}\right) = D\left(\frac{\partial^2 Y_{F,III}}{\partial x^2}\right) \quad , \quad t > 0$$

$$Y_{F,III}(0,x) = 1$$

$$Y_{F,III}(t,-\infty) = 1 \qquad (7)$$

Here T_∞ denotes the initial temperature of the oxidizer and fuel streams, and T_F is the initial temperature of the hot products. $\kappa = (k/\rho c_p)$ represents the thermal diffusivity of the gases. h_i^c denotes the standard heat of formation of a unit mass of the species i. $\dot{\omega}_i$ is the rate of production of the species i by chemical reaction (mass per unit volume per second).

Introducing non-dimensional coordinates

$$\tau = (\kappa t / L^2) \qquad \text{and} \qquad \xi = (x/L) \tag{8}$$

and, assuming unit Lewis number ($\kappa = D$), we define Schwab-Zeldovich variables [3]

$$\alpha = \left(\frac{Y_F}{\nu_F W_F}\right) - \left(\frac{Y_O}{\nu_O W_O}\right) \tag{9}$$

and

$$\beta = \left(\frac{c_p T}{q}\right) + \left(\frac{Y_O}{\nu_O W_O}\right) \tag{10}$$

where ν_O and ν_F denote, respectively, the stoichiometric coefficients for the oxidizer and the fuel. W_O and W_F are the molecular weights. $q = \sum_i \nu_i W_i h_i^c$ represents the heat released due to the chemical reaction. Since α and β satisfy ordinary heat conduction (or diffusion) equations without any source term and subject to constant initial and boundary conditions, we can easily obtain analytic expressions for them. The results are

$$\alpha(\tau,\eta) = \alpha_1 + \tfrac{1}{2}(\alpha_3-\alpha_2)\,\mathrm{erfc}\left(\frac{\eta}{2\sqrt{\tau}}\right) - \tfrac{1}{2}(\alpha_1-\alpha_2)\,\mathrm{erfc}\left(\frac{\eta-1}{2\sqrt{\tau}}\right)$$
$$\text{for} \quad \infty > \eta > 1 \qquad (11a)$$

$$= \alpha_2 + \tfrac{1}{2}(\alpha_1-\alpha_2)\,\mathrm{erfc}\left(\frac{1-\eta}{2\sqrt{\tau}}\right) + \tfrac{1}{2}(\alpha_3-\alpha_2)\,\mathrm{erfc}\left(\frac{\eta}{2\sqrt{\tau}}\right)$$
$$\text{for} \quad 1 > \eta > 0 \qquad (11b)$$

$$= \alpha_3 + \tfrac{1}{2}(\alpha_1-\alpha_2)\,\mathrm{erfc}\left(\frac{1-\eta}{2\sqrt{\tau}}\right) - \tfrac{1}{2}(\alpha_3-\alpha_2)\,\mathrm{erfc}\left(-\frac{\eta}{2\sqrt{\tau}}\right)$$
$$\text{for} \quad 0 > \eta > -\infty \qquad (11c)$$

where $\alpha_1 = (1/\nu_O W_O)$, $\alpha_2 = 0$, $\alpha_3 = (1/\nu_F W_F)$, and $\mathrm{erfc}(z) = (2/\sqrt{\pi})\int_z^\infty \exp(-z'^2)\,dz'$. The same expressions hold good for $\beta(\tau,\eta)$ when α's are replaced by β's. In this case, $\beta_1 = [(c_p T_\infty/q) + (1/\nu_O W_O)]$, $\beta_2 = (c_p T_F/q)$, and $\beta_3 = (c_p T_\infty/q)$.

In order to determine the rapid rise in chemical reaction rate or the location of the temperature maximum in region II, we must now solve one differential equation containing the reaction rate term, say, the following set of equations

$$\left.\begin{aligned} \left(\frac{\partial Y_{c,II}}{\partial \tau}\right) &= \left(\frac{\partial^2 Y_{c,II}}{\partial \eta^2}\right) + \left(\frac{L^2}{\xi K}\right)\omega_c \quad , \tau > 0 \, , \; 1 > \eta > 0 \\ Y_{c,I}(\tau,\eta) &= 0 \\ Y_{c,II}(\tau,0) &= 0 \\ Y_{c,II}(\tau,1) &= -\xi \nu_c \alpha(\tau,1) \end{aligned}\right\} \quad (12)$$

We will use an overall second order Arrhenius rate expression, that is,

$$\dot{\omega}_c = -\nu_c W_c A \xi^2 Y_c Y_F \exp(-E_a/RT) \quad (13)$$

where A, E_a & R denote, respectively, a known constant, the activation energy and the universal gas constant. Also,

$$Y_F = \nu_F W_F \left[\alpha + (Y_c/\nu_c W_c)\right] \quad . \quad (14)$$

and

$$T = (\xi/\epsilon_T)\left[\beta - (Y_c/\nu_c W_c)\right] \quad (15)$$

Thus, by making various simplifying assumptions, the problem has been reduced from a solution of equations (1) to (7) into that of a single partial differential equation (12). Because of the highly non-linear nature of the above partial differential equation, we employ a numerical method for its solution, namely, the Crank-Nicholson scheme[4].

Note that the initial conditions for the temperature as well as the oxidizer and fuel mass fractions are discontinuous. For starting any integration scheme numerically, we have to provide a continuous profile. In order to do so, we drop the reaction term altogether and obtain an analytic solution for equations (12). As long as τ is chosen small enough such that the chemical reaction term is negligible, this analytic solution is an accurate initial profile. There is an additional difficulty encountered during the initial stages of the computation. It is related to the evaluation of Y_F from Eq. (14). Since α is known very accurately from its analytic expressions given in equations (11a, b, c), and Y_O is being computed by using finite difference approximation, Y_F obtained from equation (14) turns out to be negative at some mesh points in the initial steps of computations. Therefore, we are forced to solve for all the three profiles, namely, Y_O, Y_F, and T in zone II by making use of the respective differential equations for a few initial time steps. The calculations are still proceeding and the results will be reported in the near future.

References

1. Sharma, O. P., and Sirignano, W. A., 1969, "Ignition of Stagnation Point Flow By a Hot Body", Combustion Science and Technology 1, 95-104.

2. Sharma, O. P., and Sirignano, W. A., 1970, "On the Ignition of a Premixed Fuel by a Hot Projectile", Combustion Science and Technology 1, 481-494.

3. Williams, F. A., Combustion Theory , Addison-Wesley Publishing Company, Inc., Palo Alto (1965).

4. Crank, J. and Nicolson, P., 1947, "A Practical Method for Numerical Evaluation of Solutions of Partial Differential Equations of the Heat-Conduction Type", Proc. Cambridge Philos. Soc. 43, 50-67.

C. Flame Spreading over Liquid Fuel Surfaces.

Early analysis by Glassman and Hansel[1] of the problem of a two-dimensional flame spreading across a horizontal fuel surface led to the concept that two different mechanisms could prevail. The determination of the controlling mechanism depended upon the relationship of the liquid fuel temperature to its flash point temperature. At temperatures above the flash temperature, a combustible mixture exists above the liquid surface. After ignition, a flame would propagate through the combustible mixture parallel to the surface in a similar fashion to premixed laminar flame propagation. In this case, a gas phase mechanism is controlling.

On the other hand, in the second case, where the fuel temperature is below the flash temperature, a liquid phase mechanism prevails. Here, the flame, in order to propagate, must continually heat the liquid in front of it to the flash temperature. If radiation were not important, as is the case for many fuels, then heat transfer must occur by conduction and/or convection. For the temperature range of interest, (and for typical hydrocarbon fuels), the thermal conductivity of the gas ahead of the flame varies between a value substantially less than the thermal conductivity of the liquid and a value of the same order as the liquid value. The convection in the gas phase due to buoyancy would be in a direction opposite to the flame propagation direction and, therefore, would be adverse to propagation of the flame. It will be argued later that the convection in the liquid phase has the proper direction and is typically several orders of magnitude larger than conduction. For these reasons, convection in the liquid phase (if radiation were negligible) would be the rate-controlling mechanism when the liquid temperature is initially below the flash temperature.

The present study has concentrated on this second case and, therefore, the liquid flow has been analyzed here[2]. Glassman and Hansel[1] showed experimentally that flow is induced by the spreading flame and the liquid viscosity influenced the flame spreading rate. Since these subsurface flows are believed to govern the heat transfer within the liquid, it is important to completely understand their character and their effect on the ignitability of liquids and the flame spreading rates. This paper contains the treatment of an uncoupled problem where the gas phase phenomena and the energy transfer from the gas to the liquid is ignored. Rather than determining the flame spreading rate as an eigenvalue of the problem which requires the above information, the flame spreading rate is presently taken as a parameter and the hydrodynamics are then studied.

The critical factor, in the proposed mechanism is a variation in the surface tension caused by the surface temperature variation due to the spreading flame. The temperature decreases and the surface tension increases with the distance upstream of the flame front. This variation of the surface tension amounts to a stress by which the surface liquid is pulled away from the flame front. Thus, hot liquid is carried forward in the direction of propagation and energy is transported by convection. This convective transfer is often much greater than conductive and radiative transfer, and results in spreading rates orders of magnitude greater than those achieved with flames spreading over solid surfaces. Surface-tension-driven flows have been studied by many investigators for non-reactive cases. See, for example, Reference 3.

At the surface, the stress resulting from the variation of surface tension equals the viscous stress; that is, with the superscript bars indicating dimensional quantities,*

$$\bar{\mu}\left(\frac{\partial \bar{u}}{\partial \bar{y}}\right) = \frac{d\bar{\sigma}}{d\bar{x}} \equiv \bar{\sigma}_{\bar{x}}$$

where $\bar{\mu}$ is viscosity, $\bar{u}$ is the horizontal velocity, $\bar{\sigma}$ is the surface tension, and $\bar{x}$ and $\bar{y}$ are the horizontal and vertical dimensions, respectively. If $\bar{h}$ is a characteristic dimension of the viscous layer (see the last equation), the characteristic fluid velocity $\bar{u} = O\left(\bar{h}\bar{\sigma}_{\bar{x}}/\bar{\mu}\right)$. Note that for shallow pools, $\bar{h}$ is the pool depth and, for deeper pools, a boundary layer occurs at the surface and $\bar{h}$ represents the boundary layer thickness. The theoretical analyses is, therefore, described under two separate headings. In Section C-I, we deal with fully developed flow, while Section C-II concerns with deep pools of fuel.

C-I. Shallow Pools.

Of particular interest is an estimate of the relative magnitudes of energy convection and energy conduction in the $\bar{x}$ - direction within the liquid. One must then compare $\bar{u}(\partial\bar{T}/\partial\bar{x})$ and $\bar{\alpha}(\partial^2\bar{T}/\partial\bar{x}^2)$, where $\bar{T}$ is temperature and $\bar{\alpha}$ is the thermal diffusivity. This procedure implies that the dimensionless quantity, $\bar{u}\,\Delta\bar{x}/\bar{\alpha}$, a Peclet number, be compared to unity.

---

*Later, the lack of bars will indicate nondimensional quantities.

Now, from the previous discussion

$$\frac{\bar{u}\,\Delta\bar{x}}{\bar{\alpha}} = O\left(\frac{\bar{h}\,\Delta\bar{x}}{\bar{\mu}\,\bar{\alpha}}\,\bar{\sigma}_{\bar{x}}\right) = O\left(\frac{\bar{h}\,\Delta\bar{\sigma}}{\bar{\mu}\,\bar{\alpha}}\right)$$

where $\Delta\bar{x}$ is the thickness of the thermal wave in the $\bar{x}$ - direction. The convection is much greater than the conduction in the $\bar{x}$ - direction when $(\bar{h}\,\Delta\bar{\sigma}/\bar{\mu}\,\bar{\alpha})$ is a number large compared to unity.

Consider the case in which the above Peclet number for horizontal flow is large. The ratio of the vertical conductive heat transfer to the horizontal conductive heat transfer must be of the order of $(\Delta\bar{x}/\bar{h})^2$. Since the vertical conductive heat transfer must essentially be balanced by the induced horizontal convective heat transfer, the implication is that

$$\left(\frac{\text{vertical conduction}}{\text{horizontal conduction}}\right) = O\left(\frac{\text{horizontal convection}}{\text{horizontal conduction}}\right)$$

or

$$\left(\frac{\Delta\bar{x}}{\bar{h}}\right)^2 = O\left(\frac{\bar{h}\,\Delta\bar{\sigma}}{\bar{\mu}\,\bar{\alpha}}\right)$$

It follows that

$$\left(\frac{\Delta\bar{x}}{\bar{h}}\right) = O\left(\frac{\bar{h}^2\bar{\sigma}_{\bar{x}}}{\bar{\mu}\,\bar{\alpha}}\right)$$

where the quantity on the right hand side of the equation is referred to as the Marangoni number, a Peclet number based on a surface-tension-induced velocity. It follows that this number is large compared to unity. These relations determine the order of magnitude of the $\bar{x}$ - scale over which the hydrodynamics should be examined.

It is shown later that the surface convection velocity near the flame is of the order of the characteristic velocity $\bar{U}$. This velocity is found experimentally to be of the same order as the propagation velocity $\bar{V}$ so that the Marangoni number could be approximated by $\bar{V}\bar{h}/\alpha$. Most organic fuels have a thermal diffusivity of approximately 0.0008 cm^2/sec. Thus, in the study by MacKinven, Hansel and Glassman[4] where typically the fuel depth was 0.4 cm and the propagation velocities were of the order of 3 cm/sec (at 23°C) the Marangoni (Peclet) number is of the order of 1500. In the work of Burgoyne and Roberts[5] at 23°C and with

a fuel depth of 0.25 cm, the estimated Marangoni numbers are 125 for hexanol, 200 for isopentanol, and 875 for butanol. The Marangoni number, as developed here, must be the ratio of what Burgoyne and Roberts[6] call the ratios of the appropriate effective thermal conductivities to the actual thermal conductivities in the horizontal and vertical directions, respectively. Indeed calculation of this ratio of their ratios gives about exact correspondence as it should. However, one must note that in reality the Marangoni is proportional to the square root of the ratio of the horizontal convection (effective horizontal conduction) to the vertical conduction.

C-I-1. Hydrodynamic Analysis:

Consider now the hydrodynamic problem only. If a frame of reference is fixed to an advancing heat source, a steady-state problem occurs. There are four forces of interest in this problem: inertial, gravity, viscous, and surface tension forces. Therefore, three independent similarity parameters may be found. Consider these to be the Reynolds number (R), Froude number (F), and $N_1 = (\bar{x}\,\bar{\sigma}_x / \bar{\mu}\,\bar{u})$ where $\bar{\sigma}_x$ is some representative value of the stress due to surface tension. (Typically, the maximum value might be used here). For surface-tension-driven flows, the order of magnitude of the velocity is determined by a balance between the surface-tension force and the viscous force at the surface. Therefore, $N_1=1$ in the case under consideration and only two parameters are of interest. Conveniently, they are taken to be R and $N = R/F^2N_1 = R/F^2$ which are the ratio of inertial to viscous forces and the ratio of gravity to surface-tension forces, respectively.

The velocities are nondimensionalized by the characteristic velocity $\bar{U}$, the space dimensions by the undisturbed liquid depth $\bar{h}$, the pressure by the change in pressure across the undisturbed liquid fuel layer and the surface stress by the characteristic value $\bar{\sigma}_{\bar{x}}$. Under these conditions, the equations of motion in nondimensional form become

Continuity:

$$\left(\frac{\partial u}{\partial x}\right) + \left(\frac{\partial v}{\partial y}\right) = 0 \qquad (1)$$

Horizontal Momentum:

$$R\left(u\frac{\partial u}{\partial x} + v\frac{\partial u}{\partial y}\right) + N\frac{\partial p}{\partial x} = \Delta u \qquad (2)$$

Vertical Momentum:

$$R\left(u\frac{\partial v}{\partial x}+v\frac{\partial v}{\partial y}\right)+N\left(\frac{\partial p}{\partial y}\right)=\Delta v-N \tag{3}$$

where u and v are the horizontal and vertical components of velocity and p is the pressure. Δ specifies the Laplacian operator. Buoyancy effects are not of interest (since the liquid is heated from above) and density variation with temperature can be neglected. In this manner, the energy equation has been uncoupled* from the equations which govern the dynamics of the liquid.

The boundary conditions are now considered. If $\zeta(x)$ is the local height of the fuel pool and if $(d\zeta/dx)$ is small compared to unity, the surface boundary condition in non-dimensional form is that

$$\left(\frac{\partial u}{\partial y}\right)=\sigma_x \tag{4}$$

at $y=\zeta(x)$. With $(d\zeta/dx)$ small, the shear at the surface is considered to be in the x-direction.

The solid surface at the bottom of the pool is now moving in a frame of reference fixed to the flame. If V is the absolute value of the spreading rate and if the positive x-is forward of the flame, the no-slip condition implies

$$u=-V \tag{5}$$

at y = o (which is the bottom surface).

In the problem of practical interest, $N \gg 1$ implies that the gravity force is much larger than the surface tension force. In this case, the vertical momentum equation (3) becomes

$$\left(\frac{\partial p}{\partial y}\right)\approx -1$$

which has the solution

$$p\approx p_o+\zeta(x)-y \tag{6}$$

*Since the surface tension is temperature dependent, this statement may be misleading. Therefore, the energy equation is coupled to the boundary condition on the dynamic equations.

p_c is the surface pressure and neglecting effects due to gas-phase convection, capillarity, and vaporization, it may be assumed to be independent of x and equal to the ambient pressure. It follows that

$$\left(\frac{\partial p}{\partial x}\right) = \left(\frac{d\zeta}{dx}\right) = \zeta_x$$

and the horizontal momentum equation [Equation (2)] becomes

$$R\left(u\frac{\partial u}{\partial x} + v\frac{\partial u}{\partial y}\right) + N\zeta_x = \Delta u \qquad (7)$$

If ζ_x is small, as has been considered already, then $(v/u)(= \zeta_x$ at surface) also should be small. Since $(v/u) = O(\zeta_x)$, it would be expected that $(\partial v/\partial y) = O(u\zeta_x)$ and, from Equation (1), $(\partial u/\partial x) = O(u\zeta_x)$. Considering the non-dimensional velocity u to be of order unity, the first two (inertial) terms on the left-hand-side of Equation (7) are of the order of $R\zeta_x$. For low Reynolds number flow, these two terms are negligible compared to the third. Also, $(\partial^2 u/\partial x^2)$ is negligible compared to $(\partial^2 u/\partial y^2)$ so that Equation (7) becomes

$$N\zeta_x = \left(\frac{\partial^2 u}{\partial y^2}\right) \qquad (8)$$

It is not necessary, however, to assume small Reynolds number compared to unity to obtain Equation 8. Suppose the Reynolds number were large compared to unity, but small compared to N; then the above approximations are valid and Equation (8) is obtained. This reasoning applies to the case of fully-developed flows where the velocity profile "fills" the total depth of the pool. In this sense, it is similar to the cases of Couette and Poiseuille flows where the inertial terms disappear exactly and a balance between pressure and viscous forces remain. In the present case, the inertial terms do not disappear exactly but only approximately. However, the approximate relation [Equation (8)] represents a balance between the pressure (due to hydrostatic head) and the viscous forces.

If the flow were not fully-developed, but rather a boundary layer existed near the surface, the characteristic dimension would no longer be the pool depth. Rather, it would be the boundary layer thickness and the above order of magnitude analysis and the resulting form of Equation (8) would no longer be valid.

Equation (8) implies that the slope of the surface is of the order of 1/N. It is now seen that assuming N large and ζ_x small are consistent.

The solution of Equation (8) with the boundary conditions given by Equations (4) and (5) is readily found to be

$$u = N \zeta_x y \left(\tfrac{1}{2} y - \zeta\right) + \sigma_x y - V \tag{9}$$

It follows from the previous discussion that the vertical velocity component is negligible.

Before the velocity and pressure may be evaluated from Equations (6) and (9), ζ must be determined. ζ is found by applying the principle of conservation of mass in a manner following Landau and Lifschitz[3]. Since the flow at infinity is at rest in the laboratory frame of reference, it is in uniform motion in the frame of reference moving with the flame. The phenomenon is a steady one (on such a frame) and, if the vaporization rate is negligible compared to the velocity u , there can be no change in the mass flux with the position x. That is, the upper portion of the liquid moves in direction of the flame propagation (or at reduced speed in the opposite direction) and the lower portion moves in the opposite direction in such a manner that the integral over the cross-section is invariant with the position x . This integral condition from Equation (9) yields the condition on ζ . In particular,

$$\int_c^{\zeta} u \, dy = -V \zeta(\infty) = -V = -\tfrac{1}{3} N \zeta_x \zeta^3 + \tfrac{1}{2} \sigma_x \zeta^2 - V \zeta$$

or

$$\tfrac{1}{3} N \zeta \zeta_x = \tfrac{1}{2} \sigma_x + \frac{V(1-\zeta)}{\zeta^2} \tag{10}$$

where the undisturbed, nondimensional depth $\zeta(\infty) = 1$. Equation (10) may be regarded as an ordinary differential equation which governs $\zeta(x)$.

A series solution of the form

$$\zeta(x) = \zeta_c(x) + \frac{1}{N} \zeta_1(x) + \frac{1}{N^2} \zeta_2(x) + \cdots \tag{11}$$

is sought for Equation (10). Substitution of this series into Equation (10) and separation according to powers of 1/N yields

$$\zeta_{0x} = 0 \tag{12a}$$

$$\frac{\zeta_0 \zeta_{1x}}{3} = \frac{\sigma_x}{2} + \frac{\nu(1-\zeta_0)}{\zeta_0^2} \tag{12b}$$

$$\frac{\zeta_0 \zeta_{2x} + \zeta_1 \zeta_{1x}}{3} = \nu\left(\frac{\zeta_1}{\zeta_0^2} - \frac{2\zeta_1}{\zeta_0^3}\right) \tag{12c}$$

and so forth.

Since the boundary condition on the first order differential equation is $\zeta(\infty) = 1$, it follows that $\zeta_0(\infty) = 1$ and $\zeta_1(\infty) = \zeta_2(\infty) = 0$. The solution to Equation (12a) is now obviously $\zeta_0(x) = 1$ and Equation 12b becomes

$$\zeta_{1x} = \frac{3}{2}\sigma_x$$

which has the solution

$$\zeta_1(x) = \frac{3}{2}\left[\sigma(x) - \sigma(\infty)\right] = \frac{3}{2}\Delta\sigma(x) \tag{13}$$

Now, Equation (12c) becomes

$$\zeta_{2x} = -\zeta_1\zeta_{1x} - 3\nu\zeta_1 = -\frac{9}{4}(\Delta\sigma)\sigma_x - \frac{9}{2}\nu\Delta\sigma$$

which has the solution

$$\zeta_2(x) = -\frac{9}{8}(\Delta\sigma)^2 - \frac{9}{2}\nu\int_\infty^x \Delta\sigma(x')dx' . \tag{14}$$

C-I-2. Results and Discussion.

Combining Equations (11), (13), and (14), one obtains

$$\zeta(x) = 1 + \frac{3}{2N}\Delta\sigma(x) - \frac{9}{8N^2}\left[\Delta\sigma(x)\right]^2 - \frac{9\nu}{2N^2}\int_x^\infty\left[\Delta\sigma(x')\right]dx' + O\left(\frac{1}{N^3}\right) \tag{15}$$

The surface height increases with distance upstream of the flame as shown in Figure 1 and, through the hydrostatic effect, leads to a pressure gradient that resists the motion induced by the surface tension.

It is interesting that the spreading rate has no direct influence on the surface slope until second order terms are reached. Neglect of these second order terms and substitution into Equations (6) and (9) yields

$$p = p_c + \left(1 + \frac{3}{2N}\Delta\sigma(x) - y\right) + O\left(\frac{1}{N^2}\right) \tag{16}$$

and

$$u = \left(\frac{3}{4}y^2 - \frac{1}{2}y\right)\sigma_x - V + O\left(\frac{1}{N}\right) \tag{17}$$

In particular, at the surface, $y = 1 + O(\cdot)$, and

$$u = \frac{1}{4}\sigma_x - V \tag{18}$$

It is seen that, if the surface tension gradient σ_x is large enough (and positive), there will be convection of the liquid near the surface in the direction of flame propagation (see Figure 1). However, sufficiently far in front of the flame σ_x will be small and the relative velocity near the surface must be in an opposite direction to the flame propagation. The implication is that a stagnation point must lie somewhere along the surface ahead of the flame. Actually, the analysis cannot apply in the vicinity of this point since both components of velocity become of the same order. The pressure variation given by Equation (16) is due to the hydrostatic effect while the velocity variation given by Equation (17) is parabolic. Note that the flame spreading rate does influence the velocity to lowest order even though the surface slope and the pressure are not affected until higher order.

In those cases where $(\sigma_x/4)$ is not considerably smaller than V, Equation (18) justifies the previous statement that $\bar{U}$ is the characteristic velocity. The experimental study by MacKinven, Hansel and Glassman[4] shows that $V = 2.9$ cm/sec for 4 mm of decane at a bulk temperature of 23°C. (See their Figure 8.) The gradient of surface tension with temperature for decane is

0.1 dyne/cm°C. The temperature gradient ahead of the flame is estimated to - 2.0°C/cm. This value is determined from the lergth of the precursor flame (2.5 cm); the forward end of the precursor is thought to be the flash point (45°C) and the front of the established flame is the fire point (50°C). The liquid viscosity of decane at 45°C is 0.67×10^{-2} dyne sec/cm^2. Thus, for 4 mm of decane, one calculates $(\sigma_x/4)$ to be 2.5 cm/sec. Considering the difficulties of estimating the temperature gradient ahead of the flame, one can only conclude from the above calculation that $(\sigma_x/4)$ and V are of the same order and that the proper characteristic velocity was assumed in the analysis.

The present analysis may be considered as an extension of the analysis of Landau and Lifschitz[3] in two ways: (1) the effect of the relative motion between the surface tension profile and the bottom surface of the pool has been included and (2) the analysis is not limited to Reynolds number small compared to unity. This second point is the more important one since for flame spreading problems, even for very shallow pools, the Reynolds number will be much larger than unity. Indeed, in the experiments of MacKinven, Hansel and Glassman[4], the Reynolds number based on the fuel height is found to be of the order of 25 for the minimum fuel depth at which the flame will propagate. For a 4 mm depth it is of the order of 100. Thus, $N = R/F^2$ becomes approximately 1000.

It must be realized, however, that the Reynolds number has been assumed here to be sufficiently small to consider the flow as fully-developed in the length scale of interest. This assumption may be somewhat over-restrictive since the depth will be limited to very low values. In fact, for many fuels ignition may not be possible with these shallow pools. For this reason, the results of the present analysis should be used only as a guide to the understanding of the hydrodynamic phenomenon. They should not be expected to compare too closely with the experimentally measured profiles, but rather to give only certain qualitative agreement.

In most cases, the Reynolds number based upon pool depth would be so large that fully-developed flow could not be assumed. Instead, a boundary layer would exist near the surface and the nonlinear inertial terms in the momentum equation must be retained.

The demonstration that liquid-phase convective heat transfer in the direction of flame propagation can occur is sufficiently encouraging to warrant further study of the phenomenon as a plausible rate-controlling mechanism for flame propagation.

C-II. Deep Pools

The model proposed by Sirignano and Glassman[2] and described in detail in Section C-I has been extended to the case of high Reynolds number. The analysis is not complete, and some of the results obtained thus far are given below. A schematic description of the flow field, convenient for the present analysis, is given in Figure 2.

C-II-1. Governing Equations

We employ the Boussinesq approximation, which amounts to the neglect of variations of density except in the buoyancy terms. This assumption that fluctuations in density occur principally as a result of thermal, rather than pressure, variations is a reasonably good approximation for small temperature differences in the case of a liquid. Then, the equations describing the oundary layer flow near the surface of a pool of liquid fuel, may be expressed as follows[7]:

continuity

$$\left(\frac{\partial u}{\partial x}\right) + \left(\frac{\partial v}{\partial y}\right) = 0 \tag{19}$$

x-component of momentum

$$u\left(\frac{\partial u}{\partial x}\right) + v\left(\frac{\partial u}{\partial y}\right) = -\frac{1}{\rho}\left(\frac{\partial p}{\partial x}\right) + \nu\left(\frac{\partial^2 u}{\partial y^2}\right) + g_x + g_x\beta(T-T_\infty) \tag{20}$$

y-component of momentum

$$-\frac{1}{\rho}\left(\frac{\partial p}{\partial y}\right) + g_y + g_y\beta(T-T_\infty) = 0 \tag{21}$$

energy

$$u\left(\frac{\partial T}{\partial x}\right) + v\left(\frac{\partial T}{\partial y}\right) = \kappa\left(\frac{\partial^2 T}{\partial y^2}\right) + \mu\left(\frac{\partial u}{\partial y}\right)^2 \tag{22}$$

Here x and y denote, respectively, the distances measured along the liquid fuel surface and at right angles to it, while u and v are the components of the velocity in the x- and y- directions respectively (see Figure 2). T represents the temperature of the liquid fuel, and T_∞ is its initial (or unheated) value. ρ and p denote, respectively, the density and the pressure in the liquid. ν, κ, and β are, respectively the kinematic viscosity ($=\mu/\rho$), the thermal diffusivity, and the volumetric expansion coefficient of the liquid. Finally, g_x and g_y denote the x- and y- components of the acceleration due to gravity (g).

First of all, we will show that for small scale fires as well as small curvature of the liquid surface, the pressure gradient generated by the buoyancy term is negligible. Now, setting $g_x \simeq 0$ and $g_y \simeq g$, integrating equation (21) with respect to y, and then substituting for p in equation (20), we get

$$u\left(\frac{\partial u}{\partial x}\right) + v\left(\frac{\partial u}{\partial y}\right) = \rho g\beta\int_0^y\left(\frac{\partial T}{\partial x}\right)dy + \nu\left(\frac{\partial^2 u}{\partial y^2}\right) \tag{23}$$

where we have made use of the fact that p(y = o) is equal to the constant atmospheric pressure to which the liquid surface is exposed. In order to determine the order of each term in equation (23), we define the following nondimensional variables

$$\left.\begin{aligned} \bar{x} &= (x/L) \quad , \quad \bar{u} = (u/V_F) \\ \bar{y} &= \sqrt{Re}\,(y/L) \quad , \quad \bar{v} = \sqrt{Re}\,(v/V_F) \\ \theta &= (T_{max} - T)/(T_{max} - T_\infty) \end{aligned}\right\} \tag{24}$$

where L and V_F represent some characteristic length and velocity respectively. $Re = (\rho V_F L/\mu)$ is the Reynolds number. T_{max} denotes the temperature of the liquid fuel near the flame front. Making substitutions in equation (23) from equations (24), we get

$$\bar{u}\left(\frac{\partial \bar{u}}{\partial \bar{x}}\right) + \bar{v}\left(\frac{\partial \bar{u}}{\partial \bar{y}}\right) = \left[\frac{g\beta L (T_{max} - T_\infty)}{\sqrt{Re}\, V_F^2}\right] \int_0^{\bar{y}} \left(\frac{\partial \theta}{\partial \bar{x}}\right) d\bar{y} + \left(\frac{\partial^2 \bar{u}}{\partial \bar{y}^2}\right) \tag{25}$$

All terms in equation (25) are now of unit order except for the first term on the right hand side whose coefficient is equal to $[Gr/(Re)^{5/2}]$, where $Gr \equiv [g\beta(T_{max} - T_\infty)\rho^2 L^3/\mu^2]$, is the Grashof number. Identifying V_F with the steady flame propagation speed [4], and using the data for n-decane, we find that for $(T_{max} - T_\infty) \approx 50^\circ C$, $[Gr/(Re)^{5/2}] << 1$ as long as $L < 10^2$ cms. In other words, we can altogether drop this term from equation (25) for small scale fires, and equation (20) then becomes

$$u\left(\frac{\partial u}{\partial x}\right) + v\left(\frac{\partial u}{\partial y}\right) = \nu\left(\frac{\partial^2 u}{\partial y^2}\right) \tag{26}$$

Equations (19), (21), (22), and (26) are subject to the following boundary conditions

At $y = o$

$$u = o$$
$$\mu(\partial u/\partial y) = -(d\sigma/dx)$$
$$T(x,o) \text{ is a specified function} \tag{27}$$

At $y = \infty$

$$u = V_F$$
$$T(x, \infty) = T_\infty$$

Note that the momentum equation (26) is now coupled to the energy equation (22) only through the dependence of surface tension on temperature. We have determined similar as well as non-similar velocity profiles valid upstream of the stagnation point as described next.

C-II-2. Results and Discussion.

(a) Similar Flow: Similarity in velocity profiles is achieved when surface tension varies as the square root of x, or more precisely,

$$\sigma = \sigma_c - c\,(2\rho\mu V_F^3)^{1/2} x^{1/2} \tag{28}$$

where σ_c denotes the magnitude of the surface tension at the coldest end of the liquid fuel surface ($T = T_\infty$ for $x \leq 0$), and c is a known constant. The similarity variables for this case are defined as[7]

$$\eta = \left(\frac{V_F}{2x\nu}\right)^{\frac{1}{2}} y \quad \text{and} \quad f(\eta) = \frac{\psi(x,y)}{(2x\nu V_F)^{1/2}} \tag{29}$$

where the stream function, $\psi(x, y)$, satisfies the equations

$$u = (\partial\psi/\partial y) \quad \text{and} \quad v = -(\partial\psi/\partial x) \tag{30}$$

such that the continuity equation (19) is automatically satisfied. The momentum equation (26) and the relevant boundary conditions of equations (27) now become

$$\left.\begin{aligned} f''' + f f'' &= 0 \\ f(0) = 0 \quad , \quad f''(0) &= c \quad , \quad f'(\infty) = 1. \end{aligned}\right\} \tag{31}$$

Here prime denotes differentiation with respect to η.

We have obtained numerical solutions of equations (31) for different values of c, and the results are shown in Figure 3. c is essentially a measure of the surface tension gradient, and the larger its value the greater is the reduction in the surface velocity or, in other words, the faster is the flame propagation.

(b) Non-similar Flows: In order to consider arbitrary surface tension variations, we employ an integral approach suggested by von Kármán[7]. We have so far determined only the velocity profiles, and the details of the analysis are given next. Let us assume that

$$\begin{aligned} \left(\frac{u}{V_F}\right) &= a + b\left(\frac{y}{\delta}\right) + c\left(\frac{y}{\delta}\right)^2 + d\left(\frac{y}{\delta}\right)^3 \quad \text{for} \quad 0 \leq \left(\frac{y}{\delta}\right) \leq 1 \\ &= 1 \qquad\qquad \text{for} \quad \left(\frac{y}{\delta}\right) \geq 1 \end{aligned} \tag{32}$$

Here δ denotes the viscous boundary layer thickness, and a, b, c and d are unknown quantities, which are, in general, functions of x. Besides the boundary conditions given in equations (27), we have some additional continuity conditions at $y = \delta$, namely,

$$\left(\frac{\partial u}{\partial y}\right)_{y=\delta} = 0 = \left(\frac{\partial^2 u}{\partial y^2}\right)_{y=\delta} \tag{33}$$

From equations (27), (32), and (33), we get

$$b = -\left(\frac{\delta}{\mu V_F}\right)\left(\frac{d\sigma}{dx}\right) \tag{34}$$

and

$$a = 1 - (b/3) \quad , \quad c = -b \quad , \quad d = (b/3) \tag{35}$$

Therefore, equation (32) becomes

$$\left(\frac{u}{V_F}\right) = 1 + b\left[-\frac{1}{3} + \left(\frac{y}{\delta}\right) - \left(\frac{y}{\delta}\right)^2 + \frac{1}{3}\left(\frac{y}{\delta}\right)^3\right] \quad \text{for } 0 \le \left(\frac{y}{\delta}\right) \le 1$$
$$= 1 \qquad \text{for } \left(\frac{y}{\delta}\right) \ge 1 \tag{36}$$

Note that δ may be a function of x and is still an unknown quantity. Following von Kármán, we can easily derive the momentum integral equation from equation (19) and (26), namely,

$$V_F^2\left(\frac{d\theta}{dx}\right) = \nu\left(\frac{\partial u}{\partial y}\right)_{y=0} \tag{37}$$

where θ, the so-called momentum thickness, is given by

$$\theta = \int_{y=0}^{y=\delta}\left[\left(\frac{u}{V_F}\right)\left(1 - \frac{u}{V_F}\right)\right] dy \tag{38}$$

combining equations (36) and (38), we get

$$\theta = \left(\frac{b\delta}{12}\right)\left[1 - \frac{4b}{21}\right] \tag{39}$$

Making use of one of the equations (27) in equation (37), and then integrating, we obtain

$$\theta = \left[(\sigma_e - \sigma)/\rho V_F^2\right] \tag{40}$$

where σ_e refers to the initial (or unheated) state of the liquid fuel such that θ_o at this station ($x = o$) may be set at zero. Combining equations (34), (39), and (40), we get an algebraic equation for b , that is

$$b^3 - \left(\frac{21}{4}\right) b^2 + 63\,\Sigma\,(d\Sigma/dx) = 0 \tag{41}$$

where $\Sigma = (\sigma_e - \sigma)/\sqrt{\rho\mu V_F^3}$. A graphical plot of b vs. $\Sigma\,(d\Sigma/dx)$ is shown in Figure 4. For each value of $\Sigma\,(d\Sigma/dx)$ less than 0.34, there exists three possible values for b . Note that the governing equations are the same whether the surface tension decreases or increases in the direction of the initial flow. Of course, the surface tension gradient changes sign. Thus, the negative values of b correspond to the case in which the surface tension accelerates the initial flow, and is not of any interest in the present investigation. When $b \le 3.0$, we get

a reduction in the surface velocity depending on the magnitude of b at that station x, and the velocity profile then approaches its initial value at the edge of the boundary layer. For $b > 3.0$, the fluid at the surface moves in a direction opposite to the initial velocity, and finally approaching the latter near the boundary layer edge. This portion of the curve is still under investigation because we feel that the downward trend of the curve for $b > 3.5$ might be a consequence of the assumption of a third degree polynomial for (u/V_F) [see, equation (36)]. We can check its accuracy by considering higher order polynomials.

Note that, when σ is proportional to $\sqrt{x}$, as explicitly specified in equation (28), $\Sigma\,(d\Sigma/dx)$ becomes a constant, and equal to c^2. It is then possible to compare the results of the 'similar limit' of the integral method with the exact computer calculations as described in subsection (a). For this purpose, it is interesting to compare the surface velocity $(u/V_F)_{y=0}$, the displacement thickness (δ^*), and the momentum thickness (θ). The displacement thickness is defined as follows

$$\delta^* = \int_{y=0}^{y=\delta} \left(1 - \frac{u}{V_F}\right) dy \qquad (42)$$

The results of the calculations are summarized in Table I.

Table I Comparison of the 'similar limit' of the integral method (I) with the exact computer results (II).

c	b	$(u/V_F)_{y=0}$		$(u_e/x\nu)^{1/2}\delta^*$		$(u_e/x\nu)^{1/2}\theta$	
		I	II	I	II	I	II
0.1	0.36	0.88	0.869	0.153	0.153	0.142	0.141
0.2	0.748	0.751	0.724	0.33	0.338	0.283	0.283
0.3	1.18	0.607	0.555	0.547	0.576	0.424	0.424
0.4	1.68	0.44	0.338	0.832	0.938	0.565	0.566
0.45	1.974	0.342	0.171	1.021	1.278	0.637	0.636
0.4696	2.1	0.3	0	1.107	1.721	0.664	0.664

From Table I, we can conclude that the agreement is fairly good but deteriorates as we approach the stagnation point. Again, the accuracy might be improved by including higher order polynomials. It must also be remembered that in integral approaches, the integrated variables like δ^* and θ are determined more accurately than the quantities referring to a point. The details concerning the temperature field are still under investigation.

References

1. Glassman, I. and Hansel, J. G., (1968), "Some Thoughts and Experiments on Liquid Fuel Spreading, Steady Burning and Ignitability in Quiescent Atmospheres", Fire Research Abstracts and Reviews 10, 217.

2. Sirignano, W. A. and Glassman, I., (1970), "Flame Spreading Above Liquid Fuels: Surface-Tension-Driven Flows", Comb. Sci. and Tech. 1, 307.

3. Landau, L. D. and Lifschitz, E. M., (1959) Fluid Mechanics Pergamon Press p. 241.

4. MacKinven, R., Hansel, J. G., and Glassman, I., (1970), "Influence of Laboratory Parameters on Flame Spread Across Liquid Fuels", Comb. Sci. and Tech. 1, 293.

5. Burgoyne, J. H., and Roberts, A. F., (1968a), "The Spread of a Flame Across a Liquid Surface, II. Steady State Conditions", Proc. Roy. Soc. A308, 55.

6. Burgoyne, J. H., and Roberts, A. F., (1968b), "The Spread of a Flame Across a Liquid Surface, III. A Theoretical Model", Proc. Roy. Soc. A308, 69.

7. Schlichting, H., (1960), Boundary Layer Theory , McGraw-Hill Book Company, Inc., New York, 4th Edition, p. 117, p. 243, p. 302.

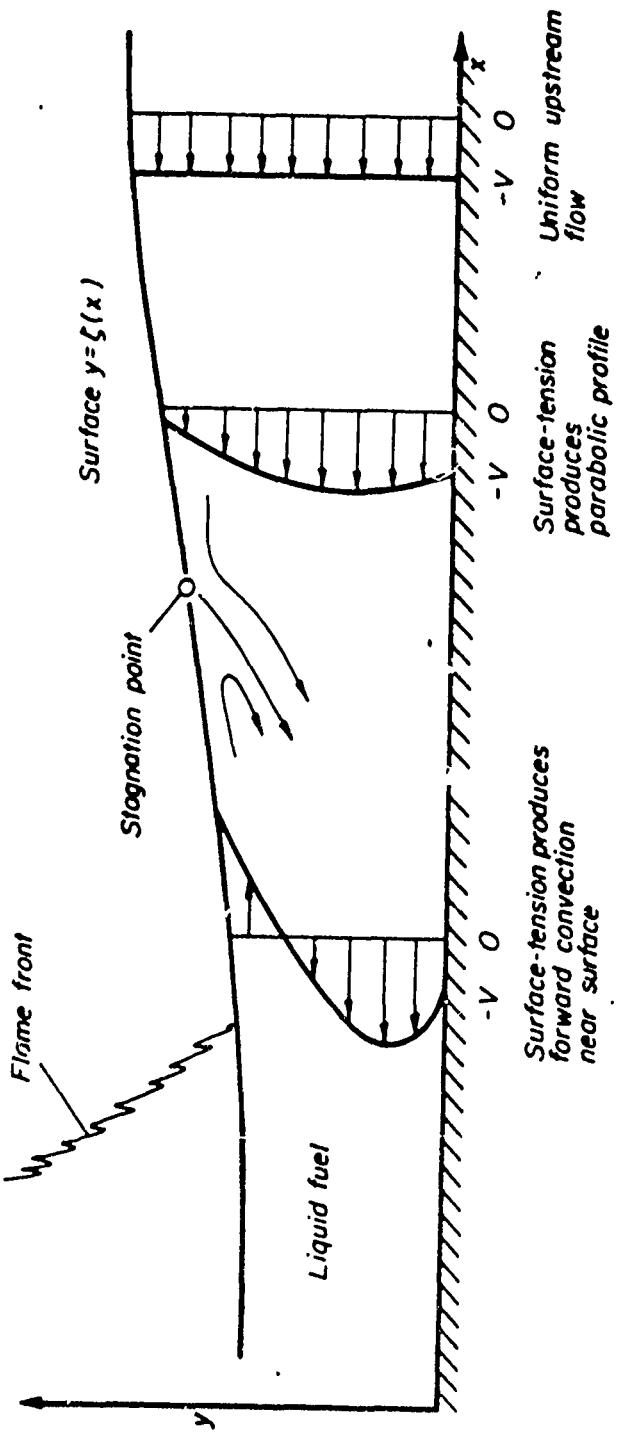

Surface - tension - driven flow field

Figure 1

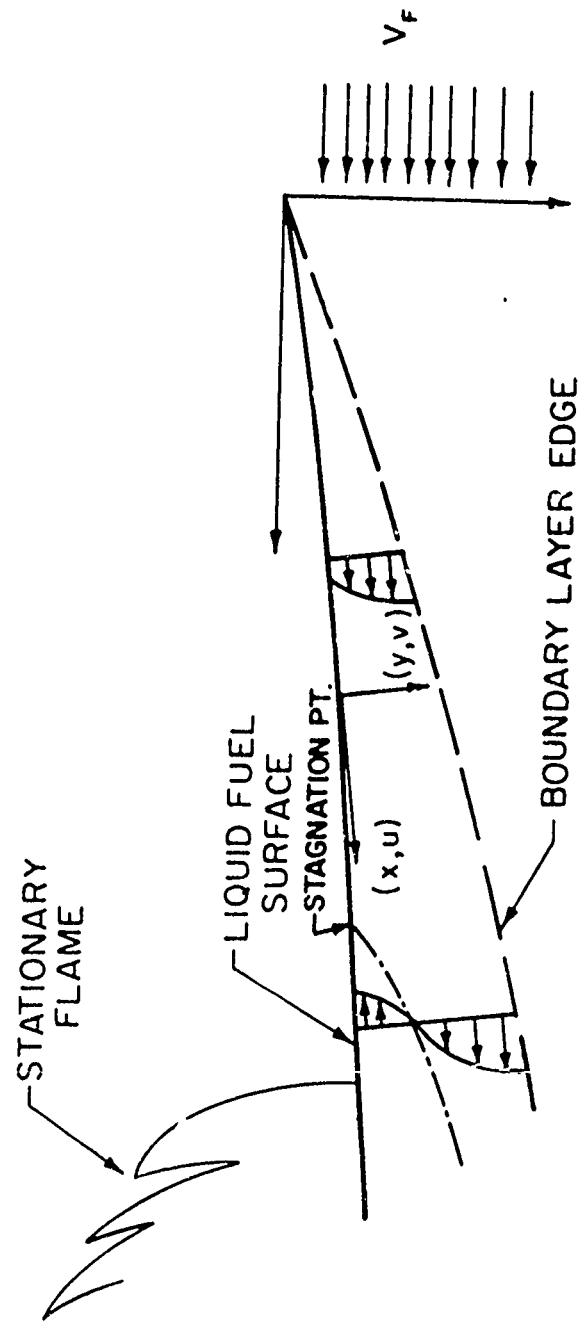

SCHEMATIC REPRESENTATION OF THE BOUNDARY LAYER FLOW FIELD

FIGURE 2

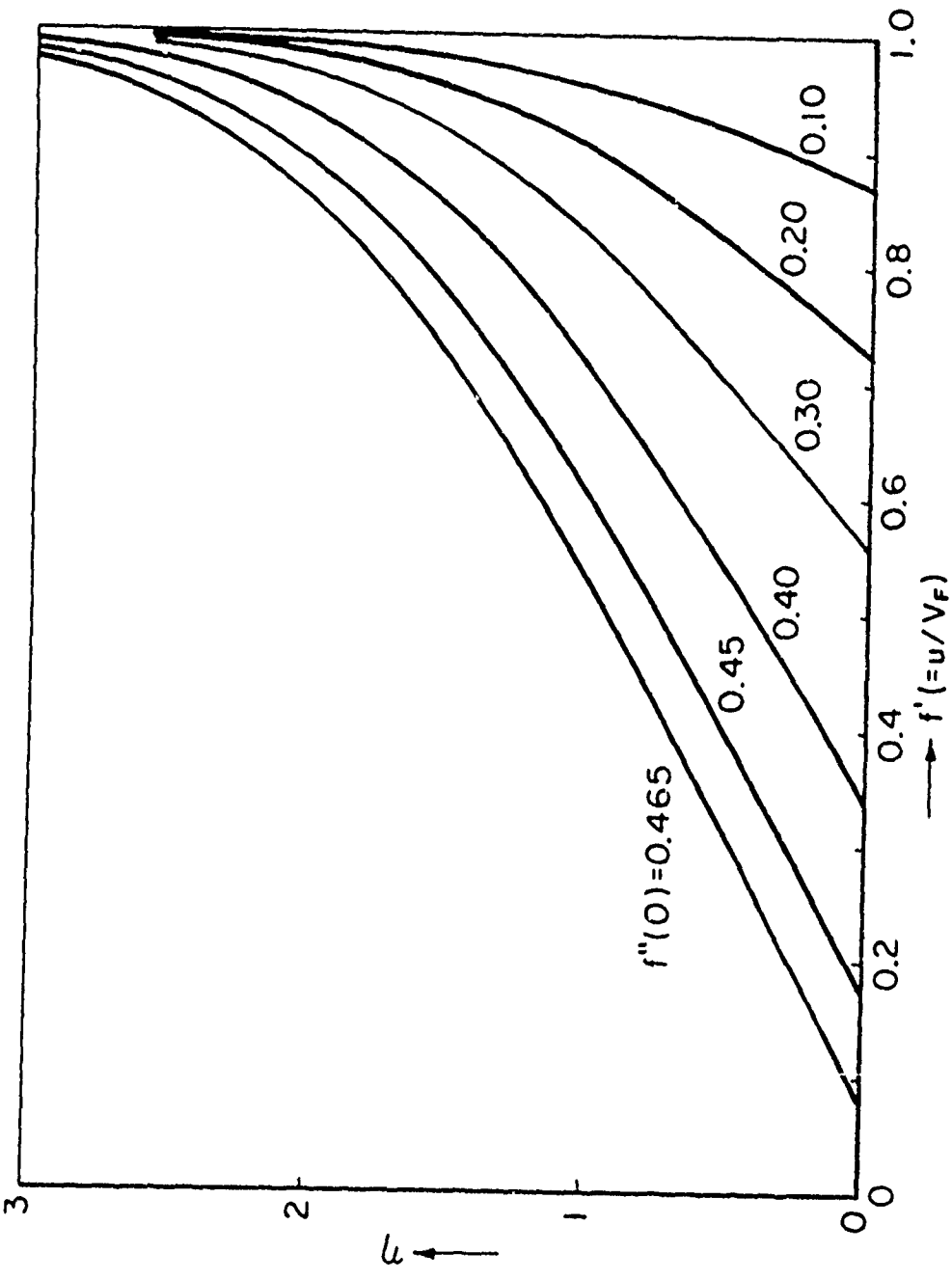

VELOCITY PROFILES ACROSS THE BOUNDARY LAYER IN THE LIQUID FUEL WITH A DECELERATING SURFACE TENSION FORCE

FIGURE 3

Part III

Table of Contents

Part III: Ignition of Pools of Liquid Fuel

List of Tables

List of Figures

Nomenclature

a_i	=	Fourier series constant
b_i	=	Fourier series constant
c	=	heat capacity
C_f	=	partial density of fuel vapor
C_{fw}	=	partial density of fuel vapor at fuel surface
d	=	depth of fuel
D	=	diffusion coefficient of vapor in air
g	=	gravitational constant
h	=	depth affected by liquid motion
k	=	thermal conductivity
k_H	=	heat transfer coefficient between the hot wire and liquid
K_T	=	thermometric conductivity
l	=	lateral width of the temperature field
$\dot{m}$	=	mass flow rate due to diffusion at the fuel surface
Ma	=	Marangoni Number
Ma_l	=	Unit Marangoni Number
Pe	=	Peclet Number
p	=	pressure
$\dot{q}$	=	heat transfer rate
Q(x)	=	heat transfer rate from the hot wire to the fluid
Ra	=	Rayleigh Number
Ra_l	=	Unit Rayleigh Number
R_{e_L}	=	Reynolds number based on length L
	=	$\rho_{air}\, U\, L / \mu_{air}$
T	=	temperature at a general point (x, y)

T_w = temperature at the fuel surface

T_∞ = temperature of the main stream of air

u = x direction velocity

U = characteristic velocity in liquid

U_∞ = velocity of the main stream of air

U_f = surface velocity of the liquid fuel

v = velocity in the y direction

W_l = mass fraction of the fuel vapor

W_{lW} = mass fraction of fuel vapor at the fuel surface

w = velocity in the z direction in the liquid

W = power input to hot wire

x = direction parallel to the surface of the fuel

y = direction normal to the surface of fuel, on air side

z = direction normal to surface within the fuel

α = $k/\rho c_p$ = thermal diffusion coefficient

β = volume expansion coefficient

δ_c = concentration boundary layer thickness

ϕ = general dependent variable

ξ = vorticity

μ_{air} = viscosity coefficient of the air

μ_f = viscosity coefficient of the fuel

ν = μ/ρ

ψ = stream function

ρ_{air} = density of the main stream of air

ρ_o = initial density of the liquid before heating

ρ_w = density at the fuel surface

ρ_∞ = density of the main stream of air

σ = surface tension coefficient

σ_T = change of surface tension per degree

γ_T = total shear stress on fuel-air boundary

Part III. Ignition of Pools of Liquid Fuel

(M. Summerfield (Principal Investigator), H. Isoda, J. F. Lamendola, R. J. Murad, B. W. MacDonald, E. G. Plett)*

A. Introduction

A.1 General Background

The study of ignition of pools of liquid hydrocarbon fuels was prompted as early as World War I when investigations on various causes of accidental aircraft crash fires and fuel spillage were undertaken in England and the United States[1]. The early investigations considered reports on actual crashes in the fields, but in subsequent studies, and particularly after World War II, full-scale experiments were carried out simulating aircraft crash fires under "controlled" conditions so as to produce actual data and film sequences[2]. Most of these experiments pointed out that the possible causes of fires, aside from the mechanical defects in engine design and other vital fuel system components, are:[3]

a) the impingement of fuel or lubricants on hot surfaces;
b) the presence of an adjacent spark, flame, or incandescent filament;
c) ignition in a fuel tank containing an inflammable air vapor mixture by electric discharge or incendiary bullet.

Laboratory experiments simulating situation (a) were conducted for many fuels and lubricants. A meaningful safety parameter determined in these experiments is the autoignition temperature[4], defined as the minimum temperature at which a fuel-air system will spontaneously ignite. The lowest ignition temperatures were obtained when known charges of liquid fuels were introduced into a heated container. The lowest container temperature which results in ignition was recorded as the autoignition temperature of the fuel. The delay time from the introduction of the fuel charge to its ignition was also recorded as a parameter of safety. The presence of sparks or burning metal chips due to friction caused by crashes on hard surfaces (such as runways for example) were also shown to have a major role in starting up fires in spilled fuel[5]. Laboratory simulations of case (b) were standardized in the form of open-cup and closed-cup flash temperatures. The closed cup flash point, (ASTM method D56) is defined as the lowest fuel temperature above which a flammable vapor air mixture exists. The closed-cup flash temperature can be utilized in measuring the safety of fuel storage tanks, and ideally it is closely related to the existence of a vapor pressure equivalent to the lean limit of flammability above the fuel surface in the container. In his Ph.D. thesis, Roberts[6] suggested that the closed flash point is a fundamental property of the fuel, and he gave some mathematical models that showed a relatively good correlation between experimental and theoretical values of both open and closed cup flash points. For the closed cup, his mathematical results gave consistently lower temperatures than the

*Dr. S. Piacsek, of the Geophysical Fluid Dynamics Laboratory, Div. of ESSA, collaborated on the numerical analysis of the preignition fluid motion, by adapting his experience with a corresponding problem involving the atmosphere and ocean when heated by the sun.

experimental values but always within 5°C. He also defined the open cup flash point to be equivalent to "the temperature of a liquid surface when the vapor at a prescribed height above the surface becomes flammable, the liquid having been heated in a prescribed way". With this definition and the assumption that the diffusion of the fuel vapor takes place up to a finite height, rather than to infinity, he succeeded in obtaining agreement between the theoretically predicted temperatures and the experimental value . The United States Institute Commerce Commission determined that a value in excess of 80°F by the method of open cup apparatus as described in ASTM D1310, would be the minimum value for classifying liquids as non-flammable.

The comparison between the flash point and autoignition temperature revealed a very interesting phenomenon. While the flash point was highly dependent on the volatility of fuel and showed a tendence to be lower for the more volatile fuels, the autoignition temperature showed a tendency to be lower for fuels with lower vapor pressure and higher molecular weight[3]. This fact gave rise to the situation whereby a volatile fuel such as benzene would be more hazardous than heavy lubricating oils in the presence of an igniting agent such as a spark, a flame, or an incandescent filament, but would be safer when spilled on hot surfaces with the absence of these igniting agents. Indeed, many engine fires were attributed to the spillage of lubricating oils on the engine nacelle.

A.2 Other Laboratory Investigations

The compilation of data on the autoignition and flash temperatures of various fuels gave a good insight into the relative safety of these fuels. Nevertheless, it was not adequate to answer the fundamental question of the burning mechanism, and hence the study of the burning characteristics of pools of fuel was undertaken. Experiments were conducted to determine the burning rate of volatile fuels in small and large trays[7]. Such investigation led to the evaluation of the energy feedback from the flame to the fuel necessary to keep it evaporating and to diffuse into the burning zone. Results of these experiments showed that the burning rate increases and approaches a maximum and constant value with increasing pool diameter; the constant value being proportional to the ratio of the net heat of combustion to the heat of vaporization of the fuel[8]. Experimental work has been carried out also to determine the minimum energy required for sparks and incandescent filaments of various sizes to ignite stationary and flowing combustible gas mixtures[9]. Since the ignition takes place in the gas phase, the contribution of these tests to the burning of liquid fuel is apparent.

The studies mentioned above covered volatile fuels that ignite and sustain flames at room temperature. However, Roberts and Burgoyne[10] reported on ignition and flame spreading over a bed of non-volatile fuel as well. They described such ignition to develop in three stages: "...an induction period in which the liquid is burning at a center of ignition; a transition period during which

the flame spreads from the center of ignition but is still affected by events occurring during the induction period; and a propagation period during which the flame spreads across the surface in a manner which is independent of events occurring during the induction period."

Similar work, but covering mostly the third period mentioned above has been carried out at Princeton University under the direction of Professor Glassman, and is described in another section of this report. The results of that study are also given in references 11 and 12.

A.3 The Current Program

When the liquid fuel temperature is above its closed-cup flash temperature (superflash), it is assumed that a flammable mixture is present above the fuel surface. In this case, the treatment of the ignition problem is very much similar to that of ignition in pre-mixed combustible gases which has been widely studied and a large volume of literature on its mechanism is available. Nevertheless, an additional and a new approach to this problem is being presented in this report. The problem here was that of a quiescent pool of liquid fuel with a flow of uncontaminated air over the pool so as to create a well defined laminar boundary layer. The objective of this investigation then, was to discover the physical principles by which the domain of ignitability could be defined. Specifically, for any given geometry of the pool of fuel, we expected to define the domain of ignitability in terms of wind velocity, fuel temperature, position of the igniter above the surface, the characteristics of the fuel, and the characteristics of the igniter. Ignition of fuel above its flash temperature requires a simple "passive" igniter (one that merely places the igniting energy at a point in the boundary layer without serving also as a flame holder, or modifying the boundary layer or heating the fuel surface).

Measurements with n-Decane and Iso-Propyl Alcohol showed that ignition is possible if the igniter is placed at a position above the fuel surface where the fuel vapor concentration lies within the lean limit of flammability, and where the laminar flame speed for the mixture at that point exceeds the boundary layer velocity. In cases where the local air velocity exceeds that of the local flame velocity, the point where these two velocities become equal indicates the maximum height at which ignition of the fuel is still possible (blow off limit). It is easy to visualize a case where the local air velocity is always above the flame speed except for regions extremely close to the fuel surface. In such regions, the ignition source may be quenched by the presence of the liquid fuel, and fire may never start. However, it is an experimental fact that once ignition takes place over a fuel at superflash temperature, no amount of blowing velocity can extinguish the flame, on the contrary, the higher the wind, the faster the burning rate of the fuel.

A theoretical discussion of the ignition of a pool at superflash temperatures subjected to an air flow system is presented in Section B. Also included is a preliminary model of the subflash ignition process. The principles expressed in the model imply the subflash ignition can occur if the igniter provides local heat transfer which augments the local vaporization rate to a level enabling the formation of flammable mixture ratio at the igniter.

In Section C, the experimental apparatus employed and the experiments at both superflash and subflash temperatures are described. Experimental results are reported and discussed. The discussion of the superflash experiment is relatively straightforward owing to the ready agreement between theory and data. However, the subflash ignition receives extensive discussion because of complexities involved in heat transfer from the igniter to the fuel pool.

In view of the complexities encountered in the study of ignition at subflash temperatures, due to the liquid motion, a further study of this motion was initiated and is reported in Section D. Moving pictures of this motion were also taken and compiled into a fifteen minute film. A numerical analysis of the fluid motion was undertaken. Preliminary results of this analysis are presented here; further results will be reported in a pending publication[22].

B. Liquid Fuel Ignition Theory

B.1 General Remarks

There are two major regimes of theoretical interest in the study of ignition of pools of liquid fuel. One is the superflash regime in which the fuel's temperature is high enough to support combustible vapor air mixture above its surface. The other is the subflash regime in which the bulk fuel temperature is below the point where combustible vapor exists. In the first case, the question of ignitability depends solely on the gas phase processes which may include aerodynamic, heat transfer, mass diffusion, as well as chemical processes. In the second case, ignition cannot occur by gas phase processes alone. Additional factors involving the liquid phase must come into play to allow ignition.

On the basis of the simple hypothesis that the edge of the domain of ignitability, for fuels at temperatures above the flash point, is determined by the line along which the flame speed equals the local air velocity, or by the line along which the fuel/air ratio equals that of the lean limit, whichever line is encountered first, it is possible to predict ignition limit contours above the pool for every value of velocity and for every fuel temperature. Accordingly, the domain of ignition is defined, for the case of a weak or "passive" igniter, (one that interferes least with the boundary layer and allows no interaction between it and the fuel surface), in terms of four variables, distance from the leading edge of the pool, distance above the liquid surface, temperature

of the fuel, and wind velocity. A theoretical analysis based on these parameters is outlined in the following paragraphs.

B.2 Theory of Ignition in the Superflash Regime:

The treatment of the boundary layer flow over the fuel surface is very similar to the treatment of a boundary layer over a flat plate if some basic assumptions are made. The fuel surface can act like a flat plate if we can show that the air flow over the fuel surface produces negligible movement of the fuel surface and that the mass diffusion from the fuel produces negligible upward velocities. Furthermore, it is possible to use the zero pressure gradient, isothermal, Blasius boundary layer solutions to describe the boundary layer for both velocity and vapor concentration if the surface temperature is not exceedingly above the room temperature or the main air flow temperature. The assumptions that are inherent in this model will be listed and discussed next.

Assumptions:

a) Incompressible flow: (ρ = const.)

There are two parameters that control the density of air flow over a flat surface, the temperature difference between the surface and the main flow, and the velocity of the main stream. Since density is inversely proportional to the temperature, the ratio between the air density at the fuel surface ρ_w and the main stream density ρ_∞ is (for constant pressure across the thin boundary layer)

$$\frac{\rho_w}{\rho_\infty} = \frac{T_\infty}{T_w}$$

If we take an average room temperature of 68°F (20°C), and allow ± 15% variation in density and still consider the flow incompressible, then this assumption would remain valid in the range -11°F to +147°F (-24°C to +64°C) of fuel surface temperature. Furthermore, the main stream velocities used for this experiment were less than 10 ft/sec well within the low Mach number range (~.01) where the effect of velocity on density variation is negligible.

b) No-slip of the fuel surface:

The total shear force on the fuel surface due to the air flow can be calculated using the equation[13]

$$\tau_r = \frac{1.33\,\rho_{air}\,U_\infty^2}{2\sqrt{R_{e_L}}} \qquad (1)$$

This force should be the driving force for the liquid fuel surface and hence:

$$\tau_r = \mu_f \frac{\bar{U}_f}{d} \qquad (2)$$

assuming the fuel is a Newtonian fluid and has a linear velocity profile with its depth. Calculations on n-Octane fuel at 95°F (35°C) and main stream air velocity of 2 ft/sec, and 4 mm of fuel depth, show that the surface slip velocity as defined in Eq. (2) would be 3.4×10^{-3} ft/sec, a mere 0.17% of the main air velocity. This slip velocity can be reduced even further with more viscous fuels. Arbitrarily choosing a tolerable slip velocity of 1/2% of the main velocity will allow a maximum air flow of 4 ft/sec over n-Octane. So, we may take the fuel surface to be stationary when we calculate the aerodynamic boundary layer.

c) Negligible Upward Velocity Due to Mass Diffusion:

In our experimental conditions, the upward velocity is controlled by diffusion processes only. The mass diffusion of the vapor at the surface of the fuel is given by the equation[14]:

$$\dot{m} = \frac{D}{1 - C_{fw}} \left(\frac{\partial C_f}{\partial y} \right)_{y=0} \tag{3}$$

when C_f is given in terms of partial density of fuel. But if C_f is given in terms of mass fraction of fuel in air, w_1, then Eq. (3) will represent the upward velocity of fuel vapor due to diffusion. It can be shown that this velocity v_w would take the form:[20]

$$\bar{V}_w = \frac{D}{1 - w_{1,w}} \left(\frac{\partial w_1}{\partial y} \right)_{y=0} = \frac{1.5\, w_{1,w}\, D}{(1 - w_{1,w})\, \delta_c} \tag{4}$$

the bar indicating average quantity. For n-Octane under the conditions specified in Assumption (b), this velocity is calculated to be 0.79×10^{-3} ft/sec having a negligible effect on the various boundary layer profiles.

It is important to add at this point that since the properties of the fuel vapor differ greatly from those of air, we have to limit ourselves to very small surface concentrations, the extent of which depends largely on the fuel properties.

The three assumptions made above are necessary if we want to consider that the fuel surface can act as a flat plate and hence use available solutions for our theory to compare with experimental results. Solutions with non-negligible upward moving velocities due to diffusion processes are available in Ref. 15, page 404, and for more refined calculations the effect of these velocities can be considered. However, Assumption (b) must be adhered to, for, if slip velocities become important, a new and complicated set of equations has to be dealt with. Once we accept the assumption that the fuel surface can be considered as a rigid surface in our analysis, then the next assumptions come from the standard ones related to the Blasius solution, listed in Ref. 13, page 283, which are repeated here briefly:

c. The flow in the channel is two-dimensional (wall effects are neglected).

d. The pressure is constant throughout the flow field (atmospheric).

e. The flow is laminar (Re_{max} from 3.3×10^3 to 3.3×10^4) and steady.

f. The physical properties of the fluid are constant.

g. The fluid flow is not affected by heat flow.

h. Body forces neglected.

With these assumptions, the following set of boundary layer equations is left to be solved:

$$\text{continuity} \qquad \frac{\partial u}{\partial x} + \frac{\partial v}{\partial y} = 0 \tag{5}$$

$$\text{momentum} \qquad u\frac{\partial u}{\partial x} + v\frac{\partial u}{\partial y} = \nu\frac{\partial^2 u}{\partial y^2} \tag{6}$$

where $\nu = \left(\frac{\mu}{\rho}\right)_{air}$

$$\text{energy} \qquad u\frac{\partial T}{\partial x} + v\frac{\partial T}{\partial y} = \alpha\frac{\partial^2 T}{\partial y^2} \tag{7}$$

where $\alpha = \left(\frac{k}{\rho c_p}\right)_{air}$

$$\text{mass diffusion} \qquad u\frac{\partial w_1}{\partial x} + v\frac{\partial w_1}{\partial y} = D\frac{\partial^2 w_1}{\partial y^2} \tag{8}$$

w_1 can be given in mass fraction or partial density of vapor in the air assuming it is a perfect gas. These equations are discussed in Ref. 14 pp. 457-463, and solutions in graphical form are shown there. The boundary conditions considered in our case are:

at $y = 0$: $u = v = 0$, $T = T_w$, $w_1 = w_{1w}$

at $y = \infty$: $u = U_\infty$, $T = T_\infty$, $w_1 = 0$

Fig. 1 shows a solution to these equations for n-Octane as calculated by Murad[20]. The ignition zone defined earlier being the zone where flammable mixture is present and where velocity is favorable for ignition is also shown superimposed on this figure. The rich limit of ignitability, in case rich vapor/air mixtures are present near the surface, can also be considered as a limiting line.

B.3 Theoretical Discussion of Ignition in the Subflash Regime:

The statement that fuel below its flash point can be considered safe is proved easily by the following example. When

benzene (Flash temp. -11°C) at room temperature is spilled and a burning match is thrown into it, a large flame is established immediately over the whole fuel surface. On the other hand, when n-Decane (Flash temp. 46°C) is spilled at room temperature, the flame of the match will be quenched by the fuel surface rather than ignite the fuel. However, if we cool the benzene to temperatures below -11°C, it will behave very much like n-Decane at room temperature. Similarly, if n-Decane is heated much above its flash temperature, it will behave like benzene.

Experimental evidence showed that by bringing a sufficiently energetic hot wire igniter close to the fuel surface, it is possible, after some ignition delay time, to start a local flame near the igniter which would spread over the fuel surface only after a second time delay while the igniter is still in operation. When the igniter is removed before the flame spreading is in progress, the local flame will be quenched immediately. In all cases the igniter must come to a close proximity to the fuel surface, and for this reason it was found that air flow over the surface did not affect the start of a local flame, but the location of the flame was shifted further downstream with increasing air velocity. All of this seems to be understandable on the hypothesis that ignition of a subflash pool takes place when the heat transfer from the igniter is sufficient, and when the waiting time is sufficient to raise the temperature of the surface locally to a temperature near the flash point. The time delay is obviously affected by those factors that determine how much heating is required to reach this stage: depth of fuel, extent of initial subflash cooling, power of the igniter, proximity of the igniter, area of the igniter, etc. Most important in determining the time delay is the fluid motion underneath the igniter stimulated by the heating, since this will determine how slowly the surface temperature will rise. Also, fuel below its flash point must involve some sort of incipient reaction, one that would ordinarily die out, but which gets going by virtue of some sort of feedback of heat from the incipient reaction zone to the surface of the fuel, accelerating the vaporization rate and hence the reaction itself to the runaway point.

Since the fluid behavior in the subflash regime is very complex and important to the understanding of ignition, it has been examined extensively and is reported in section D.

B.4 Conclusions

The theory developed predicts the maximum height at which ignition occurs with simple igniters such as sparks and hot incandescent filaments, by utilizing the following parameters: distance from leading edge, surface temperature of the fuel (or fuel concentration at the surface), wind velocity, burning velocity of the fuel, lean and rich limits of flammability. The theory can be utilized also to predict the lean limit of flammability if all other parameters are known, with the help of the experimental apparatus described in Section C.

C. Liquid Fuel Ignition Experiments

C.1 Equipment

The experimental rig, Fig. 2, was designed and built to simulate a wind blowing over a spilled liquid fuel surface in an open environment[20]. Ignition sources such as sparks and hot wire filaments were then introduced above the fuel surface to cause ignition. A carefully designed wind channel to provide a steady laminar flow over a pool of liquid fuel located inside the channel was used for this simulation. Igniters of various types and shapes were then introduced into the well defined flow boundary layer. The following are the most important features in this rig design:

1) Air supply system
2) Test section
3) Extinguishing system
4) Igniter and igniter support
5) Instrumentation

C.1.1 Air Supply System

Three pressurized dry air bottles each containing 220 cu. ft. of air were used to supply the required air flow above the pool of fuel in the test section. These bottles were placed in the same room in which the experiment took place to keep their temperature consistent with that of the room at all times. The system that was designed to deliver this air to the test section as sketched in the flow chart in Fig. 3(a). The main features of this system depicted in the figure are: the pressure regulator (R-1), the valves (NV-1, BV-1), the orifice plate, and the settling chamber.

The two-stage pressure regulator in the system was used to reduce the air bottle pressure, which initially stood at 2200 psig, to the desired range from zero to 200 psig maximum. From the regulator the air flowed through a combination of two valves. The first valve (NV-1) was a needle valve that provided the means for fine adjustment of air flow. The second valve (BV-1) was a ball valve used for quick shut-off and reproducibility of the flow. A well designed orifice section provided the necessary flow measurements. The orifice section was designed to AMSE specifications[17] with a 1" O.D. stainless steel tube 15" in length upstream of the orifice plate and a straight section 10" long 2.5" O.D. copper tube downstream of the plate. Two orifice plates were designed to cover the flow range of 0.1-1.0 cu. ft./sec which gave us the velocity range of 1.0 - 10 ft/sec above the fuel surface. One plate was 1/4" thick with a rounded nozzle type orifice with 5/32" diameter nominal hole and the other plate was 3/16" thick with 3/32" diameter hole. For the desired range indicated above, the nozzle orifice was at all times choked resulting in a linear relation between the flow velocity and the absolute static pressure upstream of the orifice. A pressure tap to measure this static pressure was placed 1" upstream of the orifice plate as required by AMSE standards.

The design features of the settling chamber can be seen in Fig. 4. Both the "braking" plate and the "distributing" plate enable faster and more even chamber filling. The honeycomb and the 20 mesh screens are used as flow straighteners and also to reduce the level of turbulence present in the chamber due to the entrance conditions. This design followed empirical considerations mentioned in Ref. 18. Finally, the air flows through a contracting nozzle with a square exit (3-3/4" sides) providing smooth and parallel flow to the test section.

C.1.2 The Test Section

As mentioned earlier, the laboratory test model was designed to simulate spilled fuel contained in an area that can be represented by a pool of liquid fuel. The side view of the test section with a representative smoke flow over the pool can be seen in Fig. 5. The flow is from left to right and the smoke was supplied by smoke generating equipment borrowed for the purpose of photographing the flow. The smoke was introduced into the lower part of the settling chamber; therefore, the smoke flow did not cover the entire channel as seen in the figure. The dimensions of the fuel surface area, are 3" wide by 7 1/4" long. The selection of these dimensions are based on practical design consideration. The depth of the fuel could be changed as follows: 1, 2, 4, 6, 7, and 8 mm by addition or removal of copper plates designed to fit into the tray. The tray itself was made of brass and a heating element was placed at the bottom to bring the fuel to a desired temperature. The temperature was monitored by a thermocouple placed in the fuel at the bottom of the tray. "Pyrex" glass walls were used for the flow channel to provide visual access to the region where the flame should appear above the fuel. The nose section for the tray represents a typical subsonic nose to prevent boundary layer separation over the fuel surface. The shape of the nose was an ellipse of 4:1 axis ratio bisected in the minor axis and tilted downward 3^{o}.

C.1.3 Extinguishing System

Extinguishing the flame appearing in the test section above the fuel surface was done through the use of CO_2 gas. A pressure regulator (Fig. 3(b) R-2) is connected to a 24 lb. pressurized bottle in order to reduce the bottle pressure (initially at 830 psig) to a delivery pressure of 60 psig. A ball valve (BV-2) is used to control the flow to the test area. The nozzle that directs the CO_2 gas over the fuel surface was originally designed with a 1/2" O.D. tube flattened at the exit and situated just above the nozzle exit of the settling chamber. This, however, proved erratic in trial extinguishing tests. It was, therefore, decided to use a nozzle from a small fire extinguisher. This proved to be the most successful method. To provide additional safety, however, a small fire extinguisher bottle was available at close range at all times.

C.1.4 Igniters and Igniter Support

Initially, tests were conducted with a diversified selection of igniters to determine the ones that would give us the best ignition results. Igniters such as a flame torch, magnesium ribbon, and a tantalum strip were tested. The flame torch, although effective in producing ignition even for fuels slightly below their flash temperature (depending on the strength of the flame), could not be accurately placed at a given position, and hence it was discarded as an igniter in our experimental tests. Similarly, while the burning magnesium ribbon could be placed at an accurate position before the start of burning, it burned unevenly. The tantalum strip was formed in a trough-like shape so as to trap a combustible vapor/air mixture from a locally heated fuel surface and ignite it. However, the temperature distribution along this electrically heated strip was extremely uneven and it tended to heat to melting at its center.

After the test results indicated above, a better choice of igniters was selected to fit every test situation. Generally, a combustible mixture of gases can be readily ignited by sparks and by red hot wire igniters requiring rather low minimum energy. Such is also the case of fuel at superflash temperatures. But, since we are dealing with a boundary layer ignition for these fuels, the igniter must have a simple shape and disturb the boundary layer least. The spark plug then is the most promising igniter for this test situation. A regular automotive spark plug but with extended electrodes was used so as to remove the main body of the plug from the vicinity of the boundary layer. These electrodes made of 1/16" stainless steel rods, had 1 mm spark gap and were fed by a 15KV neon transformer.

In extending the ignition study to fuels at subflash temperatures, it was found that the spark plug was inadequate to ignite the fuel under this test situation. A different igniter was then required to supply the necessary interaction between igniter and fuel. The shapes of the various igniters tested in this regime are shown in Fig. 6. Igniter G was first tested in connection with the superflash fuel conditions with air flow over the fuel surface. At a certain wire temperature, it was found that the results obtained from the wire are rather closely related to those of the spark plug. All of the hot-wire igniters were made of Kanthal A-1 resistance wire with a nominal diameter of .036" or roughly 0.9 mm. The effects of such a straight hot-wire on the boundary layer are rather significant, but with the necessary adjustments in the wire temperature, as mentioned above, a good result that conforms closely to the theoretical prediction of ignition limit above the fuel surface was obtained. Igniter G and all the other igniters shown in Fig. 6, were designed so as to test the effectiveness of each of the igniters in expediting the ignition of fuel at subflash temperature.

The igniter support also functioned to position the igniter accurately at the desired position. The synchronous motor (shown in Fig. 2) was used to lower and raise the igniter at constant rates. The recording of the igniter height started with measuring the distance between the igniter and its image in the fuel below by a cathetometer and halving this distance. Later, the igniter was lowered to the fuel surface and the point where it first touched the surface was recorded as zero height. The igniter was held by a micrometer and thus the positioning of the igniter was within 1/10 of a millimeter. The whole support could be moved horizontally on a railing for rough lateral placement and for finer adjustment the micrometer could be used in the lateral direction as well.

C.1.5 Instrumentation

The main stream velocity of the air and the velocity profile in the boundary layer created just above the fuel surface was measured by a DISA type 55D05 constant temperature anemometer. The hot wire probe was a miniature boundary layer type 55A36 with a wire parallel to the fuel surface. The cold resistance of the wire ranged between 3.4 to 3.7 ohms, and the operating resistance was set at 6.2 ohms. Due to the low velocity range (up to 2 ft/sec) that was used in the program, a special calibration technique had to be used. Every new wire probe was calibrated before being used for measurements. A velocity of 2 ft/sec gave an output signal from the anemometer of approximately 150mV compared with output voltage of 1.39 volts of the hot-wire anemometer itself. For this reason, a bias unit that neutralized this initial output voltage had to be added. The output was then recorded on a Honeywell Visicorder Oscillograph Model 906B, and M-100-120A galvanometers were used in the visicorder for this purpose. Since the flow was considered steady, the response of the galvanometer was not a critical parameter. For this same reason, the visicorder was operated at its slowest paper speed which was 0.4 inch of paper per second. The resistors used for the galvanometer were adjusted to give approximately 4 inch deflection for 3 ft/sec flow. After calibration of the hot-wire it was placed above the fuel surface to measure the main flow velocity in the test area, and hence to calibrate the pressure gage placed upstream of the orifice. Noise signals from the actual flow coming out of the settling chamber were extremely low 0.05 - 0.1% of main stream velocity, indicating a fairly smooth and laminar flow. Moreover, it indicates that the flow straighteners in the settling chamber worked as expected.

A temperature controller was used to monitor the fuel temperature in the tray. The controller was that of West Instrument Corp. Model JP using iron-constantan thermocouple wire. The fuel temperature could be controlled within $\pm .5^{\circ}C$ with initial overshoot of $4^{\circ}C$. The thermocouple was located at the interface between the fuel and the bottom of the tray.

Other features in the data recording setup that were used mainly for the case of ignition below flash temperature, included an ion detector (or flame detector), and two extra thermocouples to probe the fuel temperatures at various locations in the liquid fuel during the induction period. The flame detector was simply made of a 4 mm gap between two wires that are connected to 90 volt batteries, and the signal coming from the flame is recorded on the visicorder after amplification. Outputs of up to 10 mv were recorded from fully established flames. The ion detector gap was placed immediately above the hot-wire igniter where initial flame is most likely to appear. The output of the two iron-constantan thermocouples was also recorded on the visicorder with a range of 80°C per 4 inch deflection.

Arrangement of the equipment on the instrument table can be seen in Fig. 7.

C.2 Experimental Results and Discussion

The objective of the experimental program was two-fold. First to compare our theory on the ignition limit of fuels at superflash temperatures, and second to investigate and lay the foundation for an ignition prediction theory for fuels at their subflash temperature. In the superflash tests, the experimental parameters were: wind velocity, temperature of fuel surface, and height of igniter. An igniter with at least a minimum energy for ignition of the lean limit combustible mixture was used, and the maximum height to which ignition was still possible was recorded and compared with the theoretical value. However, in the subflash case, other parameters of importance were added to the ones mentioned above: fuel depth, size of tray, ignition delay, power to igniter, ignition height, and others that were believed to contribute to the change in the subflash ignition characteristics of the fuel.

C.2.1 Comparison of Predicted and Experimental Results in the Superflash Regime

The velocity profile over the fuel surface was one of the important parameters in our theory, and hence it was measured experimentally. A constant temperature hot-air anemometer was used for this purpose. The calibration of this anemometer was obtained by means of air which was expelled from a large "Pyrex" bottle (20 liter or 5 gallon capacity) by inflowing water, and thereafter fed to the hot-wire probe through a straight 9mm diameter tube, 800mm in length, thereby providing a parabolic laminar velocity profile. The calibration employed velocities up to 2 ft/sec giving a Reynold's number less than 1000 for the flow in the tube. The "Pyrex" bottle was calibrated and graduated for every liter, and the volume flow of the water to the bottle, and hence the air flow, was determined by time check on these marks. The hot-wire probe, protected against draft by a 35mm inside diameter cylinder, was placed in the center of, and 1mm in front of the mouth of the tube. Air velocity at the probe was calculated on the basis of the profile

of velocity in the tube. Maximum velocity at the center of the tube, with parabolic profile, is twice the mean velocity. The calibration data was recorded as velocity of ft/sec vs. the distance in inches traveled on the oscillograph paper. With this calibration data it was found that main flow velocities over the fuel surface of 1 ft/sec and 2 ft/sec will correspond to pressure readings upstream of the orifice plate of 26 psig and 68 psig respectively.

One difficulty encountered in the measurement of boundary layer velocity profiles over the fuel surface was the fluctuating signal from the hot-wire probe due to the cooling effect of the fuel vapor on the hot-wire itself. Therefore, a very thin aluminum plate was placed on the fuel surface to prevent the vapor from reaching the wire probe and hence allow more accurate measurements.

The fuel depth was not an important parameter in the ignition of superflash fuels, but in order to control the temperature of the fuel effectively, we chose a depth of 4mm for all of our experiments. As noted earlier the temperature of the fuel was monitored by a thermocouple and controlled by a temperature controller unit.

Although the distance from the leading edge of the fuel is also a parameter of the theoretical problem, most of the experiments were conducted at a distance of 9cm. from the leading edge. Other locations were also considered, but closer to the leading edge the ignition zone was too thin, and the igniter had to be brought too close to the surface to be considered "non-active". Further downstream was considered too close to the edge of the tray, with possible back effects on the boundary layer configuration. Thus the distance of 9 cm. from the leading edge was considered to be an optimum distance.

Two methods were employed to find the maximum height above the fuel surface at which ignition is still possible. One method was placing the hot-wire igniter at a specific height and testing for ignition at that point. Since there was a delay in the heating of the wire to its maximum temperature, a certain ignition delay time had to be chosen for this method. The other method involved heating the wire at a point 2cm. above the fuel surface and bringing it down, while heating, at the rate of approximately one millimeter per second. The first point at which ignition was sighted was recorded as the maximum height. The latter method reduced the number of experiments required to determine the desired height and also gave us better results. The first method, however, was used mainly when the igniter was a spark plug, and for subflash ignition tests.

Test results on n-Decane at various surface temperatures are compared with predicted ignition zone lines in Fig. 8. The igniter was a straight Kanthal wire with a power supply of 60 watts (equivalent to wire temperature of 1280°C) and active length of 2.3 cm. The experimental points were determined by employing the second method mentioned above. The ignition zone limit line was

based on the lower flammability limit of .67% by volume given in data available in the Fuel Research Laboratory. The laminar flame speed profile for n-Decane was not known, but was assumed to be higher than the local air velocity in the case of 1 ft/sec main flow. The correlation between the experimental point and the theoretical one was very good. Fig. 9 shows the same situation as mentioned above with n-Amyl Alcohol (F.T. 38°C), but in this experiment the igniter was a spark plug and instead of varying the fuel temperature, the main flow velocity was varied from 1 ft/sec to 2 ft/sec. Ignition with a spark plug was considered more accurate than that of the hot-wire because the spark plug is less likely to interfere with the boundary layer. But since the spark gap was 1 mm in size, the spark plug could not be brought any lower to the fuel surface. Up to a height of approximately 1.5 mm, the spark was curved toward the surface and it made the determination of the exact height of the spark rather difficult. Furthermore, it was noticed that the published flash temperature of n-Amyl Alcohol (38°C) corresponds to vapor concentration of 0.83% by volume, while the published low limit of flammability was 1.19% by volume corresponding to a fuel temperature of about 43°C. The experimental points indicated the tendency for the low limit to be lower than the published value. Fig. 10 was used for demonstration purposes. Using Iso-Propyl Alcohol (F.T.12°C) at approximately room temperature, it was shown that ignition could occur 9 cm from the leading edge and 2.5 mm above the fuel when the main flow was 1 ft/sec, while no ignition was recorded at the same point with flow of 2 ft/sec. In both cases of n-Amyl Alcohol and Iso-Propyl Alcohol, the calculated ignition zone limit corresponded to the low limit of flammability only for lack of data on the flame speed.

3.2.2 Subflash Versus Superflash Ignition

In extending our research into subflash regions, we had to establish an ignition criteria for the different regimes of interest. When the fuel is below the flash temperature, ignition is characterized first by the appearance of a localized flame near the igniter. Secondly, in a fuel that has a large range of temperatures between the flash point and fire point, the ignition criteria in this region would be the first appearance of a flash. Above the fire point, the ignition is the appearance of a flame that would spread immediately over the surface.

Fig. 11 shows clearly how these various regimes differ in response to the air flow. The test was conducted on n-Decane (F.T. 46°C) with an intense igniter so as to extend our ignition domain to the subflash region. Regime I (subflash), shows little effect on ignition height by the changing flow velocities. The relative ineffectiveness of wind on the ignition height in these circumstances is understandable when it is noted that, for subflash pools, the igniter had to be very close to the surface, so close that the wind velocity at that height is negligible, even when the main stream velocity is high enough to blow away the flame if we were to try to start ignition there. The igniter then will behave like a flame holder and the flame will appear in the wake region downstream of the igniter.

Regime II, which is very apparent in n-Decane, but absent in all the alcohols that were tested because of the proximity of their flash point to the fire point, shows a moderate effect of wind on the change of the height of ignition. The effect increases as the temperature approaches the fire point and the change becomes significant in Regime III above the fire point. Fig. 12 records the same data of Fig. 11 to show more clearly the results described above.

One interesting observation made in Regime II where the n-Decane was above flash temperature, but below fire temperature, was that ignition, when it finally occurred, seemed to take a few seconds for the strong flame to establish itself. During this time, one or more waves of pale blue flame are seen to sweep over the surface of the pool at intervals of one second or so. The first sweep corresponds to ignition and burning of the vapor present in the boundary layer; as this burns away, there is not enough vapor left for the moment to support a continuous flame. Then, half a second later, the accumulation of vapor coming from the surface is adequate once again to support a flame, and a second flame sweeps over the surface. After several such sweeps, the surface becomes heated sufficiently by feedback from the intermittently burning boundary layer to vaporize at a strong enough rate to feed a steady flame; that is when the main flame takes hold.

Fig. 13 and 14 show that in the superflash case, the surface temperature affects the height of ignition significantly, while at the subflash region with n-Butyl Alcohol, the effect is less pronounced. Fig. 14 also shows that when subflash ignition is possible at heights above 1 or 2 millimeters, the increase of main stream velocity will decrease the ignition height, as is the case with superflash fuel.

Table 1 gives results similar to those recorded in Fig. 11 with n-Decane, but in this instance the fuel is n-Amyl Alcohol, and the fuel temperature is kept below the flash temperature of 38°C for the Amyl Alcohol. It is clearly shown that the rise in initial fuel temperature and the introduction of air flow has not changed the ignition height until a temperature as close as 4°C to the flash temperature is reached. At this point, the increase in air velocity increased the height of ignition contrary to the case of superflash fuel. This is understandable if we note the presence of hot air surrounding the intense igniter. The air flowing over the fuel surface will then deflect this hot air and increase the contact between hot air and fuel surface, and hence increase the likelihood of ignition at a higher point than that of the undeflected case. Another explanation is given in the book "Flames" by Gaydon and Wolfhard[19], where they indicate that unpublished experiments by Hubner and Wolfhard showed that ignition occurs more easily in a slowly moving mixture than in a rich stagnant one. The greater difficulty of ignition was explained to be due to accumulation of spent gases following slow combustion reactions.

Table 2 again presents similar data to the one mentioned above, but now with a fuel with a very high flash temperature (101°C). The data clearly shows the extreme difficulty in igniting the Benzyl Alcohol at room temperature or approximately 75°C below the flash temperature.

C.2.3 Performance of Various Igniters in the Subflash Regime

In comparing ignition of fuels at their superflash temperatures versus ignition in the subflash regime, it was found that a simple igniter such as a spark plug or a straight hot-wire with moderate power supply is not effective in the subflash regime. Surely, even these igniters if brought in close proximity to the fuel surface may ignite the fuel after a long delay period, in the order of minutes, during which the fuel is being heated in its entirety to temperatures above the flash temperature. However, we also tested an array of igniters, shown in Fig. 6, and recorded the effectiveness of each in terms of ignition delay and height of ignition. The data collected from these tests were recorded in the form of graphs, Fig. 15 to 17, and tabulated in Table 3. Igniter A had a resistance wire with active length of 7mm (1/4") and the ring had a diameter of 13mm (1/2"). Igniter E had a wire length of 14mm and ring diameter of 26mm (1"). The distance between electrodes on igniters B and D was 1" while on C and G only 3/4". The distance between electrodes on igniter F was 3" to cover the width of our test tray. In all tests, the igniters were held at a position 9cm from the leading edge of the fuel surface.

In general, these results indicated that igniters that cover a large area of the fuel surface, are more "active", i.e., ignite the fuel more readily. The ignition delay of a straight wire such as G could be shortened by introducing a mechanical barrier into the liquid at the same time that the igniter is lowered into position. A smaller barrier produced faster ignition than a larger barrier. Discussion of the reason behind this observation will come in the next section. The long wire igniter F was tested briefly under the same conditions as the other igniters, and showed a very short ignition delay (in the order of 5 seconds). However, the height of this igniter could not be maintained constant during its operation because of the thermal expansion of the wire.

C.2.4 Ignition Delay Period in the Subflash Regime

Ignition of liquid fuel below its flash temperature can be described in the following manner:

1) An ignition delay defined by the time which elapses between the introduction of the igniter at its position to the appearance of a local flame.

2) Establishment of local flame which requires the presence of the igniter to sustain it.

3) A second time delay between the first appearance of the local flame and start of flame spreading.

4) Flame spreading on the fuel surface.

Our experimental effort was concentrated mainly on the first phase mentioned. It has been observed previously that pools of liquid fuel at subflash temperatures can be ignited, but only after significant delays (a few to many seconds). The delay is always longer than one would expect for a solid fuel, and this stretch-out of the delay was found to be due to the heat removal into the liquid phase by convection away from the site being heated by the hot igniter. Thus, fast local heating of the fuel surface to produce ignition was prevented. It is, therefore, evident that a quantitative description of the ignition delay must start with a description of the induced fluid motions and the concurrent heat removal by convection.

Observations of the fluid motions during the pre-ignition interval (see Fig. 18) led to the conclusion that the size of the fluid eddy created by the heat source just above the liquid surface was determined by intrinsic liquid properties, including probably temperature coefficient of surface tension, the viscosity, the thermal coefficient of expansion, the density, the specific heat, the thermal conductivity, etc. Some of these properties were correlated to the surface velocity of circulation and are reported in greater detail in Section D[21]. Results of an experiment with n-Decane fuel designed to test the effects of viscosity and temperature co-efficient of surface tension $\frac{d\Gamma}{dT}$ are plotted in Fig. 19. As shown in this figure ignition of pure n-Decane required relatively high igniter temperature (high power supply). Its ignition delay time increases greatly with relatively small decrease in power supplied to the igniter. The reduction of the surface tension gradient with temperature almost to zero caused generally faster ignition and more moderate increase in ignition delay time with reduction of power up to a certain low power range where the behavior of the pure n-Decane was repeated. Similar effects were noted with increasing viscosity of the fuel. However, the main difference between the reduction of surface tension gradient and the increase in viscosity other than the ones shown on the graph, was that in the first case the behavior of ignition was similar to the pure fuel by having a local flame established first, and in the latter case, the flame immediately started to spread on the fuel surface. From these observations one might conclude that the liquid surface adjacent to the igniter would become ignitable as soon as the entire eddy region had received sufficient heat to permit the nearby vapor density to reach the lean limit for ignition. For a small eddy such as being formed with a very viscous fuel, the heating of the eddy is total and fast and hence the first flame is able to sustain itself without the continuing presence of the igniter. For a large eddy, such as formed in the pure n-Decane fuel and n-Decane with surfactant, the local region on the liquid surface can be brought to ignition very quickly by making the wire very hot

well before the entire eddy becomes heated. The fact that most of the eddy region is still rather cold suggests that the flame could not remain on the surface, that it would die away as soon as the igniter is removed.

The importance of the size of the eddy could also be seen when tests were conducted with igniters A and E of Fig. 6. From Table 3, we see that for approximately the same igniter power and the same fuel depth, igniter A with the smaller size cylindrical fluid retainer ignites more readily than igniter E. However, since the fluid outside the cylinder does not warm up as well, the flame appears only within the cylinder and it can sustain itself without the igniter there. But when the cylinder is removed from the fuel or lowered further to submerge the cylinder, the flame dies out. Some efforts to determine the maximum size of the eddy being affected by the igniter will be discussed later in this section when ignition in deep circular pools is considered. However, it is evident that the mechanism that controls the ignition delay or induction interval in the case of subflash ignition, is connected with the size and fluid flow characteristics of this induced subsurface eddy.

The time delay from the first appearance of local flame to its spreading over the entire fuel surface is well described in the paper by Burgoyne, Roberts, and Quinton[10]. Their report was concerned with Iso-Pentanol (F.T. 41°C) being ignited with a wick. Their paper (Sections 2 and 3) also includes experimental observations on the steady state flame spreading, and a suggested theoretical model. Also on flame spreading, the experimental paper by MacKinven, Hansel, and Glassman (Ref. 11), and the theoretical paper on surface tension driven flows by Sirignano and Glassman (Ref. 12), and the unpublished paper on the effect of pressure head created by the high local evaporation rate by Summerfield[16] are part of the efforts made at Princeton on this subject. Since our study did not include phase 3 and 4 mentioned earlier as part of the ignition process of fuels at subflash temperatures, the above references are recommended for further study on this subject.

C.2.5 Results of Deep Pool Ignition in Cups of Various Sizes

An attempt was made to determine the maximum size of the eddy under the igniter using circular cups of various sizes. Using n-Amyl Alcohol at room temperature (F.T. 38°C) with the experimental conditions recorded on Fig. 20 and 21, it is inferred that this maximum size is within 2" diameter surface and between 3/8" to 1/2" depth. The size quoted is highly dependent on the height of the igniter and the power supplied to it. The tendency of the temperature gradient along the surface to increase with the increase of power can be seen indirectly from Fig. 22(a) and (b). Fig. 22 (a) shows the surface temperature readings opposite the igniter and at a distance of 4mm from the igniter. The temperature difference between these two stations increase with increasing power level. Figs. 23 and 24 show how ignition delay gets shorter as the height of the igniter is decreased and as the local fuel temperature approaches the flash temperature.

A rather interesting observation is made when Fig. 22(a) is compared with Fig. 25. With thermocouple placed immediately under the igniter on the fuel surface, it is learned that the temperature of the fuel remains constant with increase in power, while it increases progressively with increase in height of the igniter; contrary to the belief that we should get the same results in both cases. Although we have no exact knowledge on the mechanism of heat exchange between the fuel and the hot igniter, it can be argued that the hot air around the igniter surface must play an important role. When the igniter is placed very close to the fuel surface, a small area near the igniter is exposed to extremely hot air flowing due to natural convection, therefore, vapor that is mixed with this hot air will ignite in a smaller concentration than that given for the low limit of flammability. This is plausible in view of the decrease in this limit with increasing mixture temperature. For this reason, the fuel surface temperature does not need to be the flash temperature, but considerably lower. On the other hand, when the igniter is moved higher, the mixture present between the igniter and the fuel surface is exposed to lower air temperatures and the fuel surface area covered by the natural convection currents of the air will be larger.

C.3 Conclusions

In conclusion, the ignition of pools of fuel at temperatures above their flash point can be readily achieved and hence render the fuel dangerous. However, with the introduction of high winds over the fuel surface, the ignition possibilities become more and more limited to small heights above the fuel surface.

Although fuels such as n-Decane with flash temperature of 46°C are classified as safe by the U. S. Institute of Commerce Commission Code, they can be rendered unsafe if they are thickened (their viscosity is increased), and if the igniters are more elaborate than the spark and the straight hot wire, i.e., cover a large surface area of fuel. For this reason, the study of ignition of fuels at subflash temperatures becomes highly important as an extension to the problem of fuels at their superflash temperatures. From our observation, we can conclude that the model for such ignition would include as the essential processes, the gas phase conductive heat transfer from the hot wire to the surface, the heat transfer into the liquid below the surface in the presence of the induced convective flow field, the resulting rate of temperature rise at the surface, and the build-up of the fuel vapor concentration at the surface corresponding to the rising surface temperature.

In order to complete the model, detailed knowledge of the heat input to the fluid phase from the igniter must be available, as well as a relation between this heat input, the thermodynamic properties of the fuel (viscosity, and thermal expansion coefficient, density, surface tension) and their variation with temperature, the induced surface velocities and the extent of the surface area affected must be understood. The more detailed study of the motion preceding ignition at subflash temperatures was intended to extend knowledge of some of the above mentioned parameters.

D. Preignition Motion of the Fluid

In the course of study of ignition of liquid fuels which were initially at the subflash temperature, it was found that the fluid was set in motion as a result of the heat input at the igniter. This fluid motion was found to have a strong influence on the ignition time, and thereby became a sub-topic of this investigation of the ignition of liquid fuels. The investigation involved a detailed experimental and analytical program, which was intended to demonstrate the important mechanisms governing the fluid motion in order to allow prediction of this effect in new situations.

D.1 Experimental Program

D.1.1 Equipment

An apparatus suitable for visual and photographic study of the surface and sub-surface liquid motion was constructed, Fig. 26. It consisted of a small rectangular tray, two sides of which were made of optical quality quartz to facilitate visual observation. The bottom and ends of the tray were made of copper with a surrounding jacket for water cooling during long tests, to bring about steady state. The tray was 2 cm wide, 11.5 cm long and 4 cm deep. These dimensions together with the use of a heater wire spanning the width of the tray, assured essentially two dimensional motion of the fluid. The electrically heated wire was normally placed so that it was just wetted by the top of the liquid surface.

Thermocouples were used to measure the temperature distribution in the fluid, and streak photographs of small particles suspended in the fluid were used to obtain fluid velocities. Density gradients were observed by Schlieren photography.

D.1.2 Results of Experiments

Fig. 27 shows a series of photographs of the liquid motion in n-Decane following the initiation of power to the heater wire, taken with an exposure of 1/4 sec at zero time, 2 sec, 5 sec and 8 sec after the power was turned on. A small eddy is observed to grow and move away from the vertical plane of the hot wire, as time progresses. This is the type of motion which is responsible for the extended ignition delay of liquid fuels, which are at a temperature below the flash point, when they are being ignited by a hot metal such as this heater wire. The change of eddy dimensions with time is shown in Fig. 28.

A close examination of the typical transient fluid motion beginning when the heater power is first turned on reveals the following events. At first, a very thin layer on the top surface streams rapidly outward from the heated wire, and simultaneously the eddies beneath the surface are initiated. When the surface wave encounters the end walls of the tray, the accompanying flow deflects downward and recirculates, coming up underneath the wire. Meanwhile

the first eddie has grown somewhat so that there appears to be a concentrated circulatory motion, due to the direct heating from the wire, near the wire, with a somewhat weaker, large-scale circulation throughout the tray, resulting from the deflection of the surface motion when it encountered the end wall. Usually the large-scale weak circulation will decay with time resulting in two main counter-rotating vortices, which are symetrically spaced about the vertical plane of the heater wire.

Fig. 18 shows streak photographs of the steady state motion in n-Decane, from which maximum fluid velocities were obtained. By analyzing a series of streak photographs, it is noted that the size of the vortices increases with time, as in Fig. 27, and that the size also increases with increased power to the heater wire.

Besides the direct streak photographs, schlieren photographs and thermocouple surveys have been used to obtain temperature and density distributions in the pool. As expected, the highest temperature is reached adjacent to the wire and the central portions of the vortices are also generally warmer than other regions in the pool, Fig. 29. The maximum observed temperature difference between the fluid nearest the wire and the fluid far from the wire, for conditions comparable to those yielding Fig. 27, is less than $20^{\circ}C$.

Now, an important problem is the identification of the force or forces driving the fluid motion. There are at least two candidate forces - those due to a surface tension gradient and those due to buoyancy. The existence of a surface tension gradient is a consequence of a non-uniform fuel surface temperature coupled with the temperature dependence of surface tension; the buoyancy force results from the fact that the isotherms in the fuel are not parallel to the fuel surface, coupled with the temperature dependence of the liquid density (uniform heating from above would produce no buoyancy force).

The results of experiments tend to indicate that both of these types of forces may play a role in causing the observed fluid motion. Thus in Fig. 19, one sees that the addition of a surfactant which largely nullifies the temperature dependence of surface tension for n-decane leads to shorter ignition delays, but it does not reduce the delay down to the level that would exist if the fuel were completely immobile; evidently the fluid motion is slowed but not eliminated.

The roles played by these two types of forces can be discussed more precisely on the basis of the appropriate dimensionless groups measuring the relative influence of these factors. In the case of a flow field driven by a temperature-induced surface tension gradient, the relevant dimensionless group is a Marangoni number. Its significance for our problem can be derived in the following way. We note that there exists, in steady-state, a balance

at the free surface between the shear stress due to the surface tension gradient and viscous shear within the liquid. This yields an expression for the order of magnitude of characteristic liquid velocity at the surface

$$\mu_l \frac{\partial u}{\partial z} = \frac{\partial \sigma}{\partial x} \tag{9}$$

$$u = O\left(\frac{\sigma_T}{\mu} \cdot \frac{h}{\ell} \cdot \Delta T\right) \tag{10}$$

μ = viscosity coefficient

σ_T = change of surface tension per degree

h = depth effected by the motion

ℓ = lateral width of the temperature field

ΔT = temperature difference over the span

Using this characteristic velocity, one can compute the ratio of the heat convected to the heat conducted parallel to the surface. This ratio is, in general, a Peclet number, but in this case of a velocity driven by a surface tension gradient, it becomes a Marangoni number:

$$Pe \simeq \frac{\dot{q}_{conv.}}{\dot{q}_{cond.}} \simeq \frac{U \rho c \Delta T}{k \Delta T/\ell} = \frac{U\ell}{\alpha} = O\left(\frac{\sigma_T/\rho}{\nu \alpha} \cdot \ell \cdot \Delta T\right) \tag{11}$$

$$Ma = \left(\frac{\sigma_T/\rho}{\nu \alpha}\right) \ell \cdot \Delta T \tag{12}$$

where

ν = kinematic viscosity coefficient

This ratio of two alternative heat flows is significant for the present problem, because it measures the effectiveness of the induced motion in cooling off the liquid region adjacent to the igniting heat source and thereby delaying the occurrence of ignition.

In the case of a flow driven by the temperature-induced buoyancy, the relevant dimensionless group is the Rayleigh number. To find the characteristic convective velocity, we make use of the observation that, in the Navier-Stokes equation for the problem, the term due to buoyancy must be of the same order as the term due to viscosity:

$$\nu \frac{\partial^2 w}{\partial x^2} = O\left(\beta \cdot g \cdot \Delta T\right); \qquad w = o(u) \tag{13}$$

$$U = O\left(\frac{\beta \cdot g \cdot \Delta T}{\nu} \cdot \ell^2\right) \tag{14}$$

β = thermal expansion coefficient

g = acceleration due to gravity

Using this expression for the characteristic velocity, we form the ratio of heat flow, as before. Now the corresponding Peclet number becomes the Rayleigh number:

$$Pe = \frac{U\ell}{\alpha} = O\left(\frac{\beta g}{\nu\alpha} \ell^3 \Delta T\right) \tag{15}$$

$$Ra = \left(\frac{\beta g}{\nu\alpha}\right) \ell^3 \Delta T \tag{16}$$

Each of the two numbers depends on the physical properties of the fuel, on the imposed temperature difference, and on the size of the affected flow field. If we take a temperature difference of one degree and a dimension of one centimeter, the two numbers become the unit numbers, Ma_1 and Ra_1, defined as follows:

$$Ma = Ma_1 \cdot \ell \cdot \Delta T \tag{17}$$

(see Table 4)

$$Ra = Ra_1 \cdot \ell^3 \cdot \Delta T \tag{18}$$

In the experiment with the liquid tray described above, the power dissipated in the hot wire was measured. It is possible to replace ΔT in the expression for the Marangoni and Rayleigh numbers with the power, W, in the following way. By recognizing that the loss of heat from the hot wire can be expressed in terms of a heat transfer coefficient, k_H:

$$W = k_H \Delta T \qquad k_H \simeq C_H \rho c U \tag{19}$$

where C_H is a coefficient for convective heat transfer.

Replace ΔT, in the Marangoni and Rayleigh numbers, and take $h \propto \ell$, since vertical heat transfer must be essentially balanced by the induced horizontal heat transfer, using Eqs. 11 and 19, one obtains:

$$Pe = \frac{U\ell}{\alpha} \simeq \frac{Uh}{\alpha} \simeq \left(\frac{\sigma_T/\rho}{\nu\alpha}\right) h \frac{W}{C_H \rho c U} \quad \text{(surface tension driven)} \tag{20}$$

and using Eqs. 15 and 19, one further obtains:

$$Pe = \frac{U\ell}{\alpha} \simeq \frac{Uh}{\alpha} \simeq \left(\frac{\beta g}{\nu\alpha}\right) \frac{h^3 W}{C_H \rho c U} \quad \text{(buoyancy driven)} \tag{21}$$

Both equations can be re-arranged to take the following forms:

$$\frac{U^2}{W} = O\left(\frac{Ma_1}{C_H} \cdot \frac{\alpha}{\rho c}\right) \qquad \text{(surface tension driven)} \quad (20a)$$

$$\frac{U^2}{W} = O\left(\frac{Ra_1}{C_H} \cdot \frac{\alpha}{\rho c} h^2\right) \qquad \text{(buoyancy driven)} \quad (21a)$$

The final results indicate then that each type of driving force should yield a linear correlation between input power to the heated wire and the appropriate grouping of variables shown above. The existence of such correlations has been tested, using measured values (from streak photos) of the maximum fluid velocity leaving the wire, and appropriate values for the various other parameters in the above equations. The results for five different fuels and water are shown in Fig. 30. Both of the correlations appear to be rather good, except for water, which will be discussed separately.

Measured surface temperature by a very fine (25 microns) thermocouple shows a quick temperature rise of a few degrees centigrade a fraction of second after power on. The temperature keeps rising after this jump for the order of tens of minutes. The highest temperature at the surface in the steady-state is plotted in Fig. 31, using the same correlation factor as used in Fig. 30a. From this, we can predict the least power input to bring the surface temperature to the flash point, i.e., minimum requirement to get ignition.

It is of interest to note that the correlation for buoyancy contains an h^3 dependence while that for surface tension a linear h dependence. Therefore, although the similarity number does not directly reveal anything about the manner in which the flow begins (it comes from the steady-state equation), it is evident that the Marangoni number is dominant when the affected portion of the liquid cell is small, and that the Rayleigh number becomes more important when the entire flow field participates in the motion. This tends to indicate that the flow may start with surface tension, but that later it is sustained mainly by buoyancy effects. At what time in the starting transient the cross-over takes place cannot be determined without solving the full set of time-dependent equations. However it appears that during the pre-ignition interval of a liquid fuel both types of forces must be considered.

D.1.3 Motion of Water

Since the liquid fuel motion under study was believed to be characteristic of all fluids, the study was extended to observation of the motion of pure water. From Fig. 30 it can be seen that the motion in water is far less vigorous than in the fuels. Further, in examining the temperature distribution of water due to the local heating, it was noted that the temperature change was concentrated in a 5 mm layer near the surface, Fig. 32, as compared to almost the

entire pool depth for fuel, Fig. 29. It appears, therefore that the thermal layers are more stable in water than in the fuels. The reason for this is not completely understood at present.

In comparing the unit Marangoni and Rayleigh numbers for several of the fluids tested, Table 4, some differences can be observed. For water, the ratio of Rayleigh to Marangoni number is about 1.36 at room temperature, while the ratio for n-decane is about 7.5. When a small amount of alcohol is added to water, decreasing the surface tension, this ratio is increased to about 2.5, and the water motion becomes considerably more vigorous. From this observation, it would appear as though the surface tension, if too large, will tend to retard the motion, and when it is reduced, allows the motion to become more intense. Further study of this phenomena seems to be required for a clear understanding of the mechanisms involved. More light will be shed on this peculiarity of water in the publication which is in progress.[22]

D.2 Theoretical Program

The discussion of the possible forces causing the fluid motion, given in the previous section, stimulated interest in a more quantitative evaluation of the flow phenomena. To accomplish such an evaluation required a detailed solution of the transport equations in the fluid with boundary conditions corresponding to the physical problem. The preliminary results of this study will be reported here, with more complete solutions to be reported in a forthcoming publication.[22]

D.2.1 Theoretical Model

The tray described in section D.1.1 was used to formulate the mathematical model. Since the vertical plane of the wire defines a plane of symmetry, only one half of the pool was considered. The sketch illustrates the model. The plane of symmetry is shown

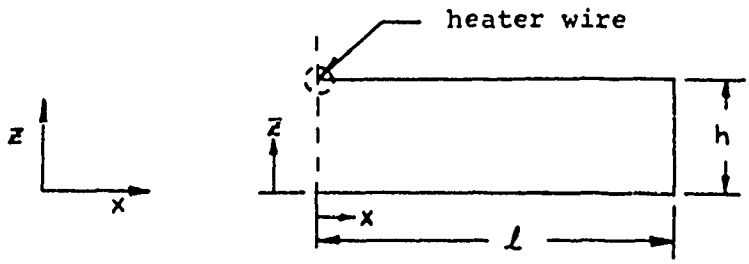

as a broken line. The heat input takes place at x = o, z = h, and begins at t = o+. Due to the large dimension in the y direction, the flow was considered uniform in that direction, resulting in a two-dimensional system.

D.2.2 Transport Equations and Boundary Conditions

The relevant transport equations may be derived from the incompressible Navier-Stokes equations for two-dimensional flow, using the assumptions that

1) only small temperature contrasts are considered, so that the variation of the physical transport properties of the fluid with temperature may be neglected;

2) the Boussinesq approximation concerning the density of an incompressible fluid in natural convection applies, i.e. density variations may be neglected everywhere except in the gravitational body force, giving rise to buoyancy effects.

Assuming a velocity vector $\bar{u} = (u,o,w)$ the relevant equations of state, continuity, and momentum and heat transport are given by

$$\rho = \rho_o\left[1 - \beta(T - T_o)\right] = \rho_o(1 - \beta T_1) \tag{22}$$

$$\frac{\partial u}{\partial x} + \frac{\partial w}{\partial z} = 0 \tag{23}$$

$$\frac{\partial u}{\partial t} + (\vec{u}\cdot\vec{\nabla})u = -\frac{1}{\rho_o}\frac{\partial p}{\partial x} + \nu\nabla^2 u \tag{24a}$$

$$\frac{\partial w}{\partial t} + (\vec{u}\cdot\vec{\nabla})w = -\frac{1}{\rho_o}\frac{\partial p}{\partial x} + \nu\nabla^2 w + \beta g T_1 \tag{24b}$$

$$\frac{\partial T_1}{\partial t} + (\vec{u}\cdot\vec{\nabla})T_1 = k_T\nabla^2 T_1 \tag{25}$$

where T_1 is defined by (22), T_o is suitably averaged mean temperature and ρ_o a corresponding density, and p is the dynamic pressure (total minus hydrostatic). The coefficients of kinematic viscosity ν, thermometric conductivity k_T and thermal expansion $\left(\beta = \frac{1}{\rho_o}\left(\frac{\partial\rho}{\partial T}\right)_{p,\rho_o}\right)$ are assumed to be constant.

For two-dimensional flow we may introduce a streamfunction ψ defined by the relations

$$u = \frac{\partial\psi}{\partial z}\quad,\quad w = -\frac{\partial\psi}{\partial x} \tag{26}$$

Cross-differentiating the first and second component of (24) to eliminate p, and introducing the vorticity (y-component)

$$\zeta = \frac{\partial u}{\partial z} - \frac{\partial w}{\partial x} = \nabla^2\psi \tag{27}$$

we obtain

$$\frac{\partial \xi}{\partial t} + (\vec{u}\cdot\vec{\nabla})\xi = \nu \nabla^2 \xi - \beta g \frac{\partial T_1}{\partial x} \tag{28}$$

The boundary conditions are now summarized as follows:

At $z = 0$ (bottom) $\quad T = T_w \,,\ \psi = 0 \,,\ \xi = \frac{\partial^2 \psi}{\partial z^2}$ (29a)

At $z = h$ (top) $\quad \frac{\partial T}{\partial z} = \frac{Q(x)}{k_T} \,,\quad \xi = 0 \,,\ \psi = 0$ (29b)

At $x = 0$ (plane of symmetry) $\quad \frac{\partial T}{\partial x} = \xi = \psi = 0$ (29c)

$x = l$ (end wall) $\quad T = T_w \,,\ \psi = 0 \,,\ \xi = \frac{\partial^2 \psi}{\partial x^2}$ (29d)

The stream function ψ has been put equal to zero on all four surfaces since no fluid enters or leaves the test volume, and ξ vanishes in view of (27) and the "frictionless wall" approximation.

Finite-difference versions of (25), (27), and (28) were programmed for a digital computer (IBM 360/91), along with the boundary conditions (29); the appropriate numerical schemes and iteration procedures are discussed next.

D.2.3 Numerical Scheme

The finite difference form of equations (25), (27) and (28) will be presented here. For a detailed discussion of the overall scheme, the reader is referred to papers by Williams [23,24] for a discussion of differencing the nonlinear advective terms and the property of conservation to a paper by Arakawa [25], and for a discussion of iterating the initial value problem in time, to two works of Richtmyer [26,27].

We discretize the time coordinate as $t = n\cdot\Delta t$ and the space coordinates as $x = i\cdot\Delta x$, $z = j\cdot\Delta z$, with n, i, j being integers, and denote the value of a dependent variable, say ϕ, at the discrete mesh points as $\phi(x,z:t) = \phi(i\cdot\Delta x, j\cdot\Delta z : n\cdot\Delta t)$. Introducing the difference operators

$$\delta_T(\phi_{ij}^n) = \frac{\phi_{ij}^{n+1} - \phi_{ij}^{n-1}}{2\,\Delta t} \tag{30}$$

$$\delta_x(\Phi_{i,j}^n) = \frac{\Phi_{i+1,j}^n - \Phi_{i-1,j}^n}{2\Delta x}, \quad \delta_z(\Phi_{i,j}^n) = \frac{\Phi_{i,j+1}^n - \Phi_{i,j-1}^n}{2\Delta z} \tag{31[a,b]}$$

$$DFX(\Phi_{i,j}^n) = \frac{\Phi_{i+1,j}^n + \Phi_{i-1,j}^n - \Phi_{i,j}^{n+1} - \Phi_{i,j}^{n-1}}{(\Delta x)^2} \tag{32a}$$

$$DFZ(\Phi_{i,j}^n) = \frac{\Phi_{i,j+1}^n + \Phi_{i,j-1}^n - \Phi_{i,j}^{n+1} - \Phi_{i,j}^{n-1}}{(\Delta z)^2} \tag{32b}$$

We may write (25) and (28) as

$$\delta_t(T_{i,j}^n) = -\delta_x[(\delta_z \psi)T]_{i,j}^n + \delta_z[(\delta_x \psi)T]_{i,j}^n + k_r[DFX(T_{i,j}^n) + DFZ(T_{i,j}^n)] \tag{33}$$

$$\delta_t(\Phi_{i,j}^n) = -\delta_x[(\delta_z \psi)\xi]_{i,j}^n + \delta_z[(\delta_x \psi)\xi]_{i,j}^n + \nu[DFX(\xi_{i,j}^n) + DFZ(\xi_{i,j}^n)] - \beta g \delta_x(T_{i,j}^n) \tag{34}$$

The particular form of spatial differencing the nonlinear advection terms is denoted by $\mathcal{F}_2$ in Arakawa's[25] work and is shown there to conserve the kinetic energy of the system. It may be also shown that it conserves T as well, i.e. the area-averaged quantity $\bar{T} = \sum\sum T_{i,j}$ is unaffected by the advection terms, as it should be. The particular form of differencing the friction terms is known as the DuFord-Frankel scheme, and the particular scheme of evaluating $\partial\Phi/\partial t$ with central differences and taking the right-hand-side at the center level n (the friction terms are slightly modified) is known as "leap-frogging".

Suppose the iteration in time has proceeded through step n so that we know all dependent variables at levels n, n-1, etc. then the values at level n+1 may be simply obtained from summing the right-hand-sides of (33) and (34), after having transferred the terms $(\Phi_k)_{i,j}^{n+1}$ appearing in the friction terms to the left-hand-side (Φ_k here denoting ξ or T). This type of time iteration, in which the new values Φ_k^{n+1} are obtained from previous values of Φ_k^n, Φ_k^{n-1} without iteration or Gaussian elimination is known as an explicit scheme.

Explicit time-iteration schemes have usually a stability condition imposed on the size of the time step Δt with which one can advance. The Von Neumann condition (p. 70, ref. 28) on the numerical stability of the equations (33) and (34) reduces essentially to two conditions: one due to the advection terms and one due to

internal gravity waves. The conditions become

$$\Delta t \leq \frac{\Delta x}{|u| + \frac{\Delta x}{\Delta z}|w|} \tag{35}$$

$$\Delta t \leq \frac{\sqrt{2}\,\pi\,\Delta x}{\sqrt{\beta g \left|\frac{\partial T}{\partial z}\right|}} \tag{36}$$

which must be observed at each mesh point i, j for the over-all scheme to remain stable. The choice of the DuFort-Frankel scheme for the friction terms eliminated one of the severest restrictions on Δt, usually $\Delta t \leq \Delta x^2/u$

The solution of the Poisson equation (27), which must be performed after each time step to obtain new values of $\psi_{i,j}^{n+1}$ (and hence $u_{i,j}^{n+1}$ and $w_{i,j}^{n+1}$), is accomplished by means of discrete Fourier series. We expand both $\zeta_{i,j}$ and $\psi_{i,j}$ as

$$\zeta_{i,j} = \sum_{m=1}^{\mathcal{J}-1} b_i^m \sin(m\pi j \Delta z) \tag{37}$$

$$\psi_{i,j} = \sum_{m=1}^{\mathcal{J}-1} a_i^m \sin(m\pi j \Delta z) \tag{38}$$

where $-1+\mathcal{J} = \frac{1}{\Delta z} - 1$ is the number of interior mesh points, and solve the resulting $\mathcal{J}-1$ ordinary difference equations

$$\frac{a_{i+1}^m + a_{i-1}^m - 2a_i^m}{(\Delta x)^2} - m^2\pi^2 a_i^m = b_i^m \tag{39}$$

for each a^m by the well-known "tri-diagonal algorithm" (p. 200, ref. 27). Here practically all the computation is spent in decomposing ζ into b_i^m, and superposing the a_i^m to obtain $\psi_{i,j}$. Utilizing the symmetry of the discrete sine functions $\sin(m\pi j/\mathcal{J})$ many multiplications can be eliminated and the total computation time shortened by large factors. In the case of a pure sine series, this factor is 3; in case of periodic boundary conditions it becomes as large as 8. For a description of the relevant algorithms, the reader is referred to the paper by Williams[24].

D.2.4 Choice of Physical Parameters

The physical parameters were chosen to correspond to the experiment involving n-decane, 2 cm deep, initially at 20°C, and heated by a power input of 1 watt/cm along the wire. The relevant

liquid properties of n-decane at 20°C are:

α = 0.000843 cm^2/sec
k_T = 0.00032 cal/sec cm °C
μ = 0.009 poise
β = 0.00103 $°C^{-1}$
ρ = 0.73g/cm^3

No evaporation or heat transfer at the upper surface is allowed, except from the wire. Around the wire ($Q(x)/k$ = 1 watt/cm $.r_w$) for $x < r_w$ and zero for $x > r_w$. No viscous shear is allowed at the upper surface of the liquid, but the shear along the tank walls is considered. The initial temperature is assumed uniform, and the wall temperatures remain constant at this value of 20°C.

D.2.5 Results and Discussion

Fig. 33 shows a preliminary plot of the calculated streamlines in the pool of n-decane at 1.55 sec after the power was turned on. The comparison in this report, with experimentally observed motion will be only qualitative, with more quantitative comparison to follow in the publication.[22] This figure considers only the effect of buoyancy, with surface tension effects to be incorporated later.[22] There is a concentrated circulation pattern set up in the region near the heater, similar to the experimentally observed vortices, with some evidence of small vortices being shed from the larger one. These shed vortices are more difficult to observe in the experiments, but are not to be discounted.

Further numerical study is continuing in order to:

a) observe the growth of the vortex with time, to compare with Fig. 28

b) observe the effect of surface tension gradient on the vortex pattern, in an attempt to explain the differences between the motion observed in water and that observed in hydrocarbon fuels

c) observe the possible effect of the containing walls on the flow pattern and intensity.

D.3 Conclusions

Convective motion of the fluid due to heat input at a point in the surface of a pool of fuel is very complex. The motion appears to be driven by buoyancy and surface tension gradients resulting from curved isotherms in the fluid. The Marangoni and Rayleigh numbers are proposed as the important dimensionless grouping of variables to explain the motion. It is observed that the motion is more vigorous in hydrocarbon fuels than in water for equivalent conditions, perhaps due to a larger ratio of Rayleigh to Marangoni number.

Preliminary results from numerical calculations based on the equations of motion, with buoyancy as the sole driving mechanism, yield results which resemble the experimentally observed vortices.

REFERENCES

1. Glendinning, W. G., and Drinkwater, J. W., "The Prevention of Fire in Aircraft", J. Roy. Aero. Soc. 51, p. 616 (1947).

2. Pinkel, I., Preston, G. M., and Pesman, G. J., "Mechanism of Start and Development of Aircraft Crash Fires", NACA RP 1133 (1953).

3. Williams, C. G., "Fuels and Lubricants for Aero Gas Turbines", Institute of Petrol J. 33 (1947), pp. 292-296.

4. Crellin, J. W., Johnson, J., and Carhart, H. W., "Relation of Minimum Ignition Point to Other Ignition Phenomena", NRL Report 4476 (Jan. 1955).

5. Campbell, J. A., "Appraisal of the Hazards of Friction-Spark Ignition of Aircraft Crash Fires", NACA TN 4024, May 1957.

6. Roberts, Ph.D. Thesis, Imperial College, England (1959).

7. Burgess, D. S., Grummer, J., and Wolfhard, H. G., "Burning Rates of Liquid Fuels in Large and Small Open Trays", First International Symposium on Fire Research (Nov. 1959), pp. 68-75.

8. Burgess, D. S., Strasser, A., and Grummer, J., "Diffusive Burning of Liquid Fuels in Open Trays", Division of Fuel Chemistry, American Chemical Society, Symposium on Fire Control Research, Chicago, Illinois (Sept. 1961).

9. Kuchta, Barkowiak, and Zabetakis, "Hot Surface Ignition Temperatures of Hydrocarbon Fuel Vapor Air Mixtures", J. of Chem. and Eng. Data 10 (1965), pp. 282-288.

10. Burgoyne, J. H., Roberts, A. F., and Quinton, P. G., "The Spread of Flame Across a Liquid Surface", Proc. Roy. Soc. A308, 39, 55, 69.

11. MacKinven, R., Hansel, J. G., and Glassman, I., "Influence of Laboratory Parameters on Flame Spread Across Liquid Fuels", Comb. Sci. and Tech. 1 No. 4 (Jan. 1970).

12. Sirignano, W. A., and Glassman, I., "Flame Spreading Above Liquid Fuels: Surface-Tension-Driven Flows", Comb. Sci. and Tech. 1 No. 4 (Jan. 1970).

13. Kreith, F., Principles of Heat Transfer, International Textbook Company, Scranton, Pa. (1966) pp. 290-291.

14. Eckert, E. R. G., and Drake, R. M., Heat and Mass Transfer, McGraw Hill Book Company, New York (1959).

15. Rohsenow, W., and Choi, H., Heat, Mass, and Momentum Transfer, Prentice Hall Inc., New Jersey (1961).

16. Summerfield, M., "A Theory of Convective Effects in Flame Spreading Over Liquid Fuels", Unpublished Report, Guggenheim Laboratories, Princeton University (Nov. 1968).

17. ASME Fluid Meters, 5th ed., N. Y. American Society of Mechanical Engineers (1958).

18. Pankhurst, R. C., and Holder, D. W., Wind Tunnel Technique, Pitman Press, London, England (1952).

19. Gaydon, A. G., and Wolfhard, H. G., Flames, 2nd ed. revised Chapman & Hall Ltd., London, England (1960) p. 26.

20. Murad, R. J., "Experimental Investigation of Ignition of Pools of Liquid Hydrocarbon Fuels", M.S.E. Thesis, Princeton University, Princeton, N. J. (1970).

21. Murad, R. J., Lamendola, J., Isoda, H., and Summerfield, M., "A Study of Some Factors Influencing the Ignition of a Liquid Fuel Pool", Submitted to Combustion and Flame, August 1970.

22. MacDonald, B. W., Piacsek, S., Isoda, H., Plett, E. G. and Summerfield, M., "Preignition Motion of Liquid Fuels Due to Local Heat Input at the Upper Surface", In progress, Sept. 1970.

23. Williams, G. P., Jour. Atmos. Sci., 24, 144 (1967).

24. Williams, G. P., Jour. Fluid Mech. 37, 727 (1969).

25. Arakawa, A., Jour. Comput. Physics 1, 119 (1966).

26. Richtmyer, R. D., N.C.A.R. Technical Note 63-2 (1963).

27. Richtmyer, R. D. and Norton, K. W., Difference Methods for Initial Value Problems, Interscience Publishers, 1967.

TABLE 1. The variation of ignition height over n-Amyl Alcohol (F.T. 38°C) with change in initial fuel temperature, air flow, and power of igniter C in the subflash regime. (Fuel depth 4mm.)

Fuel Temp. (°C)	Power to Igniter C (Watts)	Ignition Height (mm)	
		No air flow	Flow of 2 ft/sec
22	95	.5	.4
26	95	.5	.5
26	110	1.1	1.0
30	95	.6	.7
30	110	1.3	1.5
34	95	1.2	1.6
34	110	3.4	2.1

TABLE 2. The variation of ignition height over Benzyl Alcohol (F.T. 101°C) with change in initial fuel temperature, air flow and power of igniter C in the subflash regime. (Fuel depth 4mm.)

Fuel Temp. (°C)	Power to Igniter C (Watts)	Ignition Height (mm)	
		No air flow	Flow of 2 ft/sec
24	95	No Ignition	
24	110	Ignition at the surface	
40	95	Ignition at the surface	
40	110	Ignition at the surface	
70	95	.3	.3
70	110	.4	
80	95	.5	.8
96	95	3.6	2.3

TABLE 3 The effectiveness of the various igniters shown in Fig. 14, and fuel depth on the ignition delay of n-Amyl Alcohol (F.T. 38°C) at temperature of 21°C and igniter height of 1mm above the fuel surface.

Probe	Power to Probe (Watts)	Fuel Depth (mm.)	Ignition Delay (sec.)
A	56	4	12 1/2
	66	6.5	10 1/4
	68	8	9 1/2
B	61	2.5	11 1/4
	62	4	10 1/2
	62	6.5	11 1/2
	62	8	11 1/2
C	60	2.5	15 3/4
	66	4	No ignition within 90 sec.
	59.4	6.5	No ignition within 90 sec.
	59.4	8	No ignition within 90 sec.
D	56	2.5	12 1/2
	60	4	14 1/4
	63	6.5	20
	60	8	64 1/2
E	66	8	25 '2
G	64	2.5	40
	64	8,6.5,4	No ignition within 90 sec.

TABLE 4

Unit Marangoni and Rayleigh Numbers
For Liquids Studied

Liquid	Unit Marangoni Number (Ma_1)	Unit Rayleigh Number (Ra_1)
Pure water	1.1×10^4	1.5×10^4
n-Decane	1.2×10^4	9.6×10^4
n-Decane plus 1.5% surfactant*	0.13×10^4	9.6×10^4
n-Decane plus 1.5% Vistanex	0.023×10^4	0.19×10^4
Ethyl Alcohol	0.96×10^4	9.3×10^4

*Test sample by 3M Company, #FC-176

6104 RG23 70

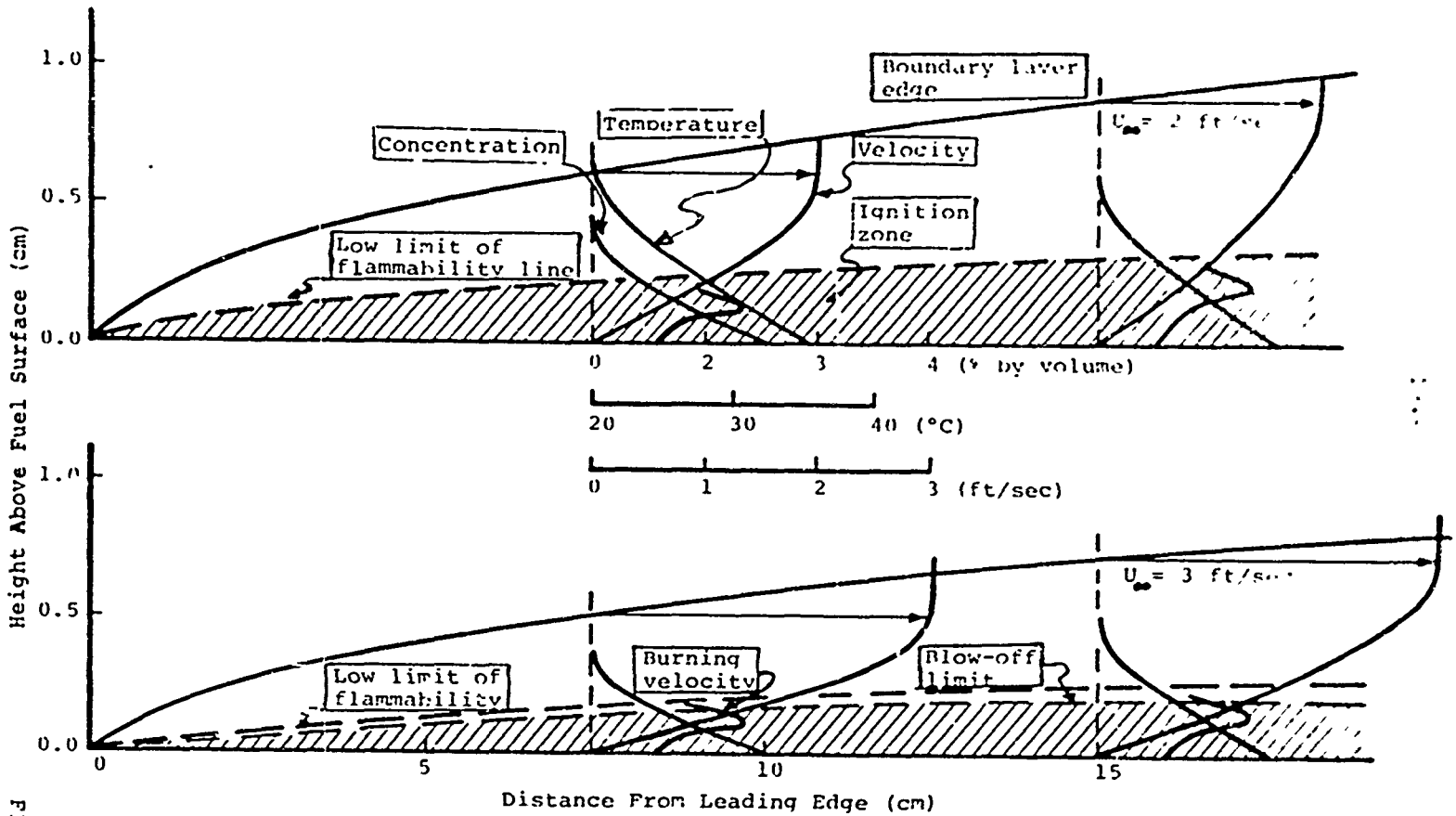

FIGURE 1

Model of Boundary Layer Profiles and Ignition Zone Over a Pool of n-Octane (Flash Temp. 13°C) With Fuel Temperature of 35°C.

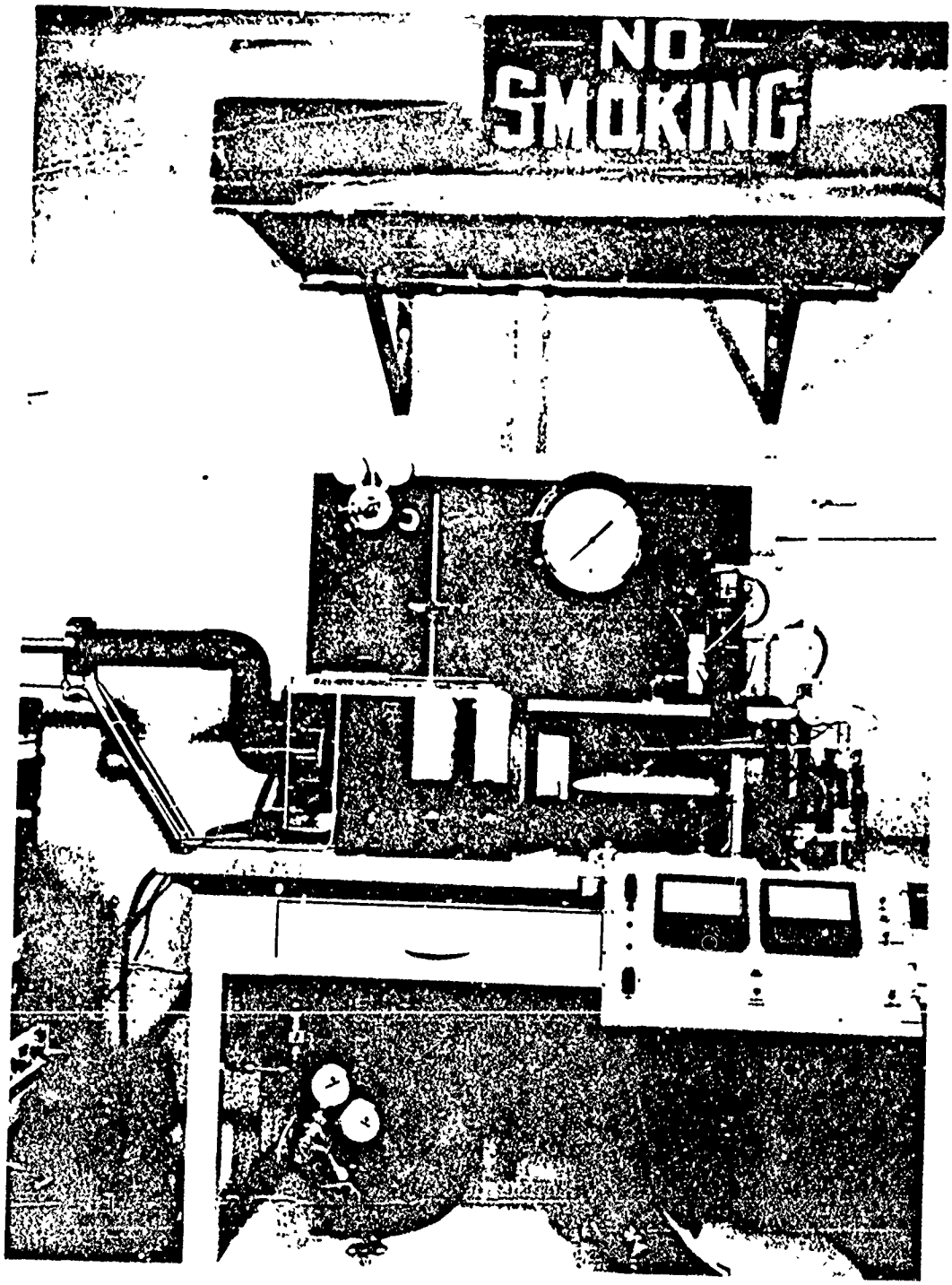

EXPERIMENTAL RIG FOR IGNITION OF LIQUID FUEL.

FIGURE 2

6104 P2 70

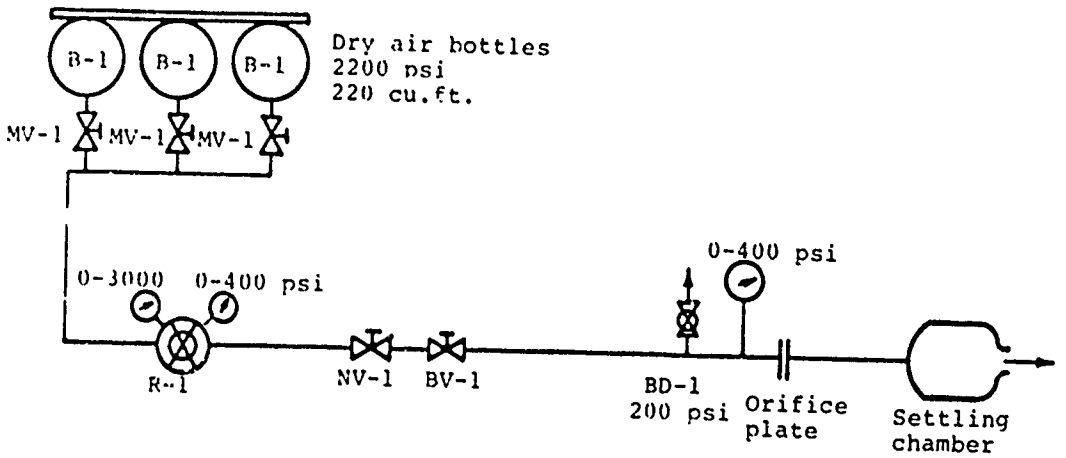

(a)

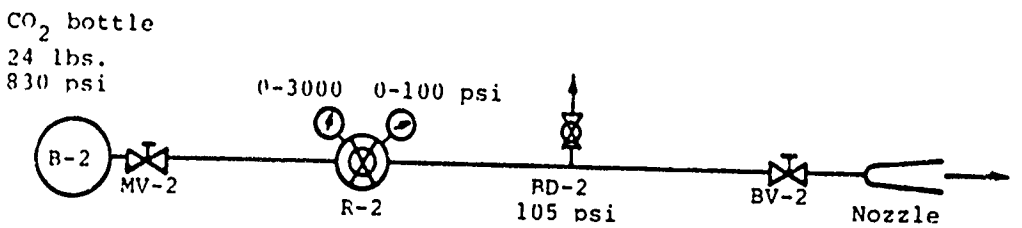

(b)

Flow Chart of the Air (a) and CO_2 Extinguishant (b) Supply Systems.

6104 R030 70

FIGURE 3

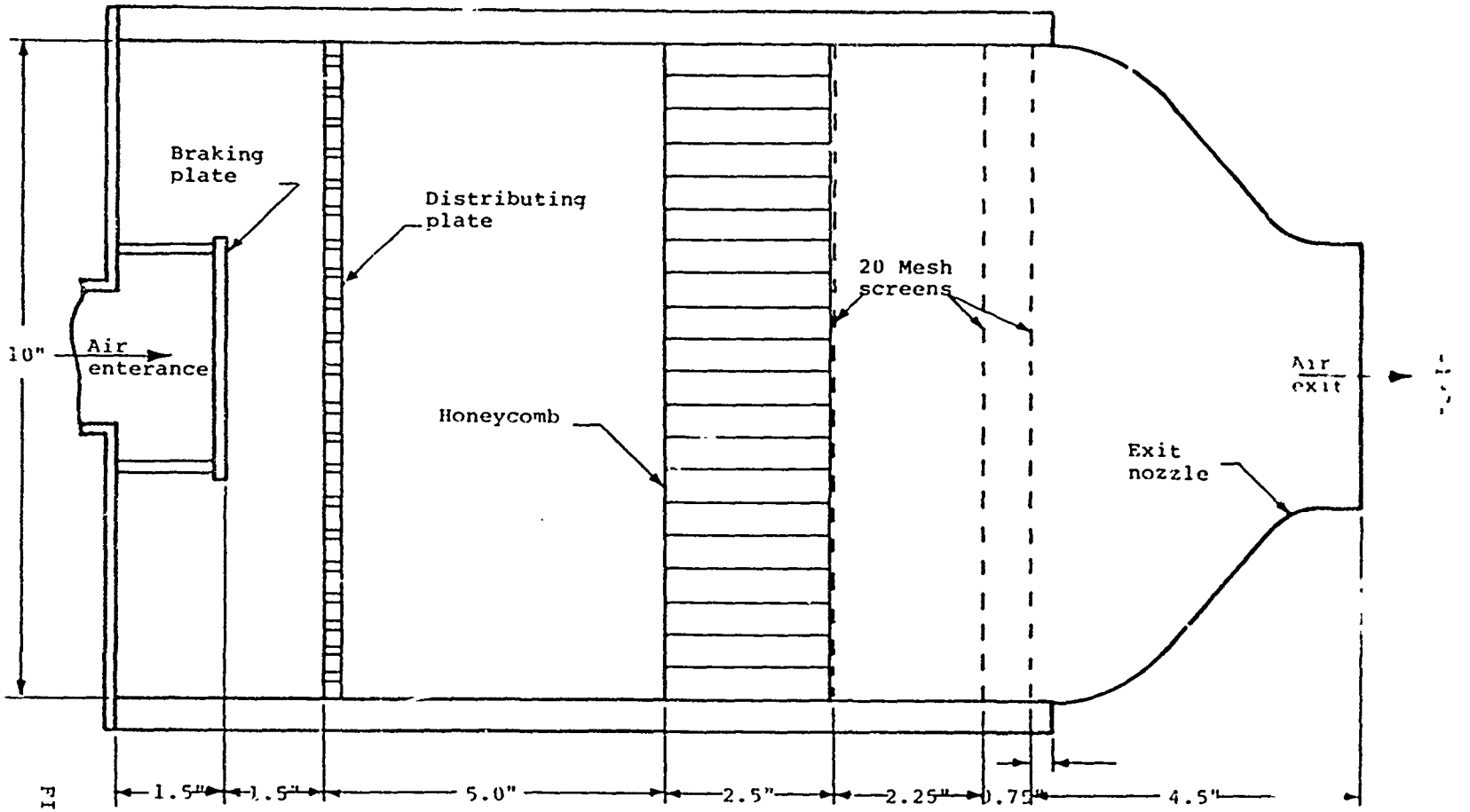

FIGURE 4

Essential Features of the Settling Chamber.

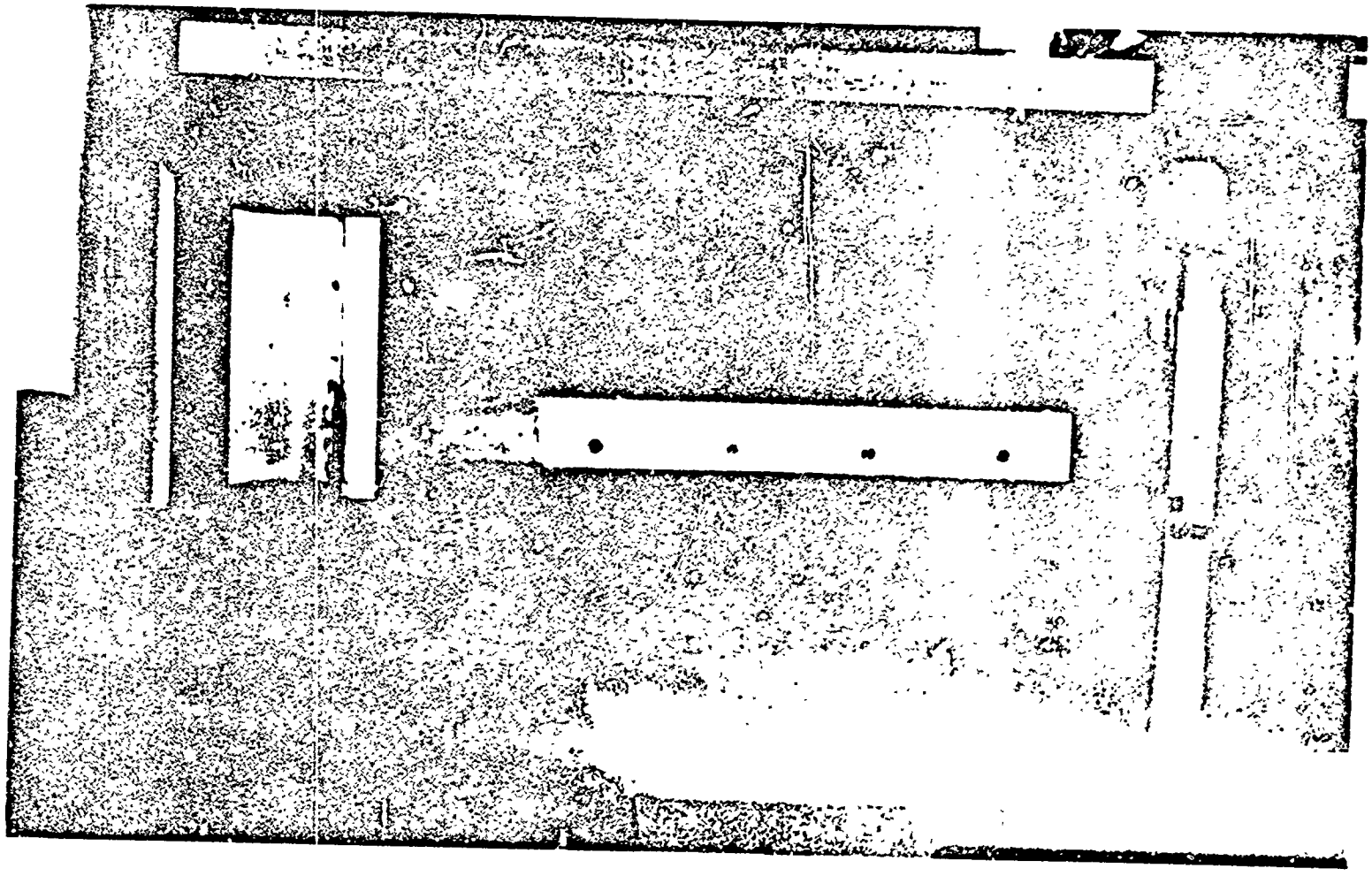

TEST SECTION WITH SMOKE FLOW FROM THE SETTLING CHAMBER TO THE FUEL TRAY.

FIGURE 5

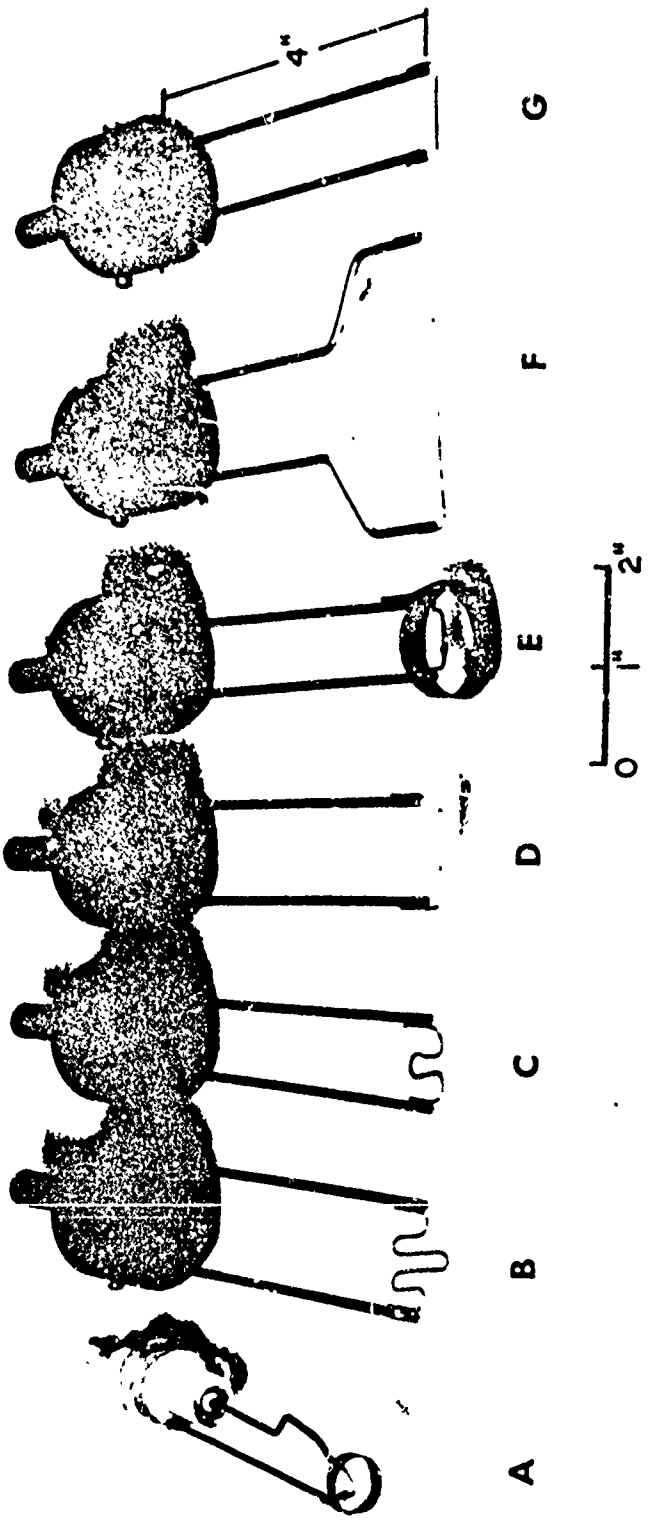

VARIOUS IGNITERS USED FOR IGNITION OF FUEL BELOW FLASH TEMPERATURE.

FIGURE 6

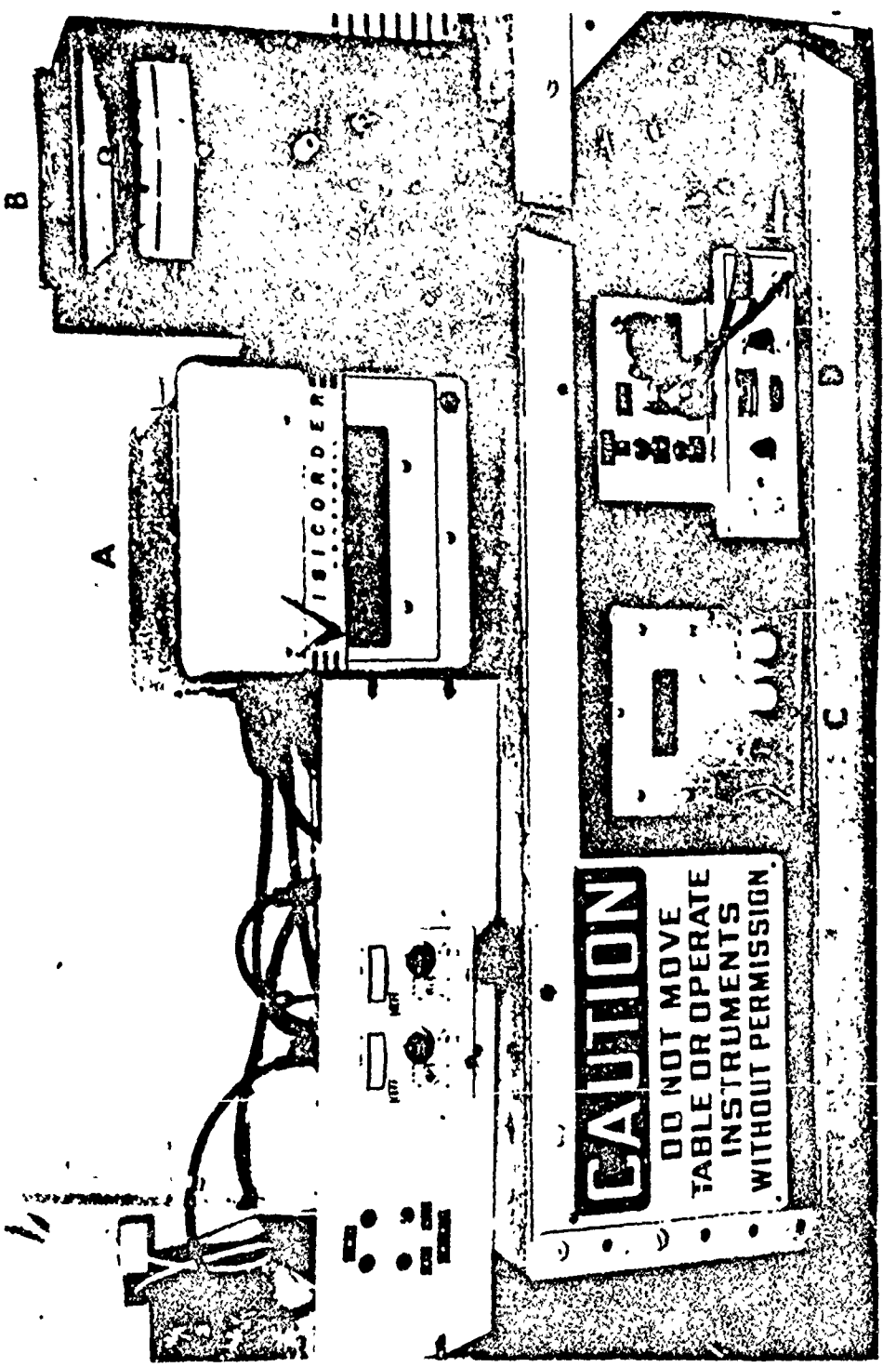

INSTRUMENT RACK: A. OSCILLOGRAPH
B. TEMPERATURE CONTROLLER
C. TIMER
D. HOT WIRE ANEMOMETER

FIGURE 7

6104 R032 70

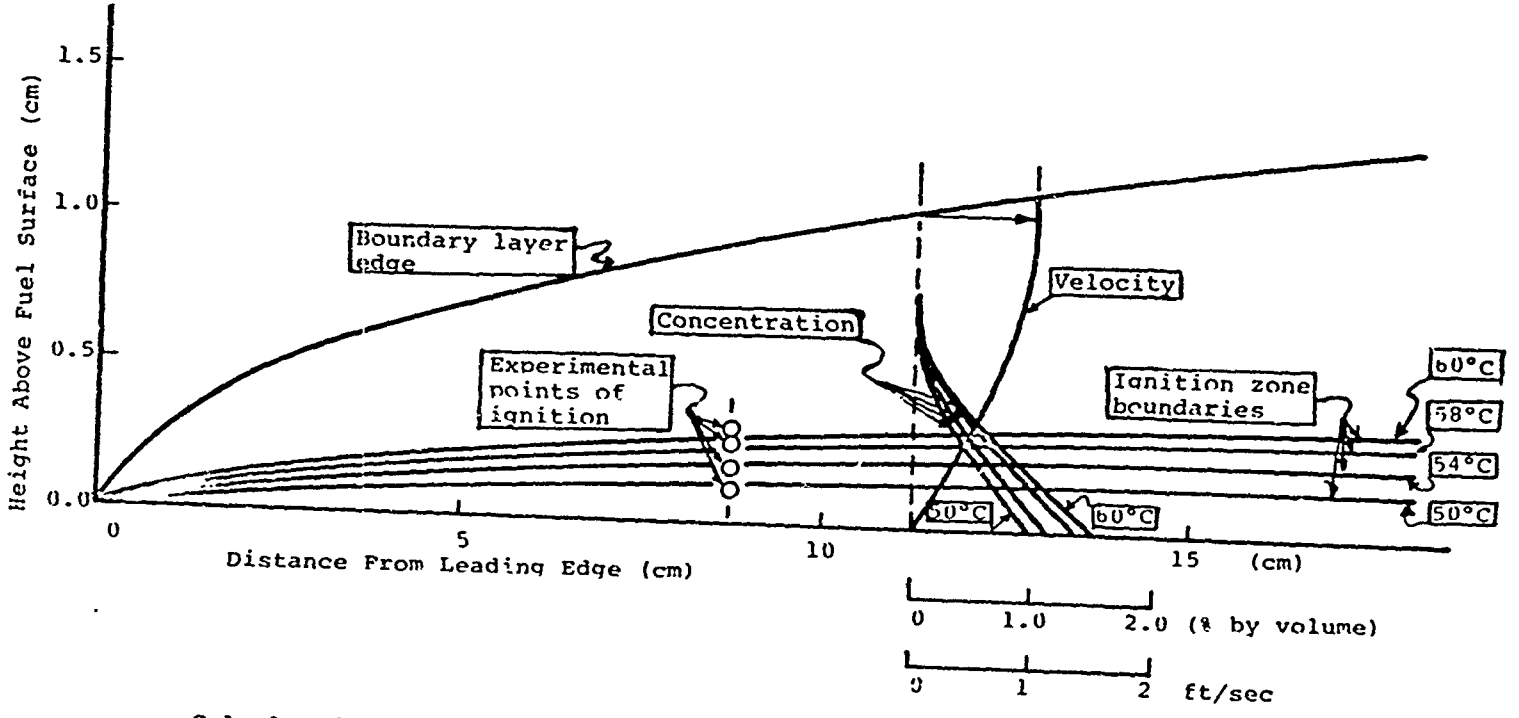

FIGURE 8

Calculated Profiles of Concentration, Velocity, and Ignition Zone Boundary Over a Pool of n-Decane (Flash Temp. 46°C) at Various Surface Temperatures Compared with Experimental Points of Ignition. (Igniter G)

6104 R 033 70

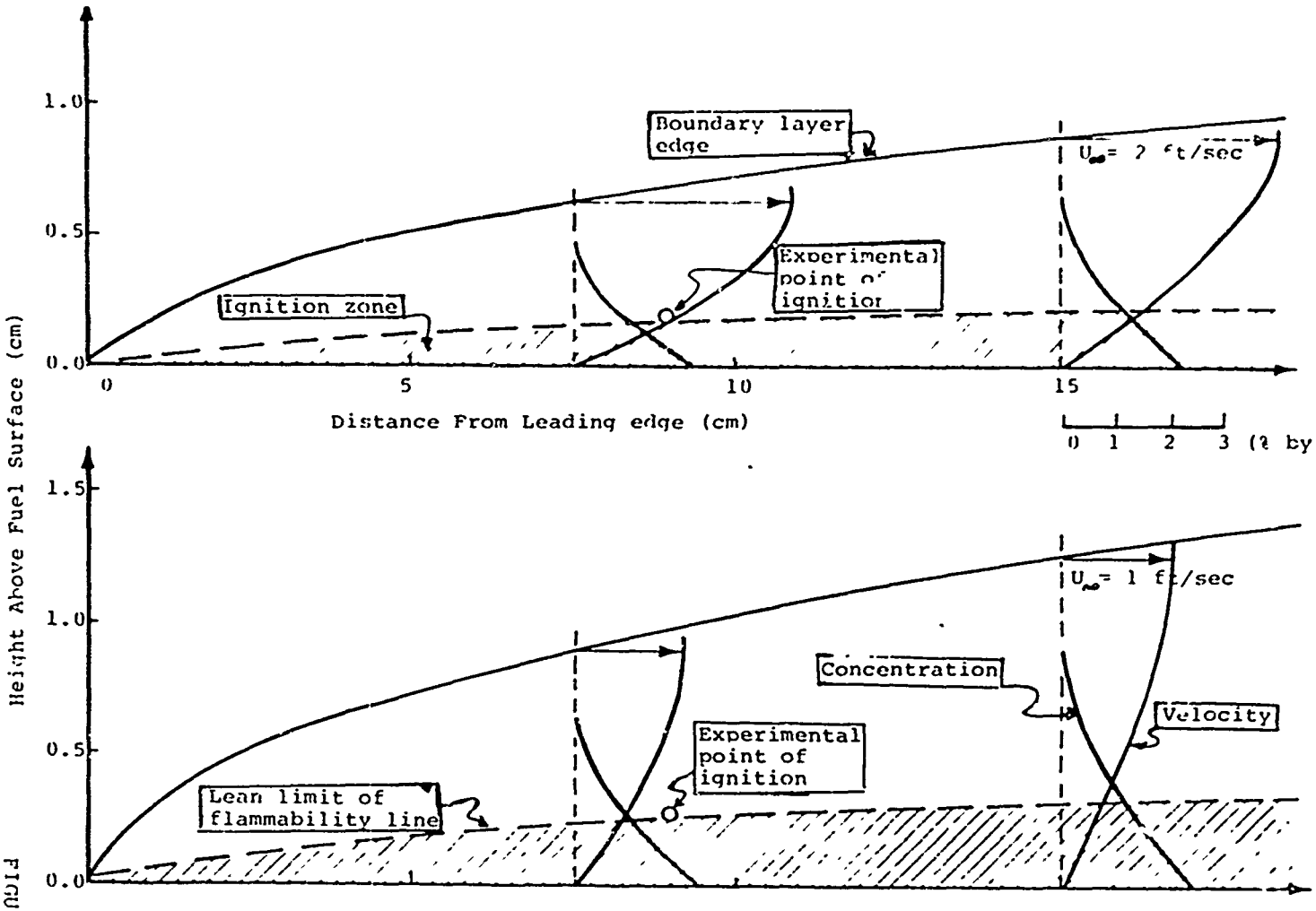

FIGURE 9

Calculated Profiles of Concentration, Velocity, and Ignition Zone Boundary Over a Pool of n-Amyl Alcohol (F.T. 38°C) at a Surface Temperature of 54°C Compared with Experimental Point. (Spark Plug Igniter)

6104 R 034 70

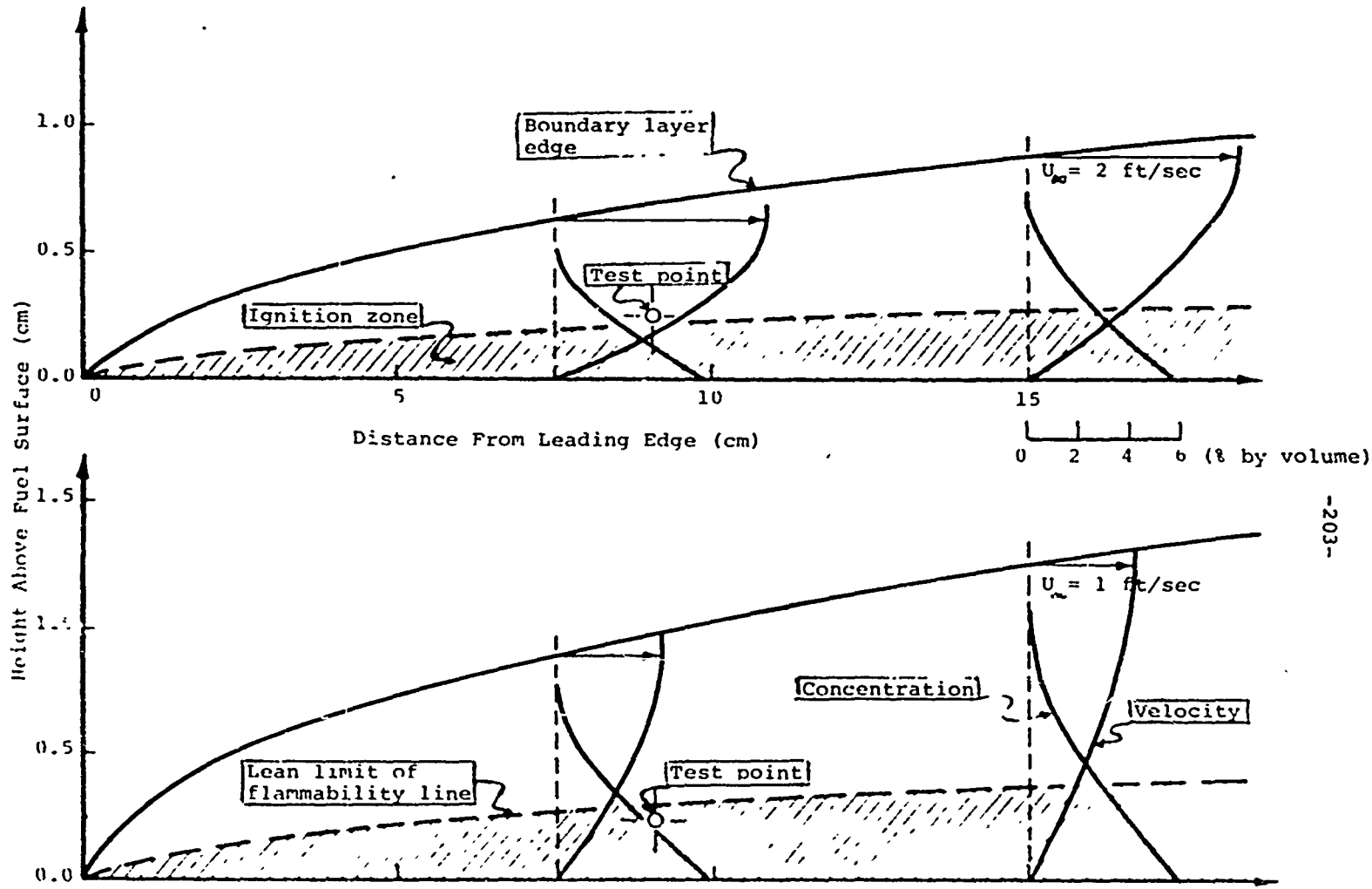

FIGURE 10

Calculated Profiles of Concentration, Velocity, and Ignition Zone Boundary Over a Pool of Iso-Propyl Alcohol (Flash Temp. 38°C) at a Surface Temperature of 25°C.

Maximum Ignition Height Above n-Decane (F.T. 46°C) Fuel Surface vs. Initial Fuel Temperature for Several Flow Velocities.

Regime I: Fuel Below Flash Temperature

Regime II: Fuel Above Flash Temperature but Below Fire Temperature

Regime III: Fuel Above Fire Temperature

Experimental Conditions: 1. Igniter C
2. Power to Igniter 95 Watts
3. Fuel Depth 4 mm

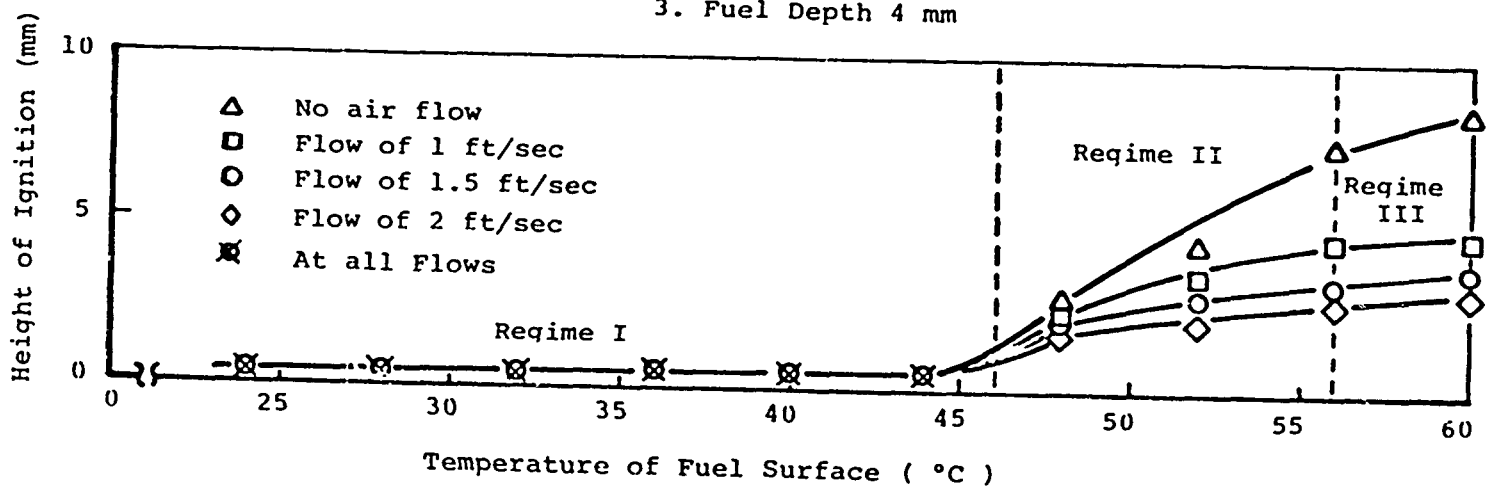

FIGURE 11

Ignition Height Over n-Decane Fuel (F.T. 46°C) vs. Main Flow Velocity, at Various Initial Fuel Temperatures.

Curves (1) & (2) Regime I

(3) & (4) Regime II

(5) Regime III

Experimental conditions: 1. Igniter C
2. Power of 95 Watts

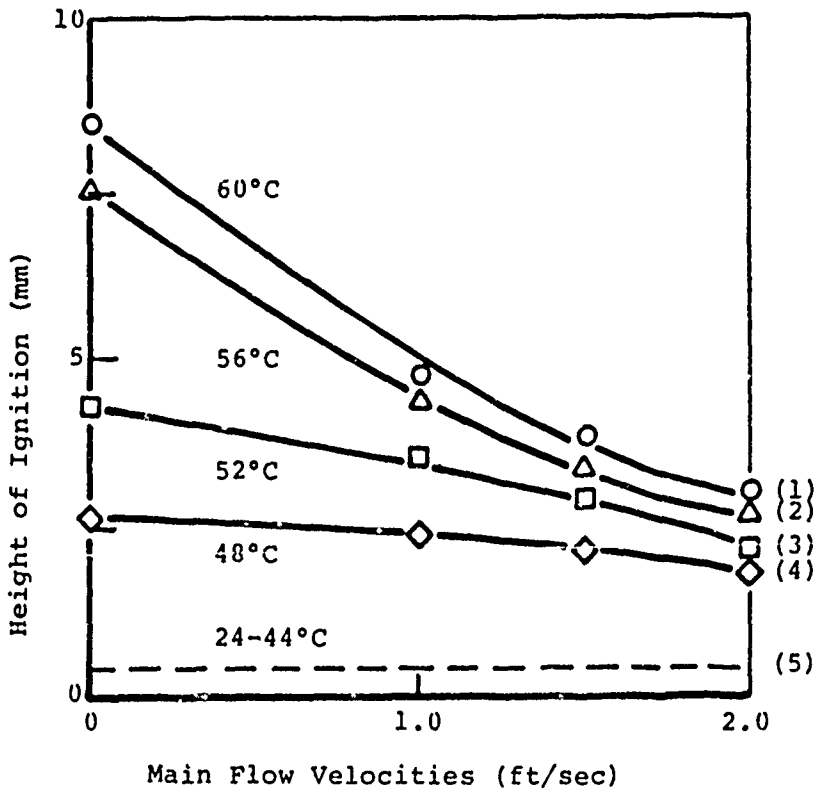

6104 R 036 70

FIGURE 12

The Variation of Ignition Height With the Change in Surface Temperature of n-Decane (F.T. 46°C).

Experimental Conditions: 1. Igniter G
2. Power of 60 Watts

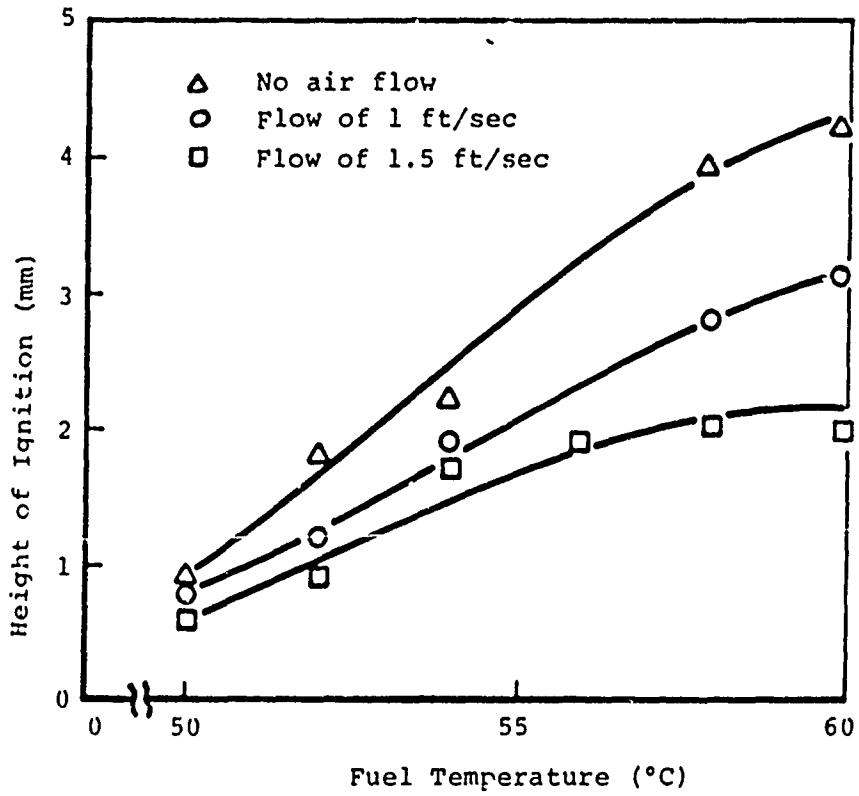

6104 R 037 70

FIGURE 13

6104 R 038 70

The Variation of Ignition Height With Change in Surface Temperature of n-Butyl Alcohol (F.T. 38°C).

Experimental Conditions: 1. Igniter G
2. Power of 60 Watts

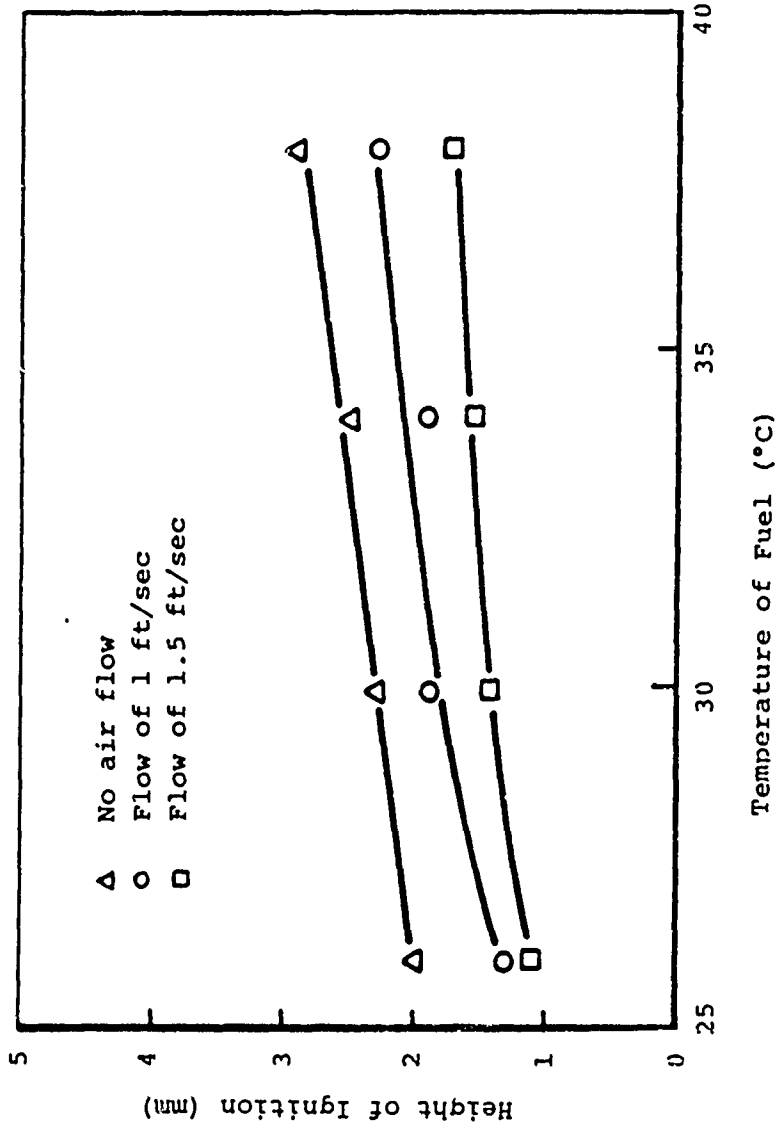

FIGURE 14

a) Temperature of Igniter as Measured by Optical Pyrometer vs. Power to Various Igniters [C,D,G].

b) Maximum Ignition Height Above n-Decane Fuel (F.T. 46°) vs. Power of Various Igniters. [C,D,G]

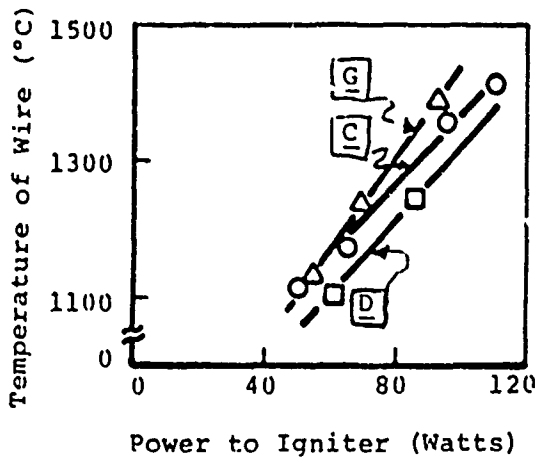

(a)

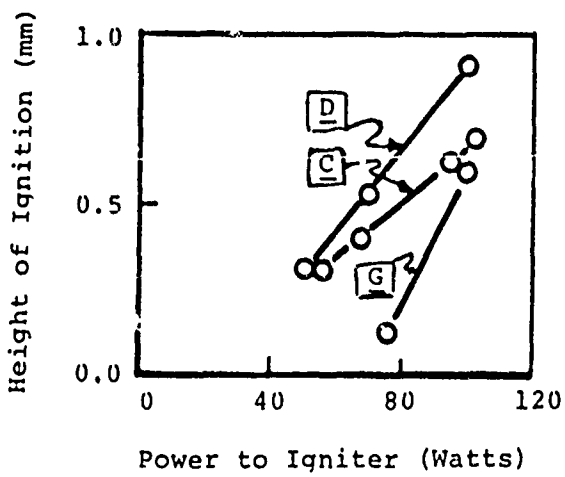

(b)

FIGURE 15

6104 R 039 70

Ignition of n-Butyl Alcohol (F.T. 38°C) at 26°C Initial Surface Temperature Showing Effect of Different Igniters on Ignition Height. (No Flow)

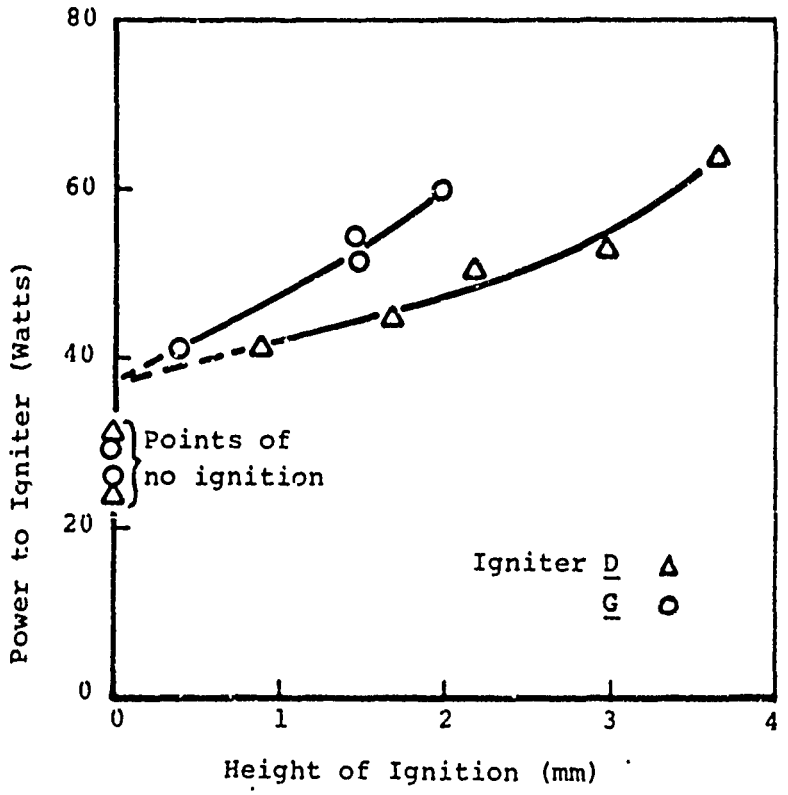

6104 R 040 70

FIGURE 16

Ignition of n-Amyl Alcohol (F.T. 38°C)
Showing Effect of Various Igniters and
Different Initial Fuel Temperatures.
(No Flow)

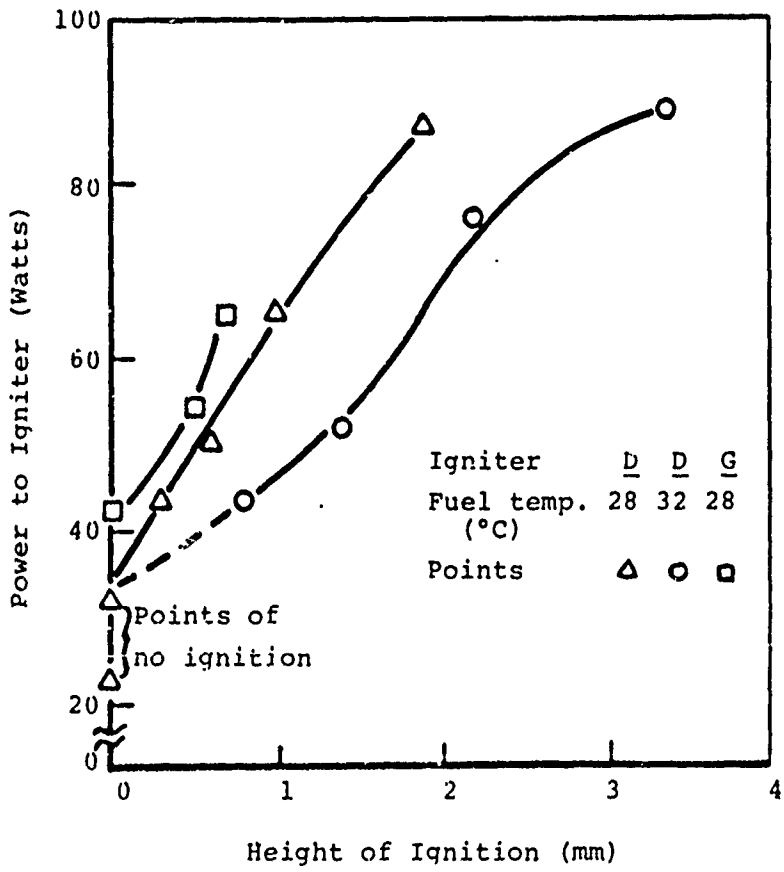

6104 R 041 70

FIGURE 17

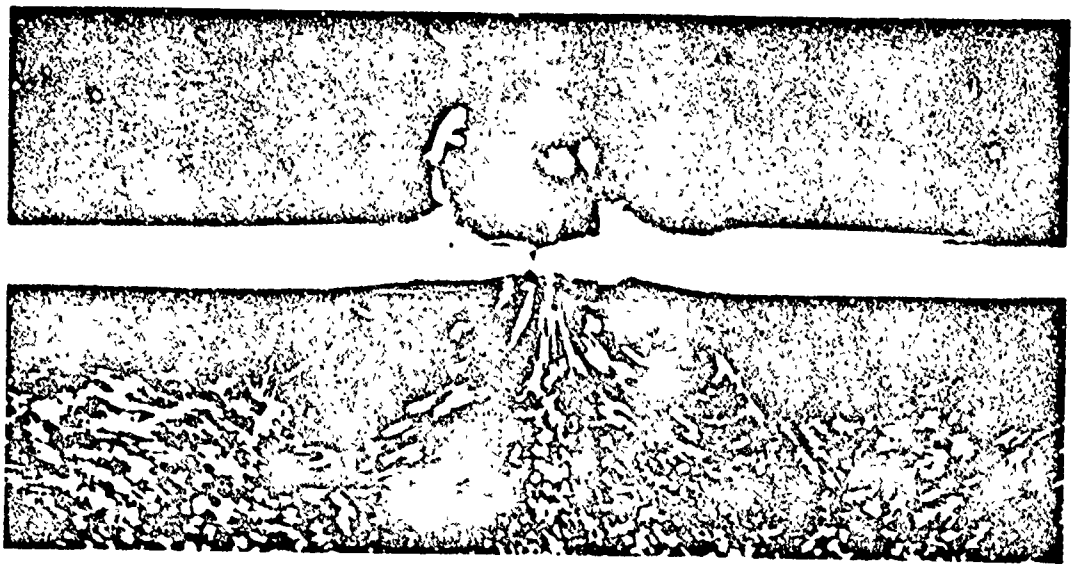

Streak Photograph of n-decane Showing Induced Eddy Motion With Probe Power Input of 0.72 Watts.

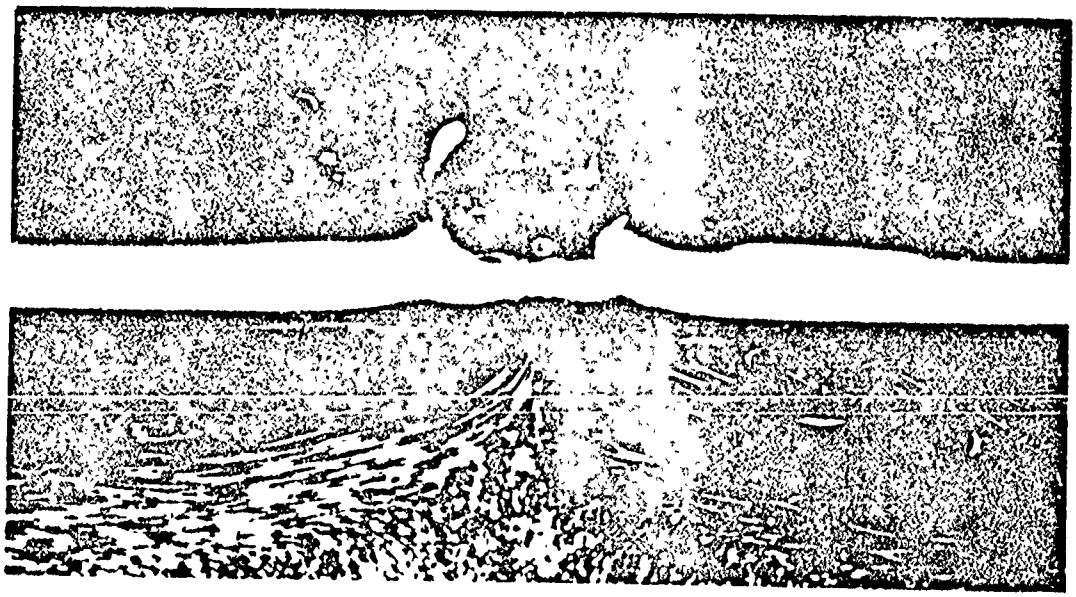

Streak Photograph of n-decane Showing Induced Eddy Motion With Probe Power Input of 2.9 Watts.

FIGURE 18

Influence of Additives on Ignition Delay vs. Power to Igniter.

Experimental Conditions:
1. Test Tray (3"x7.25")
2. Fuel Depth 4 mm
3. Initial Fuel Temp. 30°C
4. Ignition Height 0.5 mm

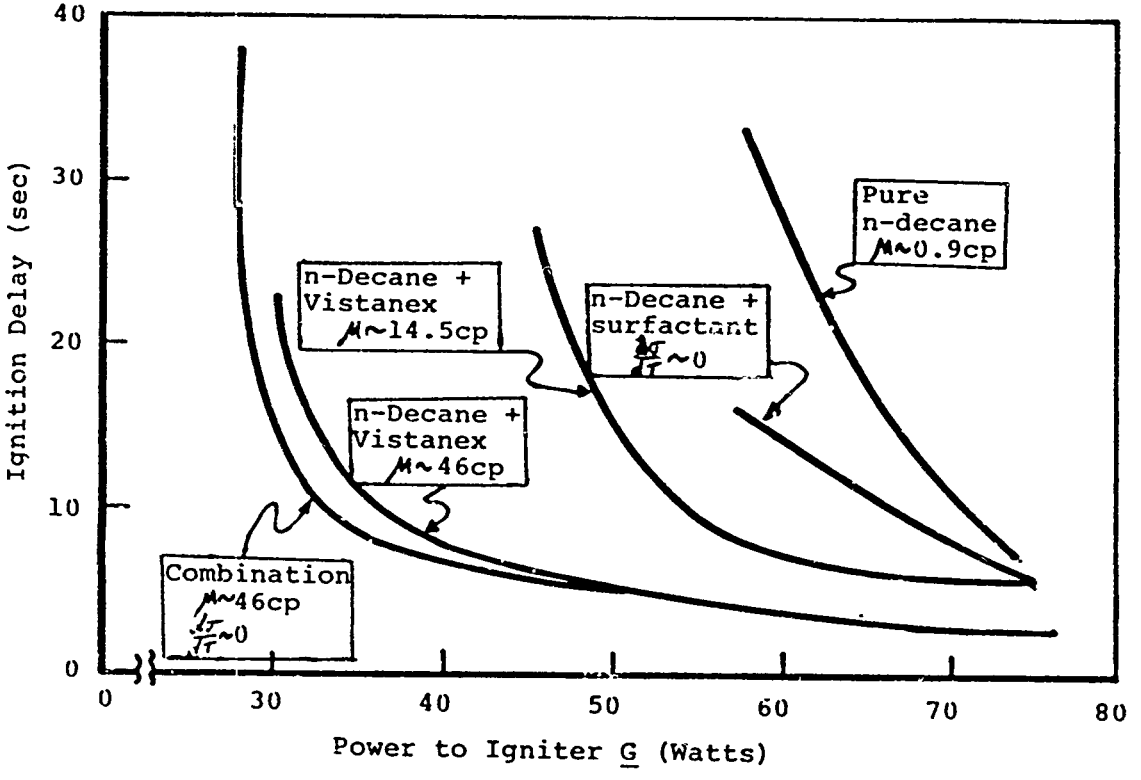

FIGURE 19

Ignition Delay vs. Diameter of Tray

Experimental Conditions:

1. n-Amyl Alcohol Fuel (F.T. 38°C)
2. Initial Fuel Temp. 23°C
3. Fuel Depth 23 mm
4. Power to Igniter G 56 Watts
5. Ignition Height 0.5 mm

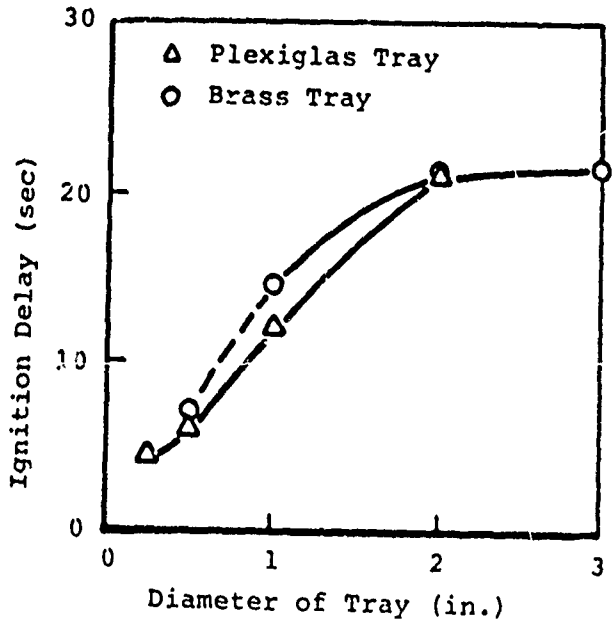

6104 R 043 70

FIGURE 20

Ignition Delay vs. Depth of Fuel

Experimental Conditions:

1. Conditions 1,2,4,and 5 of Fig. 20

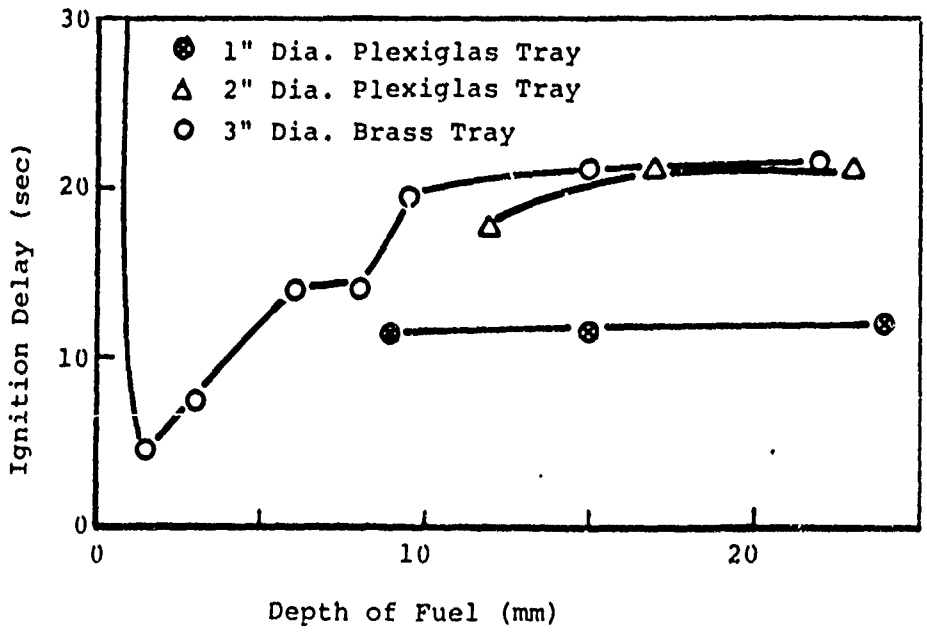

6104 R 044 70

FIGURE 21

(a) Surface Temperature at Time of Ignition vs. Power to Igniter.
    (1) Thermocouple Under Igniter
    (2) 4 mm Away

(b) Ignition Delay vs. Power to Igniter.

Experimental Conditions:

1. n-Decane Fuel (F.T. 46°C)
2. Igniter G
3. Ignition Height 0.5 mm
4. Initial Fuel Temp. 23°C
5. 2" Dia. Plexiglas Tray
6. Fuel Depth 22 mm

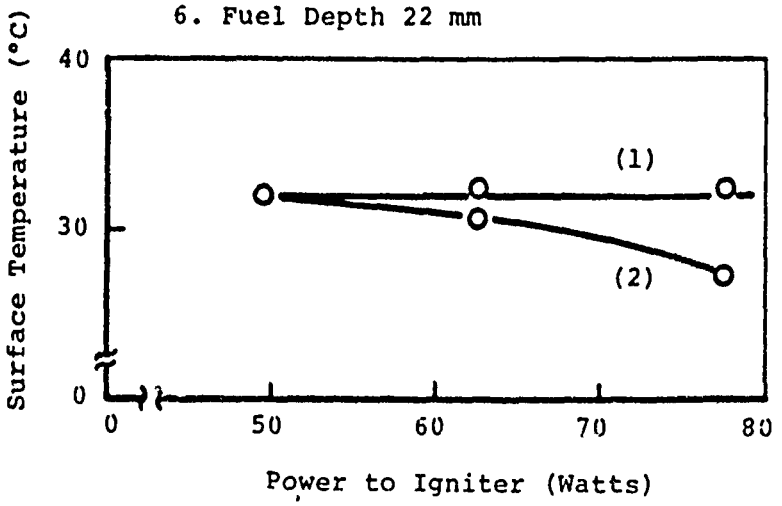

(a)

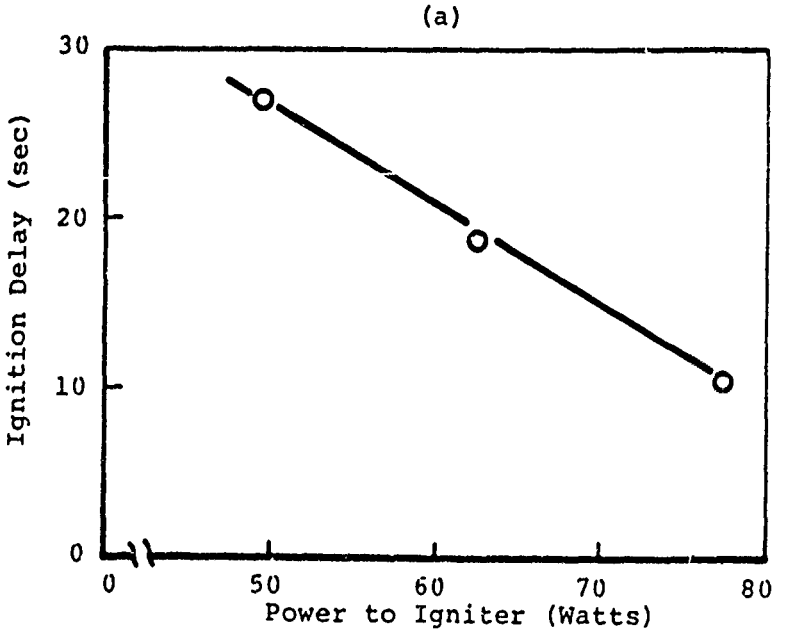

(b)

FIGURE 22

Ignition Delay vs. Ignition Height

Experimental Conditions:

1. n-Decane Fuel (F.T. 46°C)
2. Initial Fuel Temp. 21°C
3. Igniter G
4. Power to Igniter 56 Watts
5. 2" Dia. Plexiglas Tray
6. Fuel Depth 22 mm

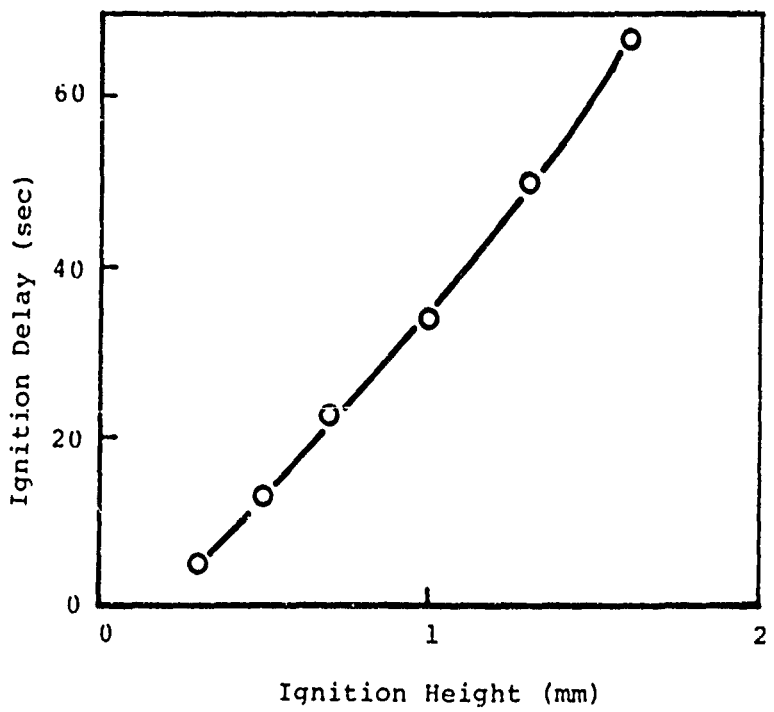

6104 R046 70

FIGURE 23

Ignition Delay vs. Initial Fuel Temperature

Experimental Conditions:

1. Conditions 1,3,5,and 6 of Fig. 23
2. Power to Igniter 58 Watts
3. Igniter Height 1.0 mm

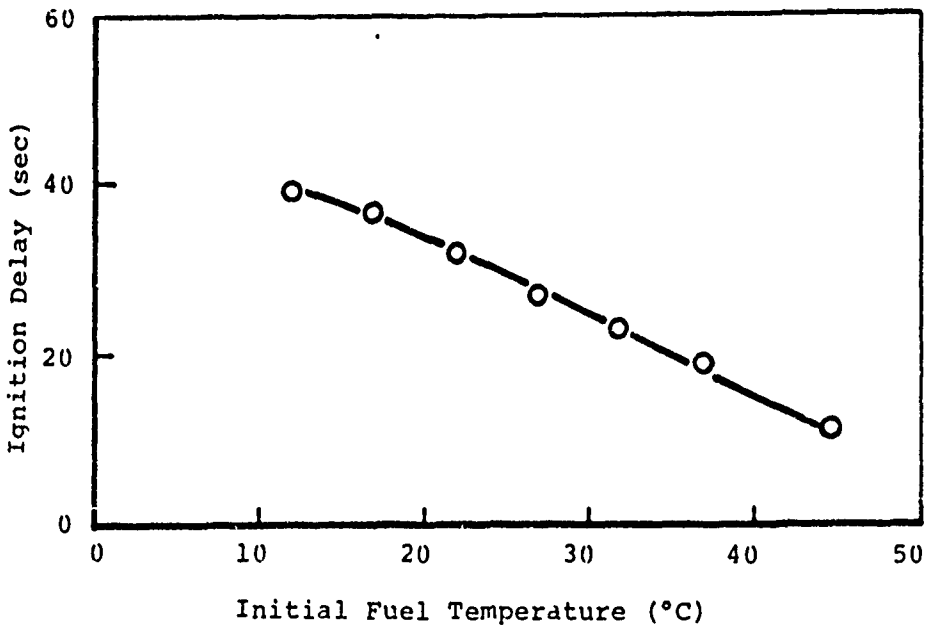

FIGURE 24

Effect of Igniter Height Over the Fuel Surface on the Fuel Surface Temperature Under the Igniter at Time of Ignition.

Experimental Conditions:

1. Conditions 1 to 6 of Fig. 23

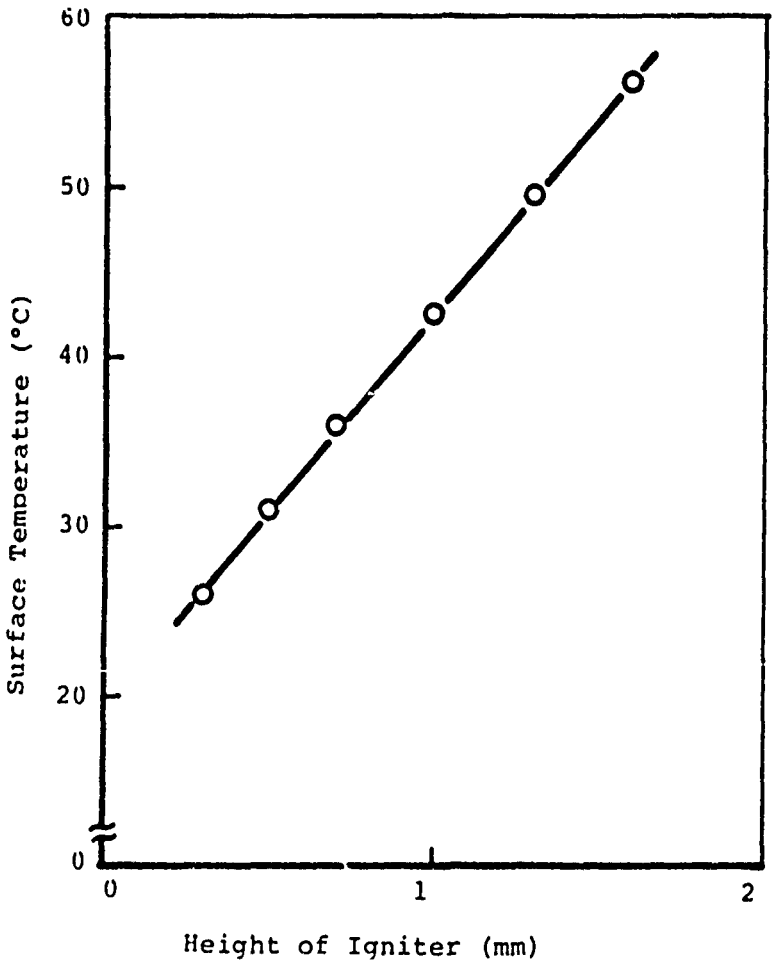

6104 R 048 70

FIGURE 25

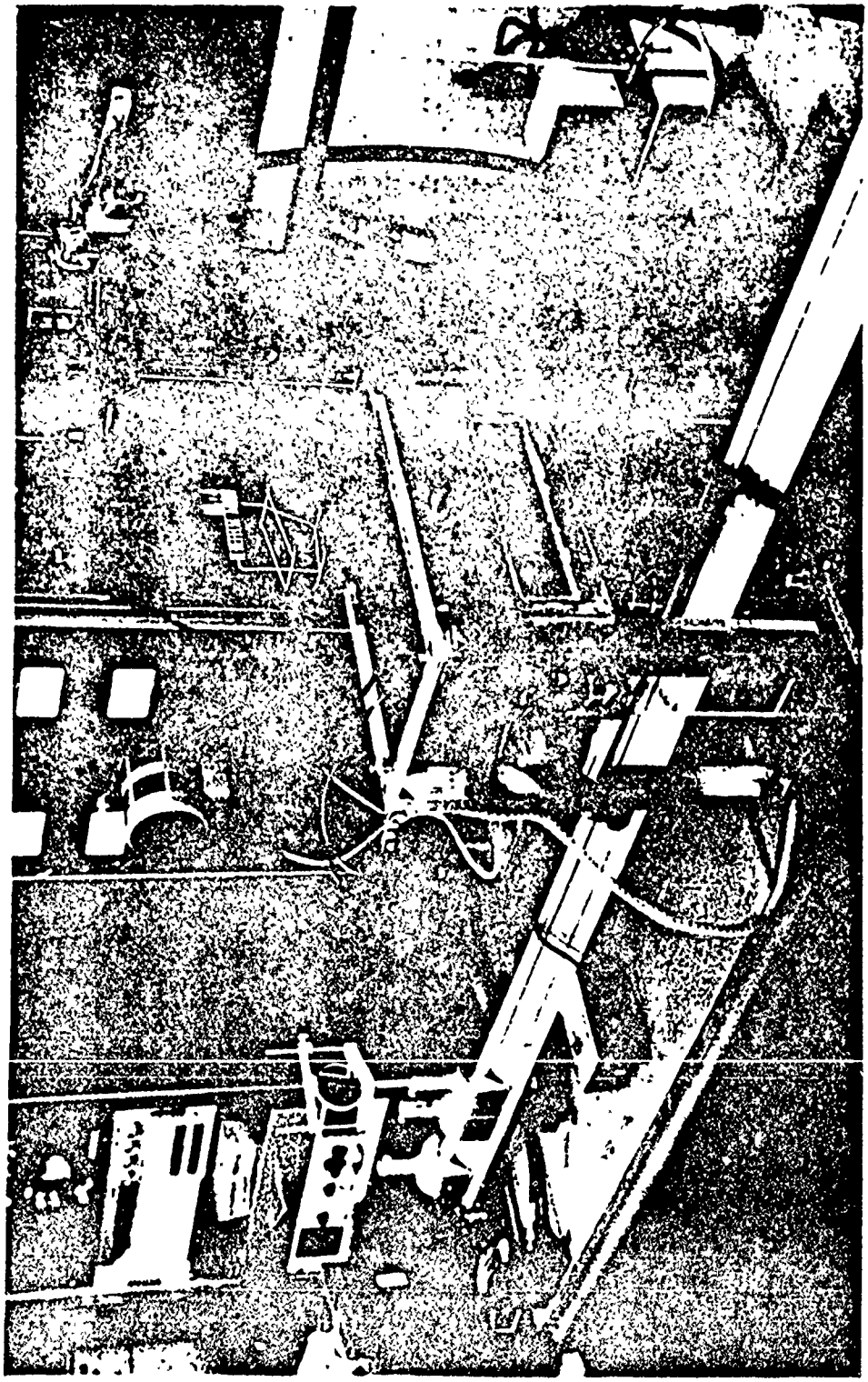

EXPERIMENTAL APPARATUS FOR LIQUID MOTION STUDY

FIGURE 26

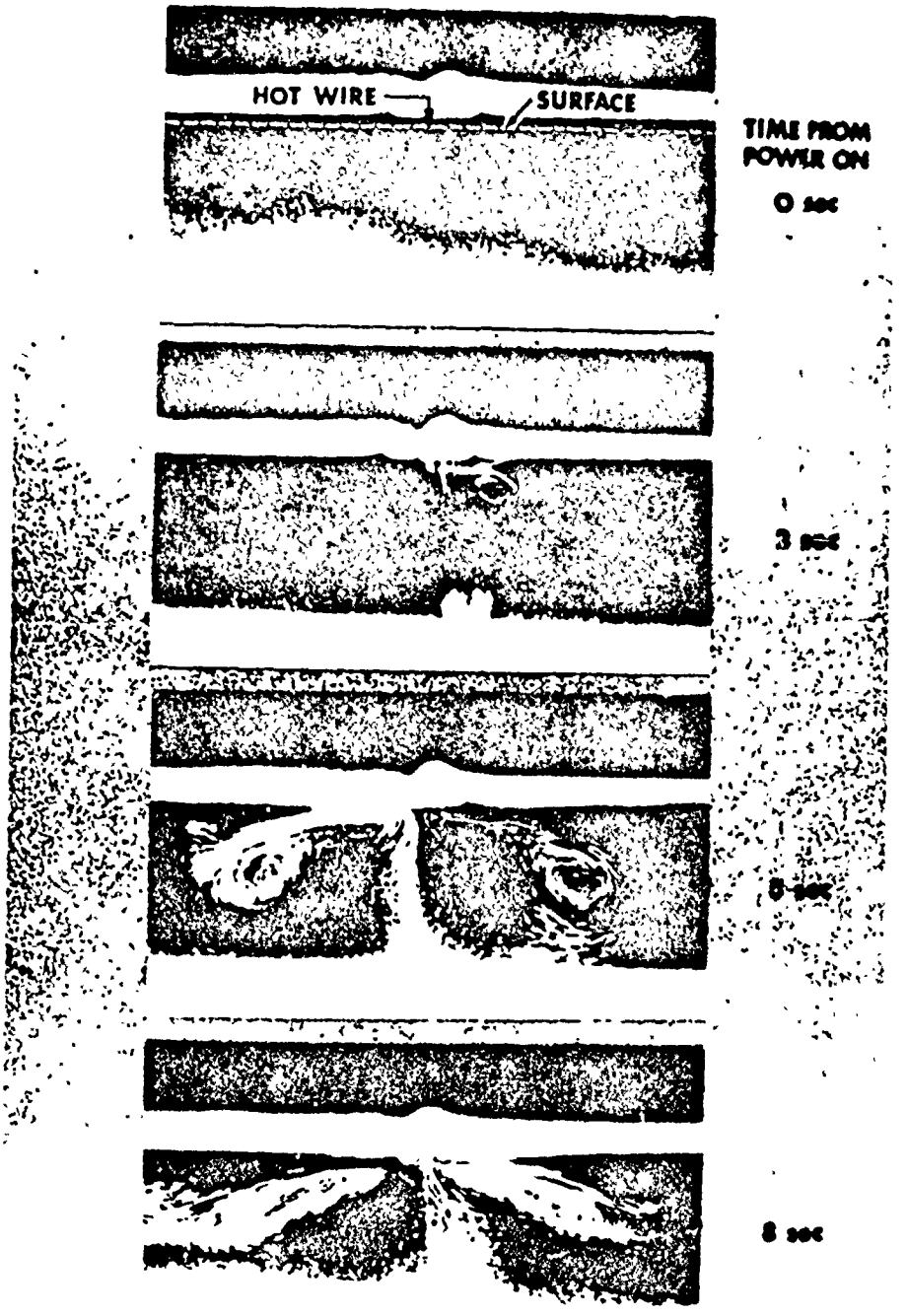

N-DECANE. 2 cm DEPTH. 20°C. 1 w/cm POWER INPUT

EDDY GROWTH IN N-DECANE FIGURE 27

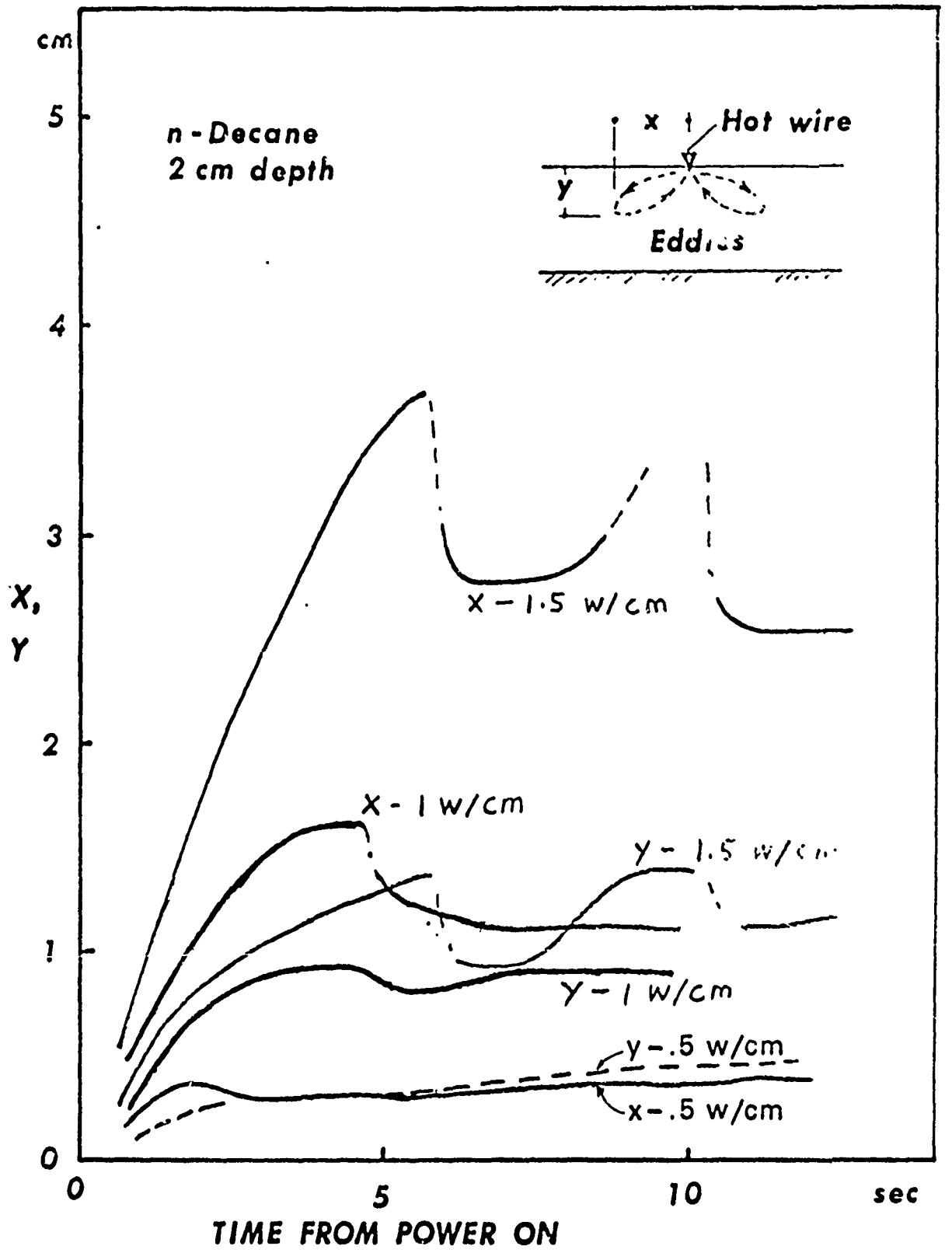

Change of Eddy Dimensions With Time

FIGURE 28

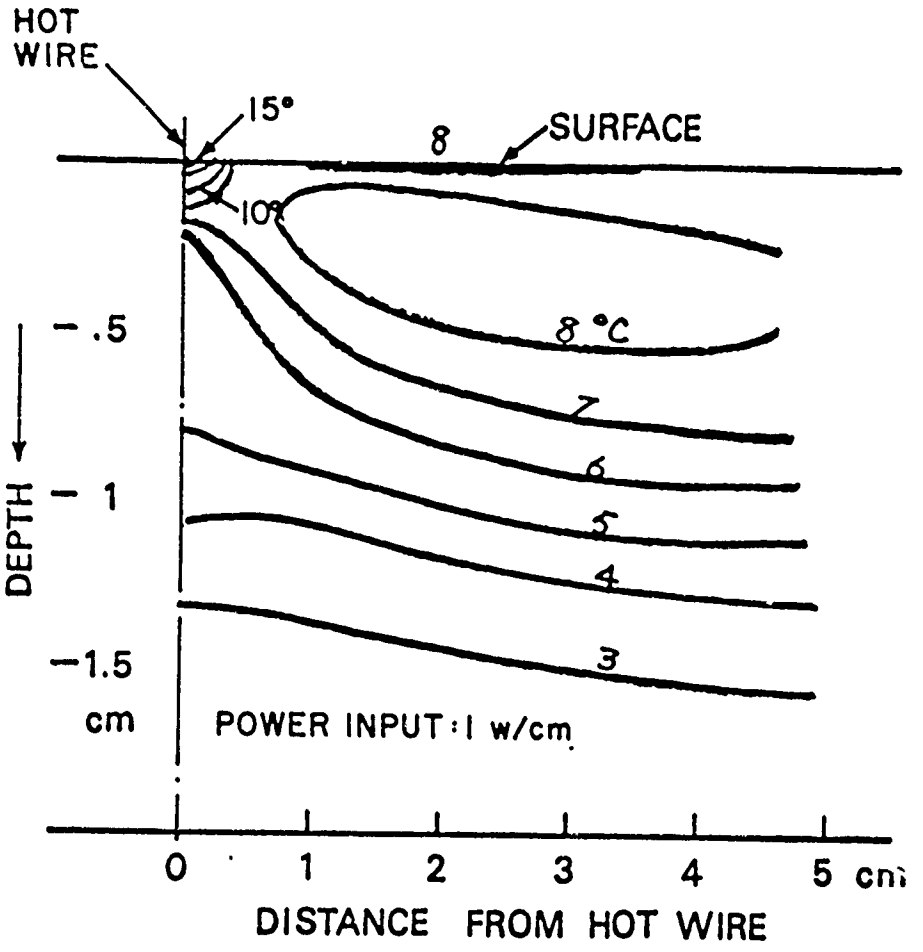

Temperature Rise in N-Decane As Measured by Fine Thermocouples

6104 R 052 70

FIGURE 29

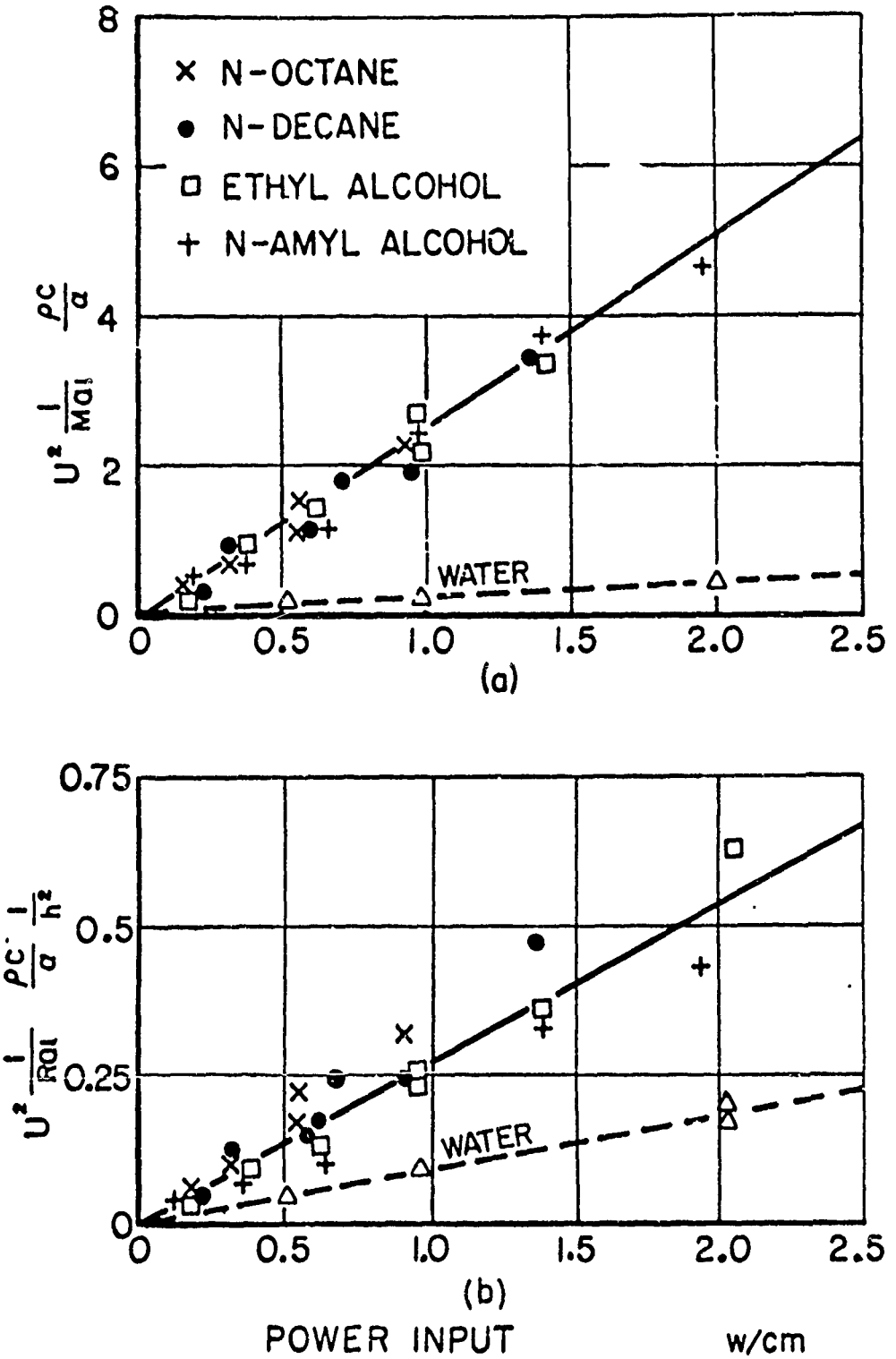

610P R 035 70

elocity Correlation vs. Power Input
a) For Surface Tension Driven Flow
b) For Buoyancy Driven Flow

FIGURE 30

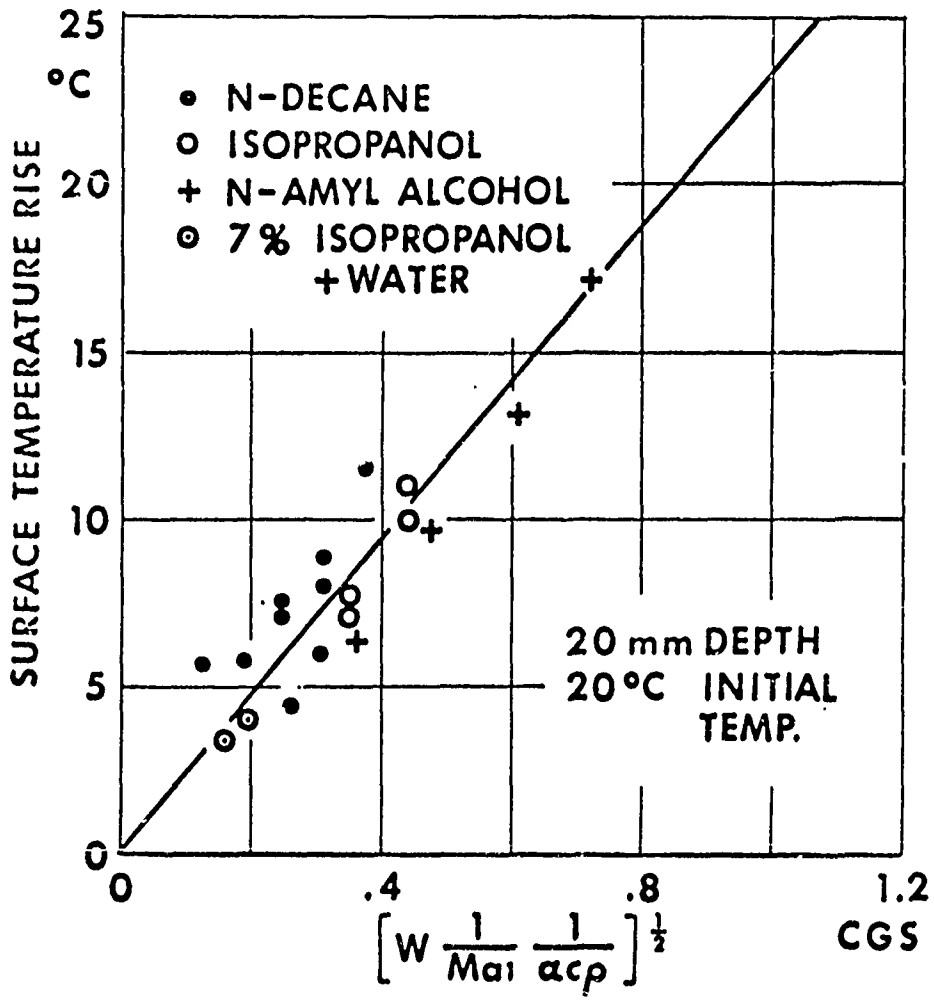

Surface Temperature Rise as Measured by Fine Thermocouples

6104 R 053 70

FIGURE 31

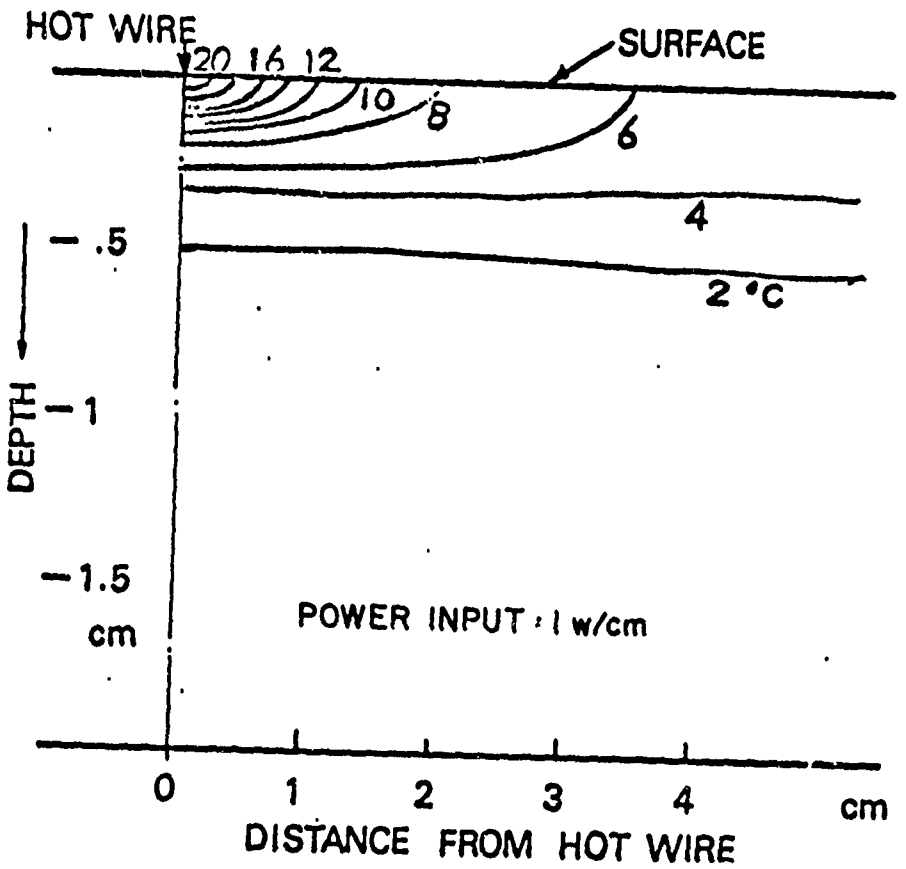

Temperature Rise in Water as Measured by Fine Thermocouples

Glad a oss to

FIGURE 32

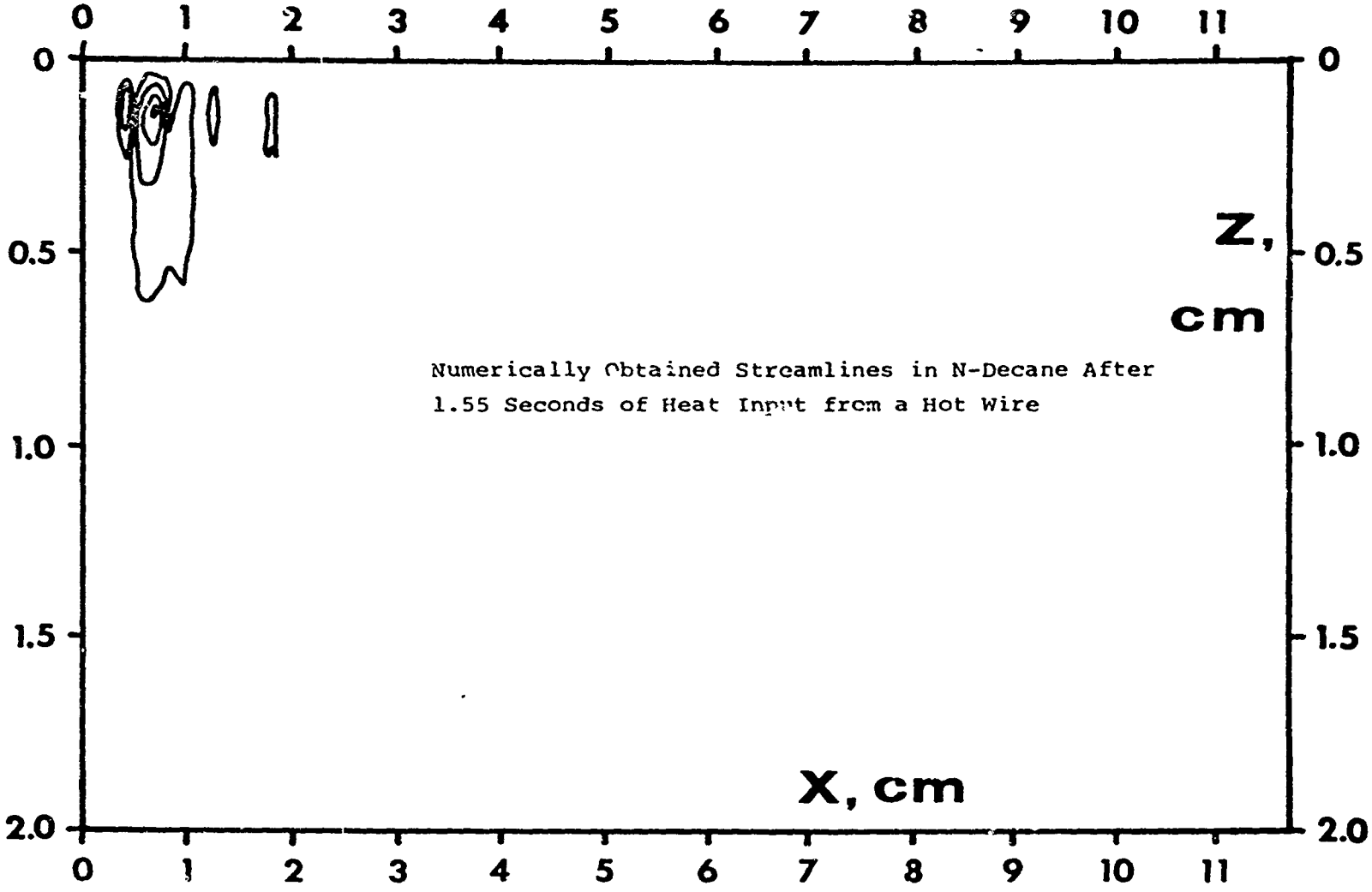

Numerically Obtained Streamlines in N-Decane After 1.55 Seconds of Heat Input from a Hot Wire

FIGURE 33

Part IV

Table of Contents

Part IV: Combustion of Nitrocellulose-Base Propellants

Figures

Figure 1 Strand burning rate ($70^{\circ}F$) of N-5 double-base propellant

Part IV. Combustion of Nitrocellulose-Base Propellants

(M. Summerfield (Principal Investigator), J. A. Steinz, H. Isoda, and N. Kubota)

The studies of the combustion characteristics of nitrocellulose-base solid propellants was begun under this contract. Unfortunately, due to funding difficulties, it was supported for only one month. The accomplishments to be reported are therefore modest.

A literature search was intended in this program and the outline of how it would be presented was made, and is included here. Some initial experiments were performed and are also described.

A. Literature Survey Outline

The main purpose of this literature survey report on the mechanism of combustion of double base propellants was to assemble all the facts about the burning of double base propellants into a coherent picture so that we would finally be able to construct an all-encompassing combustion model for this class of propellants. We would also have delineated the areas that still remain unknown, and, as a result, we should have been able to point the way to more fruitful avenues of future research. This survey report, when it was completed, would serve as the basis of our future investigations and, we hoped, as the basis for the future endeavors of other workers also. As an indication of the coverage of this report, we attach a list of the references that had been evaluated for their usefulness in the final version of the report. The findings of these references were to be placed in their proper perspective in the discussions of the report.

The survey report was intended to cover the findings of all previous investigators concerning the structure of a double base propellant flame, the chemical kinetics in the important reaction stages, and the burning rate behavior as a function of various compositional factors and also as a function of other physical parameters such as initial temperature and pressure. All of these findings were to be drawn together and compared with the predictions of several previously proposed theoretical models of propellant burning. Such comparisons would reveal the deficiencies in each of these models and, at the same time, would point to improvements that ought to be made if a "true" model of DB propellant burning is finally to be developed.

The first section of the report would discuss the practical import of DB propellants and the details of their composition and manufacture. Of particular interest would be the purpose of each constituent and the possible effects of these constituents on the overall burning behavior of a DB propellant. Special emphasis would be given to the effects of various additives such as those lead and copper compounds that produce burning rate vs pressure curves with a plateau (region of zero slope) in the normal rocket pressure range, i.e., in the range extending from 300 to 1500 psia.

The second section of the report would cover the structure of a DB propellant flame, at pressures from 0.001 atm to 100 atm. No direct information concerning the structure above 100 atm was available so for this pressure range, we intended to outline the method of inferring the structure of the flame from the predictions of a valid physical model extrapolated to these high pressures. (This method has been successful in our earlier investigations on composite type solid propellants using ammonium perchlorate oxidizer.) Much of the discussion would be aimed at giving the details of each of the three (already well-established) sequential reaction stages, one solid phase followed by two gas phase reaction stages. In this section of the report we intended to rely rather heavily on a variety of chemical kinetic studies carried out at low temperatures in bulk and on information obtained during linear regression when decomposition occurs in a surface layer at comparatively high temperature. (Naturally we would be cautious about extrapolating low temperature bulk decomposition data to the situation of linear regression at high surface temperatures.) More information would be obtained from the results of chemical kinetic studies on the liquid nitrate esters, compounds that are chemically similar to the NC/NG type DB propellants.

The discussions of the above section were to be further amplified by an elaboration of all the relevant observations concerning the structure of the solid phase, the structure of the liquid layer on the regressing propellant surface, the variation of temperature and species concentrations through each of the three (or more) stages of the flame wave, and the location of various radical emitters (indicative of the active regions) in the flame wave. Since the effect of pressure on all of these observations can be important, understanding such pressure dependencies will be of considerable help in interpreting the significance of many factors on the overall combustion process. Thus, throughout the discussions, continual reference would be made to the effects of changing pressure. With this background of information, we would be able to define qualitatively the range of physical parameters in which each of the three reaction stages become significant, or even exert the controlling influence. We would also make some specific remarks about the relative roles of conductive and radiative heat feedback, combustion inefficiency, and about the implications of a molten bubbling layer on the regressing propellant surface.

The previous section on flame structure observations would serve as the lead-in for the next section in which we would describe the combustion process in as much detail as the facts will allow. The resulting physical model, built on these more complete facts, would then be compared to the previously proposed theoretical models. Only those theories proposed for homogeneous solid propellants such as those of Spalding, of Parr and Crawford, of Rice and Ginell, and of Glazkova, would be considered in this section of the report. The comparison between theory and fact concerning the flame structure and between measurements and theoretical

predictions of the burning rate over wide ranges of pressure would disclose some of the deficiencies of the earlier theoretical models. The comparison would also suggest areas in which more experimental work must be done if reliable and accurate theoretical predictions are to be possible for the future. The comparisons between theory and experiment would exclude the effects of the various additives; the treatment of most of these effects is presently beyond analytical formulation. Nevertheless, we would have outlined the possible modes of action of the additives and also suggested how one might go about an experimental program designed to identify the specific mode of action of each of these additives.

The concluding section of the report would have summarized all that is known about the mechanism of DB propellant burning and would point also to all that has yet to be learned of this process. Specific recommendations would have been made as to future research efforts. The main thought underlying these recommendations is that the problem should be attacked by performing several parallel experiments on the same propellant composition (as outlined in Section I of the present proposal report); such parallel measurements would be self-corroborative and, only in this way, would it be possible to isolate the details of an obviously very complex combustion process. Therefore, we foresee a program in which flame structure observations are made in conjunction with burning rate measurements over the entire range of pressure. These simultaneous measurements would have been done for a series of propellants in which each constituent in the propellant was varied systematically; at this time, no such systematic variation of compositional factors has been done - it is still not possible to separate the effects of the chemical compounds that typically ender into a double base propellant composition.

B. Preliminary Experimental Results

Some initial experiments to measure the strand burning rate of N-5 double-base propellant were performed, at 70°F over the range of pressure from 1 atm to 100 atm. (see Fig. 1). Other propellants, such as M1, M9, M10, M17, M26 and T36, were also examined for the purpose of this investigation, but were not tested during this program.

Some iritial measurements of the dark zone (height vs pressure) for N-5 propellant were also obtained in a strand burner equipped with side windows for flame observation. Initial spectrograms of the gaseous part of the flame were taken at 50 psia and 200 psia. It was noted that flames of double-base propellants are rather faint in comparison with AP type propellants, so the initial spectra probably did not show all the prominent emitters. However, the radicals C_2 and CC were identified from emissions in the midst of the region of the carbon continuum. These were found at several mm above the instantaneous burning surface, not immediately above the surface as in AP composite propellants, apparently above the dark zone but within the luminous flame zone. The surface and subsurface domains of extinguished N-5 propellant were examined

photomicrographically. It was found that physical changes in the condensed phase had taken place, probably induced by the heat wave, down to about 10 microns below the surface for the 200 psi case, and about 30 microns for the 1 atm case. Surprisingly, little evidence of bubble formation even very close to the surface was found; some evidence of abundant sub-surface gas generation had been expected.

Due to termination of funding, this project was not continued further. It is felt that further conclusions would therefore be premature, based on the introductory type investigations completed.

REFERENCES

1. Adams, G. K., "The Chemistry of Solid Propellant Combustion: Nitrate Ester or Double Base Systems", Proceedings of the Fourth Symposium on Naval Structural Mechanics, Purdue University, April 19-21, 1965. "Mechanics and Chemistry of Solid Propellants", ONR Structural Mechanical Series, Pergamon Press, New York, 1967, edited by A. C. Eringen, H. Liebowitz, S. L. Koh and J. M. Crowley. pp. 117-145.

2. Adams, G. K. and Wiseman, L. A., "The Combustion of Double-Base Propellants", Selected Combustion Problems, Butterworth's Scientific Publications, London, 1954. pp. 277-288.

3. Aleksandrov, V. V., Konev, E. V., Mikheev, V. F. and Khlevnoi, S. S., "Surface Temperature of Burning Nitroglycerine Powder", Combustion, Explosion and Shock Waves, Vol. 2, No. 1, 1966. pp. 38-40.

4. Avery, W. H., "Radiation Effects in Propellant Burning", J. Phys. and Colloid Chem., Vol. 54, 1950. pp. 917-928.

5. Buechner, E. E., "Moderne Zwei-und mehrbasige Pulver", Astronautik, Vol. 4, Jan-Feb., 1967. pp. 18-21.

6. Camp, A. T. and Crescenzo, F. G., "Nitrocellulose Gas Producing Charges Containing Copper and Lead Salts and Aluminum", United States Patent No. 3,138,499, June 23, 1964.

7. Cotton, D. J. and Austin, P. D., "Solid Propellant Burning Mechanisms Study", Nav. Weps. Rept. 8573, Tech. Rept. 149, (AD 440123), May 14, 1964.

8. Crawford, B. L., Jr., Huggett, C. and McBrady, J. J., "The Mechanism of Burning of Double-Base Propellants", J. Phys. and Colloid Chem., Vol. 54, 1950. pp. 854-862.

9. Dauerman, L., Salser, G. E. and Tajima, Y. A., "Evidence for Nitrogen Trioxide in the Combustion of a Double-Base Propellant", J. Phys. Chem., Vol. 69, 1965. pp. 3668-3669.

10. Dauerman, L., "Mechanism of Catalytic Ignition and Combustion of Solid Rocket Propellants (u)", Dept. of Chemical Engineering, New York University, Bi-monthly Rept. No. 1 to Feltman Research Laboratories, Picatinny Arsenal, Dover, N. J., for June 24 to Aug. 23, 1966 (AD 648659). January, 1967.

11. Dauerman, L., Salser, G. E. and Tajima, Y. A., "Characteristics of Volatilized Species from Solid Propellants", AIAA J., Vol. 5, No. 8, 1967. pp. 1501-1503.

12. Dauerman, L. and Tajima, Y. A., "Solid-Phase Reactions of a Double-Base Propellant", AIAA J., Vol. 6, No. 4, 1968. pp. 678-683.

13. Dickson, A. D., Crawford, B. L., Jr. and Rotenberg, D. L., "Infrared Spectra of Propellant Flames", Industrial and Engineering Chemistry, Vol. 48, 1956, pp. 759-761.

14. Diederichsen, J. and Gould, R. D., "Combustion Instability of Solid Propellants: Radiation from Cordite Burning Under Conditions of Oscillating Pressure", Rocket Propulsion Establishment, Westcott, England, Tech. Memo. No. 278, (AD 414458), May, 1963.

15. Gibson, R. E., "Origin and General Significance of Study of Kinetics of Propellants", J. Phys. & Colloid Chem., Vol. 84, 1950. pp. 847-853.

16. Glazkova, A. P., "Effect of Catalytic Additives on the Burning of Ammonium Perchlorate and Certain of Its Mixtures", Combustion, Explosion, and Shock Waves, Vol. 2, No. 1, 1966. pp. 32-37.

17. Heath, G. A. and Hirst, R., "Some Characteristics of the High Pressure Combustion of Double-Base Repellants", Eighth Symposium (International) on Combustion, The Williams and Wilkins Co., Baltimore, 1967. pp. 711-720.

18. Heller, C. A. and Gordon, A. S., "Structure of the Gas Phase Combustion Region of a Solid Double Base Propellant", J. Phys. Chem., Vol. 59, 1955. pp. 773-777.

19. Huggett, C., "Combustion of Solid Propellants", Combustion Processes, High Speed Aerodynamics and Jet Propulsion Series, Vol. 2, Princeton University Press, Princeton, 1956. pp. 514-574.

20. Klein, R., Mentser, M., von Elbe, G. and Lewis, E., "Determination of the Thermal Structure of a Combustion Wave by Fine Thermocouples", J. Phys. & Colloid Chem., Vol. 54, 1950. pp. 877-884.

21. Konev, E. V. and Khlevnoi, S. S., "Influence of Light on the Rate of Burning of Nitroglycerine Powder", Journal of Applied Mechanics and Technical Physics (Russian) No. 2, March-April, 1963. Translation: Foreign Technology Division, Wright-Patterson Air Force Base, Ohio, FTD-MT-64-87, (AD 637118), (N66-37370), Feb., 1966, pp. 294-300.

22. Lenchitz, C. and Haywood, B., "Determination of the Role of the Ballistic Modifier in Propellant Combustion Using the Heat of Explosion Test", Combustion and Flame, Vol. 10, No. 2, 1966. pp. 140-146.

23. Maksimov, E. I. and Merzhanov, A. G., "Theory of Combustion of Condensed Substances", Combustion, Explosion, and Shock Waves, Vol. 2, No. 1, 1966. pp. 25-31.

24. Mal'tsev, V. M. and Pokhil, P. F., "Estimation of Thermal Effect of the Initial Stage of Burning of Powders and Explosives", Journal of Applied Mechanics and Technical Physics (Russian), No. 2, March-April, 1963. Translation: Foreign Technology Division, Wright-Patterson Air Force Base, Ohio, FTD-MT-64-87, (AD 637118), (N66-37372), Feb., 1966. pp. 309-313.

25. Markov, S., "The Foreign Technology of Solid Propellants", Surveys of Foreign Scientific and Technical Literature, Aerospace Technology Division, Library of Congress, ATD Rept. 68-30-106-2 (AD 82768), Jan., 1968.

26. Martin, S. B., "Ignition-Ablation Responses of Cellulosic Materials to High Radiant Heat Loads", 1964 Spring Meeting, Western States Section, The Combustion Institute, Stanford University, WSS/CI Paper 64-8, (AD 449601). April, 1964.

27. Marxman, G. A., Capener, E. L. and Wooldridge, C. E., "Response of a Burning Propellant Surface to Erosive Transients", Stanford Research Institute Quarterly Rept. No. 5, for Jan. 1, 1967 to March 31, 1967, (AD 819150), May, 1967.

28. Micheli, P. L. and Miller, I. E., "Travelling Charge Munition Development", Aerojet-General Corp. Rept. to Air Force Armament Laboratory, Air Force Systems Command, Elgin Air Force Base, Florida, Tech. Rept. AFATL-TR-67-36, (AD 819335), March, 1967.

29. Mikheev, V. F., Khlevnoi, S. S. and Khudyakov, A. V., "Thin-Film Resistance Thermometer for Registering the Surface Temperature of a Powder at High Heat Transfer Rates", Combustion, Explosion, and Shock Waves, Vol. 2, No. 2, 1966. pp. 27-31.

30. Military Specification "N-5 Double-Base Propellant", MIL-P-17689A(A5) superseding C-MIL-P-17659 (Nord), 23 March 1953.

31. Musso, R. C., "Decomposition Studies of CMDB Propellant Ingredients", Proceedings of the 3rd ICRPG Combustion Conference, CPIA Publication No. 162, Vol. 1, Dec., 1967. pp. 551-559.

32. Musso, R. C. and Grigor, A. F., "Decomposition Studies of Propellant Ingredients and Ingredient Combinations", ICRPG/AIAA 3rd Solid Propulsion Conference, Atlantic City, New Jersey, June 4-6, 1968. AIAA Preprint 68-495.

33. Parr, R. C. and Crawford, B. L., Jr., "A Physical Theory of Burning of Double-Base Propellants", J. Phys. & Colloid Chem., Vol. 54, 1950. pp. 929-954.

34. Phillips, L., "Comment on 'Evidence for Nitrogen Trioxide in the Combustion of a Double-Base Propellant", J. Phys. Chem., Vol. 72, No. 6, 1968. p. 2279.

35. Pleshanov, A. S., "The Structure of a Flame Front", Journal of Applied Mechanics and Technical Physics (Russian), No. 2, March-April, 1963. Translation: Foreign Technology Division, Wright-Patterson Air Force Base, Ohio, FTD-MT-64-87, (AD 637118), (N66-37371), Feb. 1966. pp. 301-308.

36. Pokhil, P. F. and Mal'tsev, V. M., "About the Mechanism of Combustion of Powders", Inzhenerno-Fizicheskiy Zhurnal (Engineering-Physical Journal), Vol. 6, No. 6, 1963. pp. 94-99. Translation: Foreign Technology Division, Air Force Systems Command, Wright-Patterson Air Force Base, Ohio, FTD-MT-63-242, (AD 606751), March, 1964.

37. Preckel, R. F., "Plateau Ballistics in Nitrocellulose Propellants", ARS J., Vol. 31, No. 9, 1961. pp. 1286-1287.

38. Preckel, R. F., "Plateau Ballistics in Nitrocellulose Propellants", AIAA J., Vol. 3, No. 2, 1965. pp. 346-347.

39. Price, E. W., "Solid Propellant Combustion: State of Knowledge 1967", 62nd. National Meeting, American Institute of Chemical Engineering, Salt Lake City, Utah, May 21-24, 1967. Paper No. 3b.

40. Price, E. W., "Combustion of Solid Rocket Propellants", AIAA Professional Study Series, to be published.

41. Reid, D. L., "The Dependence of Several Solid Propellant Burning Anomalies on Flame Structure", M.S.E. Thesis, Department of Aeronautical Engineering, Princeton University, July, 1967.

42. Rice, O. K. and Ginell, R., "The Theory of the Burning of Double-Base Rocket Powders", J. Phys. and Colloid Chem., Vol. 54, 1950. pp. 885-917.

43. Roginskii, S. Z. and Sapozhnikov, L. M., "Explosive Reactions in Condensed Systems and the Kinetics of the Thermal Decomposition of Trinitroglycerine", Zh. fiz. Khim (J. of Phys. Chem.), Vol. 2, No. 1, 1931. pp. 80-101. Translation: Technical Information and Library Services, Ministry of Aviation, TIL./T. 5414, (N66 28227), March, 1966.

44. Sabadell, A. J., Wenograd, J. and Summerfield, M., "Measurement of Temperature Profiles Through Solid Propellant Falmes Using Fine Thermocouples", AIAA J., Vol. 3, No. 9, 1965. pp. 1580-1584.

45. Sinha, S. K. and Patwardhan, W. D., "Burning of Platonized Propellants", Explosivstoffe, No. 10, 1968, (A69-12881). pp. 223-225.

46. Steinberger, R., "Advances in Double-Base Propellants for Launch Vehicles", Proceedings of the International Symposium on Space Technology and Science, Tokyo, Japan, May 15-22, 1967. Agne Publishing, Inc., 1968. pp. 63-68.

47. Tsai, C. L., Woodward, E. C., Jr. and Suh, N. P., "The Surface Temperature of M-2 Double Base Propellants at Low Pressures", College of Engineering, University of South Carolina, Columbia, Progress Report to Picatinny Arsenal, U. S. Army, Dover, New Jersey, on work performed under Grant No. DA-ARO-D-31-124-61029, 1969.

48. Vandenckerckhove, J., "Erosive Burning of Colloidal Solid Propellant", Jet Propulsion, Vol. 28, No. 9, 1958. pp. 599-603.

49. Vilyunov, V. N., "On the Thermal Theory of Ignition", Combustion, Explosion, and Shock Waves, Vol. 2, No. 2, 1966. pp. 48-51.

50. Wilfong, R. E., Penner, S. S. and Daniels, F., "A Hypothesis for Propellant Burning", J. Phys. & Colloid Chem., Vol. 54, 1950. pp. 863-872.

51. Zenin, A. A., "Burning of Nitroglycerine Powder in Vacuum and at Subatmospheric Pressure", Combustion, Explosion, and Shock Waves, Vol. 2, No. 1, 1966. pp. 42-44.

52. Zenin, A. A., "Formal Kinetic Characteristics of the Reactions Accompanying the Burning of a Powder", Combustion, Explosion, and Shock Waves, Vol. 2, No. 2, 1966. pp. 17-19.

53. Collection of Articles in "Theory of Explosives", Ed. by K. K. Andreyev, A. F. Belyayev, A. I. Gol'binder and A. G. Gorst, State Scientific-Technical Publishing House, Moscow, 1963. Translation: Foreign Technology Division, Air Force Systems Command, Wright-Patterson Air Force Base, Ohio, FTD-MT-63-254, (AD 605706), January, 1964.

    a) Svetlov, B. S., "On the Thermal Decomposition of Nitroglycerine in the Liquid-Phase", p. 252.

    b) Gorvunov, V. V. and Svetlov, B. S., "Concerning the Influence of Temperature on Decomposition of Nitroglycerine", p. 262.

c) Svetlov, B. S., "On the Role of Nitrogen Dioxide in the Self-Accelerated Decomposition of Nitroglycerine", p. 291.

d) Gorbunov, V. V. and Svetlov, B. S., "On the Roll of Condensation Products in the Disintegration of Nitroglycerine", p. 300.

e) Andreyev, K. K., "On the Thermal Disintegration of Nitroglycerine and the Possibility of Its Transition to Explosion", p. 318.

f) Andreyev, K. K. and Kaydymov, B. I., "Thermal Disintegration of PETN", p. 341.

g) Svetlov, B. S., "Thermal Disintegration of Diethyleneglycol Nitrate in the Liquid Phase", p. 385.

h) Lur'ye, B. A. and Svetlov, B. S., "On the Influence of Certain Impurities on Thermal Disintegration of Diethyleneglycol Dinitrate", p. 396.

i) Kondrikov, B. N., "Thermal Decomposition of Dinitrate of Ethylene Glycol and Trinitrate of Glycerine", p. 420.

54. Collection of Articles from "Journal of Applied Mechanics and Technical Physics", No. 6, Nov.-Dec., 1963. Translation: Foreign Technology Division, Air Force Systems Command, Wright-Patterson Air Force Base, Ohio, FTD-MT-64-66, (AD 618314), April, 1965.

a) Librovich, V. B., "On the Ignition of Powders and Explosives", p. 110.

b) Velyayev, A. F. and Lukashenya, G. V. "Effective Temperature of Burning of Certain Explosive Substances", p. 183.

c) Bakhman, N. N., "Remarks About the Influence of Condensed Remainder on Dependency of Burning Rate on Pressure", p. 195.

6104 C 056 70

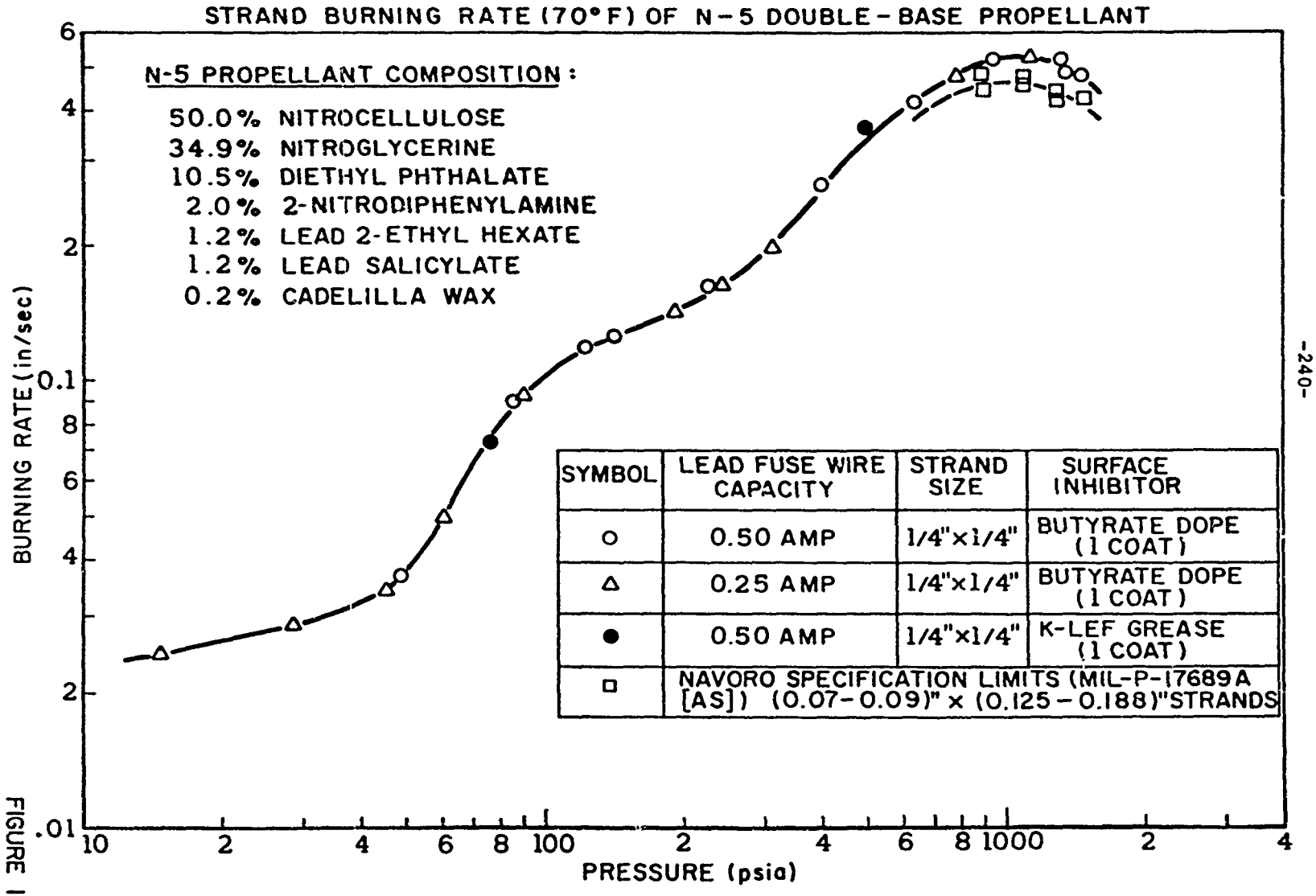

FIGURE 1

Unclassified

Security Classification

DOCUMENT CONTROL DATA · R&D

(Security classification of title, body of abstract and indexing annotation must be entered when the overall report is classified)

1 ORIGINATING ACTIVITY (Corporate author) Department of Aerospace and Mechanical Sciences Princeton University Princeton, New Jersey 08540	2a REPORT SECURITY CLASSIFICATION Unclassified 2b GROUP

3 REPORT TITLE

Physics of Flames

4 DESCRIPTIVE NOTES (Type of report and inclusive dates)

Final Report (July 1, 1968 to June 30, 1970)

5 AUTHOR(S) (Last name, first name, initial)

Glassman, I., Sirignano, W. A., and Summerfield, M.

6 REPORT DATE	7a TOTAL NO OF PAGES	7b NO OF REFS
September, 1970	237	121

8a CONTRACT OR GR . T NO DAAO5-68-C-0450 b PROJECT NO c d	9a ORIGINATOR'S REPORT NUMBER(S) AMS Dept. T.R. 952 9b OTHER REPORT NO(S) (Any other numbers that may be assigned this report)

10 AVAILABILITY/LIMITATION NOTICES

This document has been approved for public release and sale; its distribution is unlimited.

11 SUPPLEMENTARY NOTES	12 SPONSORING MILITARY ACTIVITY
	Ballistic Research Laboratories, U. S. Army Aberdeen Proving Grounds, Md.

13 ABSTRACT

Theoretical and experimental analyses of flame spreading across pools of liquid fuels and the ignitability of such pool under quiescent and flowing environments are presented. The fundamental concept is that, when the temperature of the liquid fuel is below the flash point, convection currents in the liquid play a dominant role in both ignitability and flame spreading. These currents are induced by either or both surface tension and buoyancy forces.

A theoretical analyses related to ignition of fuels by projectiles is presented. A brief section on the combustion of nitrocellulose-base propellants is included.

DD FORM 1 JAN 64 1473

Unclassified

Security Classification

Unclassified

Security Classification

14. KEY WORDS	LINK A		LINK B		LINK C	
	ROLE	WT	ROLE	WT	ROLE	WT
Flame Spreading Ignition of Fuels Ignition by Projectiles Hydrocarbon Combustion Nitrocellulose Combustion						

INSTRUCTIONS

1. ORIGINATING ACTIVITY: Enter the name and address of the contractor, subcontractor, grantee, Department of Defense activity or other organization *(corporate author)* issuing the report.

2a. REPORT SECURITY CLASSIFICATION: Enter the overall security classification of the report. Indicate whether "Restricted Data" is included. Marking is to be in accordance with appropriate security regulations.

2b. GROUP: Automatic downgrading is specified in DoD Directive 5200.10 and Armed Forces Industrial Manual. Enter the group number. Also, when applicable, show that optional markings have been used for Group 3 and Group 4 as authorized.

3. REPORT TITLE: Enter the complete report title in all capital letters. Titles in all cases should be unclassified. If a meaningful title cannot be selected without classification, show title classification in all capitals in parenthesis immediately following the title.

4. DESCRIPTIVE NOTES: If appropriate, enter the type of report, e.g., interim, progress, summary, annual, or final. Give the inclusive dates when a specific reporting period is covered.

5. AUTHOR(S): Enter the name(s) of author(s) as shown on or in the report. Enter last name, first name, middle initial. If military, show rank and branch of service. The name of the principal author is an absolute minimum requirement.

6. REPORT DATE: Enter the date of the report as day, month, year; or month, year. If more than one date appears on the report, use date of publication.

7a. TOTAL NUMBER OF PAGES: The total page count should follow normal pagination procedures, i.e., enter the number of pages containing information.

7b. NUMBER OF REFERENCES: Enter the total number of references cited in the report.

8a. CONTRACT OR GRANT NUMBER: If appropriate, enter the applicable number of the contract or grant under which the report was written.

8b, 8c, & 8d. PROJECT NUMBER: Enter the appropriate military department identification, such as project number, subproject number, system numbers, task number, etc.

9a. ORIGINATOR'S REPORT NUMBER(S): Enter the official report number by which the document will be identified and controlled by the originating activity. This number must be unique to this report.

9b. OTHER REPORT NUMBER(S): If the report has been assigned any other report numbers *(either by the originator or by the sponsor)*, also enter this number(s).

10. AVAILABILITY/LIMITATION NOTICES: Enter any limitations on further dissemination of the report, other than those imposed by security classification, using standard statements such as:

(1) "Qualified requesters may obtain copies of this report from DDC."

(2) "Foreign announcement and dissemination of this report by DDC is not authorized."

(3) "U. S. Government agencies may obtain copies of this report directly from DDC. Other qualified DDC users shall request through _____."

(4) "U. S. military agencies may obtain copies of this report directly from DDC. Other qualified users shall request through _____."

(5) "All distribution of this report is controlled. Qualified DDC users shall request through _____."

If the report has been furnished to the Office of Technical Services, Department of Commerce, for sale to the public, indicate this fact and enter the price, if known.

11. SUPPLEMENTARY NOTES: Use for additional explanatory notes.

12. SPONSORING MILITARY ACTIVITY: Enter the name of the departmental project office or laboratory sponsoring *(paying for)* the research and development. Include address.

13 ABSTRACT: Enter an abstract giving a brief and factual summary of the document indicative of the report, even though it may also appear elsewhere in the body of the technical report. If additional space is required, a continuation sheet shall be attached.

It is highly desirable that the abstract of classified reports be unclassified. Each paragraph of the abstract shall end with an indication of the military security classification of the information in the paragraph, represented as *(TS) (S) (C), or (U)*

There is no limitation on the length of the abstract. However, the suggested length is from 150 to 225 words.

14 KEY WORDS: Key words are technically meaningful terms or short phrases that characterize a report and may be used as index entries for cataloging the report. Key words must be selected so that no security classification is required. Identifiers, such as equipment model designation, trade name, military project code name, geographic location, may be used as key words but will be followed by an indication of technical context. The assignment of links, rules, and weights is optional

GPO 886-551